Development, Validation, and Application of Methods for High Time-Response Measurement of Gaseous Atmospheric Chlorinated Species

Teles Carlo Furlani

A DISSERTATION SUBMITTED TO THE FACULTY OF GRADUATE STUDIES IN PARTIAL FULFILMENT OF THE REQUIREMENTS FOR THE DEGREE OF

DOCTOR OF PHILOSOPHY

GRADUATE PROGRAM IN CHEMISTRY

YORK UNIVERSITY

TORONTO, ONTARIO

November 2021

Abstract

Halogenated compounds that participate in catalytic cycles in the atmosphere can influence the fate of chemicals, including ozone (O_3), methane, and volatile organic compounds (VOCs) in the troposphere. These halogen radicals, in particular atomic chlorine (Cl), can deplete O_3 and will react rapidly with VOCs.

Reliable, sensitive, and widely available hydrogen chloride (HCl) measurements are important for understanding Cl initiated oxidation in many regions of the troposphere. We configured a commercial HCl cavity ring-down spectrometer (CRDS) for sampling HCl in the ambient atmosphere and developed validation techniques to characterize the measurement uncertainties. The CRDS makes fast, sensitive, and robust measurements of HCl, comparing favourably to other techniques for measurement of HCl described in the literature. An ambient intercomparison with a standard HCl quantification method showed excellent agreement.

The same analyzer was used to make continuous HCl measurements in the polluted marine boundary layer during the Halifax Fog and Air Quality Study (HaliFAQS). HCl throughout the campaign was elevated when high irradiance was observed. Bimodal HCl features in the high irradiance days indicated two photochemical processes; (1) morning time photolysis of Cl precursors, and (2) midday formation of nitric acid (HNO_3) followed by acid displacement onto chloride (Cl^-) containing aerosols. A simple box model was used to estimate peak nighttime nitryl chloride ($ClNO_2$) mixing ratios that showed good agreement between measured and simulated HCl on 6 days with high irradiance. Modelled estimates on June 18 showed that production of Cl from $ClNO_2$ photolysis was 13% as large as production of OH from O_3 photolysis when considering the full day, and 37% in the morning indicating Cl contributes to oxidative capacity in Halifax.

Chlorine containing compounds in the atmosphere can impact air quality, climate, and health. Total gaseous chlorine (TCl_g) measurements can illuminate unknown sources of Cl to the atmosphere. Techniques for measuring TCl_g have been limited to offline analysis of extracted filters and do not provide suitable temporal information on fast atmospheric process. High-time resolution in-situ measurements of TCl_g can be captured by combusting ambient air on a catalytic platinum (Pt) substrate contained in a high temperature furnace followed by measurement of HCl by CRDS. This method depends on the complete combustion of TCl_g to release Cl atoms that readily react with supplied excess propane to form HCl. Complete conversion of the strong chlorine-containing bonds found in dichloromethane, 1-chlorobutane, and 1,3-dichloropropene, was demonstrated. Breaking these relatively strong C-Cl bonds is a good proof of concept for complete conversion of all similar or weaker bonds that characterize all other TCl_g. We applied this technique to both outdoor and indoor environments and measured 2.0–3.5 and 5–18 ppbv of TCl_g, respectively. These measurements were in reasonable agreement with the sum of expected HCl from known Cl species. The method validated here is capable of measuring in-situ total Cl_y and has a broad range of applications to make routine TCl_g measurements in a variety of regions. The utility of this novel TCl_g measurement technique will be crucial to future estimates and assessments of chlorinated compounds and their impact on air quality, climate, and health.

The measurements described above would not be possible without the ability to deliver consistent quantities of trace compounds at atmospherically relevant mixing ratios. We demonstrated a method by which these compounds can be generated using permeation devices (PDs). We discussed the efficacy of two different calibration techniques, gravimetric and offline analysis. We characterized the physical dependence of temperature and showed the emission stability of PDs using in-situ online analysis.

Acknowledgements

First and foremost, I would like to thank my supervisor Cora Young. You showed me how to be not just a better atmospheric chemist but also how to be Persistent, Observant, and Precise (POPs), forgive the pun. Your guidance while I have navigated what chemist I want to be is greatly appreciated and you deserve recognition. I would also like to thank my committee members Rob McLaren and John Liggio for all their help and suggestions throughout my time at York. Thank you to Trevor VandenBoer for your experimental expertise and for always reminding us to RTFM.

I have been lucky to find many friends throughout my degree and because of them my experience changed for the better. I have to thank every CJY group member I had the pleasure of working with: The MUN crew – Rob, Joseph, John, Kathryn, Bryan, Heidi, Kat, Li, and Devon. John and Joseph, thank you for all the weird jokes and office hand ball, and Kathryn for being a cool desk neighbour. The York crew – Lisa, Andrea, Alessia, Shira, Melodie, Leigh, Leyla, Alex, and others. A special thank you to my York office mates, Andrea and Lisa. Andrea the time spent in that office was a ~golden experience~. *Lisa*, you were and are the best oxygen out of the 324 "Ozone".

To my MUN friends; Liam, Alison, Lucas, Kathleen, Josh, Nicole, Doug, Kerri, Jake, and Nick. Thank you for all the fun times in and out of the chemistry society room. Special thanks to Lucas and Kathleen for housing me when my apartment flooded and adopting me as an honorary Burke manor member. A big thank you to my non-chemistry friends, Lauren, Niall, Victoria, and Al, for all the fun times at Wing'n it trivia, you carried me to greatness; immortalized as trivia gods for all of time in the pantheon of chicken wing legends.

A big thank you to my family Frank, Elaine, Blair, Krystal, Nonna-Nina, and Chica who supported me throughout my entire undergraduate and graduate degrees. With special thanks to the cutest dog in the world, Chica, who actually ghost wrote this thesis and deserves all the treats in the world.

Table of Contents

List of Tables

List of Figures

List of Symbols, Nomenclature, and Abbreviations

°C	degree Celsius
Δ	delta, change
ΔE_D	activation energy of diffusion
ΔH_S	heat of solution
%	percent
Σ	sum
σ	standard deviation
μm	micrometre/micron
μL	microlitre
γ	reactive uptake coefficient for N_2O_5
ADT	Atlantic daylight-saving time
AGAGE	advanced global atmospheric gases experiment
BDE	bond dissociation energy
cm	centimetre
CB	1-chlorobutane
CH_4	methane
C_2H_6	ethane
C_3H_8	propane
CH_3OH	methanol
CH_3CHO	acetaldehyde
CH_3Cl	methyl chloride
CH_3CCl_3	methyl chloroform
CH_2Cl_2	dichloromethane
$CHCl_3$	trichloromethane
$CCl_2=CCl_2$	tetrachloroethylene
$CHClF_2$	chlorodifluoromethane
CIMS	chemical ionization mass spectrometry

Cl	chlorine atom
Cl^-	chloride
Cl_y	reactive chlorine
Cl_2	molecular chlorine
CFC	chlorofluorocarbon
$ClNO_2$	nitryl chloride
ClO	chlorine monoxide
ClO_x	Cl + ClO
$ClONO_2$	chlorine nitrate
CO	carbon monoxide
CONTRAST	CONvective Transport of Active Species in the Tropics
CRDS	cavity ring-down spectroscopy
D_0	pre-exponential constant for diffusion
DCM	dichloromethane
DCP	1,3-dichloropropene
ECCC	Environment and Climate Change Canada
EDT	Eastern daylight-savings time
GC-MS	gas chromatography mass spectrometry
GEM	global environmental multiscale
H	Henry's law coefficient
H_2SO_4	sulfuric acid
HaliFAQS	Halifax Fog and Air Quality Study
HCFC	hydrochlorofluorocarbon
HCHO	formaldehyde
HCl	hydrochloric acid
HCl-TCl	HCl and total chlorine
HEPA	high efficiency particulate air
HO_x	OH + HO_2

HO_2	hydroperoxyl radical
HOCl	hypochlorous acid
HONO	nitrous acid
HNO_3	nitric acid
HPLC	high performance liquid chromatography
HRDPS	high resolution deterministic prediction system
i.d.	inner diameter
IC-CD	ion chromatography with conductivity conduction
kJ	kilojoules
km	kilometre
KOH	potassium hydroxide
kW	kilowatts
L	litre
LOD	limit of detection
LOQ	limit of quantification
m	metre
M	molar concentration mol L^{-1}
MΩ	megaohm
MBL	marine boundary layer
MFC	mass flow controller
min	minute
mL	millilitre
mm	millimetre
mM	millimolar
mol	moles
ng	nanogram
N_2	molecular nitrogen
N_2O_5	dinitrogen pentoxide

NCAR	national center for atmospheric research
NaCl	sodium chloride
NaOH	sodium hydroxide
NH_3	ammonia
NCl_3	nitrogen trichloride
NH_2Cl	monochloramine
$NHCl_2$	dichloramine
NO	nitric oxide
NO_2	nitrogen dioxide
NO_3	nitrate radical
NO_x	$NO + NO_2$
NOAA	National Oceanic and Atmospheric Administration
o.d.	outer diameter
O (^1D)	first excited state of singlet oxygen
O_2	oxygen
O_3	ozone
OH	hydroxyl radical
OP-FTIR	open-path Fourier transform infrared spectroscopy
PD	permeation device
PFA	perfluoroalkoxy
pH	scale of acidity, $-\log(H^+)$
PID	proportional-integral-differential
PM	particulate matter
$PM_{2.5}$	particulate matter >2.5 μm
PP	polypropylene
pptv	parts per trillion by volume
ppbv	parts per billion by volume
ppmv	parts per million by volume

psi	pounds per square inch
Pt	platinum
PTFE	polytetrafluoroethylene
QMS	quadrupole mass spectrometry
R	ideal gas constant
RH	relative humidity
s	seconds
S_0	pre-exponential constant for solubility
sccm	standard cubic centimeter per minute
SML	sea surface micro layer
SO_2	sulfur dioxide
SSA	sea spray aerosols
T	temperature
TCl_g	total gaseous chlorine
Tg	teragram
ToF	time of flight
TUV	tropospheric ultraviolet and visible radiation model
UV	ultraviolet
V	volts
v/v	volume by volume
VSLS	very short-lived substances
VOC	volatile organic compound
w/v	weight by volume
WINTER	Wintertime Investigation of Transport, Emissions, and Reactivity aircraft campaign
yr	year

List of Appendices

Preface

This thesis is comprised of a series of manuscripts that have been published or are in preparation for submission to be published in peer-reviewed scientific journals. Consequently, repetition of introductory and experimental details was inevitable. All manuscripts were written by Teles C. Furlani with critical comments provided by Cora J. Young. All research and manuscript preparation was conducted under the guidance of Cora J. Young. The contributions of co-authors are detailed below:

Chapter 1: Introduction

Contributions – Prepared by Teles C. Furlani with editorial comments by Cora J. Young

Chapter 2: Compact Permeation Devices for Stable Emission of Gas-Phase Analytical Standards

Teles C. Furlani[1] and Cora J. Young[1]

[1] Department of Chemistry, York University, Toronto, Canada

Contributions – Teles C. Furlani collected and analyzed the data. Teles C. Furlani and Cora J. Young conceived of and designed the experiments. Funding was obtained by Cora J. Young. The manuscript was written by Teles C. Furlani with input from Cora J. Young.

Chapter 3: Validation of a new cavity ring-down spectrometer for measuring tropospheric gaseous hydrogen chloride

Teles C. Furlani[1], Patrick R. Veres[2], Kathryn E.R. Dawe[3, a], J. Andrew Neuman[2, 4], Steven S. Brown[2,5], Trevor C. VandenBoer[1], Cora J. Young[1]

[1] Department of Chemistry, York University, Toronto, ON, Canada

[2] NOAA Chemical Sciences Laboratory, Boulder, CO, USA

[3] Department of Chemistry, Memorial University of Newfoundland, St. John's, NL, Canada

[4] Cooperative Institute for Research in Environmental Sciences, University of Colorado, Boulder, CO, USA

[5] Department of Chemistry, University of Colorado, Boulder, CO, USA

[a] Now at SEM Ltd., St. John's, NL, Canada

Contributions – Teles C. Furlani collected and analyzed the data with collection assistance from Kathryn E.R. Dawe. Humidity change response time data was collected by Patrick R. Veres. Teles C. Furlani, Patrick R. Veres, J. Andrew Neuman, Steven S. Brown, Trevor C. VandenBoer, and Cora J. Young conceived of and designed the experiments. Funding was obtained by Cora J. Young. The manuscript was written by Teles C. Furlani with input from all authors.

Acknowledgements

We acknowledge the Natural Sciences Engineering and Research Council of Canada and York University for funding. We thank Andrea Angelucci and Sonya Daljeet for assistance with data collection.

Chapter 4: Hydrogen Chloride (HCl) as a Tracer for Morning Reactive Chlorine Cycling in the Polluted Marine Boundary Layer during the Halifax Fog and Air Quality Study (HaliFAQS)

Teles C. Furlani[1], Alex Moravek[1, a], Wanmin Gong[2], Aldona Wiacek[3,4], Rachel Y.-W. Chang[5], Trevor C. VandenBoer[1], and Cora J. Young[1]

[1] Department of Chemistry, York University, Toronto, Canada

[2] Environment and Climate Change Canada, Toronto, Canada

[3] Department of Environmental Science, Saint Mary's University, Halifax, Canada

[4] Department of Astronomy and Physics, Saint Mary's University, Halifax, Canada

[5] Department of Physics and Atmospheric Science, Dalhousie University, Halifax, Canada

[a] Now at German Environment Agency, Section II 4.3, Dessau-Rosslau, Germany

Contributions – Teles C. Furlani collected and analyzed the data with collection assistance from Alex Moravek. OP- FT-IR data was collected and analyzed by Aldona Wiacek. Planetary boundary layer height data was collected by Wanmin Gong. Teles C. Furlani, Alex Moravek, Trevor C.

VandenBoer, and Cora J. Young conceived of and designed the experiments. Funding was obtained by Cora J. Young and Rachel Y.-W. Chang. The manuscript was written by Teles C. Furlani with input from all authors.

Acknowledgements

We acknowledge the Natural Sciences Engineering and Research Council of Canada, Ocean Frontier Institute, and York University for funding. We thank Cameron Power, Baban Nagare, and Joelle Dionne for assistance with data collection.

Chapter 5: Characterization of a Conversion Technique to Measure Total Chlorine in Ambient Air

Teles C. Furlani[1] and Cora J. Young[1]

[1] Department of Chemistry, York University, Toronto, Canada

Contributions – Teles C. Furlani collected and analyzed the data. Teles C. Furlani and Cora J. Young conceived of and designed the experiments. Funding was obtained by Cora J. Young. The manuscript was written by Teles C. Furlani with input from Cora J. Young.

Acknowledgements

We acknowledge the Sloan Foundation, Natural Sciences Engineering and Research Council of Canada, and York University for funding.

Chapter 6: Conclusions and Future Directions

Contributions – Prepared by Teles C. Furlani with editorial comments by Cora J. Young

Other Publications During PhD

Angelucci, A.A.; **Furlani, T.C.**; Wang, X.; Jacob, D.J.; VandenBoer, T.C.; Young, C.J. Understanding sources of atmospheric hydrogen chloride in coastal spring and continental winter. ACS Earth Sp. Chem. 2021. https://doi.org/10.1021/acsearthspacechem.1c00193.

Joudan, S.; Orlando, J.J.; Tyndall, G.S.; **Furlani, T.C.**; Young, C.J.; Mabury, S. A. Atmospheric Fate of a New Polyfluoroalkyl Building Block, $C_3F_7OCHFCF_2SCH_2CH_2OH$. Environ. Sci. Technol. 2021. https://doi.org/10.1021/acs.est.0c07584.

Lao, M.; Crilley, L.R.; Salehpoor, L.; **Furlani, T.C.**; Bourgeois, I.; Neuman, J.A.; Rollins, A.W.; Veres, P.R.; Washenfelder, R.A.; Womack, C.C.; Young, C.J.; VandenBoer, T.C. A Portable, Robust, Stable and Tunable Calibration Source for Gas-Phase Nitrous Acid (HONO). Atmos. Meas. Tech. 2020, 13, 5873–5890. https://doi.org/10.5194/amt-13-5873-2020.

Dawe, K.E.R.; **Furlani, T.C.**; Kowal, S.F.; Kahan, T.F.; VandenBoer, T.C.; Young, C.J. Formation and Emission of Hydrogen Chloride in Indoor Air. Indoor Air. 2019, 70–78. https://doi.org/10.1111/ina.12509.

Chapter 1.

Introduction

1.1 Introduction to atmospheric chemistry

1.1.1 Oxidation chemistry

The chemistry and fate of trace gases have significant impacts on climate and air quality. Oxidative capacity in the atmosphere is what dictates the removal of trace gases. Oxidation is the primarily loss mechanism for greenhouse gases (e.g., methane (CH_4)) and some toxic gases (e.g., carbon monoxide (CO)). The most abundant oxidants in the atmosphere are oxygen (O_2), ozone (O_3), and the hydroxyl radical (OH), with the latter being the major oxidation driving force in the troposphere despite being the least abundant of the three. The oxidation of the troposphere is of importance as it dictates the fate of all surface emissions. The bond energies for O_2 and O_3 are relatively large compared to OH, and usually only react with radical species with exception to epoxidation reactions of O_3 adding onto alkenes. In contrast, OH reacts readily with non-radical species that have either/both an abstractable hydrogen and a double bond. The dominant source of OH in the troposphere is initiated by the photolysis of O_3 (R1.1.1), followed by the reaction between $O(^1D)$ and water (R1.1.2).

$$O_3\,(g) + h\nu \rightarrow O_2\,(g) + O(^1D)\,(g) \qquad \text{R1.1.1}$$

$$O(^1D)\,(g) + H_2O\,(g) \rightarrow 2OH\,(g) \qquad \text{R1.1.2}$$

The level of OH in the troposphere is estimated using a steady-state approach including sources (e.g., R1.1.1 and R1.1.2) and sinks, and is usually estimated as 1×10^6 molecules cm^{-3}. As long as there is O_3, water, and light, then there is a myriad of different reactions that can take place involving trace gases and OH as the primary oxidant. When NO_x ($NO + NO_2$) is added to the equation, oxidation chemistry becomes more complex. With enough sunlight, NO_x will catalytically promote O_3 formation via reactions R1.1.3–R1.1.6, using methane as an example (M here represents a molecule of air, e.g., N_2 or O_2).

$CH_4\,(g) + OH\,(g) \rightarrow CH_3\,(g) + H_2O\,(g)$ R1.1.3

$CH_3\,(g) + O_2\,(g) + M \rightarrow CH_3OO\,(g) + M$ R1.1.4

$CH_3OO\,(g) + NO\,(g) \rightarrow CH_3O\,(g) + NO_2\,(g)$ R1.1.5

$NO_2\,(g) + O_2\,(g) + h\nu \rightarrow NO\,(g) + O_3\,(g)$ R1.1.6

$CH_3O\,(g) + O_2\,(g) \rightarrow HCHO\,(g) + HO_2\,(g)$ R1.1.7

Leading to the net reaction:

$CH_4\,(g) + OH\,(g) + 3O_2\,(g) \rightarrow HCHO\,(g) + HO_2\,(g) + H_2O\,(g) + O_3\,(g)$ R1.1.8

The catalytic formation of O_3 from NO_x (R1.1.3–1.1.8) is required to maintain the levels of OH observed in the troposphere.[1] While oxidation reactions with OH is the most important globally, oxidation initiated by the chlorine atom (Cl) cannot be neglected.[2] Reactions involving Cl can be faster for some trace gases that resist oxidation by OH. Chlorine chemistry in stratosphere was the primary focus from the 1970s to 1980s and the impacts are well understood. There is more uncertainty in chlorine chemistry in the troposphere due the greater complexity and lack of understanding on all the chemical processes necessary for constraining all sources and sinks.

1.1.2 Stratospheric and tropospheric chlorine chemistry

Stratospheric chemistry began when the presence ozone in the upper atmosphere was theorized by Hartley in 1881,[3] and the mechanisms for ozone behaviour was proposed by Chapman in 1930 (R1.2.1 to R1.2.4).[4]

$O_2\,(g) + h\nu \rightarrow 2O\,(g)$ R1.2.1

$O_2\,(g) + O\,(g) + M\,(g) \rightarrow O_3\,(g) + M\,(g)$ R1.2.2

$O_3\,(g) + h\nu \rightarrow O\,(g) + O_2\,(g)$ R1.2.3

$O_3\,(g) + O\,(g) \rightarrow 2O_2\,(g)$ R1.2.4

Ozone in the stratosphere is necessary for life as it acts as a filter by absorbing harmful ultraviolet radiation before it reaches the earths surface. The catalytic destruction of ozone has been observed due to the influence of HO_x (H + OH + peroxy radicals),[5] NO_x (NO + NO_2),[6] and halogen chemistry.[7–10] Halogens from primarily chlorine containing compounds have long since been attributed to stratospheric O_3 destruction since the mechanism (R1.2.5 to R1.2.7) was first hypothesized by Molina and Rowland in 1974.[10]

$$Cl\,(g) + O_3\,(g) \rightarrow ClO\,(g) + O_2\,(g) \qquad \text{R1.2.5}$$

$$ClO\,(g) + O\,(g) + h\nu \rightarrow Cl\,(g) + O_2\,(g) \qquad \text{R1.2.6}$$

Leading to the net reaction:

$$O_3\,(g) + O\,(g) \rightarrow 2O_2\,(g) \qquad \text{R1.2.7}$$

Cl impacts on ozone become much more complex in the troposphere, with many more competing and ozone producing reactions. In polluted continental and coastal cities, elevated Cl emissions have been observed to enhance O_3 production.[2,11–15] On average, O_3 levels are enhanced when Cl is present, but this change can be drastically different given the local conditions. Ozone peak concentrations changes in continental urban regions can range from -10.5–27%.[13] An increase in Cl_y emissions in China due to coal combustion was shown to increase the monthly average of ozone by 4.1%.[15] There is no direct mechanism for why Cl oxidation would provide an increase in O_3 formation, the uncertainty in observed increase in ozone from these modelling studies are possibly a erroneous artifact. OH reactions still dominate radical propagation, but the propensity of Cl to initiate radical propagation chains provides more opportunities to yield O_3. Oxidation chemistry has the greatest impact on the fate of many trace gases, but the contributions to tropospheric chemistry involving aerosols that offer a large surface area for heterogenous reactions can also play an important role.

1.1.3 Atmospheric aerosols

Atmospheric chemistry and climate can be impacted by the presence of small, condensed liquid or solid matter suspended in air called aerosols or particulate matter (PM). Aerosols are typically characterized by their size distribution and composition. Sources of aerosols to the atmosphere can be natural (sea spray, dust, volcanic emissions, and biogenic aerosols) and anthropogenic (dust mobilization from human activity, nitrate and sulfate emissions, fossil fuel combustion, and waste and biomass burning). Among natural sources, the sea spray generated from wind stress at the ocean surface is the largest emission of global aerosol by mass (but typically a low number concentration).[16,17] The mobilization of chloride (Cl^-) from sea salt can lead to interesting chlorine chemistry (see Section 1.1.3). Size distribution is usually indicative of the source, commonly separated into two categories, coarse mode particles which have an aerodynamic diameter of 1 – 100 μm, and fine mode particles which have an aerodynamic diameter of < 1 μm. Fine mode particles can be further categorized into ultrafine particles < 0.1 μm, but there is some debate between what is a particle and what is a molecular cluster at nanometer ranges.[18–20] The size and composition of aerosols affect their impacts. For example, PM with aerodynamic diameter less than 2.5 μm or $PM_{2.5}$ is of particular concern for human health. $PM_{2.5}$ is at the critical size that allows it to partition into and clog the small alveolar lung cavities, which can to contribute to cancer.[20] Furthermore, aerosol size and composition has an impact on climate. At an aerodynamic diameter of approximately < 0.2 μm, PM can start acting as cloud condensation nuclei, the solid surface of these particles offers a large surface area for liquids to condense on.[18,19] By aiding in the formation of clouds, aerosols of this size have a direct effect on surface albedo, by reflecting oncoming solar radiation thus giving a net negative radiative forcing.[21,22] Radiative forcing is the measurement of energy flux within the planetary boundary layer that offers a net warming (positive) or cooling (negative). Some aerosols contain

organic matter that is capable of absorbing actinic radiation giving them a net positive radiative forcing.[23] By mass there is very little fine and ultrafine particles, but they are numerically greater and contribute the most to overall PM surface area.[24]

Understanding the composition of particles in the atmosphere is a major challenge for atmospheric science because aerosols are typically heterogeneous in nature. Composition can vary from individual particle to particle, but most studies report bulk composition results by the size fraction collected.[24,25] The reactive species within and on aerosols can undergo chemical transformations. In some cases, aerosol age and source can be inferred by studying its composition. Understanding the different mechanisms of aerosol chemical transformation has been a challenge for atmospheric scientists, due to analytical limitations hindering our ability to study the very dilute air media.

1.1.4 Marine boundary layer (MBL)

The marine boundary layer (MBL) is where the ocean meets the atmosphere, it is at this interface that we can study the transportation of soluble and insoluble compounds from the ocean to the atmosphere.[16,26–29] The top 1000 μm ocean is where most sea-air exchange takes place and is denominated as the sea surface micro layer (SML),[30] which is enriched with organics that are continuously partitioning from the bulk ocean due to torrential mixing.[16,17] Chemical partitioning of gases is another method by which the ocean and atmosphere exchange, this is a concentration and temperature driven process.[30,31]

Nascent sea spray aerosols (SSA, also known as marine aerosols) derived from oceans represent the most significant contribution to the global aerosol load. The composition of SSA is dominated by inorganic sea salt by mass at larger diameters, while the smaller particles are enriched in organic species. Formation of SSA occurs when strong ocean currents become

turbulent, and this turbulence will form breaking waves that can eject coarse and fine mode aerosols that are enriched in dissolved sea salt and organic matter. Breaking waves can entrap air bubbles that scrub organics from the bulk ocean, the entrapped air bubbles rise to the surface, burst and release SSA.[16] The larger coarse particles do not have a long atmospheric lifetime (hours–days) compared to the smaller longer-lived aerosols (day–weeks) which can be found much farther from the ocean and can serve as a source of ocean emissions well inland.[32,33]

1.2 Reactive chlorine

Reactive chlorine (Cl_y) represents all chlorine-containing species which can undergo common atmospheric reactions to yield a chlorine atom. A typical background mixing ratio of Cl_y in the troposphere is approximately 1.5 ppbv (subject to change from region to region). The dominant Cl_y species include methyl chloride (CH_3Cl, 43%), methyl chloroform (CH_3CCl_3, 29%), dichloromethane (CH_2Cl_2, 3%), trichloromethane ($CHCl_3$, 4%), tetrachloroethylene ($CCl_2=CCl_2$, 2%), and chlorodifluoromethane ($CHClF_2$, 8%), see Figure 1-1. These are mostly emitted directly naturally or anthropogenically; the latter is the end oxidation product of a litany of larger alkyl chlorides (~4%).[34,35] Inorganic sources account for 7% by mass; these emissions are small in comparison to organic Cl_y, yet due to their higher reactivity are more likely to increase the total Cl atom concentration.[36,37] The most abundant inorganic forms and the focus of the majority of Cl_y chemistry are molecular chlorine (Cl_2), hydrochloric acid (HCl), hypochlorous acid (HOCl), and nitryl chloride ($ClNO_2$), see Figure 1-2.

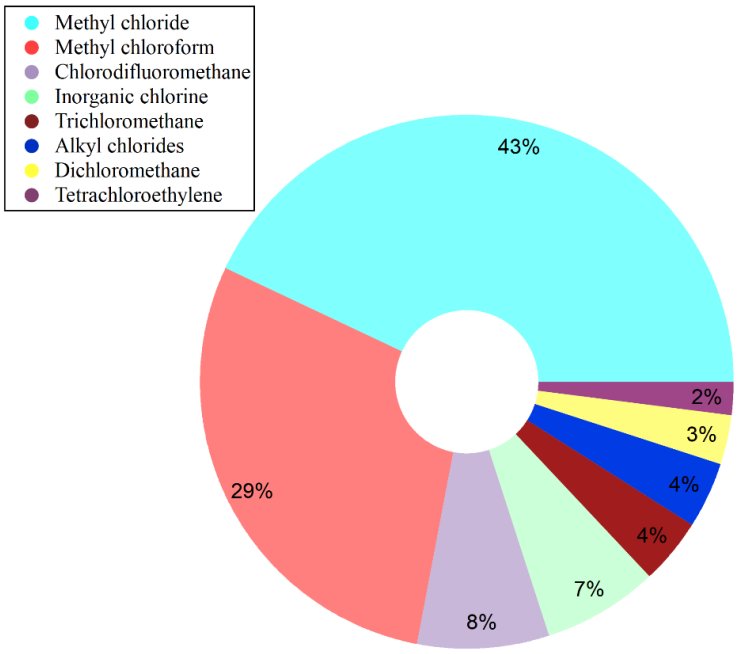

Figure 1-1. Typical speciation of Cl_y (percent). Data taken from Khalil et. al., (1999).[35]

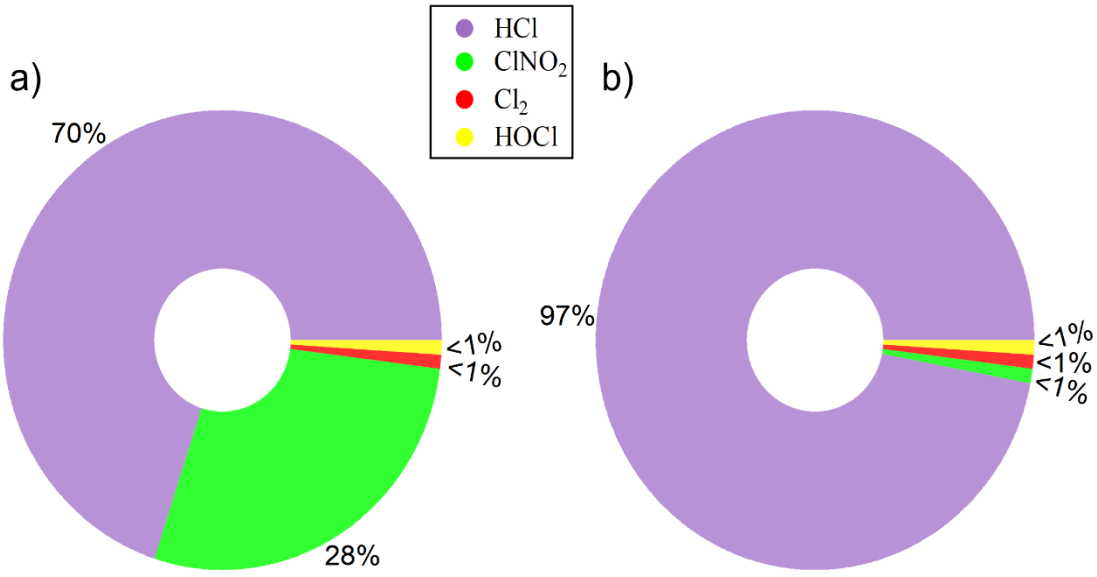

Figure 1-2. Inorganic Cl_y percent contribution for a coastal area during the wintertime for a) nighttime and b) daytime. Data taken from Haskins et. al., (2018).[38]

Photolysis of Cl_y is the most common pathway to form Cl, doing so changes the oxidative chemistry of the troposphere. Oxidation initiated with Cl yields more O_3 than oxidation initiated with OH.[2] Reasons for this are not fully understood, but the implications for mechanisms of

oxidation chemistry are significant.[2,39] Cl atoms have not been directly measured to date in the atmosphere. Instead, their abundance has been inferred through steady-state approximations from all known formation and loss processes. Levels of Cl vary from region to region but are estimated to be 0.5×10^{3}–7.6×10^{4} atoms cm^{-3}.[2,40–42]

1.3 Sources of Cl_y

1.3.1 Direct emissions

Direct emissions of organic and inorganic Cl_y are derived mainly from natural sources (~90%), such as the ocean, terrestrial (soil, wetlands, etc.), biomass burning, volcanic activity, anthropogenic pollution (Figure 1-3). Oceanic emissions is the largest contributor, accounting for ~80 % by mass emitted per year.[34,35] There are many reasons why the amount of chlorinated organics is high in the ocean which leads to their significant emissions to the atmosphere. The sources of chlorinated species to the ocean includes, but is not limited to, atmospheric deposition, sediment leaching, biodegradation and metabolic waste of ocean life, direct pollution, and polluted runoff from estuaries.[34,35,37] The contribution of individual sources is not quantified and difficult to deconvolute. At best, each region can be modelled, but this is very challenging due to the changing variables and constraints. There are two mechanisms for ocean derived emission of organic Cl_y. The first is straightforward partitioning of volatile and semi-volatile organics from the organic-rich SML. Individual compound partitioning depends on the Henry's law coefficient (H) and concentration in the SML (H range for most organic Cl_y is 1.1×10^{-4}–5.9×10^{-3} Pa mol m^{-3}).[43] The second mechanism for ocean emissions is classified as more physical rather than a chemical process and is due to emission of SSAs. Organic-rich SSAs can, in some circumstances, evaporate and emit their compounds into the atmosphere, via induced partitioning.

The second most prominent contribution to direct emissions is by terrestrial geocycling.[35] Although these emissions are the second largest, they are poorly understood. The theorized contributions to terrestrial emissions are due to volatilization from plant life and biological activity in soil. Cl_y emitted into the atmosphere from combustion processes (i.e., biomass burning, and volcanic activity) is almost solely in the form of HCl, and to a lesser extent, Cl_2. Anthropogenic emission of Cl_y is dominated by the coal burning industry and incineration of chlorinated waste.[15,36] Under stable Cl_y levels in the stratosphere, the transfer rate from the stratosphere to the troposphere was calculated in 1993 to be 0.03 Tg Cl yr^{-1}.[44,45] A recent study suggests that Cl_y levels are increasing in the stratosphere. The calculated mean growth rate for stratospheric Cl_y is 3.7 ppt Cl yr^{-1}.[46] Direct emissions are more challenging to predict and model, yet these emission fluxes control the majority of Cl_y inventory.

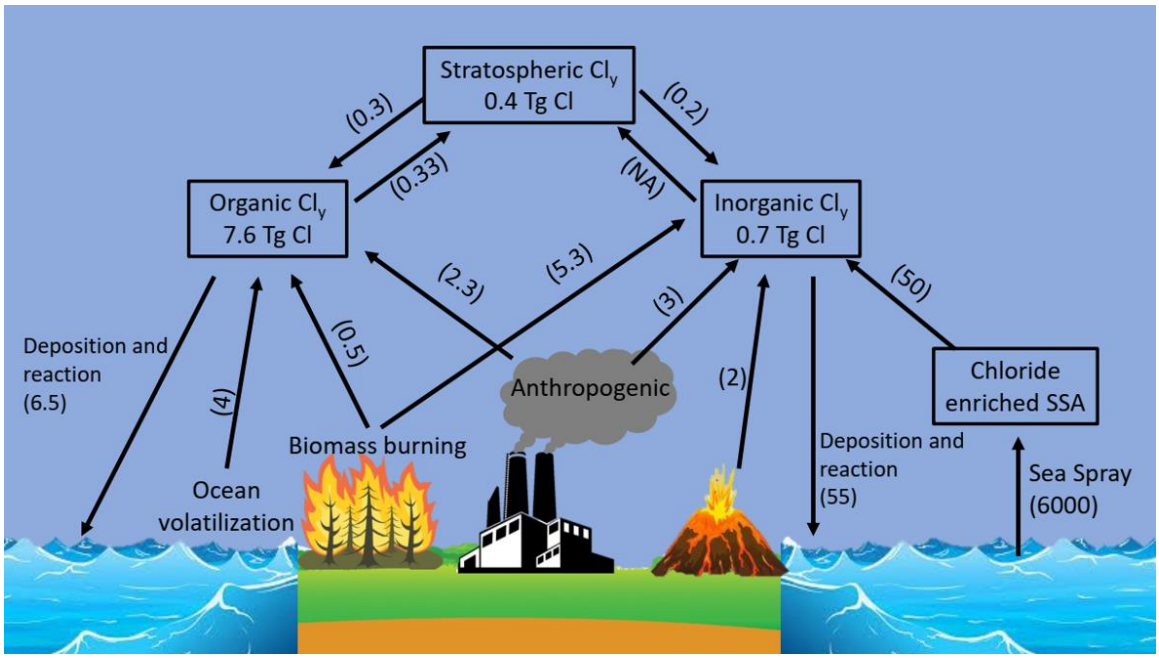

Figure 1-3. Total chlorine inventory for natural and anthropogenic sources. Numbers in brackets are in Tg Cl yr^{-1}. Data taken from Khalil et al., (1999), Keene et al., (1999), Graedel et al., (1995), Graedel et al., (1996), and Lobert et al., (1999).[34–37,45]

1.3.2 Indirect formation via chlorine activation

Mobilization of Cl^- in SSA has been a key reactive pathway for transforming unreactive aqueous Cl^- into Cl_y; these transformations are known as chlorine activation. There are three known major pathways for chlorine activation (Figure 1-4); HCl production via acid displacement,[47–52] formation of Cl_y (e.g., $ClNO_2$) from reactive dinitrogen pentoxide (N_2O_5) uptake in aqueous aerosols,[53–59] and molecular chlorine volatilization from SSA influenced by the photolysis of O_3.[60]

Acid displacement reactions occur when both the produced gas has a lower proton affinity, and the formation energy of the new salt is greater than the reactants (R3.1).[48]

$$HX + MCl\ (s\ or\ aq) \rightarrow MX\ (s\ or\ aq) + HCl\ (g) \qquad \text{R1.3.1}$$

Where M is any generic cation pair for the salt (e.g., Na^+) and HX is a strong acid. Due to the abundance of Cl^- in SSA, the factor limiting the rate of HCl production from acid displacement is the presence of gaseous strong acids in the MBL. The most common atmospheric gases that displace surface Cl^- are nitric acid (HNO_3) and sulfuric acid (H_2SO_4):

$$HNO_3\ (g) + MCl\ (s\ or\ aq) \rightarrow MNO_3\ (s\ or\ aq) + HCl\ (g) \qquad \text{R1.3.2}$$

$$H_2SO_4\ (g) + MCl\ (s\ or\ aq) \rightarrow MHSO_4\ (s\ or\ aq) + HCl\ (g) \qquad \text{R1.3.3}$$

When continental urban pollution mixes with SSA, HNO_3 mixing ratios dictates HCl acid displacement production.[50,53] In regions with large emissions of natural and anthropogenic sulfur dioxide (SO_2), the precursor compound for H_2SO_4, acid displacement production of HCl is dictated by H_2SO_4 mixing ratios.[34,61,62] Acid displacement reactions are exclusively modelled as a function of gaseous [H_2SO_4] and [HNO_3]. These reactions have been shown to occur when other weak organic acids are present, representing a potential negative bias in modelled HCl levels in regions with high organic acid concentrations.[63]

Urban NO_x pollution is closely tied to the chemistry of chlorine activation (Figure 1-4).[13,52,55,64,65] N_2O_5 is a night time reservoir for NO_x, and it is produced from reaction between NO_2 and nitrate radical (NO_3, R3.2 – 3.4).[53,54,66] Reactive uptake of N_2O_5 into Cl^- containing aqueous aerosols is known to yield $ClNO_2$ (R3.5).[53] A higher yield of $ClNO_2$, and in some cases, Cl_2 is observed under low pH and high $[Cl^-]$.[58] Due to competing reactions with other halides, it is noted that more information on solvated HCl is vital to understand the constraints on the reactive uptake coefficient (γ) for N_2O_5.[54,58,59,67–69] Notable variables on reactive uptake coefficient include relative humidity,[47] aerosol composition,[65] and a high nitrate concentration in aerosols inhibits uptake by 1 order of magnitude (R3.6).[54,65,70] Conversion of N_2O_5 to HNO_3 is a major night-time NO_x loss mechanism.[53,54] The reactive uptake suppression by nitrate is negated by a small presence of Cl^- due to competing reactions with N_2O_5 ionization product NO_2^+.[65,68] In areas where NO_x is present in appreciable amounts the major nighttime Cl reservoir species is $ClNO_2$.

$$NO\,(g) + O_3\,(g) \rightarrow NO_2\,(g) + O_2\,(g) \qquad \text{R1.3.4}$$

$$NO_2\,(g) + O_3\,(g) \rightarrow NO_3\,(g) + O_2\,(g) \qquad \text{R1.3.5}$$

$$NO_2\,(g) + NO_3\,(g) \rightleftharpoons N_2O_5\,(g) \qquad \text{R1.3.6}$$

$$N_2O_5\,(g) + Cl^-\,(aq) + H^+\,(aq) \rightarrow ClNO_2\,(g) + HNO_3\,(aq) \qquad \text{R1.3.7}$$

$$N_2O_5\,(g) + H_2O\,(l) \rightarrow 2HNO_3\,(aq) \qquad \text{R1.3.8}$$

Finally, the Cl^- in SSA can react with O_3 to form OCl^-, and under acidic conditions HOCl and Cl_2 are emitted.[71–73] This form of activation is very slow and is not a significant source of global Cl_y. However, the reaction has been shown to occur on saline snow,[74] and is considered the dominant pathway in Arctic regions due to very low levels of NO_x. The reaction proceeds faster when light is present; the mechanism to support this is unknown. It is suggested that the O_3 is photolyzed first or that a reactive halogen intermediate requires ultraviolet (UV) irradiation.[71]

Understanding the chemistry of reservoir species of Cl is essential in determining Cl levels accurately. The dominant daytime reservoir for Cl in the troposphere is HCl. HCl can cycle back and forth by reactions with hydroxyl radicals and compounds with an available hydrogen.[75–79]

$Cl\ (g) + RH\ (g) \rightarrow HCl\ (g) + R\ (g)$ R1.3.9

$HCl\ (g) + OH\ (g) \rightarrow Cl\ (g) + H_2O\ (g)$ R1.3.10

The balance between loss and formation processes of chlorine atoms from HCl is highly dependent on many external factors, such as deposition rate and the presence of particulate Cl^- and NO_x. Cl_2 and $ClNO_2$ formation pathways are also dependent on Cl^- containing marine aerosols. Cl_2 can be emitted from the photolysis of O_3 in the presence of Cl^- aerosols.[71] $ClNO_2$ is formed in the presence of NO_x and Cl^- containing aqueous aerosols.[39,52,54,56,57] Both Cl_2 and $ClNO_2$ are photolabile nighttime reservoirs for Cl, which means Cl cycling depends on the available sunlight and precursor compounds. These processes are depicted in Figure 1-4.

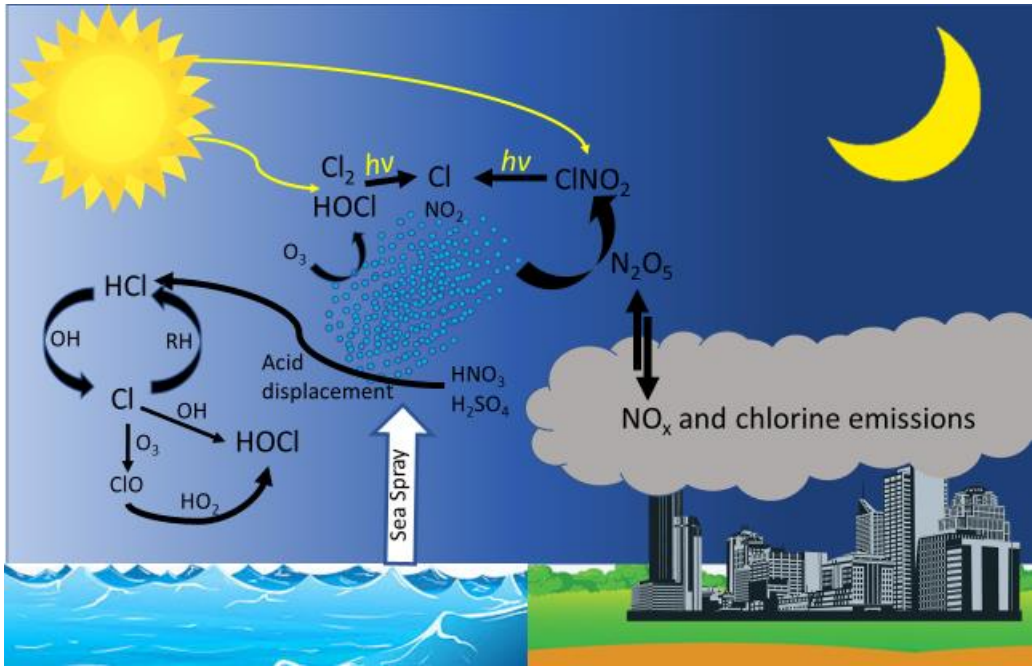

Figure 1-4. Primary Cl_y reactions for both day and nighttime chemistry.[71,80–83]

1.4 Sinks for Cl_y

1.4.1 Dry and wet deposition

The deposition of most Cl_y species have not been investigated explicitly and are estimated from the deposition of other species (e.g., HCl). One major exception is HCl, for which deposition is well understood. Global concentrations of HCl are inversely proportional to relative humidity. HCl is a polar gas that is very soluble in water, and susceptible to deposition to wet surfaces. The estimated dry deposition rate of HCl is 15 ± 5 Tg Cl yr^{-1}, calculated using an average mixing ratio of 200 pptv and mean deposition velocity of 1.0 cm s^{-1} and therefore, is a lower estimate as deposition velocities can be as high as 6 cm s^{-1}.[36] Other inorganic forms of Cl_y are much more photolabile, and their daytime deposition loss is unimportant with respect to their fast chemical sinks. Organic Cl_y is less soluble than HCl and its dry and wet deposition is estimated to be small enough to not be a major sink.[36]

1.4.2 Reactions of Cl_y

Currently, with the information we have on both organic and inorganic Cl_y reaction pathways, ascertaining the contribution each has on the total global Cl production is difficult to gauge accurately. Organic Cl_y emissions are much greater than inorganic and could, therefore, dominate Cl atom production, but reaction rates tend to be relatively slow. The lifetimes for two dominant organochlorines methyl chloride and dichloromethane are 573 and 109 days, respectively (Table 1-1).[42] The major loss mechanism for organic Cl_y is oxidation with OH. In a model study by Hossaini et al., (2016) chlorocarbon oxidation was calculated to yield a tropospheric Cl_y source of ~4320 Gg Cl/yr, which gives a [Cl] background of 0.5×10^3 atoms cm^{-3}.[42] These estimates are based on a 1999 Cl_y inventory study, and therefore require more modern measurements to assess current chlorine chemistry.[34]

Table 1-1. Lifetimes of common organic Cl_y in the troposphere with respect to OH and photolysis. Data taken from Hossaini et al.,(2016).[42]

Chlorocarbon	Formula	Lifetime (Days)
Methyl chloride	CH_3Cl	573
Chloroform	$CHCl_3$	112
Dichloromethane	CH_2Cl_2	109
Bromochloromethane	CH_2BrCl	103
Tetrachloroethene	C_2Cl_4	67
1,2-Dichloroethane	CH_2ClCH_2Cl	47
Bromodichloromethane	$CHBrCl_2$	41
Dibromochloromethane	$CHBr_2Cl$	32
Trichloroethene	C_2HCl_3	5
Chloroiodomethane	CH_2ICl	0.1

Inorganic Cl_y can be more complex, due to the cyclicity, meaning the resulting Cl atom produced reacts to reform precursor compounds. The major loss mechanism for inorganic Cl_y is photolysis. The dominant photolabile inorganic Cl_y depends on the region. Cl_2 is a relatively unimportant Cl reservoir and is readily lost via photolysis. Cl_2 has the highest photolysis rate constant compared to other inorganic photolabile Cl_y (Figure 1-5). Measurements have been made in coastal regions with a mixing ratio maximum of 35 pptv.[73,84] While Cl_2 mixing ratios are highest at night, without more information on the nighttime source and sink chemistry of Cl_2 it is tentatively classified as a nighttime reservoir. When considering the chemistry of Cl_2 we must talk about HOCl, the two most intertwined Cl_y cycles (R1.4.2). Due to the different and sometimes convoluted mechanisms involved in the formation of these Cl_y species, it is difficult

to approximate the amount of Cl released. While HOCl is very photolabile, it readily reacts on acidic chloride containing heterogenous surfaces to form Cl_2; via reactions R4.1 and R1.4.2.[72,73,85]

$HOCl\,(g) \rightleftharpoons HOCl\,(aq)$ R1.4.1

$HOCl\,(aq) + Cl^-\,(aq) + H^+\,(aq) \rightleftharpoons Cl_2\,(aq) + H_2O\,(l)$ R1.4.2

$Cl_2\,(aq) \rightleftharpoons Cl_2\,(g)$ R1.4.3

$Cl_2\,(g) + h\nu \rightarrow 2Cl\,(g)$ R1.4.4

$HOCl\,(g) + h\nu \rightleftharpoons Cl\,(g) + OH\,(g)$ R1.4.5

Photolysis of $ClNO_2$ (R1.4.6) in the morning has been shown to be the primary early morning radical source in polluted coastal cities.[2] The lifetime of $ClNO_2$ is <1 hour during the day and as long as 31 hours under sustained low light conditions.[86] The photolysis rate is comparable to HOCl and less than Cl_2, yet the abundance of $ClNO_2$ is typically greater and, therefore, it contributes more to Cl production (Figure 1-5). As a minor loss mechanism, $ClNO_2$ has also been observed to react on Cl^- containing aerosols to form Cl_2 via R1.4.7.[53] $ClNO_2$ formation has significant impacts on Cl and NO_x budgets, and both play key roles in the overall oxidative capacity of the troposphere. In some regions in the polluted MBL photolysis of $ClNO_2$ is considered the largest source of Cl at sunrise.[2,57,87]

$ClNO_2\,(g) + h\nu \rightarrow Cl\,(g) + NO_2\,(g)$ R1.4.6

$ClNO_2\,(g) + Cl^-\,(aq) \rightarrow Cl_2\,(g) + NO_2^-\,(g)$ R1.4.7

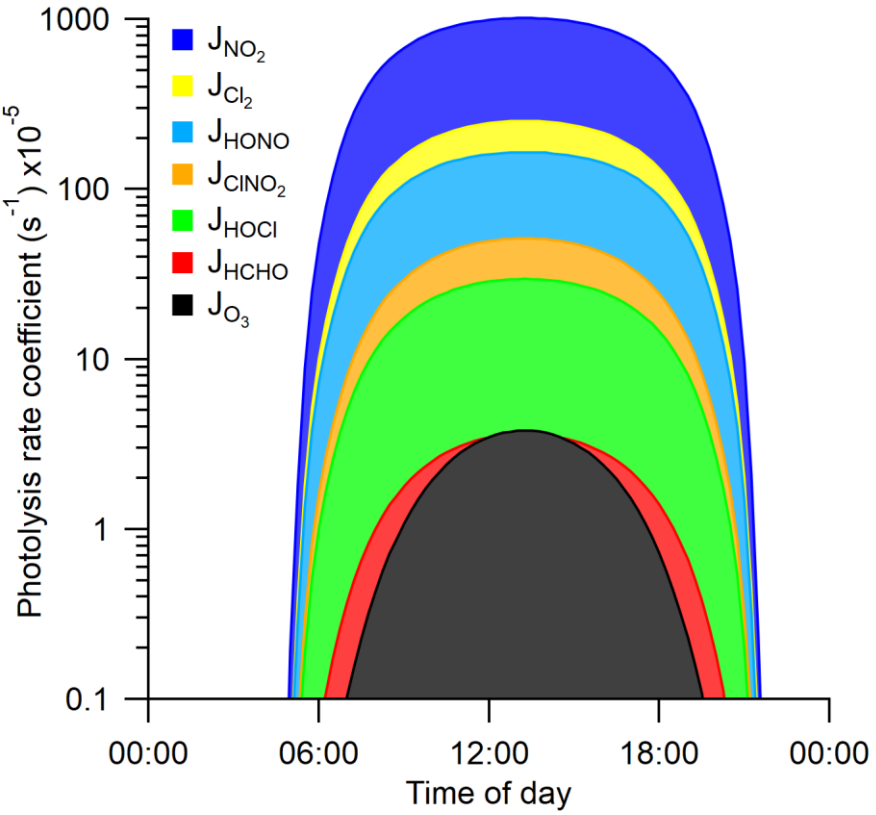

Figure 1-5. Lognormal photolysis rate coefficients over a given day for inorganic Cl_y and select common photolabile species. Rate coefficients calculated using the national center for atmospheric research (NCAR) tropospheric ultraviolet and visible (TUV) radiation model-version 5.3. Rate coefficients were determined using default conditions for June 18, 2019, in Halifax, Nova Scotia, Canada (44°37'55.8"N, 63°34'48.4"W).

Reactions involving chlorine monoxide (ClO) can easily be overlooked when discussing the total chlorine inventory in the troposphere. This is in part due to the fact it is more of an intermediate species that reacts very fast, making it very difficult to measure and accurately access its contributions to the total inventory. ClO_x (Cl+ClO) cycling is more notoriously attributed to the catalytic destruction of ozone in the stratosphere,[10] particularly in the Arctic where there are little to no competing reactive sinks for ClO.[88] Reaction rates and kinetics data on ClO is essential for properly modelling Cl_y rather than routine inventory measurements. ClO in the troposphere is formed primarily through (R1.4.8), and lost via (R1.4.9), and (R1.4.10). Under high NO_x conditions, reactions (R1.4.11) and (R1.4.14) can yield chlorine nitrate

($ClONO_2$) and $ClNO_2$, respectively, and these products will build up overnight and lost to photolysis in the morning.[53,88]

$Cl\,(g) + O_3\,(g) \rightarrow ClO\,(g) + O_2\,(g)$ R1.4.8

$ClO\,(g) + OH\,(g) \rightarrow Cl\,(g) + HO_2\,(g)$ R1.4.9

$ClO\,(g) + HO_2\,(g) \rightarrow HOCl\,(g) + O_2\,(g)$ R1.4.10

$ClO\,(g) + NO_2\,(g) \rightarrow ClONO_2\,(g)$ R1.4.11

$ClONO_2\,(g) + hv \rightarrow ClO\,(g) + NO_2\,(g)$ R1.4.12

$ClONO_2\,(g) + hv \rightarrow Cl\,(g) + NO_3\,(g)$ R1.4.13

$ClO\,(g) + NO\,(g) \rightarrow Cl\,(g) + NO_2\,(g)$ R1.4.14

When considering the chemistry of Cl_y, it is crucial to consider the contribution HCl has on the overall chlorine inventory. Unless we have a grasp on the all the sources and sinks for HCl, we can not properly access the total chlorine inventory. In the troposphere HCl is the only daytime reservoir for Cl. While HCl is primarily lost by dry/wet deposition it can be lost to oxidation by OH (R1.3.10), but will likely be immediately reformed again in R1.3.9.[35,42,78] The chemistry of HCl formation and its importance as not only the dominant daytime Cl reservoir but also in estimating daily chlorine production is explored further in Chapter 4.

1.5 Global implications

1.5.1 Measurements of Cl_y

Current measurements techniques are continually being developed to assess Cl_y species. There is currently no literature precedent for measuring total Cl_y using just one method, and therefore, many different approaches are needed to understand the total tropospheric chlorine budget. Organochlorines are usually analyzed directly from collected ambient air samples by gas chromatography, sometimes collected on polyurethane foam first and extracted before

analysis.[89–92] Current literature focuses primarily on improving online techniques of the relatively more reactive inorganic Cl_y such as $ClNO_2$, Cl_2, HOCl, and HCl. The species that has been measured the most, by far, is HCl. The classic or "gold standard" approach to measuring HCl is by scrubbing ambient air with a denuder (or similar diffusion scrubber) and analyzing the extract by ion chromatography.[93–99] The denuder is a diffusion based technique, wherein a laminar sample stream passes over a coated substrate (alkaline coating for acidic gases) and the collisions due to diffusivity onto the substrate result in an effective scrubbing of the desired gases. These samples are collected over hours to days, depending on the expected baseline mixing ratio and the sensitivity of the extract analyzing instrument. The mean data is reported over that integrated timeframe resulting in a major loss of temporal trends. Another typical method to measure HCl is by using a tandem mist chamber whose extracts are similarly analyzed by ion chromatography.[100–108] The time resolution of HCl measurements is typically 2 hours, which is better than denuder based methods but still not fast enough to capture fast processes. Tandem mist chambers are also capable of measuring Cl_2 and HOCl (presumably also ClO, Cl, $ClNO_2$, $ClNO_3$, and BrCl) when an alkaline mist solution is adopted, but it is not able to speciate between inorganic chlorines and these studies report total inorganic chlorine minus HCl.[100,102,103]

1.5.2 Cl initiated reactions and impacts on O_3 and OH

Reactions involving Cl in the troposphere have been largely underestimated since it was first seriously considered by Finlayson-Pitts et al., in the 1990s.[11] Currently, our best method for estimating the concentration of Cl atoms for a region is by steady-state approximation, and to do that we need an understanding Cl reactivity with all types of volatile organic compounds (VOCs). It is generally understood in the literature that Cl atoms are much more reactive than OH, usually 2 orders of magnitude higher in reactivity depending on the VOC mixture.[40,109] The

chemistry of Cl reactivity is very different from OH; studies have shown that each radical has a very different reactivity profile.[2] When compared with OH, Cl tends to be more reactive to more long-lived VOC species such as alkanes, and much less reactive towards NO_x. Cl almost exclusively reacts via hydrogen abstraction, forming HCl in the process. Despite the higher reactivity of Cl relative to OH, secondary radical formation from reactions initiated by either OH or Cl results predominately in OH formation. This highlights a considerable challenge when determining primary radical contributions due to the similar end products, as VOC tracer ratios was not shown to accurately reflect the impact of Cl initiated oxidation.[2] The obscured impact of Cl oxidation is due to the secondary OH produced from the Cl initiated reactions. Oxidative capacity of the troposphere is therefore determined by the ratio of OH/Cl and the VOC profile.

Table 1-2. Reaction rate ranges for common VOC classes. Determined at 295–298 K. Data taken from Young et al., 2014, and JPL 2020.[2,109]

Compound class	OH Rate constant range ($cm^3\ molec^{-1}\ s^{-1}$)	Cl Rate constant range ($cm^3\ molec^{-1}\ s^{-1}$)
Alkanes	$6.3*10^{-15} – 1.1*10^{-11}$	$1.0*10^{-13} – 1.4*10^{-10}$
Alkenes	$7.02*10^{-12} – 1.1*10^{-11}$	$1.11*10^{-10} – 4.2*10^{-10}$
Alcohols	$9..1*10^{-13} – 5.5*10^{-12}$	$5.5*10^{-11} – 1.0*10^{-10}$
Aldehydes	$8.5*10^{-12} – 2.4*10^{-11}$	$3.8*10^{-11} – 1.38*10^{-10}$
Aromatics	$7.21*10^{-13} – 5.24*10^{-11}$	$1.0*10^{-15} – 3.6*10^{-10}$
Acids	$1.54*10^{-13} – 4.5*10^{-12}$	$<2*10^{-16} – 2.0*10^{-13}$
Biogenics	$2.0*10^{-11} – 1.61*10^{-10}$	$2.2*10^{-10} – 6.4*10^{-10}$
Ketones	$2.48*10^{-13} – 1.1*10^{-12}$	$5.27*10^{-13} – 4.0*10^{-11}$

Methane removal in the atmosphere by hydrogen-abstraction from Cl is largest sink for Cl atoms and considered the biggest impact Cl has on the greenhouse effect.[78,80,81,110,111] Some studies have used the isotopic ratio of methane $^{13}C/^{12}C$ depletion to approximate Cl concentrations. The kinetic isotope effect of Cl yields a higher increase in the $^{13}C/^{12}C$ fraction when compared to OH, from this data Cl oxidation is responsible for 1.4–3.8% of the total

methane sink.[110,111] Other VOC oxidations initiated by Cl have only been modelled to date, accounting for 20%, 14%, 10%, and 4% of the global losses of ethane (C_2H_6), propane (C_3H_8), higher alkanes, and methanol (CH_3OH) respectively.[78] Cl atoms can also affect the oxidation cycling for alkyl sulfides, yielding primarily HCl, SO_2, acetaldehyde (CH_3CHO), and formaldehyde (HCHO) products.[112–114] The impact of enhanced reactivity of Cl on the global sulfur cycle has not been extensively studied, but suspected to be significant in the MBL during sunrise when Cl levels are the highest.[112]

1.5.3 Current questions in the sources and chemistry of Cl_y

Recent work on Cl_y has been focusing on wintertime chlorine activation, the impacts on indoor air quality, and improving chlorine chemistry models.[38,115–119] Currently, parameters on wintertime modelling of Cl_y has not been accurately accessed due to a lack of wintertime ambient measurements. There are many theorized sources of Cl_y during the wintertime, such as an increase in controlled biomass/coal burning for heat and an increase in automobile use to avoid harsh weather conditions.[38,84,120,121] The increase in biomass/coal burning will have a direct impact on Cl_y emissions in the form of emitted HCl and Cl_2.[122] Automobile use is a major NO_x emission source for urban areas and (as discussed in Section 1.2.2) will have an indirect contribution on Cl_y emissions in the form of emitted $ClNO_2$ and HCl.[38,121] Vehicles are also a suggested direct source for chlorinated VOCs, emissions that can sustain low levels (<20ppt) of daytime Cl_2 and HOCl.[121] There is also a noticeable enhancement in Cl^- in regions affected by harsh icy conditions, this is due to the practice of salting icy roads for safer driving.[120] Evidence from Wintertime Investigation of Transport, Emissions, and Reactivity (WINTER) aircraft campaign has shown that inorganic tropospheric Cl_y is dominated by HCl.[38] High mixing ratios of HCl, in this case, are the products of biomass/coal burning inland, and a greater number of

acid displacement reactions due to elevated NO_x and Cl^- over both land and sea.[38] Another emerging area of Cl_y research is indoor air quality/chemistry. Known Cl_y species Cl_2, HOCl, $ClNO_2$ emissions have been observed to evolve from everyday cleaning activities, including cleaning with chlorine bleach.[123] When these chlorine-containing cleaning supplies mix with other ammoniated cleaners, harmful chloramines will be emitted.[123] Gaseous HOCl in indoor air can also undergo interesting chlorinating chemistry with unsaturated oils on indoor surfaces, including skin oils, cooking oils, dust, etc.[124] HCl has also been observed to be emitted from common household activities, such as cooking and cleaning.[117] The impacts of high levels of Cl_y has on indoor air quality have not been accessed. Because the emissions of indoor Cl_y is activity-based it is difficult to impose the emissions of one household onto another without a high degree of uncertainty. It is unclear whether Cl_y is transferred from indoor into outdoor environments and, if so, whether it acts as a significant source of urban Cl_y pollution. All current studies agree that more ambient measurements of not only Cl_y, but all the parameters that affect its chemistry are required to model Cl_y fluxes and the impacts on climate properly. Cl_y modelling studies are a powerful resource to better understanding chlorine chemistry on a global scale, but are limited in that they need more measurements that help reflect different regions.[42,78,125] A recent study by Zhai et. al., (2021), estimated that an increase of up to 170% of total Cl_y can be attributed to anthropogenic sources.[125] It must be mentioned that not all local sources and emissions can be captured in a global model, and in our group we have found that modelled HCl can be underestimated by up to 3 orders of magnitude in continental regions where local emissions can mask the effects of modelled chemical sources.[126]

1.6 Thesis Objectives

The main goal of this work is to better understand tropospheric Cl_y through three objectives: (1) Validating a new spectroscopic instrument for HCl; (2) Applying quality HCl measurements to elucidate chlorine chemistry trends in an urban MBL; and (3) Developing novel instrumentation to measure total reactive chlorine. This will be accomplished in three milestones that address each of the goals in Chapters 3–5 of this thesis, respectively. A necessity underlying Cl_y work is the generation of accurate, stable standards through permeation devices, which will be described in Chapter 2. The first Cl_y milestone (Chapter 3) combined multiple approaches to validate a new commercial cavity ring-down spectroscopy (CRDS) HCl analyzer for ambient measurements of HCl. This was achieved through lab generated HCl gas and an ambient intercomparison with annular denuder extracts analysed by ion chromatography. The instrument performance of the CRDS was further compared to other HCl measurement techniques and the response time of the instrument was characterized. The second Cl_y milestone (Chapter 4) describes CRDS-measured HCl during the Halifax Fog and Air Quality Study (HaliFAQS). Using HCl and supporting measurements, the sources of HCl were assessed. Trends observed in the diurnal HCl were used to develop an irradiance-dependent model to estimate $ClNO_2$ mixing ratios and compare its production of Cl to primary sources of OH. The final Cl_y objective (Chapter 5) was to develop a novel total chlorine measurement. This was achieved using a high-temperature platinum catalyzed flow tube capable of combusting chlorine species transforming them into HCl that can be easily and accurately measured using the CRDS.

1.7 References

(1) Seinfeld, J. H.; Pandis, S. N. Atmospheric Chemistry and Physics : From Air Pollution to Climate Change. 2016.

(2) Young, C. J.; Washenfelder, R. A.; Edwards, P. M.; Parrish, D. D.; Gilman, J. B.; Kuster, W. C.; Mielke, L. H.; Osthoff, H. D.; Tsai, C.; Pikelnaya, O.; et al. Chlorine as a Primary Radical: Evaluation of Methods to Understand Its Role in Initiation of Oxidative Cycles. *Atmos. Chem. Phys.* **2014**, *14* (7), 3427–3440. https://doi.org/10.5194/acp-14-3427-2014.

(3) Hartley, W. N. XXI.—On the Absorption of Solar Rays by Atmospheric Ozone. *J. Chem. Soc. Trans.* **1881**, *39*, 111–128.

(4) Chapman, S. A Theory of Upperatmospheric Ozone. *Mem. Roy. Meteor.* **1930**, *3*, 103–125.

(5) Bates, D. R.; Nicolet, M. The Photochemistry of Atmospheric Water Vapor. *J. Geophys. Res.* **1950**, *55* (3), 301–327.

(6) Crutzen, P. J. The Influence of Nitrogen Oxides on the Atmospheric Ozone Content. *Q. J. R. Meteorol. Soc.* **1970**, *96* (408), 320–325.

(7) Farman, J. C.; Gardiner, B. G.; Shanklin, J. D. Large Losses of Total Ozone in Antarctica Reveal Seasonal ClOx/NOx Interaction. *Nature* **1985**, *315* (6016), 207–210. https://doi.org/10.1038/315207a0.

(8) Solomon, S.; Garcia, R. R.; Rowland, F. S.; Wuebbles, D. J. On the Depletion of Antarctic Ozone. *Nature* **1986**, *321* (6072), 755–758.

(9) Stolarski, R. S.; Cicerone, R. J. Stratospheric Chlorine: A Possible Sink for Ozone. *Can. J.*

Chem. **1974**, *52* (8), 1610–1615.

(10) Molina, M. J.; Rowland, F. S. Stratospheric Sink for Chlorofluoromethanes: Chlorine Atom-Catalysed Destruction of Ozone. *Nature* **1974**, *249* (5460), 810–812. https://doi.org/10.1038/249810a0.

(11) Finlayson-Pitts, B. J. Chlorine Atoms as a Potential Tropospheric Oxidant in the Marine Boundary Layer. *Res. Chem. Intermed.* **1993**, *19* (3), 235–249. https://doi.org/10.1163/156856793X00091.

(12) Tanaka, P. L.; Oldfield, S.; Neece, J. D.; Mullins, C. B.; Allen, D. T. Anthropogenic Sources of Chlorine and Ozone Formation in Urban Atmospheres. *Environ. Sci. Technol.* **2000**, *34* (21), 4470–4473. https://doi.org/10.1021/es991380v.

(13) Faxon, C. B.; Allen, D. T. Chlorine Chemistry in Urban Atmospheres: A Review. *Environ. Chem.* **2013**, *10* (3), 221–233. https://doi.org/10.1071/EN13026.

(14) Tanaka, P. L.; Riemer, D. D.; Chang, S.; Yarwood, G.; McDonald-Buller, E. C.; Apel, E. C.; Orlando, J. J.; Silva, P. J.; Jimenez, J. L.; Canagaratna, M. R.; et al. Direct Evidence for Chlorine-Enhanced Urban Ozone Formation in Houston, Texas. *Atmos. Environ.* **2003**, *37* (9), 1393–1400. https://doi.org/https://doi.org/10.1016/S1352-2310(02)01007-5.

(15) Liu, Y.; Fan, Q.; Chen, X.; Zhao, J.; Ling, Z.; Hong, Y.; Li, W.; Chen, X.; Wang, M.; Wei, X. Modeling the Impact of Chlorine Emissions from Coal Combustion and Prescribed Waste Incineration on Tropospheric Ozone Formation in China. *Atmos. Chem. Phys.* **2018**, *18* (4), 2709–2724. https://doi.org/10.5194/acp-18-2709-2018.

(16) O'Dowd, C. D.; De Leeuw, G. Marine Aerosol Production: A Review of the Current

Knowledge. *Philos. Trans. R. Soc. A Math. Phys. Eng. Sci.* **2007**, *365* (1856), 1753–1774. https://doi.org/10.1098/rsta.2007.2043\n10.1038/17508; Allan, B.J., Plane, J.M.C., McFiggans, G., Observations of 010 in the remote marine boundary layer (2001) Geophys. Res. Lett, 28, pp. 1945-1948. , doi:10.1029/2000GL012468; Andreas, E. L. 1998 A new sea spray generation function for wind speeds up to 32 m s-1. J. Phys. Oceanogr. 28, 2175-2184. (doi:10.1175/1520-0485(1998)028〈2175:ANSSGF〉2.0.CO;2)Andreas, E.L., A review of the sea spray generation function for the open ocean (2002) Atmosphere-ocean interacti.

(17) O'Dowd, C. D.; Facchini, M. C.; Cavalli, F.; Ceburnis, D.; Mircea, M.; Decesari, S.; Fuzzi, S.; Yoon, Y. J.; Putaud, J.-P. Biogenically Driven Organic Contribution to Marine Aerosol. *Nature* **2004**, *431* (7009), 676–680. https://doi.org/10.1038/nature02959.

(18) Vogel, A. L.; Schneider, J.; Müller-Tautges, C.; Phillips, G. J.; Pöhlker, M. L.; Rose, D.; Zuth, C.; Makkonen, U.; Hakola, H.; Crowley, J. N.; et al. Aerosol Chemistry Resolved by Mass Spectrometry: Linking Field Measurements of Cloud Condensation Nuclei Activity to Organic Aerosol Composition. *Environ. Sci. Technol.* **2016**. https://doi.org/10.1021/acs.est.6b01675.

(19) Taylor, J. W.; Choularton, T. W.; Blyth, A. M.; Flynn, M. J.; Williams, P. I.; Young, G.; Bower, K. N.; Crosier, J.; Gallagher, M. W.; Dorsey, J. R.; et al. Aerosol Measurements during COPE: Composition, Size and Sources of CCN and IN at the Interface between Marine and Terrestrial Influences. *Atmos. Chem. Phys. Discuss.* **2016**, No. February, 1–39. https://doi.org/10.5194/acp-2016-84.

(20) Abbey, D. E.; Ostro, B. E.; Petersen, F.; Burchette, R. J. Chronic Respiratory Symptoms

Associated with Estimated Long-Term Ambient Concentrations of Fine Particulates Less than 2.5 Microns in Aerodynamic Diameter (PM2.5) and Other Air Pollutants. *J. Expo. Anal. Environ. Epidemiol.* **1995**, *5* (2), 137–159.

(21) Wood, R.; Wyant, M.; Bretherton, C. S.; Rémillard, J.; Kollias, P.; Fletcher, J.; Stemmler, J.; De Szoeke, S.; Yuter, S.; Miller, M.; et al. Clouds, Aerosols, and Precipitation in the Marine Boundary Layer: An Arm Mobile Facility Deployment. *Bull. Am. Meteorol. Soc.* **2015**, *96* (3), 419–439. https://doi.org/10.1175/BAMS-D-13-00180.1.

(22) Satheesh, S. K.; Krishna Moorthy, K. Radiative Effects of Natural Aerosols: A Review. *Atmos. Environ.* **2005**, *39* (11), 2089–2110. https://doi.org/10.1016/j.atmosenv.2004.12.029.

(23) Haywood, J.; Boucher, O. Estimates of the Direct and Indirect Radiative Forcing Due to Tropospheric Aerosols: A Review. *Rev. Geophys.* **2000**, *38* (4), 513–543. https://doi.org/10.1029/1999RG000078.

(24) Whitby, K. .; Husar, R. .; Liu, B. Y. . The Aerosol Size Distribution of Los Angeles Smog. *J. Colloid Interface Sci.* **1972**, *39* (1), 177–204. https://doi.org/10.1016/0021-9797(72)90153-1.

(25) Hodshire, A. L.; Lawler, M. J.; Zhao, J.; Ortega, J.; Jen, C.; Yli-Juuti, T.; Brewer, J. F.; Kodros, J. K.; Barsanti, K. C.; Hanson, D. R.; et al. Multiple New-Particle Growth Pathways Observed at the US DOE Southern Great Plains Field Site. *Atmos. Chem. Phys.* **2016**, *16* (14), 9321–9348. https://doi.org/10.5194/acp-16-9321-2016.

(26) Walker, R. Marine Aerosol Chemistry. **2016**, 8306–8313. https://doi.org/10.1002/2016GL069070.Received.

(27) Fitzgerald, J. W. Marine Aerosols: A Review. *Atmos. Environ. Part A, Gen. Top.* **1991**, *25* (3–4), 533–545. https://doi.org/10.1016/0960-1686(91)90050-H.

(28) Fairall, C. W.; Larsen, S. E. Dry Deposition, Surface Production and Dynamics of Aerosols in the Marine Boundary Layer. *Atmos. Environ.* **1984**, *18* (1), 69–77. https://doi.org/10.1016/0004-6981(84)90229-4.

(29) Roberts, M. J.; Hewitt, H. T.; Hyder, P.; Ferreira, D.; Josey, S. A.; Mizielinski, M.; Shelly, A. Impact of Ocean Resolution on Coupled Air-sea Fluxes and Large-scale Climate. *Geophys. Res. Lett.* **2016**. https://doi.org/10.1002/2016GL070559.

(30) Wurl, O.; Wurl, E.; Miller, L.; Johnson, K.; Vagle, S. Formation and Global Distribution of Sea-Surface Microlayers. *Biogeosciences* **2011**, *8* (1), 121–135. https://doi.org/10.5194/bg-8-121-2011.

(31) Lee, C.; Sultana, C. M.; Collins, D. B.; Santander, M. V.; Axson, J. L.; Malfatti, F.; Cornwell, G. C.; Grandquist, J. R.; Deane, G. B.; Stokes, M. D.; et al. Advancing Model Systems for Fundamental Laboratory Studies of Sea Spray Aerosol Using the Microbial Loop. *J. Phys. Chem. A* **2015**, *119* (33), 8860–8870. https://doi.org/10.1021/acs.jpca.5b03488.

(32) Claeys, M.; Roberts, G.; Mallet, M.; Arndt, J.; Sellegri, K.; Sciare, J.; Wenger, J.; Sauvage, B. Optical, Physical and Chemical Properties of Aerosols Transported to a Coastal Site in the Western Mediterranean: Focus on Primary Marine Aerosols. *Atmos. Chem. Phys. Discuss.* **2016**, *1* (August), 1–42. https://doi.org/10.5194/acp-2016-602.

(33) Salter, M. E.; Hamacher-Barth, E.; Leck, C.; Werner, J.; Johnson, C. M.; Riipinen, I.; Nilsson, E. D.; Zieger, P. Calcium Enrichment in Sea Spray Aerosol Particles. *Geophys.*

Res. Lett. **2016**, *43* (15), 8277–8285. https://doi.org/10.1002/2016GL070275.

(34) Keene, W. C.; Khalil, M. A. K.; Erickson, D. J.; McCulloch, A.; Graedel, T. E.; Lobert, J. M.; Aucott, M. L.; Gong, S. L.; Harper, D. B.; Kleiman, G.; et al. Composite Global Emissions of Reactive Chlorine from Anthropogenic and Natural Sources: Reactive Chlorine Emissions Inventory. *J. Geophys. Res. Atmos.* **1999**, *104* (D7), 8429–8440. https://doi.org/10.1029/1998JD100084.

(35) Khalil, M. A. K.; Moore, R. M.; Harper, D. B.; Lobert, J. M.; Erickson, D. J.; Koropalov, V.; Sturges, W. T.; Keene, W. C. Natural Emissions of Chlorine-Containing Gases: Reactive Chlorine Emissions Inventory. *J. Geophys. Res. Atmos.* **1999**, *104* (D7), 8333–8346. https://doi.org/10.1029/1998JD100079.

(36) Graedel, T. E.; Keene, W. C. Tropospheric Budget of Reactive Chlorine. *Global Biogeochem. Cycles* **1995**, *9* (1), 47–77. https://doi.org/10.1029/94GB03103.

(37) Lobert, J. M.; Keene, W. C.; Logan, J. A.; Yevich, R. Global Chlorine Emissions from Biomass Burning: Reactive Chlorine Emissions Inventory. *J. Geophys. Res. Atmos.* **1999**, *104* (D7), 8373–8389. https://doi.org/10.1029/1998JD100077.

(38) Haskins, J. D.; Jaeglé, L.; Shah, V.; Lee, B. H.; Lopez-Hilfiker, F. D.; Campuzano-Jost, P.; Schroder, J. C.; Day, D. A.; Guo, H.; Sullivan, A. P.; et al. Wintertime Gas-Particle Partitioning and Speciation of Inorganic Chlorine in the Lower Troposphere Over the Northeast United States and Coastal Ocean. *J. Geophys. Res. Atmos.* **2018**, *123* (22), 12,812-897,916. https://doi.org/10.1029/2018JD028786.

(39) Osthoff, H. D.; Roberts, J. M.; Ravishankara, A. R.; Williams, E. J.; Lerner, B. M.; Sommariva, R.; Bates, T. S.; Coffman, D.; Quinn, P. K.; Dibb, J. E.; et al. High Levels of

Nitryl Chloride in the Polluted Subtropical Marine Boundary Layer. *Nat. Geosci* **2008**, *1* (5), 324–328.

(40) Knipping, E. M.; Dabdub, D. Impact of Chlorine Emissions from Sea-Salt Aerosol on Coastal Urban Ozone. *Environ. Sci. Technol.* **2003**, *37* (2), 275–284. https://doi.org/10.1021/es025793z.

(41) Riemer, D. D.; Apel, E. C.; Orlando, J. J.; Tyndall, G. S.; Brune, W. H.; Williams, E. J.; Lonneman, W. A.; Neece, J. D. Unique Isoprene Oxidation Products Demonstrate Chlorine Atom Chemistry Occurs in the Houston, Texas Urban Area. *J. Atmos. Chem.* **2008**, *61* (3), 227–242. https://doi.org/10.1007/s10874-009-9134-5.

(42) Hossaini, R.; Chipperfield, M. P.; Saiz-Lopez, A.; Fernandez, R.; Monks, S.; Feng, W.; Brauer, P.; von Glasow, R. A Global Model of Tropospheric Chlorine Chemistry: Organic versus Inorganic Sources and Impact on Methane Oxidation. *J. Geophys. Res. Atmos.* **2016**, *121* (23), 14,214-271,297. https://doi.org/10.1002/2016JD025756.

(43) Sander, R. Compilation of Henry's Law Constants (Version 4.0) for Water as Solvent. *Atmos. Chem. Phys.* **2015**, *15* (8), 4399–4981. https://doi.org/10.5194/acp-15-4399-2015.

(44) Graedel, T. E.; Crutzen, P. J. *Atmospheric Change: An Earth System Perspective*.; W.H. Freeman and Co.: New York, 1993.

(45) Graedel, T.; Keene, W. The Budget and Cycle of Earth's Natural Chlorine. *Pure and Applied Chemistry*. 1996, p 1689. https://doi.org/10.1351/pac199668091689.

(46) Hossaini, R.; Chipperfield, M. P.; Saiz-Lopez, A.; Harrison, J. J.; von Glasow, R.; Sommariva, R.; Atlas, E.; Navarro, M.; Montzka, S. A.; Feng, W.; et al. Growth in

Stratospheric Chlorine from Short-Lived Chemicals Not Controlled by the Montreal Protocol. *Geophys. Res. Lett.* **2015**, *42* (11), 4573–4580. https://doi.org/10.1002/2015GL063783.

(47) Saul, T. D.; Tolocka, M. P.; Johnston, M. V. Reactive Uptake of Nitric Acid onto Sodium Chloride Aerosols Across a Wide Range of Relative Humidities. *J. Phys. Chem. A* **2006**, *110* (24), 7614–7620. https://doi.org/10.1021/jp060639a.

(48) Gard, E. E.; Kleeman, M. J.; Gross, D. S.; Hughes, L. S.; Allen, J. O.; Morrical, B. D.; Fergenson, D. P.; Dienes, T.; E. Gälli, M.; Johnson, R. J.; et al. Direct Observation of Heterogeneous Chemistry in the Atmosphere. *Science (80-.).* **1998**, *279* (5354), 1184 LP – 1187. https://doi.org/10.1126/science.279.5354.1184.

(49) Laskin, A.; Moffet, R. C.; Gilles, M. K.; Fast, J. D.; Zaveri, R. A.; Wang, B.; Nigge, P.; Shutthanandan, J. Tropospheric Chemistry of Internally Mixed Sea Salt and Organic Particles: Surprising Reactivity of NaCl with Weak Organic Acids. *J. Geophys. Res. Atmos.* **2012**, *117* (D15). https://doi.org/10.1029/2012JD017743.

(50) Pechtl, S.; von Glasow, R. Reactive Chlorine in the Marine Boundary Layer in the Outflow of Polluted Continental Air: A Model Study. *Geophys. Res. Lett.* **2007**, *34* (11). https://doi.org/10.1029/2007GL029761.

(51) Rossi, M. J. Heterogeneous Reactions on Salts. *Chem. Rev.* **2003**, *103* (12), 4823–4882. https://doi.org/10.1021/cr020507n.

(52) Raff, J. D.; Njegic, B.; Chang, W. L.; Gordon, M. S.; Dabdub, D.; Gerber, R. B.; Finlayson-Pitts, B. J. Chlorine Activation Indoors and Outdoors via Surface-Mediated Reactions of Nitrogen Oxides with Hydrogen Chloride. *Proc. Natl. Acad. Sci.* **2009**, *106*

(33), 13647 LP – 13654. https://doi.org/10.1073/pnas.0904195106.

(53) Finlayson-Pitts, B. J.; Ezell, M. J.; Pitts, J. N. Formation of Chemically Active Chlorine Compounds by Reactions of Atmospheric NaCl Particles with Gaseous N2O5 and ClONO2. *Nature* **1989**, *337* (6204), 241–244. https://doi.org/10.1038/337241a0.

(54) Roberts, J. M.; Osthoff, H. D.; Brown, S. S.; Ravishankara, A. R.; Coffman, D.; Quinn, P.; Bates, T. Laboratory Studies of Products of N2O5 Uptake on Cl− Containing Substrates. *Geophys. Res. Lett.* **2009**, *36* (20). https://doi.org/10.1029/2009GL040448.

(55) Li, Q.; Zhang, L.; Wang, T.; Tham, Y. J.; Ahmadov, R.; Xue, L.; Zhang, Q.; Zheng, J. Impacts of Heterogeneous Uptake of Dinitrogen Pentoxide and Chlorine Activation on Ozone and Reactive Nitrogen Partitioning: Improvement and Application of the WRF-Chem Model in Southern China. *Atmos. Chem. Phys.* **2016**, *16* (23), 14875–14890. https://doi.org/10.5194/acp-16-14875-2016.

(56) Riedel, T. P.; Bertram, T. H.; Crisp, T. A.; Williams, E. J.; Lerner, B. M.; Vlasenko, A.; Li, S.-M.; Gilman, J.; de Gouw, J.; Bon, D. M.; et al. Nitryl Chloride and Molecular Chlorine in the Coastal Marine Boundary Layer. *Environ. Sci. Technol.* **2012**, *46* (19), 10463–10470. https://doi.org/10.1021/es204632r.

(57) Sarwar, G.; Simon, H.; Xing, J.; Mathur, R. Importance of Tropospheric ClNO2 Chemistry across the Northern Hemisphere. *Geophys. Res. Lett.* **2014**, *41* (11), 4050–4058. https://doi.org/10.1002/2014GL059962.

(58) Roberts, J. M.; Osthoff, H. D.; Brown, S. S.; Ravishankara, A. R. N2O5 Oxidizes Chloride to Cl2 in Acidic Atmospheric Aerosol. *Science (80-.).* **2008**, *321* (5892), 1059–1059. https://doi.org/10.1126/science.1158777.

(59) Thornton, J. A.; Abbatt, J. P. D. N2O5 Reaction on Submicron Sea Salt Aerosol: Kinetics, Products, and the Effect of Surface Active Organics. *J. Phys. Chem. A* **2005**, *109* (44), 10004–10012. https://doi.org/10.1021/jp054183t.

(60) Oum, K. W.; Lakin, M. J.; DeHaan, D. O.; Brauers, T.; Finlayson-Pitts, B. J. Formation of Molecular Chlorine from the Photolysis of Ozone and Aqueous Sea-Salt Particles. *Science (80-.).* **1998**, *279* (5347), 74–77. https://doi.org/10.1126/science.279.5347.74.

(61) Evans, C. D.; Monteith, D. T.; Fowler, D.; Cape, J. N.; Brayshaw, S. Hydrochloric Acid: An Overlooked Driver of Environmental Change. *Environ. Sci. Technol.* **2011**, *45* (5), 1887–1894. https://doi.org/10.1021/es103574u.

(62) Sipilä, M.; Berndt, T.; Petäjä, T.; Brus, D.; Vanhanen, J.; Stratmann, F.; Patokoski, J.; Mauldin, R. L.; Hyvärinen, A.-P.; Lihavainen, H.; et al. The Role of Sulfuric Acid in Atmospheric Nucleation. *Science (80-.).* **2010**, *327* (5970), 1243 LP – 1246. https://doi.org/10.1126/science.1180315.

(63) Laskin, A.; Moffet, R. C.; Gilles, M. K.; Fast, J. D.; Zaveri, R. A.; Wang, B.; Nigge, P.; Shutthanandan, J. Tropospheric Chemistry of Internally Mixed Sea Salt and Organic Particles : Surprising Reactivity of NaCl with Weak Organic Acids. **2012**, *117*, 1–12. https://doi.org/10.1029/2012JD017743.

(64) Wang, Z.; Wang, W.; Tham, Y. J.; Li, Q.; Wang, H.; Wen, L.; Wang, X.; Wang, T. Fast Heterogeneous N2O5 Uptake and ClNO2 Production in Power Plant Plumes Observed in the Nocturnal Residual Layer over the North China Plain. *Atmos. Chem. Phys. Discuss.* **2017**, No. x, 1–26. https://doi.org/10.5194/acp-2017-492.

(65) Wagner, N. L.; Riedel, T. P.; Young, C. J.; Bahreini, R.; Brock, C. A.; Dubé, W. P.; Kim,

S.; Middlebrook, A. M.; Öztürk, F.; Roberts, J. M.; et al. N2O5 Uptake Coefficients and Nocturnal NO2 Removal Rates Determined from Ambient Wintertime Measurements. *J. Geophys. Res. Atmos.* **2013**, *118* (16), 9331–9350. https://doi.org/10.1002/jgrd.50653.

(66) Morris, E. D.; Niki, H. Reaction of Dinitrogen Pentoxide with Water. *J. Phys. Chem.* **1973**, *77* (16), 1929–1932. https://doi.org/10.1021/j100635a001.

(67) Bertram, T. H.; Thornton, J. A.; Riedel, T. P. An Experimental Technique for the Direct Measurement of N2O5 Reactivity on Ambient Particles. *Atmos. Meas. Tech* **2009**, *2*, 231–242. https://doi.org/10.5194/amt-2-231-2009.

(68) Bertram, T. H.; Thornton, J. A. Toward a General Parameterization of N_2O_5 Reactivity on Aqueous Particles: The Competing Effects of Particle Liquid Water, Nitrate and Chloride. *Atmos. Chem. Phys.* **2009**, *9* (21), 8351–8363. https://doi.org/10.5194/acp-9-8351-2009.

(69) Anttila, T.; Kiendler-Scharr, A.; Tillmann, R.; Mentel, T. F. On the Reactive Uptake of Gaseous Compounds by Organic-Coated Aqueous Aerosols: Theoretical Analysis and Application to the Heterogeneous Hydrolysis of N2O5. *J. Phys. Chem. A* **2006**, *110* (35), 10435–10443. https://doi.org/10.1021/jp062403c.

(70) F. Mentel, T.; Sohn, M.; Wahner, A. Nitrate Effect in the Heterogeneous Hydrolysis of Dinitrogen Pentoxide on Aqueous Aerosols. *Phys. Chem. Chem. Phys.* **1999**, *1* (24), 5451–5457. https://doi.org/10.1039/A905338G.

(71) Oum, K. W.; Lakin, M. J.; DeHaan, D. O.; Brauers, T.; Finlayson-Pitts, B. J. Formation of Molecular Chlorine from the Photolysis of Ozone and Aqueous Sea-Salt Particles. *Science (80-.).* **1998**, *279* (5347), 74 LP – 76. https://doi.org/10.1126/science.279.5347.74.

(72) Donaldson, D. J.; Ravishankara, A. R.; Hanson, D. R. Detailed Study of HOCl + HCl → Cl2 + H2O in Sulfuric Acid. *J. Phys. Chem. A* **1997**, *101* (26), 4717–4725. https://doi.org/10.1021/jp9633153.

(73) Lawler, M. J.; Sander, R.; Carpenter, L. J.; Lee, J. D.; von Glasow, R.; Sommariva, R.; Saltzman, E. S. HOCl and Cl_2 Observations in Marine Air. *Atmos. Chem. Phys.* **2011**, *11* (15), 7617–7628. https://doi.org/10.5194/acp-11-7617-2011.

(74) Wren, S. N.; Donaldson, D. J.; Abbatt, J. P. D. Photochemical Chlorine and Bromine Activation from Artificial Saline Snow. *Atmos. Chem. Phys.* **2013**, *13* (19), 9789–9800. https://doi.org/10.5194/acp-13-9789-2013.

(75) Simpson, W. R.; Brown, S. S.; Saiz-Lopez, A.; Thornton, J. A.; Von Glasow, R. Tropospheric Halogen Chemistry: Sources, Cycling, and Impacts. *Chem. Rev.* **2015**, *115* (10), 4035–4062. https://doi.org/10.1021/cr5006638.

(76) Saiz-Lopez, A.; Von Glasow, R. Reactive Halogen Chemistry in the Troposphere. *Chem. Soc. Rev.* **2012**, *41* (19), 6448–6472. https://doi.org/10.1039/c2cs35208g.

(77) Crisp, T. a; Lerner, B. M.; Williams, E. J.; Quinn, P. K.; Bates, T. S.; Bertram, T. H. Observations of Gas Phase Hydrochloric Acid in the Polluted Marine Boundary Layer. *J. Geophys. Res. Atmos.* **2014**, 6897–6915. https://doi.org/10.1002/2013JD020992.Received.

(78) Wang, X.; Jacob, D. J.; Eastham, S. D.; Sulprizio, M. P.; Zhu, L.; Chen, Q.; Alexander, B.; Sherwen, T.; Evans, M. J.; Lee, B. H.; et al. The Role of Chlorine in Global Tropospheric Chemistry. **2019**, 3981–4003.

(79) Kim, S.; Huey, L. G.; Stickel, R. E.; Pierce, R. B.; Chen, G.; Avery, M. A.; Dibb, J. E.;

Diskin, G. S.; Sachse, G. W.; McNaughton, C. S.; et al. Airborne Measurements of HCl from the Marine Boundary Layer to the Lower Stratosphere over the North Pacific Ocean during INTEX-B. *Atmos. Chem. Phys. Discuss.* **2008**, *2008*, 3563–3595. https://doi.org/10.5194/acpd-8-3563-2008.

(80) Simpson, W. R.; Brown, S. S.; Saiz-Lopez, A.; Thornton, J. A.; von Glasow, R. Tropospheric Halogen Chemistry: Sources, Cycling, and Impacts. *Chem. Rev.* **2015**, *115* (10), 4035–4062. https://doi.org/10.1021/cr5006638.

(81) Saiz-Lopez, A.; von Glasow, R. Reactive Halogen Chemistry in the Troposphere. *Chem. Soc. Rev.* **2012**, *41* (19), 6448–6472. https://doi.org/10.1039/C2CS35208G.

(82) Finlayson-Pitts, B. J. The Tropospheric Chemistry of Sea Salt: A Molecular-Level View of the Chemistry of NaCl and NaBr. *Chem. Rev.* **2003**, *103* (12), 4801–4822. https://doi.org/10.1021/cr020653t.

(83) Thornton, J. A.; Kercher, J. P.; Riedel, T. P.; Wagner, N. L.; Cozic, J.; Holloway, J. S.; Dubé, W. P.; Wolfe, G. M.; Quinn, P. K.; Middlebrook, A. M.; et al. A Large Atomic Chlorine Source Inferred from Mid-Continental Reactive Nitrogen Chemistry. *Nature* **2010**, *464*, 271.

(84) Lee, B. H.; Lopez-Hilfiker, F. D.; Schroder, J. C.; Campuzano-Jost, P.; Jimenez, J. L.; McDuffie, E. E.; Fibiger, D. L.; Veres, P. R.; Brown, S. S.; Campos, T. L.; et al. Airborne Observations of Reactive Inorganic Chlorine and Bromine Species in the Exhaust of Coal-Fired Power Plants. *J. Geophys. Res. Atmos.* **2018**, *123* (19), 11,211-225,237. https://doi.org/10.1029/2018JD029284.

(85) Von Clarmann, T. CHLORINE IN THE STRATOSPHERE. *Atmósfera; Vol 26, No 3*

2013.

(86) Ganske, J. A.; Berko, H. N.; Finlayson-Pitts, B. J. Absorption Cross Sections for Gaseous ClNO2 and Cl2 at 298 K: Potential Organic Oxidant Source in the Marine Troposphere. *J. Geophys. Res. Atmos.* **1992**, *97* (D7), 7651–7656. https://doi.org/https://doi.org/10.1029/92JD00414.

(87) Phillips, G. J.; Tang, M. J.; Thieser, J.; Brickwedde, B.; Schuster, G.; Bohn, B.; Lelieveld, J.; Crowley, J. N. Significant Concentrations of Nitryl Chloride Observed in Rural Continental Europe Associated with the Influence of Sea Salt Chloride and Anthropogenic Emissions. *Geophys. Res. Lett.* **2012**, *39* (10). https://doi.org/10.1029/2012GL051912.

(88) Bonne, G. P.; Stimpfle, R. M.; Cohen, R. C.; Voss, P. B.; Perkins, K. K.; Anderson, J. G.; Salawitch, R. J.; Elkins, J. W.; Dutton, G. S.; Jucks, K. W.; et al. An Examination of the Inorganic Chlorine Budget in the Lower Stratosphere. *J. Geophys. Res. Atmos.* **2000**, *105* (D2), 1957–1971. https://doi.org/10.1029/1999JD900996.

(89) Kolusu, S. R.; Schlünzen, K. H.; Grawe, D.; Seifert, R. Chloromethane and Dichloromethane in the Tropical Atlantic Ocean. *Atmos. Environ.* **2017**, *150*, 417–424. https://doi.org/https://doi.org/10.1016/j.atmosenv.2016.11.037.

(90) Esen, F. Development of a Passive Sampling Device Using Polyurethane Foam (PUF) to Measure Polychlorinated Biphenyls (PCBs) and Organochlorine Pesticides (OCPs) near Landfills. *Environ. Forensics* **2013**, *14* (1), 1–8. https://doi.org/10.1080/15275922.2012.729008.

(91) Leedham Elvidge, E. C.; Oram, D. E.; Laube, J. C.; Baker, A. K.; Montzka, S. A.; Humphrey, S.; O'Sullivan, D. A.; Brenninkmeijer, C. A. M. Increasing Concentrations of

Dichloromethane, CH_2Cl_2, Inferred from CARIBIC Air Samples Collected 1998–2012. *Atmos. Chem. Phys.* **2015**, *15* (4), 1939–1958. https://doi.org/10.5194/acp-15-1939-2015.

(92) Kallenborn, R.; Oehme, M.; Wynn-Williams, D. D.; Schlabach, M.; Harris, J. Ambient Air Levels and Atmospheric Long-Range Transport of Persistent Organochlorines to Signy Island, Antarctica. *Sci. Total Environ.* **1998**, *220* (2), 167–180. https://doi.org/https://doi.org/10.1016/S0048-9697(98)00257-5.

(93) Appel, B. R.; Tokiwa, Y.; Povard, V.; Kothny, E. L. The Measurement of Atmospheric Hydrochloric Acid in Southern California. *Atmos. Environ. Part A. Gen. Top.* **1991**, *25* (2), 525–527. https://doi.org/https://doi.org/10.1016/0960-1686(91)90325-2.

(94) Eldering, A. M.; Solomon, P. A.; Salmon, L. G.; Fall, T.; Cass, G. R. Hydrochloric Acid: A Regional Perspective on Concentrations and Formation in the Atmosphere of Southern California. *Atmos. Environ. Part A, Gen. Top.* **1991**, *25* (10), 2091–2102. https://doi.org/10.1016/0960-1686(91)90086-M.

(95) Keuken, M. P.; Schoonebeek, C. A. M.; van Wensveen-Louter, A.; Slanina, J. Simultaneous Sampling of NH3, HNO3, HC1, SO2 and H2O2 in Ambient Air by a Wet Annular Denuder System. *Atmos. Environ.* **1988**, *22* (11), 2541–2548. https://doi.org/https://doi.org/10.1016/0004-6981(88)90486-6.

(96) Lindgren, P. F. Diffusion Scrubber-Ion Chromatography for the Measurement of Trace Levels of Atmospheric HCl. *Atmos. Environ. Part A. Gen. Top.* **1992**, *26* (1), 43–49. https://doi.org/https://doi.org/10.1016/0960-1686(92)90259-N.

(97) Bari, A.; Ferraro, V.; Wilson, L. R.; Luttinger, D.; Husain, L. Measurements of Gaseous HONO, HNO3, SO2, HCl, NH3, Particulate Sulfate and PM2.5 in New York, NY. *Atmos.*

Environ. **2003**, *37* (20), 2825–2835. https://doi.org/10.1016/S1352-2310(03)00199-7.

(98) Dasgupta, P. K.; Campbell, S. W.; Al-Horr, R. S.; Ullah, S. M. R.; Li, J.; Amalfitano, C.; Poor, N. D. Conversion of Sea Salt Aerosol to NaNO3 and the Production of HCl: Analysis of Temporal Behavior of Aerosol Chloride/Nitrate and Gaseous HCl/HNO3 Concentrations with AIM. *Atmos. Environ.* **2007**, *41* (20), 4242–4257. https://doi.org/https://doi.org/10.1016/j.atmosenv.2006.09.054.

(99) United States Environmental Protection Agency. Compendium of Methods for the Determination of Inorganic Compounds in Ambient Air: Determination of Reactive Acidic and Basic Gases and Strong Acidity of Atmospheric Fine Particles (<2.5 Mm) (Compendium Method IO-4.2). **1999**.

(100) Keene, W. C.; Maben, J. R.; Pszenny, A. A. P.; Galloway, J. N. Measurement Technique for Inorganic Chlorine Gases in the Marine Boundary Layer. *Environ. Sci. Technol.* **1993**, *27* (5), 866–874. https://doi.org/10.1021/es00042a008.

(101) Pszenny, A. A. P.; Keene, W. C.; Jacob, D. J.; Fan, S.; Maben, J. R.; Zetwo, M. P.; Springer-Young, M.; Galloway, J. N. Evidence of Inorganic Chlorine Gases Other than Hydrogen Chloride in Marine Surface Air. *Geophys. Res. Lett.* **1993**, *20* (8), 699–702. https://doi.org/10.1029/93GL00047.

(102) Keene, W. C.; Savoie, D. L. The PH of Deliquesced Sea-Salt Aerosol in Polluted Marine Air. *Geophys. Res. Lett.* **1998**, *25* (12), 2181–2184. https://doi.org/https://doi.org/10.1029/98GL01591.

(103) Pszenny, A. A. P.; Moldanová, J.; Keene, W. C.; Sander, R.; Maben, J. R.; Martinez, M.; Crutzen, P. J.; Perner, D.; Prinn, R. G. Halogen Cycling and Aerosol PH in the Hawaiian

Marine Boundary Layer. *Atmos. Chem. Phys.* **2004**, *4* (1), 147–168. https://doi.org/10.5194/acp-4-147-2004.

(104) Jourdain, B.; Legrand, M. Year-Round Records of Bulk and Size-Segregated Aerosol Composition and HCl and HNO3 Levels in the Dumont d'Urville (Coastal Antarctica) Atmosphere: Implications for Sea-Salt Aerosol Fractionation in the Winter and Summer. *J. Geophys. Res. Atmos.* **2002**, *107* (D22), ACH 20-1-ACH 20-13. https://doi.org/https://doi.org/10.1029/2002JD002471.

(105) Keene, W. C.; Pszenny, A. A. P.; Maben, J. R.; Stevenson, E.; Wall, A. Closure Evaluation of Size-Resolved Aerosol PH in the New England Coastal Atmosphere during Summer. *J. Geophys. Res. Atmos.* **2004**, *109* (D23). https://doi.org/https://doi.org/10.1029/2004JD004801.

(106) Keene, W. C.; Long, M. S.; Pszenny, A. A. P.; Sander, R.; Maben, J. R.; Wall, A. J.; O'Halloran, T. L.; Kerkweg, A.; Fischer, E. V; Schrems, O. Latitudinal Variation in the Multiphase Chemical Processing of Inorganic Halogens and Related Species over the Eastern North and South Atlantic Oceans. *Atmos. Chem. Phys.* **2009**, *9* (19), 7361–7385. https://doi.org/10.5194/acp-9-7361-2009.

(107) Keene, W. C.; Stutz, J.; Pszenny, A. A. P.; Maben, J. R.; Fischer, E. V; Smith, A. M.; von Glasow, R.; Pechtl, S.; Sive, B. C.; Varner, R. K. Inorganic Chlorine and Bromine in Coastal New England Air during Summer. *J. Geophys. Res. Atmos.* **2007**, *112* (D10). https://doi.org/10.1029/2006JD007689.

(108) Lawler, M. J.; Finley, B. D.; Keene, W. C.; Pszenny, A. A. P.; Read, K. A.; von Glasow, R.; Saltzman, E. S. Pollution-Enhanced Reactive Chlorine Chemistry in the Eastern

Tropical Atlantic Boundary Layer. *Geophys. Res. Lett.* **2009**, *36* (8). https://doi.org/10.1029/2008GL036666.

(109) Burkholder, J. B.; Sander, S. P.; Abbatt, J. P. D.; Barker, J. R.; Cappa, C.; Crounse, J. D.; Dibble, T. S.; Huie, R. E.; Kolb, C. E.; Kurylo, M. J.; et al. Chemical Kinetics and Photochemical Data for Use in Atmospheric Studies Evaluation Number 19. *Pasadena, CA Jet Propuls. Lab. Natl. Aeronaut. Sp. Adm. 2020* **2020**, No. 19–5.

(110) Platt, U.; Allan, W.; Lowe, D. Hemispheric Average Cl Atom Concentration from $^{13}C/^{12}C$ Ratios in Atmospheric Methane. *Atmos. Chem. Phys.* **2004**, *4* (9/10), 2393–2399. https://doi.org/10.5194/acp-4-2393-2004.

(111) Allan, W.; Struthers, H.; Lowe, D. C. Methane Carbon Isotope Effects Caused by Atomic Chlorine in the Marine Boundary Layer : Global Model Results Compared with Southern Hemisphere Measurements. **2007**, *112*, 1–10. https://doi.org/10.1029/2006JD007369.

(112) Oksdath-Mansilla, G.; Peñéñory, A. B.; Barnes, I.; Wiesen, P.; Teruel, M. A. Product Distribution Study of the Cl-Atom Initiated Oxidation of Ethyl Methyl Sulfide and Diethyl Sulfide. *Atmos. Environ.* **2014**, *85*, 41–47. https://doi.org/https://doi.org/10.1016/j.atmosenv.2013.11.063.

(113) Thompson, K. C.; Canosa-Mas, C. E.; Wayne, R. P. Kinetics and Mechanism of the Reaction between Atomic Chlorine and Dimethyl Selenide; Comparison with the Reaction between Atomic Chlorine and Dimethyl Sulfide. *Phys. Chem. Chem. Phys.* **2002**, *4* (17), 4133–4139. https://doi.org/10.1039/B204657A.

(114) Stickel, R. E.; Nicovich, J. M.; Wang, S.; Zhao, Z.; Wine, P. H. Kinetic and Mechanistic Study of the Reaction of Atomic Chlorine with Dimethyl Sulfide. *J. Phys. Chem.* **1992**, *96*

(24), 9875–9883. https://doi.org/10.1021/j100203a055.

(115) McNamara, S. M.; Kolesar, K. R.; Wang, S.; Kirpes, R. M.; May, N. W.; Gunsch, M. J.; Cook, R. D.; Fuentes, J. D.; Hornbrook, R. S.; Apel, E. C.; et al. Observation of Road Salt Aerosol Driving Inland Wintertime Atmospheric Chlorine Chemistry. *ACS Cent. Sci.* **2020**, *6* (5), 684–694. https://doi.org/10.1021/acscentsci.9b00994.

(116) Wang, X.; Jacob, D. J.; Fu, X.; Wang, T.; Breton, M. Le; Hallquist, M.; Liu, Z.; McDuffie, E. E.; Liao, H. Effects of Anthropogenic Chlorine on PM2.5 and Ozone Air Quality in China. *Environ. Sci. Technol.* **2020**, *54* (16), 9908–9916. https://doi.org/10.1021/acs.est.0c02296.

(117) Dawe, K. E. R.; Furlani, T. C.; Kowal, S. F.; Kahan, T. F.; Vandenboer, T. C.; Young, C. J. Formation and Emission of Hydrogen Chloride in Indoor Air. *Indoor Air* **2019**, No. April 2018, 70–78. https://doi.org/10.1111/ina.12509.

(118) Wang, C.; Collins, D. B.; Abbatt, J. P. D. Indoor Illumination of Terpenes and Bleach Emissions Leads to Particle Formation and Growth. *Environ. Sci. Technol.* **2019**, *53* (20), 11792–11800. https://doi.org/10.1021/acs.est.9b04261.

(119) Mattila, J. M.; Lakey, P. S. J.; Shiraiwa, M.; Wang, C.; Abbatt, J. P. D.; Arata, C.; Goldstein, A. H.; Ampollini, L.; Katz, E. F.; DeCarlo, P. F.; et al. Multiphase Chemistry Controls Inorganic Chlorinated and Nitrogenated Compounds in Indoor Air during Bleach Cleaning. *Environ. Sci. Technol.* **2020**, *54* (3), 1730–1739. https://doi.org/10.1021/acs.est.9b05767.

(120) Kolesar, K. R.; Mattson, C. N.; Peterson, P. K.; May, N. W.; Prendergast, R. K.; Pratt, K. A. Increases in Wintertime PM2.5 Sodium and Chloride Linked to Snowfall and Road

Salt Application. *Atmos. Environ.* **2018**, *177*, 195–202.

https://doi.org/https://doi.org/10.1016/j.atmosenv.2018.01.008.

(121) Priestley, M.; le Breton, M.; Bannan, T. J.; Worrall, S. D.; Bacak, A.; Smedley, A. R. D.; Reyes-Villegas, E.; Mehra, A.; Allan, J.; Webb, A. R.; et al. Observations of Organic and Inorganic Chlorinated Compounds and Their Contribution to Chlorine Radical Concentrations in an Urban Environment in Northern Europe during the Wintertime. *Atmos. Chem. Phys.* **2018**, *18* (18), 13481–13493. https://doi.org/10.5194/acp-18-13481-2018.

(122) Lee, B. H.; Lopez-Hilfiker, F. D.; Schroder, J. C.; Campuzano-Jost, P.; Jimenez, J. L.; McDuffie, E. E.; Fibiger, D. L.; Veres, P. R.; Brown, S. S.; Campos, T. L.; et al. Airborne Observations of Reactive Inorganic Chlorine and Bromine Species in the Exhaust of Coal-Fired Power Plants. *J. Geophys. Res. Atmos.* **2018**, *123* (19), 11,225-11,237. https://doi.org/10.1029/2018JD029284.

(123) Wong, J. P. S.; Carslaw, N.; Zhao, R.; Zhou, S.; Abbatt, J. P. D. Observations and Impacts of Bleach Washing on Indoor Chlorine Chemistry. *Indoor Air* **2017**, No. June, 1082–1090. https://doi.org/10.1111/ina.12402.

(124) Schwartz-Narbonne, H.; Wang, C.; Zhou, S.; Abbatt, J. P. D.; Faust, J. Heterogeneous Chlorination of Squalene and Oleic Acid. *Environ. Sci. Technol.* **2019**, *53* (3), 1217–1224. https://doi.org/10.1021/acs.est.8b04248.

(125) Zhai, S.; Wang, X.; McConnell, J. R.; Geng, L.; Cole-Dai, J.; Sigl, M.; Chellman, N.; Sherwen, T.; Pound, R.; Fujita, K.; et al. Anthropogenic Impacts on Tropospheric Reactive Chlorine Since the Preindustrial. *Geophys. Res. Lett.* **2021**, *48* (14), e2021GL093808. https://doi.org/https://doi.org/10.1029/2021GL093808.

(126) Angelucci, A. A.; Furlani, T. C.; Wang, X.; Jacob, D. J.; VandenBoer, T. C.; Young, C. J. Understanding Sources of Atmospheric Hydrogen Chloride in Coastal Spring and Continental Winter. *ACS Earth Sp. Chem.* **2021**. https://doi.org/10.1021/acsearthspacechem.1c00193.

Chapter 2.

Compact Permeation Devices for Stable Emission of Gas-Phase Analytical Standards

2.1 Introduction

2.1.1 History of commercial use

Atmospheric analytical chemists require methods to generate and deliver consistent low concentration (less than 1 parts per billion by volume (ppbv)) of analytes for a variety of applications, such as calibrations. Permeation devices (PDs) offer a straightforward method to provide known gas phase mixing ratios that are stable over a long time. There are a variety of commercially available PDs containing environmentally relevant compounds in different device configurations. The most common configuration is a liquid hermetically sealed in a polymer tube (e.g., perfluoroalkoxy (PFA)) plugged on both ends with a porous polymer (e.g., polytetrafluoroethylene (PTFE)).[1,2] Other common configurations include a porous PTFE plug or wafer coupled to a stainless-steel or a glass reservoir. The simple permeation tube is the cheapest and easiest configuration to construct. Configurations that include a stainless-steel reservoir have longer lifetimes and are used for high vapour pressure compounds when needed in large amounts. Gas ampules or cylinders coupled with porous wafers can also be used but are much more difficult to work with and are not discussed further in this work. Regardless of the configuration, PDs are suitable for compounds that are volatile or semi-volatile, which can partition into the gas phase allowing them to then permeate through the material.

The simplicity of PDs has made them integral to environmental field and air quality studies. There are many different techniques to quantify PD emissions, including but not limited to, gravimetric or volumetric analysis and offline methods that involve scrubbing the sample stream into a solution amenable to an appropriate analytical instrument. The gases generated from PDs can be analytes for in-situ measurements or reagents for heterogenous chemistry.

2.1.2 Permeation device theory

Permeation devices work, as the name implies, by the permeation of a known compound through a permeable material. The permeation rate is dependent on the partial pressure between the inside of the sealed tube and outer walls containing the tube. The permeation process is also dependent on temperature, and therefore, temperature must be carefully controlled to maintain stable permeation rates.[3] There are three stages over the lifetime of a PD: the first is the saturation phase, the second is the steady-state phase, and finally the decay phase. The saturation phase is the initial buildup of the analyte in the gas phase as it permeates through the different microchannels through the polymer effectively saturating the all the pores. The steady-state phase is when the emission of the analyte from the tube is in steady-state, effectively allowing for a stable flow of the emitting compound into the delivery sample stream. The decay stage is when is the partial pressure in the tube starts to decrease due to insufficient quantity of analyte, at this stage the PD is no longer usable as it will not be able to provide a stable emission.

The difference in partial pressure between the inner environment (inside the PD) saturated with the analyte and outer "clean" environment (PD housing) is the major driving force for the permeation process. The basic operating principle for all PDs is best described by combining Fick's second law and Henry's law of solubility.[1–3] Fick's second law of diffusion through a porous substance is defined as (E1; units $m^2\ s^{-1}$):

$$D = D_0 e^{-\frac{\Delta E_D}{RT}} \qquad \text{(E1)}$$

Where D_0 is the pre-exponential constant for diffusion of the permeating compound, ΔE_D is the activation energy for the thermodynamic diffusion process, R is the ideal gas law constant, and T

is temperature. The effective Henry's Law solubility coefficient is defined as (E2; units of mol Pa^{-1} m^{-3}):

$$S = S_0 e^{-\frac{\Delta H_S}{RT}} \quad \text{(E2)}$$

Where S_0 is the pre-exponential constant for solubility and ΔH_S is the heat of solution of the permeating compound. The product of these two equations yields the overall permeability term (E3; units of mol Pa^{-1} m^{-1} s^{-1}):

$$P \equiv D \times S \quad \text{(E3)}$$

Therefore, permeation depends on both kinetic and thermodynamic properties of the system. The rate of permeation is not solely dependent on the physical properties of the desired gas and permeation material, but also external factors such as the temperature and pressure, as well as the potential chemical interactions between the analyte and the permeating material. To continue to produce a stable emission of the analyte, there must be a steady-state of diffusion of the permeating gas and a constant stream of diluent flow to reduce build-up of the gas in sample stream. At steady-state, the emission rate (E4; units of mol s^{-1}) through the porous plug or wafer can be expressed by:

$$E_s = P \times S_A \times \frac{(p_i - p_o)}{w} \quad \text{(E4)}$$

Where E_s is the emission rate of the sample, P is the permeability defined in E3, S_A is the surface area of the inner tube, p_i is the partial pressure of the sample in the tube, p_o is the partial pressure outside the tube, and w is the porous material wall thickness. Similarly, the emission rate from a PD with a porous tube and impermeable plug is expressed by:

$$E_s = 2\pi r L \times P \times \frac{(p_i - p_o)}{w} \quad \text{(E5)}$$

Where r is the radius of the tube and L is tube length. When the tube and plug materials are both permeable to the analyte, E4 and E5 can be combined to determine $E_{s,\,tot}$.

$$E_{s,tot} = 2\pi rL \times P_t \times \frac{(p_i - p_o)}{w_t} + P_p \times \pi r^2 \times \frac{(p_i - p_o)}{w_p} \qquad \text{(E6)}$$

Where P_t and w_t are the permeability coefficient and wall thickness of the tube, respectively, and P_p and w_p are the permeability coefficient and wall thickness of the plug, respectively. Emission rates can be theoretically determined if the physicochemical properties of the analyte and permeation material are known, but most emission rate determinations are performed empirically using analytical measuring techniques.

2.1.3 Chapter objectives

In this work we provide a basic understanding of the chemical properties that affect PDs. We apply PD theory to accomplish the following: (i) construct and maintain PDs with consistent emissions; (ii) demonstrate different calibration techniques and provide guidance for selection of calibration techniques; (iii) characterize the physical dependence of temperature and demonstrate PD stability; and (iv) explain how PDs have been applied to various experiments.

2.2 Methods

2.2.1 Chemicals and materials

Commercially available reagents were purchased from Sigma-Aldrich: Dichloromethane (DCM, HPLC grade, Oakville, Ontario, Canada), cis-1,3-dichloropropene (DCP, 97%, Milwaukee, Wisconsin, USA), 1-chlorobutane (CB, 99.5%, Milwaukee, Wisconsin, USA), reagent grade hydrochloric acid (HCl, 12 M, Oakville, Ontario, Canada), and acetic anhydride (ReagentPlus®, ≥99%, Oakville, Ontario, Canada) were used in permeation device construction.

Potassium hydroxide (KOH) pellets were used to create scrubbing solution for permeation device gas collection. Nitrogen (N_2, grade 4.8) gas was from Praxair (Toronto, Ontario, Canada). Experiments used deionized water generated by a Barnstead Infinity Ultrapure Water System (Thermo Fisher Scientific, Waltham, Massachusetts, USA; 18.2 MΩ cm−1). Eluent for annular denuder IC analysis was prepared from sodium hydroxide solution (NaOH, 50% w/w, Thermo Fisher Scientific, Sunnyvale, California, USA). IC calibration standards were prepared through serial dilution of a mixed anion standard concentrate (Thermo Fisher Scientific, Dionex Seven-Anion II, P/N: 057590). Material for permeation tube construction include porous PTFE rod (3.17 mm o.d., P/N: 84935K64; McMaster-Carr) and PFA tubing (3 mm o.d., P/N: 5733K73; McMaster-Carr).

2.2.2 Temperature controlled oven

To effectively maintain a stable temperature for the PDs, we built a custom aluminium oven designed to contain up to four PFA flow cells (½" o.d.). All components were purchased from either Omega™ Environmental (St. Eustache, QC) or Allied Electronics, Inc. (Fort Worth, TX). The aluminum oven rested on a L-shaped sheet of aluminum that was fitted with a process controller (Omega™; CN 7823), solid state-relay relay (Allied; SSR, D1210, Crydom) mounted on an aluminium heat sink (Allied; HS172, Crydom), and 10-amp fuse (Omega™; Tron, KAX-10 A). The aluminum oven depicted in Figure 1 was 8" by 3" by 3", the four holes were machined to snugly fit four PFA flow cells that offer an inert working surface for delivering the emitting gases. The aluminum oven was machined along the longest axis to contain a cartridge heater with an integrated K-type thermocouple housed in a high-temperature incoloy sheath (Omega™; CIR, 300 W, 120 V, 8" length and a 3/8" o.d.). The aluminum oven is designed to fit snugly with the cartridge heater and maximize contact between the oven and the heating element along the

cartridge. The heater is a high watt density cartridge with maximum working temperature of 760 ºC with fiberglass insulation. The K-type thermocouple is integrated into the cartridge heater and measures temperature based of the principles of the Seebeck effect, a derivative of the thermoelectric effect. The potential in volts for two different materials of the thermocouple between the hot and cold surface is measured and the potential difference between these junctions is used to calculate the temperature using a process controller. The two materials used in a K-type thermocouple are chromel (Ni-Cr) and alumel (Ni-Al) alloys that yields a temperature range of 0 to 1250 ºC. The process controller monitors the feedback from the thermocouple and the output voltage. The solid state-relay is an electronic switching device that takes power from 120 V outlet. The output voltage (5 V DC) from the process controller is regulates the power allowed through the solid state-relay by turning the bypass switch on or off. The process controller uses a proportional-integral-differential (PID) function and works by first plotting the output voltage vs the measured temperatures for multiple overshoots and undershoots of a setpoint. The three correction parameters are for the PID function are the proportional, integral, and derivative terms. The controlled feedback loop takes the measured over and undershoots to tune these three terms to lower the variability around the setpoint. The process controller used in these experiments has a temperature stability of ± 0.1 °C. All electronics used were protected by a Bussman rectifier fuse against excess current flow.

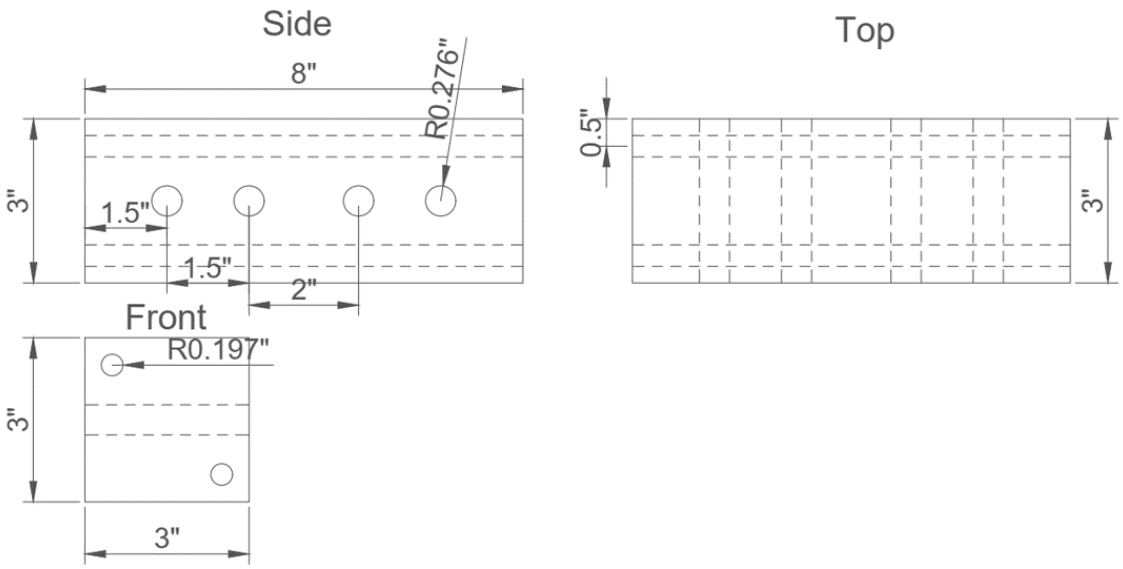

Figure 2-1. Schematic of the heated aluminium block.

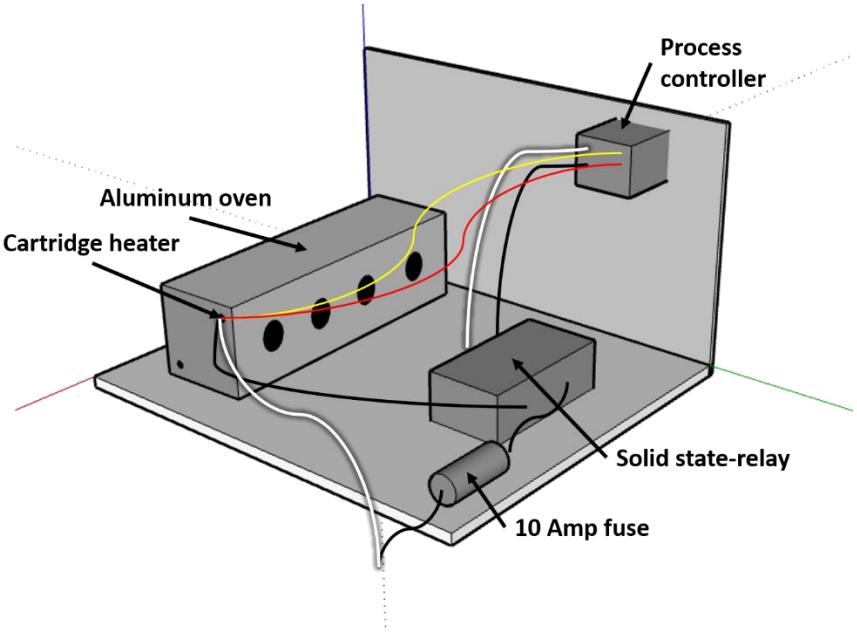

Figure 2-2. Schematic of the PD oven apparatus. Black lines represent live wires. White lines represent neutral wires. Red and yellow lines represent positive and negative polarity wires, respectively, for the integrated K-type thermocouple for the cartridge heater.

2.2.3 Ion chromatography with conductivity detection (IC-CD) analysis

Aqueous samples collected into an impinger was transferred and diluted into a 25 mL polypropylene (PP) volumetric flask (±0.08 mL). Aliquots of the diluted samples were analyzed using an ICS-2100 (Thermo Fisher Scientific, Sunnyvale, California, USA). An AS-DV autosampler loaded 1.0 mL of sample onto a concentration column (5 x 23 mm, TAC-ULP1, P/N: 061400) and injected into the IC-CD. Acetate and chloride were analyzed at a flowrate of 1.5 mL min^{-1} using an eluent gradient from 1–60 mM KOH controlled by a Dionex EGC III KOH Potassium Hydroxide Eluent Generator Cartridge (Thermo Fisher Scientific, Sunnyvale, California, USA), and separated on an AS11-HC analytical column thermostated to 30°C, and protected by an IonPac AG11 guard column (4 × 250 mm, P/N: 052960, and 4 x 50 mm, P/N: 052962, respectively). The gradient program, described by Place et al.,[4] started with 1.0 mM KOH held for 7 min followed by a linear increase to 16 mM KOH over the next 9 min. The KOH was held at 16 mM for 4 min then linearly increased to 25 mM from 20 min to 25 min. At 25 min the concentration was linearly increased to 60 mM over a period of 8 min, followed by a step decrease back to 1.0 mM KOH and held for 1 min to re-equilibrate the column, yielding a total run time of 33 min. The eluent was suppressed in legacy mode with 124 mA (AERS 500, 4 mm, P/N: 082540) before Cl^- was detected by the CD (DS6 heated conductivity cell, 30 °C). IC-CD calibration standards were prepared through serial dilution of a mixed anion standard concentrate (Thermo Fisher Scientific, Dionex Seven-Anion II, P/N: 057590).

2.3 Results and discussion

2.3.1 In-house permeation device construction

A simple method developed for the construction of custom permeation tubes for use in PDs is described here in detail with visual depictions in Figure 2-3. (1) PFA tube (3 mm i.d. with 1 mm

thickness) was cut to desired length (7.6 cm is used here). (2) The end of the tube was heated using a heat-gun at the highest output setting and the tube was rotated to evenly distribute the heat. Once sufficiently heated, the tube end takes on a glossy appearance and swell slightly. (3) The heated end was plugged with the porous PTFE rod by inserting the rod in a twisting motion until the desired length had been inserted (1 cm used here). While still hot, the plugged end was gently rolled between two flat surfaces to help seal and reduce any air pockets that may have formed. Any protruding PTFE rod was removed. (4) Aliquots of 100–400 µL of analyte liquid/solution were carefully delivered until the tube was ~1/2 – 3/4 full. Final volume will depend on PFA tube length. The filled tube was left to rest standing up-right on a tissue for ~10 minutes to ensure no visible leakages were present. (5) Step (2) was repeated, taking special precaution when heating the liquid-containing tube as it can boil over rapidly if using highly volatile compounds. (6) In situations where lower emissions rates were desired; instead of plugging the filled open end described in step (5), the filled open-ended tubing was hermetically sealed closed by heating the end until very pliable and almost melted, followed by 1 minute of firmly pinching the end closed with thick needle nose pliers.

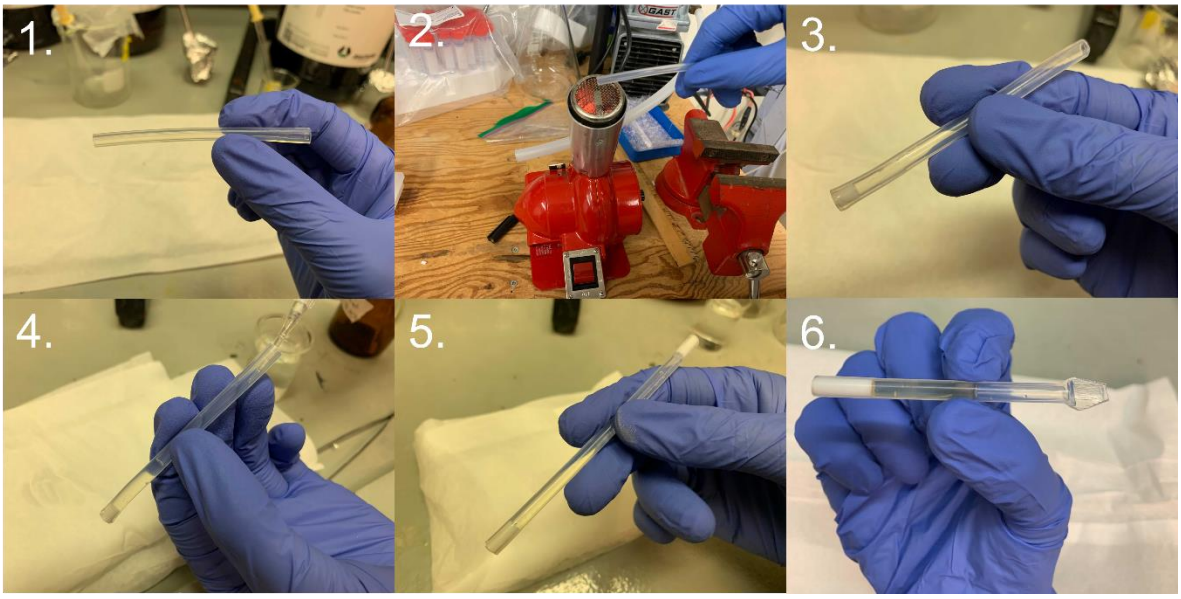

Figure 2-3. Steps in the construction of a custom permeation tube for use in a PD.

The temperature-controlled aluminum block described in section 2.2.1 housed the permeation tube and can regulate the temperature to 30.0–80.0 ± 0.1 °C. Dry N_2 flowed through a PFA flow tube (1.27 cm o.d.) in the block, containing the permeation tube. The N_2 gas flows over the permeation tube housed in the flow cell collecting the emitted analyte and acts as the delivery flow. Stable flows through the oven are maintained with a 50 µm diameter critical orifice (Lenox laser, Glen Arm, Maryland, USA, SS-4-VCR-2-50). The critical orifice is a flow restricting plate that allows a constant and stable flows when the back pressure and temperature are kept constant. We supply a 30 psi back pressure of N_2 to generate delivery gas flowrates, that typically fluctuate around 50 standard cubic centimeter per minute (sccm). Flows are measured using a DryCal Definer 220 (Mesa Labs, Lakewood, Colorado, USA).

2.3.2 PD emission rate determination

Gravimetric analysis is the most common--and sometimes only--method for commercial PD emission rate determination. MacInnis et al., (2016) conducted an independent calibration of a PD

containing gravimetrically validated commercial permeation tubes filled with an aqueous solution of the analyte. They observed an 7–16 times difference between their measured emission rate and the reported rate.[5] This is due to the inherent loss of water from the PDs. While the vapour pressure of water is typically much lower than the analytes, it is a non negligible component of the PD emission. The contribution to mass loss cannot be decoupled from the mass loss of the analyte, leading to an inflated emission rate. Emission rates for pure liquid PDs (e.g., DCM, Figure 2-4) can be accurately determined by gravimetric analysis in the PD saturation phase. The time required for the PD to reach the saturation phase is dependent on the porous material and the emitting compound. For the compounds tested here, the time needed to wait for the build-up phase to finish is estimated, at minimum, to be 24 hours. After reaching the stabilization period (which can be difficult to observe using gravimetric calibration), the permeation rates can be measured, within relatively short measurement periods limited by the sensitivity of the analytical balance and the emission rate of the PD. If the emission rate is high, then the time required to overcome the limitations of the analytical balance is lessened. As an example, the gravimetric determination of the emission rate for a PD of DCM required 37 days (Figure 2-4) to accurately measure the mass loss using a balance with precision of ±0.001 g and generate a five-point graph of mass loss versus elapsed time. The emission rate, at 30 °C, of the DCM PD was 640 ± 13 ng min^{-1}; the error in gravimetric calibrations is the uncertainty (σ) in the best fit line combined with the error in the analytical balance (±0.001 g, for this work). It should be noted that the PD can be used during the calibration period if the emission rate is not needed prior to its application. A similar approach was taken to determine emission rates of 240 ± 36 and $1.20\times10^4 \pm 0.02\times10^4$ for 1-chlorobutane and 1,3-dichlorobutane, respectively (Table 2-1).

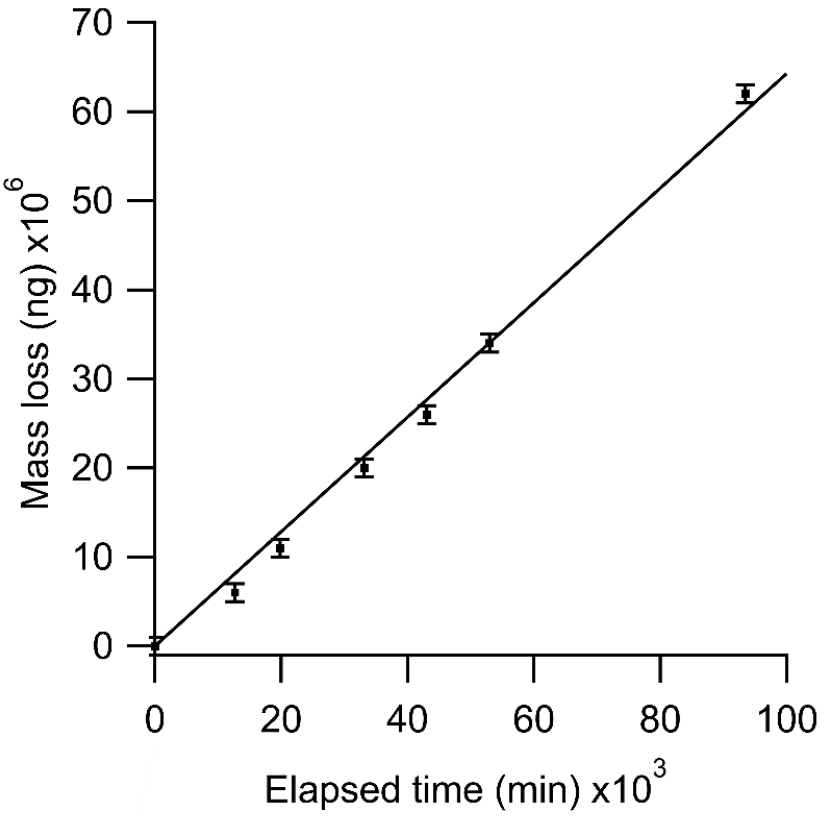

Figure 2-4. Gravimetric determination of a dichloromethane PD. The emission rate was calculated from the slope of the plot of mass loss over elapsed time and determined to be 640 ± 13 ng min^{-1}. Error bars in the y-axis are derived from the uncertainty of the analytical balance.

For targets that cannot be produced as a pure liquid, another technique must be used to accurately assess the emission rate. For example, the solvated nature of concentrated acids precludes the use of gravimetric analysis. A suitable alternative is experimentally determined emission rates using sample collection and offline analysis. The emission rate of PDs for HCl and acetic anhydride at 30–60 °C were tested using scrubbing followed by analysis with IC-CD (Figure 2-5). These acidic gases were collected by scrubbing the delivery gas into a 25 mL glass impinger containing approximately 15 mL of 1 mM potassium hydroxide over a known time period; collection times ranged from 15–60 minutes. Mass emission rates and the uncertainty for the PDs were determined by averaging of collected samples (n=3) and propagating IC measurement error (±σ). The IC-CD determined emission rate for HCl PD used in Chapter 3 was 140 ± 18 ng min^{-1}

(Table 2-1). The IC-CD determined emission rates for a 30 °C acetic anhydride PD was 900 ± 42 ng min^{-1} (Table 2-1). To test collection efficiencies, a second bubbler was place inline such that the exhaust from the primary bubbler was directed into the input of the second. Anion concentrations in the second bubbler were below limit of quantification (LOQ), < 20.0 ng for acetate and < 8 ng for chloride.[4] Thus, collection efficiency is expected to be near 100%. Inlet effects (adsorption/absorption) may delay surface active gases (most acidic gases), but the loss is negligible at the high concentrations in these sample streams.[6–8] Collection and analysis for PDs by IC-CD can roughly take a day to complete, which is quite fast in comparison to gravimetric techniques. Although not used in this work, high performance liquid chromatography (HPLC) is another technique used for determining aqueous extracts, and can be advantageous for measuring water soluble organic compounds and the neutral form of acidic gaseous.[5,9] PD gases can also be captured on an appropriate sorbent trap (e.g., Tenax) and either extracted or directly analyzed using gas chromatography mass spectrometry (GC-MS).[10,11] In-situ determinations of PD emission rates of generated nitric acid and ammonia gases have be performed using established spectroscopy techniques, such ultra-violet optical absorption.[12] There are many techniques that can be applied to determine PD emission rates, but each will be analyte specific and therefore must be chosen on a case-by-case basis. While gravimetric techniques for emission rate determination are relatively inexpensive (given that most labs have an analytical balance) and can be applied to any pure substance, offline approaches (or in-situ spectroscopy) are often faster (~1 day compared to weeks) and can effectively determine emission rates of mixtures.

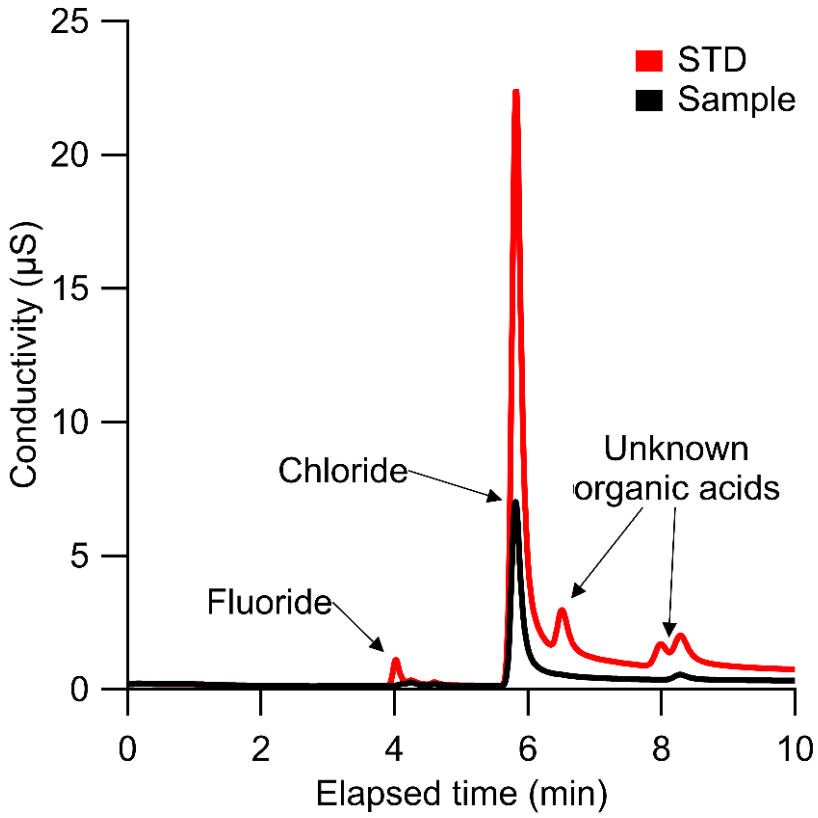

Figure 2-5. IC-CD chromatogram for a calibration standard and a HCl PD extract collected for 60 minutes. IC-CD method cut to 10 min for brevity.

Table 2-1. Summary of custom PDs.

Compound	Emission rate (ng min^{-1})	Temperature (°C)	Volume and composition	Method of determination
HCl	140 ± 18	60	200 µL of 37 % w/v aqueous solution	IC-CD
Acetic anhydride	900 ± 42 1700 ± 1.8×10^2 3700 ± 3.9×10^2	30 40 50	200 µL of pure liquid	IC-CD
Dichloromethane	640 ± 13	30	400 µL of pure liquid	Gravimetric
1-chlorobutane	240 ± 36	30	400 µL of pure liquid	Gravimetric
1, 3-dichlorobutane	1.20×10^4 ± 0.02×10^4	30	400 µL of pure liquid	Gravimetric

2.3.3 Temperature dependence of PDs

Thermostating the PD emitting environment, in this case the PFA housing, plays an important role in producing a consistent emission rate. Both terms from E1 and E2 have an exponential dependence on temperature, due to the Arrhenius behaviour of the factors that influence permeation rate. For most compounds, a change in 1°C can change the emission rate by 5–10%.[3,13] The sensitivity of PD systems to temperature change emphasizes the need to accurately maintain the housing temperature with good precision.

A temperature dependent equation was determined from acetic anhydride PD extracts collected at different temperatures. The data is fitted to a modified E3 to yield:

$$Emission\ rate = S_0 D_0 e^{-\frac{\Delta E_D + \Delta H_S}{RT}} + C \qquad \text{(E7)}$$

Using the PD emission rate and the temperature of the oven, we can determine the coefficients from E7. Acetic anhydride PD emission rates were determined under three temperatures (Table 2-1, Figure 2-6), and S_0D_0 was calculated to be 2.63×10^5 ng min^{-1}, the term $-(\Delta E_D + \Delta H_S)$ was calculated to be 1.87 kJ mol^{-1}, and the C term was 754.72 ng min^{-1}. The C term is the lower limit of the emission rate where the best fit line converges until the freezing point of acetic anhydride when emission rate does not follow dynamic liquid behaviour.

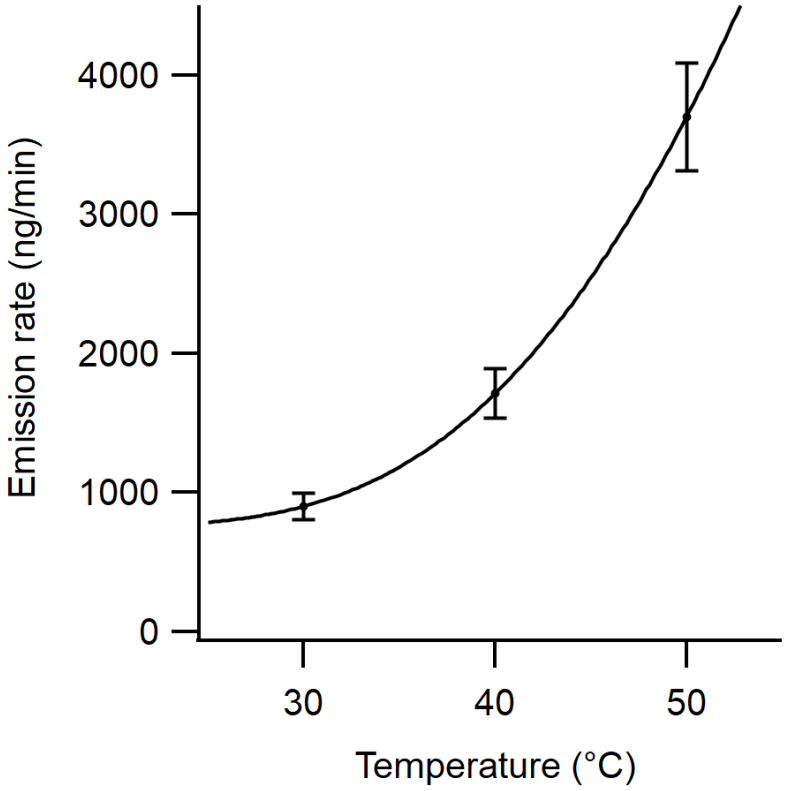

Figure 2-6. Temperature dependence of acetic anhydride emission rate fitted to E7. Error bars represent the error in triplicate analysis of IC samples at each temperature.

2.3.4 Stability of PDs

Stability can be defined as a consistent mass output over time for PDs having reached equilibrium. The stability of an HCl PD system was monitored by cavity ring-down spectroscopy (CRDS). The output of an HCl PD carried by ~50 sccm of dry N_2 was met with 3000 sccm of clean air and directed into the inlet of the CRDS over 12 hours (Figure 2-7). The stable output of this PD is shown in Figure 2-7a, and the precision (±σ) over this timeframe was 0.05 ppbv. Figure 2-7b helps illustrates the stability of the measured HCl, showing the percent difference from the mean (7.0 ppbv). This is our best estimate on the high-time resolution stability of a PD but is likely a conservative estimate due to the limitations and inherent challenges in measuring HCl gas. As described briefly in Section 2.3.1., HCl is a surface-active gas and will readily sorb to surfaces,

observed by the decrease from 2–6 hours in Figure 7b due to these surface effects. Characterizing these effects will be discussed in more detail in Chapter 3.

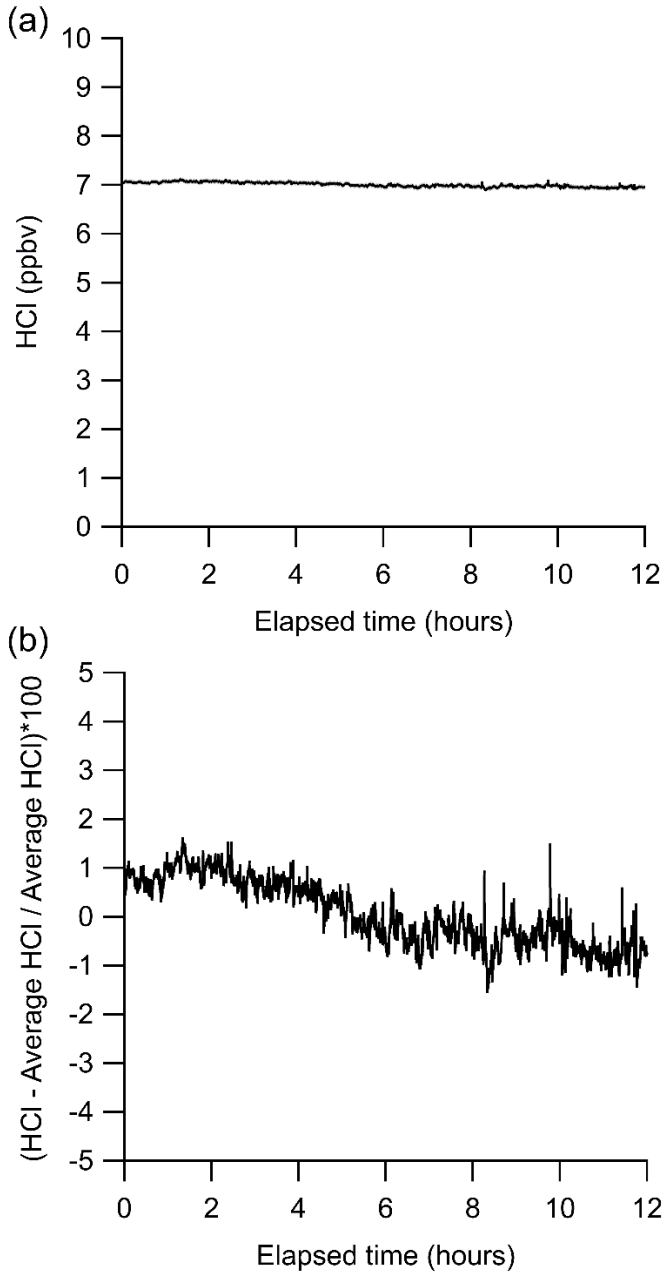

Figure 2-7. (a) CRDS measuring HCl emitted from a PD over 12 hours at 0% relative humidity (RH). (b) PD stability illustrated by the percent difference from the mean over 12 hours.

2.3.5 Applications

There are a wide range of applications in which PDs can be used; this section will focus on some of the applications in which PDs constructed using the methods described herein have been used (see Table 2-1). The most common application is that of a gas phase standard for in-situ online detection. One of the primary challenges in making accurate online measurements of uncommon analytes is finding the appropriate standards. Commercial premade and certified gas cylinders do not exist for every compound one might be interested in, or can be prohibitively expensive, which is why custom PDs that can be easily made in lab are an attractive solution to in-situ calibrations. For example, custom HCl PDs with known emission rates were used to generate a standard gas sample used to validate and help characterize the in-situ CRDS, see Chapter 3 where this work is discussed in more detail. In Chapter 5 of this thesis, PDs were used to generate three organochlorines, dichloromethane, 1-chlorobutane, and 1, 3-dichloropropene. These compounds are not commercially available as either premade certified PDs or gas cylinders, and therefore the ability to construct these custom PDs was crucial for this work. Because we could generate these gases, we are able to validate and characterize a novel method to measure total chlorine.

While using PDs to generate a calibrant gas is the primary application, they can also be used to generate low levels of a reagent gas. Low levels of HCl gas from our PDs were used as a reagent to generate nitrous acid (HONO) in work discussed in Lao et al., (2020).[14] Due to the inability to directly generate HONO, our PDs can produce a robust and stable supply of the reagent gas offering consistent reaction rates needed to apply the HONO generating method to in-situ field calibrations.

PD use is not only limited to calibration techniques, but they can also be used as a reagent ion source, such as for chemical ionization mass spectrometry (CIMS), a widely used in situ

measurement technique in atmospheric sciences. The most common reagent ions for CIMS are acetic anhydride and methyl iodide.[15–17] Generating consistent low levels of these reagent ions is crucial for chemical ionization, which is controlled by the presence of reagent ion to neutral compound (sometimes the analyte) clusters that changes with RH and the concentration of the reagent ions.

2.4 Conclusions

In conclusion we have provided a basic understanding of the chemical properties that affect permeation devices such as the activation energy for thermodynamic diffusion and the heat of solution of the permeating compound. We demonstrated the efficacy of two different calibration techniques, gravimetric and offline collection followed by IC-CD analysis. Gravimetric analysis is relatively inexpensive and robust for pure liquid compounds but is limited by analytical balance uncertainty and generally requires more time to accomplish (~weeks). Offline analysis is quicker (~days) but requires analysis techniques specific to individual analytes, which is typically more expensive. We characterized the physical dependence of temperature on the emission rate for an acetic anhydride PD. The stability of an HCl PD was monitored using a CRDS and the fluctuation/precision of the experiment with the longest equilibration time was 0.2%. We recognize that the stability monitored here is a combination of the true error of the emission rate and the uncertainty of the CRDS method we used to monitor it. This work also described in detail how we construct and maintain consistent emissions using inert and porous fluorinated polymers combined with a custom-built temperature-controlled oven. The variety of applications our PDs have been used is broad and extend to the entirety of the work explained in this thesis.

2.5 References

(1) Mitchell, G. D. A Review of Permeation Tubes and Permeators. *Sep. Purif. Methods* **2000**, *29* (1), 119–128. https://doi.org/10.1081/SPM-100100005.

(2) Washenfelder, R. A.; Roehl, C.; Mckinney, K.; Julian, R.; Wennberg, P. A Compact, Lightweight Gas Standards Generator for Permeation Tubes. *Rev. Sci. Instrum.* **2003**, *74*, 3151–3154. https://doi.org/10.1063/1.1570949.

(3) Tumbiolo, S.; Vincent, L.; Gal, J.-F.; Maria, P.-C. Thermogravimetric Calibration of Permeation Tubes Used for the Preparation of Gas Standards for Air Pollution Analysis. *Analyst* **2005**, *130* (10), 1369–1374. https://doi.org/10.1039/B508536E.

(4) Place, B. K.; Young, C. J.; Ziegler, S. E.; Edwards, K. A.; Salehpoor, L.; VandenBoer, T. C. Passive Sampling Capabilities for Ultra-Trace Quantitation of Atmospheric Nitric Acid (HNO3) in Remote Environments. *Atmos. Environ.* **2018**, *191* (November 2017), 360–369. https://doi.org/10.1016/j.atmosenv.2018.08.030.

(5) MacInnis, J. J.; VandenBoer, T. C.; Young, C. J. Development of a Gas Phase Source for Perfluoroalkyl Acids to Examine Atmospheric Sampling Methods. *Analyst* **2016**, *141* (12), 3765–3775. https://doi.org/10.1039/C6AN00313C.

(6) Crisp, T. a; Lerner, B. M.; Williams, E. J.; Quinn, P. K.; Bates, T. S.; Bertram, T. H. Observations of Gas Phase Hydrochloric Acid in the Polluted Marine Boundary Layer. *J. Geophys. Res. Atmos.* **2014**, 6897–6915. https://doi.org/10.1002/2013JD020992.Received.

(7) Ellis, R. a; Murphy, J. G.; Pattey, E.; Haarlem, R. Van; Brien, J. M. O. Characterizing a Quantum Cascade Tunable Infrared Laser Differential Absorption Spectrometer (QC-TILDAS) for Measurements of Atmospheric Ammonia. *Atmos. Meas. Tech.* **2010**, 3309–

3338.

(8) Roscioli, J. R.; Zahniser, M. S.; Nelson, D. D.; Herndon, S. C.; Kolb, C. E. New Approaches to Measuring Sticky Molecules: Improvement of Instrumental Response Times Using Active Passivation. *J. Phys. Chem. A* **2016**, *120* (9), 1347–1357. https://doi.org/10.1021/acs.jpca.5b04395.

(9) Joudan, S.; Orlando, J. J.; Tyndall, G. S.; Furlani, T. C.; Young, C. J.; Mabury, S. A. Atmospheric Fate of a New Polyfluoroalkyl Building Block, C3F7OCHFCF2SCH2CH2OH. *Environ. Sci. Technol.* **2021**. https://doi.org/10.1021/acs.est.0c07584.

(10) Pellizzari, E.; Demian, B.; Krost, K. Sampling of Organic Compounds in the Presence of Reactive Inorganic Gases with Tenax GC. *Anal. Chem.* **1984**, *56* (4), 793–798.

(11) Doucette, W. J.; Wetzel, T. A.; Dettenmaier, E.; Gorder, K. Emission Rates of Chlorinated Volatile Organics from New and Used Consumer Products Found during Vapor Intrusion Investigations: Impact on Indoor Air Concentrations. *Environ. Forensics* **2018**, *19* (3), 185–190. https://doi.org/10.1080/15275922.2018.1475433.

(12) Huey, L. G.; Jakoubek, R. Calibration and Evaluation of Nitric Acid and Ammonia Permeation Tubes by UV Optical Absorption. **2003**, *37* (13), 2975–2981. https://doi.org/10.1021/es026422l.

(13) Gómez, J. I. S.; Takhtehfouladi, E. S.; Schlögl, R.; Ruland, H. Design and Implementation of a Gas Generating System for Complex Gas Mixtures and Calibration Gases. *Chemie Ing. Tech.* **2020**, *92* (10), 1574–1585. https://doi.org/https://doi.org/10.1002/cite.202000110.

(14) Lao, M.; Crilley, L. R.; Salehpoor, L.; Furlani, T. C.; Bourgeois, I.; Neuman, J. A.; Rollins, A. W.; Veres, P. R.; Washenfelder, R. A.; Womack, C. C.; et al. A Portable, Robust, Stable and Tunable Calibration Source for Gas-Phase Nitrous Acid (HONO). *Atmos. Meas. Tech.* **2020**, *13*, 5873–5890. https://doi.org/10.5194/amt-13-5873-2020.

(15) Woodward-Massey, R.; Taha, Y. M.; Moussa, S. G.; Osthoff, H. D. Comparison of Negative-Ion Proton-Transfer with Iodide Ion Chemical Ionization Mass Spectrometry for Quantification of Isocyanic Acid in Ambient Air. *Atmos. Environ.* **2014**, *98* (x), 693–703. https://doi.org/10.1016/j.atmosenv.2014.09.014.

(16) Veres, P.; Roberts, J. M.; Warneke, C.; Welsh-Bon, D.; Zahniser, M.; Herndon, S.; Fall, R.; de Gouw, J. Development of Negative-Ion Proton-Transfer Chemical-Ionization Mass Spectrometry (NI-PT-CIMS) for the Measurement of Gas-Phase Organic Acids in the Atmosphere. *Int. J. Mass Spectrom.* **2008**, *274* (1–3), 48–55. https://doi.org/10.1016/j.ijms.2008.04.032.

(17) Brophy, P.; Farmer, D. K. Clustering, Methodology, and Mechanistic Insights into Acetate Chemical Ionization Using High-Resolution Time-of-Flight Mass Spectrometry. *Atmos. Meas. Tech.* **2016**, *9* (8), 3969–3986. https://doi.org/10.5194/amt-9-3969-2016.

Chapter 3.

Validation of a New Cavity Ring-Down Spectrometer for Measuring Tropospheric Gaseous Hydrogen Chloride

Abstract

Reliable, sensitive, and widely available hydrogen chloride (HCl) measurements are important for understanding oxidation in many regions of the troposphere. We configured a commercial HCl cavity ring-down spectrometer (CRDS) for sampling HCl in the ambient atmosphere and developed validation techniques to characterize the measurement uncertainties. The CRDS makes fast, sensitive, and robust measurements of HCl in a high finesse optical cavity coupled to a laser centered at 5739 cm^{-1}. The accuracy was determined to reside between 5–10%, calculated from laboratory and ambient air intercomparisons with annular denuders. The precision and limit of detection (3σ) in the 0.5 Hz measurement were below 6 pptv and 18 pptv, respectively for a 30 second integration interval in zero air. The response time of this method is primarily characterized by fitting decay curves to a double exponential equation and is impacted by inlet adsorption/desorption, with these surface effects increasing with RH and decreasing with decreasing HCl mixing ratios. The minimum 90% response time was 10 seconds and the equilibrated response time for the tested inlet was 2–6 minutes under the most and least optimal conditions, respectively. An intercomparison with the EPA compendium method for quantification of acidic atmospheric gases showed good agreement, yielding a linear relationship statistically equivalent to unity (slope of 0.97 ± 0.15). The CRDS from this study can detect HCl at atmospherically relevant mixing ratios, often performing comparable or better in sensitivity, selectivity, and response-time from previously reported HCl detection methods.

3.1 Introduction

Halogenated compounds that participate in catalytic cycles in the atmosphere have major impacts on atmospheric chemistry. Chlorine-containing species have long been known to catalytically destroy stratospheric ozone[1] and can have similar impacts on tropospheric ozone in polar regions.[2,3] In particular, early morning oxidation in the troposphere can be influenced heavily

by chlorine atoms released by photolabile chlorine species.[4–7] It is estimated that reactions involving chlorine atoms account for 14–27% of global tropospheric oxidation of abundant volatile organic compounds (VOCs).[8]

The role of chlorine chemistry in the troposphere remains uncertain in part due to a lack of a complete understanding of the contribution of chlorine reservoir species to the tropospheric chlorine inventory.[4,7] Sources of inorganic chlorine to the troposphere are important because many of them are photochemically active (e.g., $ClNO_2$). A near-complete budget of inorganic tropospheric chlorine from aircraft transects of polluted North American continental outflow during the WINTER campaign demonstrated that hydrogen chloride (HCl) makes up 48–62 % of total inorganic chlorine, and approximately 98% of total gaseous inorganic chlorine.[9] Troposphere HCl levels are typically between 10 and 1000 parts per trillion by volume (pptv) (e.g., Crisp et al. (2014); Haskins et al. (2018); and Young et al. (2013)). Elevated levels of HCl are typically found near marine environments polluted with NO_x; where reactions involving the chloride in sea spray aerosols can be a major source of chlorine to the troposphere.[9,11–13]

HCl is directly emitted to the atmosphere predominantly from volcanic activity, biomass burning, and industrial sources.[11,14,15] HCl is also produced through heterogeneous acid displacement reactions of strong acids, such as nitric acid, with particulate chloride (pCl^-):[13,16–19]

$$HA_{(g,\,aq)} + MCl_{(aq,\,s)} \rightarrow MA_{(aq,\,s)} + HCl_{(g)} \qquad \text{R3.1.1}$$

where M represents a cation in a chloride salt (often sodium). Elevated levels of chlorine atoms may also be present in both indoor and outdoor environments due to the emission of photolabile reactive chlorine compounds.[4,7,20–22]

$$XCl_{(g)} + h\upsilon \rightarrow Cl\cdot_{(g)} + X\cdot_{(g)} \qquad \text{R3.1.2}$$

Secondary production of HCl predominantly occurs *via* the reaction of chlorine atoms with methane or VOCs by hydrogen abstraction:

$$Cl\cdot_{(g)} + CH_{4(g)} \rightarrow HCl_{(g)} + \cdot CH_{3(g)} \qquad \text{R3.1.3}$$

$$Cl\cdot_{(g)} + RH_{(g)} \rightarrow HCl_{(g)} + R\cdot_{(g)} \qquad \text{R3.1.4}$$

The loss of gas-phase HCl occurs predominantly through wet or dry deposition which are terminal sinks for tropospheric chlorine,[13] with minor loss by reaction with the hydroxyl radical (OH) to re-form chlorine atoms:

$$HCl_{(g)} + OH\cdot_{(g)} \rightarrow Cl\cdot_{(g)} + H_2O_{(g)} \qquad \text{R3.1.5}$$

The balance between loss and formation of chlorine atoms from HCl is highly dependent on factors such as the presence of pCl^-, NO_x (NO_x=NO+NO_2), and HCl deposition rate.[12,23]

Measuring HCl in the gas phase is challenging as it readily adsorbs to surfaces. Methods for atmospheric HCl detection must be sensitive, robust, and selective and address HCl interactions with instrument surfaces. Mass spectrometry based measurement techniques have been developed for the detection of HCl in both the stratosphere and troposphere (e.g., Huey et al., (1996) and Marcy et al., (2004)).[24,25] Other methods include scrubbing ambient air using an annular denuder and/or a tandem mist chambers to collect HCl, followed by offline analysis such as ion chromatography (IC).[10,26–28] Online detection methods such as chemical ionization time of flight mass spectrometry (CI-ToF-MS),[11] negative ion proton transfer chemical ionization mass spectrometry (NI-PT-CIMS),[29] and negative mode atmospheric pressure chemical ionization coupled to triple quadrupole mass spectrometry (APCI-MS-MS) have been shown to be reliable and sensitive methods for HCl detection.[30] Limitations to these existing HCl measurement techniques include some or all of the following; detection limits that are not suitable for the low

level of HCl in the troposphere, slow time response, lack of portability, and calibration challenges. Spectroscopic techniques offer distinct advantages over some previous methods. Spectroscopic techniques for measuring atmospheric HCl reported by Hagen et al., (2014) and Wilkerson et al., (2021) have shown the precedent for fast time response, as well as sensitive, selective, and robust detection.[31,32] The portability and fast time response for instruments is of great importance for spatial resolution and is therefore a key factor for field deployment.

Measurements of HCl are typically calibrated using HCl from permeation devices and or standards in compressed gas cylinders. Method validation for HCl measurements are rare, but can reduce these uncertainties.[31,32] In this paper we demonstrate the versatility and validation of a new commercial cavity ring-down spectrometer (CRDS) for in-situ atmospheric gas phase HCl measurements. First, we compare this CRDS with existing HCl measurement techniques through lab and field intercomparisons. We then describe and characterize surface effects and recommend inlet configurations for best practices when conducting ambient sampling.

3.2 Materials and experimental methods

3.2.1 Chemicals

Reagent grade hydrochloric acid (HCl, 12 M) was used in permeation device construction (see Section 3.2.3). Potassium hydroxide (KOH) pellets were used to create scrubbing solution for permeation device gas collection. Commercially available reagents were obtained from Sigma-Aldrich (Oakville, Ontario, Canada). Nitrogen (grade 4.8) and Ultra Zero Air (grade 5.0) gases were from Praxair (Toronto, Ontario, Canada). Experiments used deionized water generated by a Barnstead Infinity Ultrapure Water System (Thermo Fisher Scientific, Waltham, Massachusetts, USA; 18.2 MΩ cm^{-1}). Annular denuder coating solution was prepared with reagent grade (>95.5%) sodium carbonate (Sigma-Aldrich, St. Louis, Missouri, USA), reagent grade glycerol

(Sigma-Aldrich, St. Louis, Missouri, USA), HPLC grade methanol (Fisher Chemicals, Ottawa, Ontario, Canada), and 18.2 MΩ cm^{-1} deionized water. Eluent for annular denuder IC analysis was prepared from sodium hydroxide solution (NaOH, 50% w/w, Thermo Fisher Scientific, Sunnyvale, California, USA). IC calibration standards were prepared through serial dilution of a mixed anion standard concentrate (Thermo Fisher Scientific, Dionex Seven-Anion II, P/N: 057590).

3.2.2 Cavity ring-down spectrometer (CRDS)

The Picarro G2108 Hydrogen Chloride Gas Analyzer system was used for all analyses (Figure A-1). The basic operating principles of this CRDS are similar to analogous Picarro greenhouse gas instruments that have been described in detail by Crosson (2008).[33] The CRDS consists of a tunable laser, a wavelength monitor, and a heated optical cavity (80 °C). All the components of this analyzer and internal stainless-steel fittings are contained within a heat-regulated metal case maintained at 45 °C. The laser radiation (1742 nm, 5739 cm^{-1}) is directed by a fiber optic cable to the wavelength monitor and optical cavity. The first overtone (2-0 absorption band) of HCl is easily discernable from other absorbing species (e.g., H_2O and CH_4), has a relatively high intensity compared to the fundamental absorption transition, and is accessible to near-infrared (IR) diode laser light sources. The optical cavity is fitted with three highly reflective dielectric-coated fused silica mirrors (R > 99.995%, ring down time constant of 53 µsec, equivalent to a path length of 16 km) oriented in an acute triangular arrangement supported by an invar housing. The reflectivity of the mirrors is measured from the laser signal loss in an analyte-free optical cavity under inert gas flow. The CRDS flow rate is 2 L min^{-1} and the cavity is held at a reduced pressure of 18.70 ± 0.02 kPa (140.0 Torr) thermostated to 80.000 ± 0.005°C. One mirror is mounted on a piezoelectric actuator to achieve optical resonance between the laser frequency and the longitudinal modes of the cavity. The laser is shut off rapidly (<1 µsec) once resonance is

achieved. A photodetector monitors the decay of the photons exiting the cavity through another mirror. Custom electronics digitize the signal for fitting of an exponential decay; the time constant of the decay, τ, is converted to absorbance, α, using the expression

$$\alpha = 1 / c\tau - 1 / c\tau_0 \qquad \text{(E1)}$$

where c is the speed of light. The instrument measures 30 specific frequencies within ~1 cm^{-1} centered at 5739 cm^{-1} to fit the absorption spectra of trace species in this region (see Figure A-2). HCl, H_2O, and CH_4 mixing ratios are reported every 2 seconds, though the true time response of the measurement method is limited by surface effects (see Section 3.3.4). Gaseous inorganic chlorine reservoir species (e.g., $ClNO_2$) cannot thermally dissociated under the cavity (80 °C) conditions.[34] The instrument zero measurement drift is reduced by a high precision distributed feedback laser centered at 5739.2625 cm^{-1} coupled with a custom-designed wavelength monitor to determine the frequency axis of each spectrogram. To mitigate particulate matter optical extinction and surface deposition on the high reflectivity mirrors, two high efficiency particulate air (HEPA) filters are placed upstream of the cavity, contained within the 45 °C heat-regulated compartment.

3.2.3 In-house HCl permeation device validation

The in-house assembly of HCl permeation devices (PDs) is described in detail in Lao et al., (2020).[35] Briefly, 200 µL of 12 M aqueous HCl solution was pipetted into a 7.62 cm perfluoroalkoxy (PFA) tube (3 mm i.d. with 1 mm thickness) plugged at both ends with porous polytetrafluoroethylene (PTFE) (1 cm length by 3.17 mm o.d.). The polymers allow a consistent mass of HCl to permeate at a given temperature and pressure. An aluminum block that was temperature-controlled using a cartridge heater (Omega™; CIR-2081/120V, Saint-Eustache, QC, Canada) housed the PD and was regulated to 60.0 ± 0.1 °C by a process controller. Dry N_2 flowed through a PFA tube (1.27 cm o.d.) in the block, containing the PD. Stable flows of 49 ± 2 standard

cubic centimeters per minute (sccm) through the oven were maintained with a 50 µm diameter critical orifice (Lenox laser, Glen Arm, Maryland, USA, 15 psi; SS-4-VCR-2-50). Flows were measured using a DryCal Definer 220 (Mesa Labs, Lakewood, Colorado, USA). The mass emission rate of HCl from the PD was quantified by scrubbing into a 25 mL glass impinger containing 1 mM KOH over 24 h followed by analysis using IC with conductivity detection (CD). Mass emission rates for the PD were determined as 140 ± 18 ng min^{-1} (n=3, ± 1σ) at 60 °C.

3.2.4 Laboratory intercomparison

A laboratory intercomparison between the CRDS and offline-measured HCl scrubbed into a basic solution of 100 mM KOH by delivering gaseous HCl from the permeation device to the sampling systems. The 140 ng min^{-1} of HCl in dry N_2 from the PD was mixed into a zero air dilution flow of 2.1 to 8.0 L min^{-1}, to provide standard addition HCl mixing ratios that ranged from 12 to 45 ppbv.

The dilution flow was maintained using a 10 L min^{-1} mass flow controller (GM50A, MKS instruments, Andover, Massachusetts, USA). All inlet lines and fittings were kept at ambient temperature (~25 °C) and were made of PFA unless stated otherwise. The inlet mixing line between the PD emissions and the humidified dilution flow was 3.17 mm i.d. and 45 cm in length. Residence times for HCl in the sampling line ranged from 0.02 to 0.08 seconds. To vary relative humidity (RH), a controlled flow of zero air was directed into a glass impinger at room temperature containing deionized water to yield a water-saturated air stream. The humidified flow was passed through a 2 µm Teflon filter (TISCH scientific, North Bend, Ohio, USA) in a PFA holder to prevent any aqueous droplets from entering the experimental lines. The RH was set by mixing with dry zero air to generate 0, 20, 50, and 80 % RH values.

3.2.5 Ambient intercomparison

An ambient intercomparison was undertaken by measuring outdoor air with the CRDS in parallel with sodium carbonate-coated annular denuders. A total of 11 denuder samples were collected alongside continuous CRDS observations, each for approximately 24 hours between 4–11 April 2019. The measurement site was the air quality research station, located on the roof of the Petrie Science and Engineering building at York University in Toronto, Ontario, Canada (43.7738° N, 79.5071° W, 220 m above sea level). All indoor inlet lines and fittings were kept at room temperature while the outdoor temperature ranged from -2 to 14 °C. All inlet lines and fittings were made of PFA unless stated otherwise. A full schematic of the sampling apparatus indicating the separation between the outdoor and indoor inlet positions is provided in Figure A-5. A 22 L min^{-1} sampling flow was pulled through a URG Teflon Coated Aluminum Cyclone (URG Corporation, Chapel Hill, North Carolina, USA) with a 2.5 µm cut-off for particulate matter. The inlet lines were such that each sampling setup collected HCl at equal residence time to ensure equivalent wall losses of HCl. The shared inlet line was 4.65 m in length and had an i.d. of 4.76 mm. The flow was split between the 1.5 m denuder sampling line (20 L min^{-1}) and the 0.15 m CRDS sampling line (2 L min^{-1}), yielding a 0.375 sec residence time for both methods. The denuder line flow was equally divided into two multichannel etched glass annular denuders (URG Corporation, Chapel Hill, North Carolina, USA, 4 channel, 242 mm length, URG-2000-30x242-4CSS) at 10 L min^{-1}. The denuders collected HCl in parallel to each other with flows controlled using two separate 10 L min^{-1} mass flow controllers (GM50A, MKS instruments). Denuders were coated with a solution of 2% w/w sodium carbonate and 0.1% w/w glycerol in a solution of 1:1 methanol:water. A 15 mL aliquot of coating solution was dispensed into a denuder and two polypropylene caps affixed. The sealed denuders were inverted and rotated for a few minutes to ensure an even coating. The excess coating solution was decanted, and the denuder was dried for

15 min with 2 L min^{-1} of zero air. After sampling, denuders were extracted with 2 aliquots of 5.00 mL deionized water, following the same sealing and inversion procedure, for a total extraction volume of 10.00 mL. Extracts were collected into a 15 mL polypropylene tube for storage at 4 °C until analysis. Instances of flagged instrument errors in the CRDS data during ambient observations were removed as standard practice in quality control procedures (see Figure A-3). The loss of observational data during such periods corresponds to a negative bias. The CRDS data loss during a given denuder sampling period was included in setting the overall measurement error when intercomparing measurements.

3.2.6 Ion chromatography analysis

Samples collected into an impinger from the HCl PD were analyzed as the chloride anion by IC-CD using an ICS-2100 (Thermo Fisher Scientific, Sunnyvale, California, USA) according to the method described in Place et al., (2018).[36] Annular denuder extracts were analyzed by IC-CD using an ICS-6000 (Thermo Fisher Scientific, Sunnyvale, California, USA). Details of both separation methods can be found in the Appendix A. Chloride was quantified using external calibration with a 5-point calibration curve. Two check standards, located at the high and low ends of the working range, were used to evaluate the accuracy of quantification.

3.3 Results and discussion

3.3.1 Suitability for atmospheric measurements

The selectivity of this CRDS analyzer arises from monitoring a high-intensity spectral line (5739.2625 cm^{-1}). The absorption used by this instrument is suitable for HCl measurements in the ambient atmosphere because abundant atmospheric gaseous species such as CO, CO_2, NO_x, and N_2O do not have major absorption features in the same region.[37,38] Absorption features of H_2O and CH_4 in this spectral region are part of the fitting parameters used to determine number densities of HCl, as described in Section 3.2.2. Most organic and inorganic compounds commonly found at

trace levels in the atmosphere do not absorb strongly in this region.[37,38] For these compounds to interfere with the CRDS measurement, their mixing ratios would need to be very high (>10 parts per million by volume, ppmv). Under conditions where the peak shape is compromised by the presence of interfering absorbing species or instrument instabilities (e.g., cavity pressure fluctuations), the instrument fitting is interrupted and the "bad" data is flagged, thereby allowing simple quality control (see Figure A-3).

The limit of detection (LOD) of the CRDS analyzer is suitable for expected HCl levels in the atmosphere. Instrument LODs were calculated as three times the Allan-Werle deviation (Figure 3-1, Hagen et al., 2014) when overflowing a 15 cm inlet (3.17 mm i.d.) with zero air directed into the CRDS for ~10 hours. The LODs determined in the CRDS measurements for 2 second, 30 second, 5 minute, and 1 hour integration times were 66, 18, 5, and 2 pptv, respectively. Similarly, precision was determined from the Allan-Werle deviation in the blank over the same 10 hours of zero air sampling. Precision in a 2 second, 30 second, 5 minute, and 1 hour integration time was 22, 6, 2, and 0.8 pptv, respectively.

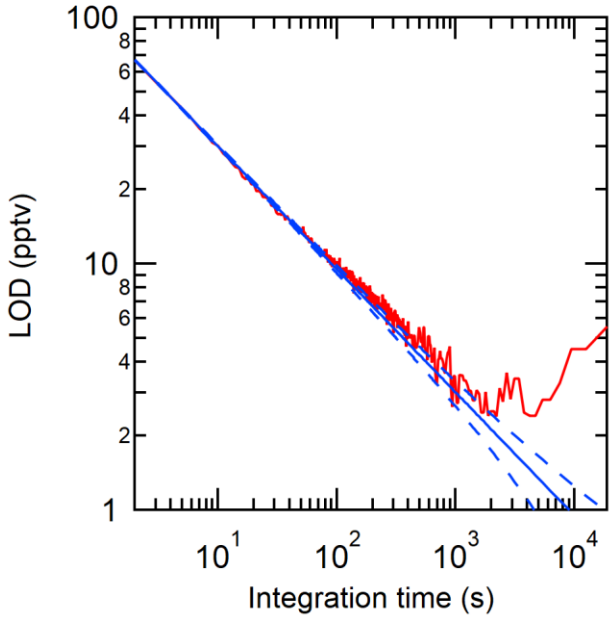

Figure 3-1. Allan-Werle deviation (3σ) in the optical cavity purged with zero-air (red line) shown with the ideal deviation (no drift, solid blue line) and associated error in the deviation (dashed blue line).

3.3.2 Instrument performance

This CRDS has many advantages compared to methods previously used to measure HCl in the ambient atmosphere (Table 3-1). The LOD and precision of the instrument is comparable to prior high time-resolution methods, allowing changes in HCl mixing ratio of a few pptv to be measured. The accuracy/uncertainty is the hardest to compare due to the differences in assessment. A particular challenge is that other methods require external calibrations to determine accuracy and a stable, accurately calibrated HCl source at atmospherically relevant mixing ratios is challenging to obtain.[35,39] In contrast, spectroscopic techniques offer a distinct advantage as they are absolute measurements and accuracy determinations rely on propagating uncertainty in the measured parameters (i.e., wavelength and the time constant τ). In the absence of determining accuracy of the CRDS from its operating parameters we use the deviations in our intercomparisons to estimate the accuracy of the full system, i.e., the instrument and ambient sampling inlet combined. We assess the total method uncertainty using intercomparisons with the gold standard for atmospheric acid detection (EPA Compendium method IO-4.2, United States Environmental Protection Agency)[26] due to the greater uncertainty when considering the potential total system error from the sorption/desorption to all sampling surfaces (i.e., instrument and inlet). We measured that the accuracy of the analyzer ranges from 5 to 15%. This is a conservative range based on the methods we used to validate the instrument, which is further described in Section 3.3.3. The response time of the CRDS used in this work is fast compared to most measurements; the limitation for all online-line methods compared in Table 3-1 is not the measurement frequency, but rather the time required for HCl to adsorb and desorb from the inlet to the sample stream, which is discussed further in Section 3.3.4. Lastly, instrument size and power consumption of this

CRDS are much lower than many other techniques and are major advantages when considering use in the field, particularly for mobile platforms.

Table 3-1. Performance characteristics of CRDS HCl analyzer compared to previously reported methods.

Instrument	LOD	Accuracy/ Uncertainty	Precision	Measurement frequency	Instrument Size	Power Consumption	Reference
Near-IR CRDS	<18 pptv[a] (30 sec)	5–15%	6 pptv (30 sec)	2 s[e]	31.75 kg 43.2 x 17.9 x 44.6 cm	110 W (analyzer) 75 W (pump)	This study
Near-IR CRDS	60 pptv[a] (1 min)	<10%	20 pptv (1 min)	<15 s	NR	NR	Hagen et al. (2014)[31]
Off-axis integrated cavity output spectrometer (OA-ICOS)	78 pptv (30 sec)	<11%	26 pptv (30 sec)	1 s	NR	NR	Wilkerson et al. (2021)[32]
Aircraft laser infrared absorption spectrometer	33 pptv[b]	10 %	0.1 ppbv (30 sec)	<30 s	72 kg	NR	Webster et al. (1994), Voss et al. (2001)[40,41]
Quartz-enhanced photoacoustic spectroscopy (QEPAS)	550 ppbv[a]	NR	526 ppbv	NR	NR	NR	Ma et al. (2016)[42]
Acetate CI-ToF-MS	97 pptv[a]	30%	32.3 pptv	<1 s	59 x 42 x 83 cm	<2000 W peak	Crisp et al. (2014)[11]
Iodide CI-HR-ToF-MS	30 pptv[a] (30 sec)	30%	10 pptv (30 sec)	0.22 s	~ 59 x 42 x 83 cm	<2000 W peak	Lee et al. (2018)[43]
Sulfur pentaflouride ion trap CIMS	66 pptv[a]	10%	22 pptv	1.6 s	NR	NR	Jurkat et al. (2010)[44]
APCI-MS-MS	335 pptv[a]	NR	NR	5 s	NR	< 17.5 kW	Karellas et al. (2003)[30]
Tandem mist chamber and IC-CD	48 pptv[c]	<25 %	24 pptv[c]	2 h	NR	NR	Keene et al. (2009), Keene et al. (2007)[27,28]

Annular denuder and IC-CD	6.9–42 pptv[d]	10%	NR	Hours–Days	>10 kg	400 W (Sampling equipment only)	This study

a: 3σ, b: predicted assuming a minimum detectable line-center absorption of 1×10^{-5} can be achieved in 30 s, c: precision (σ) determined from averaged paired measurements in 2 h samples on IC-CD and LOD was calculated at 2σ, d: 3σ calculated range for a 24-hour sampling time from three denuder method blanks, e: instrument data reporting frequency. The true measurement frequency will also be affected by surface effects, as described in section 3.4, and NR: not reported.

3.3.3 Laboratory and ambient intercomparison

We compared the CRDS analyzer-measured HCl with the gas standard mixing ratios provided by an IC-certified PD under dry conditions and observed a close to 1:1 correlation. We explored 5 mixing ratios 12, 16, 21, 32, and 45 ppbv (Figure 3-2). These levels are greater than what are observed in the ambient atmosphere but demonstrate good signal response linearity. When the HCl gas entrained in flows of higher RH (≥ 50 %) a negative bias was observed, although the measurements generally remained within the quantified error in the PD output. Negative bias from the provided HCl mixing ratios at 50 % and 80 % RH were 9.6 % and 14.9 %, respectively. As described above, there is no spectroscopic water absorption interference in the HCl measurement indicating that water increased HCl losses to gas handling surfaces for experiments conducted in humidified air. Inlet surface effects are well established for gaseous strong acids and bases, as these compounds readily sorb at interfaces (e.g., Eisele and Tanner (1993), Kim et al. (2008), Neuman et al. (1999), Pszenny et al. (1993), Roscioli et al. (2016)).[45–49] The comparison presented here is a best-case scenario because the sampled mixing ratios were much greater than expected in the ambient atmosphere, and therefore less likely to be impacted by surface effects. Surface effects under humid conditions necessitated the mitigation and quantification efforts described further in Section 3.3.4. To practically validate the CRDS under real-world conditions and atmospherically relevant mixing ratios, an ambient intercomparison was performed over a period of 7 days (4–11 April 2019).

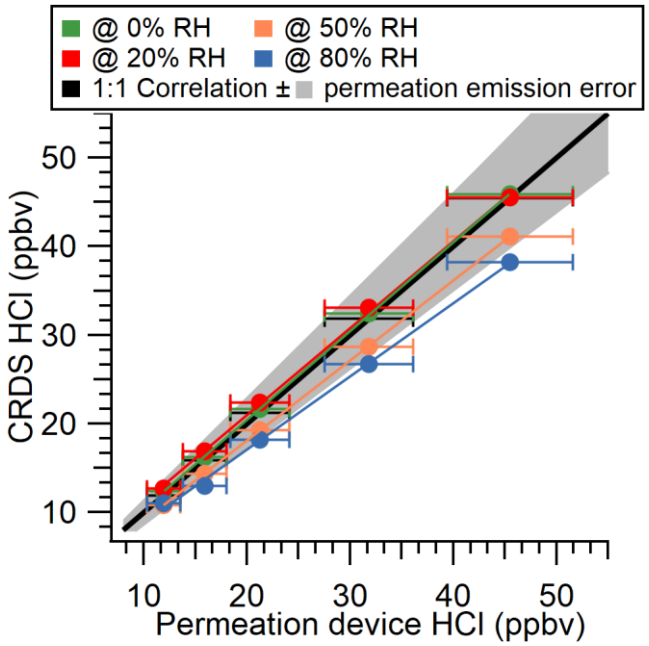

Figure 3-2. Comparison of CRDS HCl measurements and output from an HCl permeation device over a range of RHs. Error bars in the x direction represent propagated IC measurement error, while error bars in the y direction represent the standard deviation of online sampling plateau for each mixing ratio (low magnitudes mean these error bars do not extend beyond the points). A 1:1 correlation (solid black line) is shown with the uncertainty in the permeation device emission rate (shaded grey area).

Online HCl detection by CRDS showed good agreement with HCl mixing ratios quantified from ten annular denuder extracts collected according to EPA Compendium method IO-4.2,[26] which is a standard offline method for quantitation of acidic atmospheric gases (see Figure 3-3a). Measurements from the two instruments were linearly related with a slope of 0.97 ± 0.15, as determined by orthogonal least distance regression, with a y-intercept of -0.001 ± 0.021. Half of the measurements are within 10 % of a 1:1 correlation and the remaining half fall within 25 %. To further validate the comparison a linear correlation coefficient (see Figure A-6) of 0.93 ± 0.14 was determined for the two methods and shows good agreement with the orthogonal least distance regression. Changes in RH had no systematic bias on the correlation. Our intercomparison indicates that CRDS measures HCl with comparable results to those obtained by carbonate-coated

annular denuders. While the latter requires offline analysis, the CRDS has the additional benefit of continuous high time resolution measurements at 0.5 Hz and dramatically better precision.

Although average HCl measurements between the CRDS and denuders agreed well, much of the useful temporal variability were lost in the time-integrated denuder data (Figure 3-3b). For example, from 19:00 April 5 to 01:00 April 6 (All times EDT) the CRDS measured mixing ratios between 91 and 598 pptv. This rapid change of mixing ratios is not captured by the 24-hour average denuder-measured mixing ratio of 348 pptv. The fast time response of the CRDS also captured other rapidly changing HCl features such as the peak observed on between 00:00–06:00 on April 7. The 6-hour event started at 80 pptv and increased at a rate of 1.2 pptv min^{-1} to 230 pptv over ~120 minutes, followed by a decrease at a rate of 0.5 pptv min^{-1} for ~240 minutes to 98 pptv. The fast time response of the CRDS on the order of minutes is crucial when applying the technique to the real atmosphere for the purpose of fully constraining the sources and sinks for HCl, for which many precursors have similar lifetimes, and ultimately improve our understanding of the Cl budget.[11]

Results from the laboratory and ambient intercomparisons were used to determine the accuracy of the HCl analyzer as 5 to 15 %. The lower bound of uncertainty (5 %) was determined from the laboratory intercomparison under the optimal dry conditions (Figure 3-2). The upper bound of uncertainty (15 %) was consistent across the laboratory intercomparison under the highest RH (80%) conditions tested (Figure 3-2) and the standard deviation of the orthogonal distance regression slope from the ambient intercomparison (Figure 3-3a).

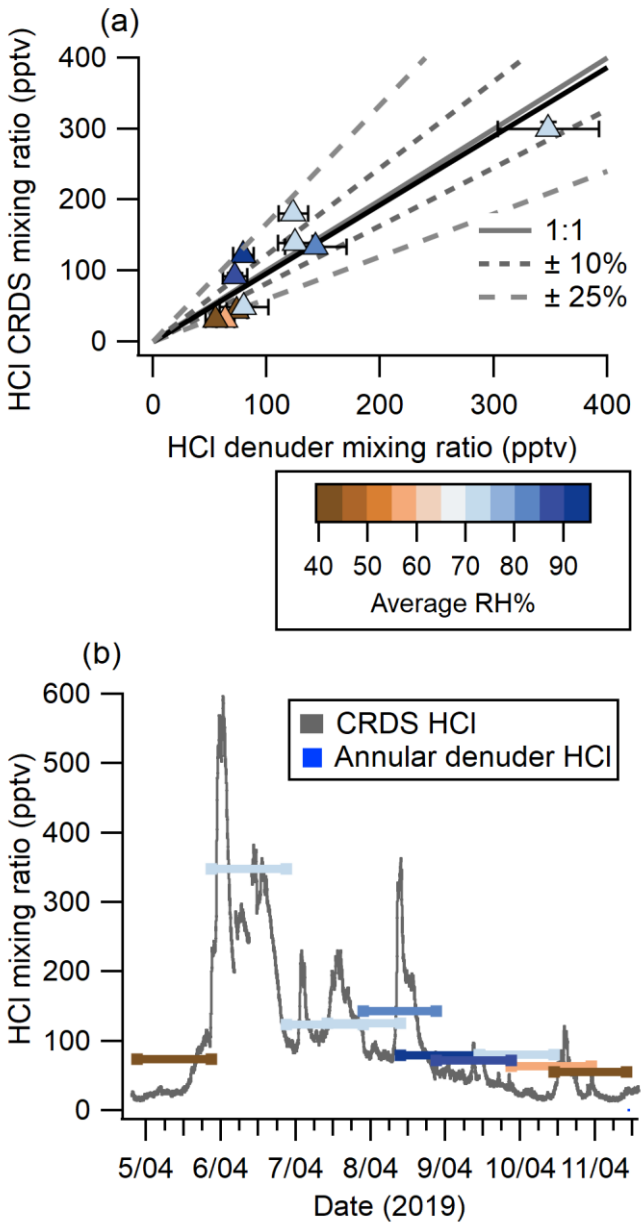

Figure 3-3. (a) Comparison of HCl measured 4–11 April 2019 using annular denuders and CRDS (averaged to the collection time of denuders). Denuder error bars are derived from the error in the IC calibration, standard deviation of method blanks, and extraction recovery. CRDS measurement errors are the precision in a single measurement combined with data loss for flagged instrument errors. Also shown are a 1:1 correlation line (solid grey), 10 % (short grey dash) and 25 % (long grey dash) deviation from 1:1, and the orthogonal distance regression (solid black). Points are coloured by the average RH during sampling. (b) Continuous HCl mixing ratio timeseries by CRDS overlaid with averaged 24-hour denuder measurement analyzed by IC with lines coloured according to the average RH during sampling.

3.3.4 Sampling line and instrument response time assessment

We have thus far demonstrated the efficacy of the CRDS for accurately analyzing gas standards and ambient HCl. However, the potential for sampling losses or desorption sources of surface-active gases that could affect the quality of such measurements is ubiquitous, and the study of these effects are well established.[11,49–51] This makes quantification a challenge as there are typically long equilibration times associated with signal stabilization. Long equilibrations make fast time response detection difficult without first characterizing line sorption and desorption, followed by making inlet modifications to minimize losses.[50,52,53] To ensure accurate field measurements of HCl, a characterization of the magnitude of HCl loss and desorption during sampling was made. The response time of an instrument to a rapid change in HCl can be calculated by both the time it takes for the measurement to go from zero to 100 % of the HCl quantity being delivered, as well as the time it takes to return from the HCl quantity being delivered back to zero.

Inlet and instrument surface effects for surface active gases such as HCl can be characterized by fitting decay curves to a double exponential;[50,51,54,55]

$$y = y_0 + A_1 e^{\left(-\frac{t-t_0}{\tau_1}\right)} + A_2 e^{\left(-\frac{t-t_0}{\tau_2}\right)} \quad \text{(E2)}$$

Where y is the mixing ratio of HCl, y_0 is the mixing ratio at the end of the decay, A_1 and A_2 are proportionality coefficients that determine how much the decay is governed by τ_1 and τ_2 respectively, t is the time elapsed, and t_0 is the initial time. The first time constant (τ_1) represents air exchange within the instrument, while the second (τ_2) is the surface interaction equilibrium time between HCl adsorbed to surfaces and the overlying airstream mixing ratio. The only term in this equation that can be optimized for the CRDS is τ_2, which can be reduced by decreasing the amount of time HCl interacts with inlet surfaces. The sampling flow rate and cavity temperatures

are constant for the commercial software and not adjustable, therefore changing the value of τ_1 was not explored in this study. In most reports τ_1 represents the largest change in signal and represents instrument response time. For example, Whitehead et al., (2008) found that τ_1 values governed >75% (i.e., A_1) of changes in measured NH_3.[56] For the CRDS, measured values of τ_1 were between 5 and 10 seconds under all conditions and could be improved with a faster inlet flowrate for the CRDS to subsample from.

An additional set of experiments was undertaken in which a 24 ppbv HCl standard was sampled while varying RH from 0 to 33% (Figure 3-4). The effect of RH on the response time of the CRDS was measured using a method similar to that described in Section 3.2.4. The HCl standard gas was sampled over three 10 min pulses at each RH (± 2%). The HCl standard was introduced into a 3.17 mm i.d. PFA tube and 10 cm long inlet line. Data was background corrected to levels measured prior to the standard addition and the signal was normalized to the HCl enhancement during the final 10 seconds of each HCl pulse. Due to a lack of inlet characterization for systems measuring HCl, we compare our decay constants to literature values for compounds with similar surface-active properties (e.g., HNO_3 and NH_3). The instrument exchange rate (τ_1) values for spectroscopic methods measuring HNO_3 and NH_3 are generally faster than our measured values for HCl. However, it should be noted that measurements of τ_1 reflect differences in sampling flow rates and internal volume and are likely affected by the internal filters present in the HCl CRDS. Typically, τ_1 was <2 seconds,[49–51] but could be as high as 4.5 seconds for larger pulses (1 ppmv) of analyte.[49] We observed a highly variable surface interaction equilibrium time constant (τ_2), with values ranging between 97 and 350 seconds. Reported values of τ_2 for other surface-active gases are similarly variable, with values <50 seconds for heated short clean inlets,[49–51] and ~300 seconds for a contaminated inlet measuring NH_3.[51] Major differences in the surface area

between our instrument and the instruments to which we compare are likely to cause τ_2 differences. Our method employs the use of three filters that increase the gas to surface interactions, and therefore increase our equilibrated response time τ_2.

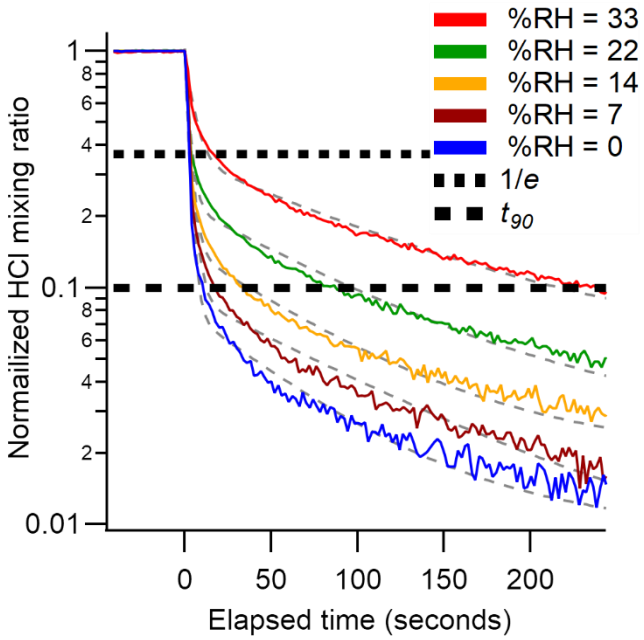

Figure 3-4. Background corrected and normalized signal decay curves observed for pulsed HCl (24 ppbv) performed at various RHs. Dashed grey lines represent a double exponential fit to the average of three cycles at each water mixing ratio. The short and long dashed black lines indicate 37 % (1/e) and 90 % (t_{90}) decrease from the initial signal, respectively.

Another method for quantifying response time is by calculating the e-folding (1/e) signal loss with respect to time. Calculated e-folding response times demonstrated the fast exchange within the system with values comparable to τ_1. Similarly, a signal decrease of 90% (t_{90}) illustrates the total decay of the sampling line. Using e-folding response time and t_{90} offers a better visual understanding of the relative roles for instrument and inlet responses and the impacts of increasing RH. We summarize the double exponential decay constants, e-folding response time, and t_{90} for the rise and decay of HCl mixing ratios from pulses delivered to the instrument in Table 3-2 and tables A-1–4. Increasing the RH increases the response time of the inlet (Figure 3-4). At the highest

experimental RH (33 %), τ_2 is increased by almost a factor of two compared to dry conditions, from seconds to minutes. At lower mixing ratios the higher RH increased the response times to a greater extent (Table 3-2 and Tables S1–S4). The increased response time at high ambient RH would not compromise stationary measurements in which HCl mixing ratios changed on time scales of minutes to hours but would not capture more rapid changes. The largest impact on CRDS time response likely comes from unavoidable effects of partitioning on the large surface area of the HEPA filters located before the optical cavity. Minimizing inlet effects for the CRDS where observation of HCl mixing ratio changes over <1 min is required (e.g., aircraft or mobile measurements) are most important. The wall interactions of HCl can be reduced by increasing the inlet flow rate and/or decreasing the tubing length.[53]

Physical approaches to improving inlet response include inlet material substitution, heating, and pressure reduction, to reduce adsorption of surface-active analytes through removal of surface water and promoted mass transfer of analytes to the gas phase.[57] Deming et. al., (2019) found that PFA tubing had the lowest delay times for semivolatile compounds and would likely extend to small polar molecules like HCl.[52] For a clean thermally-equilibrated inlet, HCl artifacts can be minimized, but if semivolatile aerosol chloride is sampled (e.g., NH_4Cl), the thermodynamic equilibrium can be shifted to result in a positive bias in the HCl measurement, equivalent to similar considerations when measuring HNO_3 and NH_3.[50,56,57] While HEPA filters prevent aerosol from entering the cavity, their elevated temperature (45 °C) could lead to volatilization bias and therefore the use of an inlet filter held at ambient temperature to reduce such effects is recommended at a minimum.

Chemical approaches can also help mitigate adsorption of surface-active molecules to inlet surfaces through derivatization or passivation. The silanization of glass or stainless-steel to form

an inert fluorinated or silicon coating on a virtual impactor or the introduction of a gaseous fluorinated compound that adsorbs competitively to instrument surfaces in place of the analytes have been demonstrated to substantially reduce surface adsorption on PFA.[32,49–51,55] However, environmental impacts must be considered when constantly adding fluorinated compounds to sampling flows as they may have deleterious environmental consequences.[58] In particular, perfluorobutanesulfonic acid, the fluorinated chemical suggested for passivating inlets,[49] is subject to usage restrictions in some European countries based on potential negative human and environmental health impacts.[59–61] The high surface activity of perfluorobutanesulfonic acid is likely to cause issues in the analyzer used in this work because the gas sample comes into direct contact with the high reflectivity mirrors. Acid deposition onto mirrors will degrade their reflectivity. Silicon coatings on all plumbed surfaces have been successfully used for atmospheric HCl measurements,[32] and recommended for applications where PFA use is impractical. Although a direct comparison has not been conducted for HCl, PFA inlet material has been reported to yield better response times than silicon coatings for nitric acid.[45] Differences in instrument configurations and applications may warrant the use of different inlet materials and coatings for successful measurement of atmospheric HCl.

Table 3-2. Summary of the fit parameters for the double exponential decay curves as a function of mixing ratio and humidity, e-folding response time, and t_{90}.

Mixing ratio (ppbv)	Residence time (seconds)	RH (%)	τ_1 (seconds)	τ_2 (seconds)	$1/e$ (seconds)	t_{90} (seconds)
12	0.021	0	10.3	123	26.5	101
16	0.028	0	9.6	200	24.7	82
21	0.037	0	10.1	300	26.4	74
24	–	0	2.7	97	2.5	10
		7	5.0	124	2.5	18
		14	5.0	114	2.5	32
		22	5.0	123	3.9	86

		33	10.0	189	16.1	239
32	0.056	0	9.4	188	24.5	62
45	0.079	0	9.7	350	25.6	54

3.4 Conclusions

The suitability of a CRDS analyzer for measuring ambient atmospheric HCl were explored through laboratory and ambient air intercomparisons, assessing their inlet and analyzer sampling challenges to established atmospheric sampling techniques for strong acids. In comparison to other reported instrumentation, the CRDS is shown performing similar or better than the most sensitive HCl measurements reported. As with many in situ measurements of HCl, the most significant limitation is adsorption/desorption loss and release on inlet surfaces, with the deposition effects increasing with increasing RH and decreasing HCl mixing ratios. Given the longstanding knowledge of these issues for surface active gases, such as HNO_3 and NH_3, there are a variety of chemical and physical options, discussed in this study, to mitigate inlet effects and achieve faster response times for the CRDS. Increasing the flowrate of the sampling inlet, while maintaining laminar flow, is the simplest approach to reducing surface effects discussed in Section 3.3.4. Spectra capturing errors in the measurement of HCl for the CRDS can occur at high levels of VOCs (e.g., near emission point sources or biomass burning plumes) or instrument instabilities (e.g., pressure fluctuations), however potential instrument errors are minimal under most operating and atmospheric conditions. Finally, comparison with annular denuder observations agreed within the combined uncertainties, with the CRDS measurement rate demonstrating the power of capturing transient events that are important to constraining atmospheric chlorine chemistry (e.g., photolysis of precursors, thermodynamic partitioning, and direct emissions).

3.5 References

(1) Solomon, S. Stratospheric Ozone Depletion: A Review of Concepts and History. *Rev. Geophys.* **1999**, *37* (3), 275–316. https://doi.org/10.1029/1999RG900008.

(2) Simpson, W. R.; Glasow, R. Von; Riedel, K.; Anderson, P.; Ariya, P.; Bottenheim, J.; Burrows, J.; Carpenter, L. J. Halogens and Their Role in Polar Boundary-Layer Ozone Depletion. *Atmos. Chem. Phys.* **2007**, 4375–4418.

(3) Simpson, W. R.; Brown, S. S.; Saiz-Lopez, A.; Thornton, J. A.; Von Glasow, R. Tropospheric Halogen Chemistry: Sources, Cycling, and Impacts. *Chem. Rev.* **2015**, *115* (10), 4035–4062. https://doi.org/10.1021/cr5006638.

(4) Osthoff, H. D.; Roberts, J. M.; Ravishankara, A. R.; Williams, E. J.; Lerner, B. M.; Sommariva, R.; Bates, T. S.; Coffman, D.; Quinn, P. K.; Dibb, J. E.; et al. High Levels of Nitryl Chloride in the Polluted Subtropical Marine Boundary Layer. *Nat. Geosci* **2008**, *1* (5), 324–328.

(5) Thornton, J. A.; Kercher, J. P.; Riedel, T. P.; Wagner, N. L.; Cozic, J.; Holloway, J. S.; Dubé, W. P.; Wolfe, G. M.; Quinn, P. K.; Middlebrook, A. M.; et al. A Large Atomic Chlorine Source Inferred from Mid-Continental Reactive Nitrogen Chemistry. *Nature* **2010**, *464*, 271.

(6) Young, C. J.; Washenfelder, R. A.; Roberts, J. M.; Mielke, L. H.; Osthoff, H. D.; Tsai, C.; Pikelnaya, O.; Stutz, J.; Veres, P. R.; Cochran, A. K.; et al. Vertically Resolved Measurements of Nighttime Radical Reservoirs in Los Angeles and Their Contribution to the Urban Radical Budget. *Environ. Sci. Technol.* **2012**, *46* (20), 10965–10973. https://doi.org/10.1021/es302206a.

(7) Young, C. J.; Washenfelder, R. A.; Edwards, P. M.; Parrish, D. D.; Gilman, J. B.; Kuster, W. C.; Mielke, L. H.; Osthoff, H. D.; Tsai, C.; Pikelnaya, O.; et al. Chlorine as a Primary Radical: Evaluation of Methods to Understand Its Role in Initiation of Oxidative Cycles. *Atmos. Chem. Phys.* **2014**, *14* (7), 3427–3440. https://doi.org/10.5194/acp-14-3427-2014.

(8) Sherwen, T.; Schmidt, J. A.; Evans, M. J.; Carpenter, L. J.; Großmann, K.; Eastham, S. D.; Jacob, D. J.; Dix, B.; Koenig, T. K.; Sinreich, R.; et al. Global Impacts of Tropospheric Halogens (Cl, Br, I) on Oxidants and Composition in GEOS-Chem. *Atmos. Chem. Phys.* **2016**, *16* (18), 12239–12271. https://doi.org/10.5194/acp-16-12239-2016.

(9) Haskins, J. D.; Jaeglé, L.; Shah, V.; Lee, B. H.; Lopez-Hilfiker, F. D.; Campuzano-Jost, P.; Schroder, J. C.; Day, D. A.; Guo, H.; Sullivan, A. P.; et al. Wintertime Gas-Particle Partitioning and Speciation of Inorganic Chlorine in the Lower Troposphere Over the Northeast United States and Coastal Ocean. *J. Geophys. Res. Atmos.* **2018**, *123* (22), 12,812-897,916. https://doi.org/10.1029/2018JD028786.

(10) Young, A. H.; Keene, W. C.; Pszenny, A. A. P.; Sander, R.; Thornton, J. A.; Riedel, T. P.; Maben, J. R. Phase Partitioning of Soluble Trace Gases with Size-Resolved Aerosols in near-Surface Continental Air over Northern Colorado, USA, during Winter. *J. Geophys. Res. Atmos.* **2013**, *118* (16), 9414–9427. https://doi.org/10.1002/jgrd.50655.

(11) Crisp, T. a; Lerner, B. M.; Williams, E. J.; Quinn, P. K.; Bates, T. S.; Bertram, T. H. Observations of Gas Phase Hydrochloric Acid in the Polluted Marine Boundary Layer. *J. Geophys. Res. Atmos.* **2014**, 6897–6915. https://doi.org/10.1002/2013JD020992.Received.

(12) Finlayson-Pitts, B. J.; Ezell, M. J.; Pitts, J. N. Formation of Chemically Active Chlorine Compounds by Reactions of Atmospheric NaCl Particles with Gaseous N2O5 and

ClONO2. *Nature* **1989**, *337* (6204), 241–244. https://doi.org/10.1038/337241a0.

(13) Wang, X.; Jacob, D. J.; Eastham, S. D.; Sulprizio, M. P.; Zhu, L.; Chen, Q.; Alexander, B.; Sherwen, T.; Evans, M. J.; Lee, B. H.; et al. The Role of Chlorine in Global Tropospheric Chemistry. **2019**, 3981–4003.

(14) Keene, W. C.; Khalil, M. A. K.; Erickson, D. J.; McCulloch, A.; Graedel, T. E.; Lobert, J. M.; Aucott, M. L.; Gong, S. L.; Harper, D. B.; Kleiman, G.; et al. Composite Global Emissions of Reactive Chlorine from Anthropogenic and Natural Sources: Reactive Chlorine Emissions Inventory. *J. Geophys. Res. Atmos.* **1999**, *104* (D7), 8429–8440. https://doi.org/10.1029/1998JD100084.

(15) Butz, A.; Dinger, A. S.; Bobrowski, N.; Kostinek, J.; Fieber, L.; Fischerkeller, C.; Giuffrida, G. B.; Hase, F.; Klappenbach, F.; Kuhn, J.; et al. Remote Sensing of Volcanic CO2, HF, HCl, SO2, and BrO in the Downwind Plume of Mt. Etna. *Atmos. Meas. Tech.* **2017**, *10* (1), 1–14. https://doi.org/10.5194/amt-10-1-2017.

(16) Gard, E. E.; Kleeman, M. J.; Gross, D. S.; Hughes, L. S.; Allen, J. O.; Morrical, B. D.; Fergenson, D. P.; Dienes, T.; Ga, M. E.; Johnson, R. J.; et al. Direct Observation of Heterogeneous Chemistry in the Atmosphere. **1998**, *279* (February).

(17) Valach, R. The Origin of the Gaseous Form of Natural Atmospheric Chlorine ’. *Tellus Ser. B Chem. Phys. Meteorol.* **1967**.

(18) Clegg, S. L.; Brimblecombe, P. Potential Degassing of Hydrogen Chloride from Acidified Sodium Chloride Droplets. *Atmos. Environ.* **1985**, *19* (3), 465–470. https://doi.org/https://doi.org/10.1016/0004-6981(85)90167-2.

(19) Bondy, A. L.; Wang, B.; Laskin, A.; Craig, R. L.; Nhliziyo, M. V; Bertman, S. B.; Pratt, K. A.; Shepson, P. B.; Ault, A. P. Inland Sea Spray Aerosol Transport and Incomplete Chloride Depletion: Varying Degrees of Reactive Processing Observed during SOAS. *Environ. Sci. Technol.* **2017**, No. 51, 9533–9542. https://doi.org/10.1021/acs.est.7b02085.

(20) Mattila, J. M.; Lakey, P. S. J.; Shiraiwa, M.; Wang, C.; Abbatt, J. P. D.; Arata, C.; Goldstein, A. H.; Ampollini, L.; Katz, E. F.; DeCarlo, P. F.; et al. Multiphase Chemistry Controls Inorganic Chlorinated and Nitrogenated Compounds in Indoor Air during Bleach Cleaning. *Environ. Sci. Technol.* **2020**, *54* (3), 1730–1739. https://doi.org/10.1021/acs.est.9b05767.

(21) Dawe, K. E. R.; Furlani, T. C.; Kowal, S. F.; Kahan, T. F.; Vandenboer, T. C.; Young, C. J. Formation and Emission of Hydrogen Chloride in Indoor Air. *Indoor Air* **2019**, No. April 2018, 70–78. https://doi.org/10.1111/ina.12509.

(22) Young, C. J.; Zhou, S.; Siegel, J. A.; Kahan, T. F. Illuminating the Dark Side of Indoor Oxidants. *Environ. Sci. Process. Impacts* **2019**, *21* (8), 1229–1239. https://doi.org/10.1039/C9EM00111E.

(23) Roberts, J. M.; Osthoff, H. D.; Brown, S. S.; Ravishankara, A. R. N2O5 Oxidizes Chloride to Cl2 in Acidic Atmospheric Aerosol. *Science (80-.).* **2008**, *321* (5892), 1059–1059. https://doi.org/10.1126/science.1158777.

(24) Huey, L. G.; Villalta, P. W.; Dunlea, E. J.; Hanson, D. R.; Howard, C. J. Reactions of CF3O- with Atmospheric Trace Gases. *J. Phys. Chem.* **1996**, *100* (1), 190–194. https://doi.org/10.1021/jp951928u.

(25) Marcy, T. P.; Fahey, D. W.; Gao, R. S.; Popp, P. J.; Richard, E. C.; Thompson, T. L.;

Rosenlof, K. H.; Ray, E. A.; Salawitch, R. J.; Atherton, C. S.; et al. Quantifying Stratospheric Ozone in the Upper Troposphere with in Situ Measurements of HCl. *Science (80-.).* **2004**, *304* (5668), 261 LP – 265. https://doi.org/10.1126/science.1093418.

(26) United States Environmental Protection Agency. Compendium of Methods for the Determination of Inorganic Compounds in Ambient Air: Determination of Reactive Acidic and Basic Gases and Strong Acidity of Atmospheric Fine Particles (<2.5 Mm) (Compendium Method IO-4.2). **1999**.

(27) Keene, W. C.; Long, M. S.; Pszenny, A. A. P.; Sander, R.; Maben, J. R.; Wall, A. J.; O'Halloran, T. L.; Kerkweg, A.; Fischer, E. V; Schrems, O. Latitudinal Variation in the Multiphase Chemical Processing of Inorganic Halogens and Related Species over the Eastern North and South Atlantic Oceans. *Atmos. Chem. Phys.* **2009**, *9* (19), 7361–7385. https://doi.org/10.5194/acp-9-7361-2009.

(28) Keene, W. C.; Stutz, J.; Pszenny, A. A. P.; Maben, J. R.; Fischer, E. V; Smith, A. M.; von Glasow, R.; Pechtl, S.; Sive, B. C.; Varner, R. K. Inorganic Chlorine and Bromine in Coastal New England Air during Summer. *J. Geophys. Res. Atmos.* **2007**, *112* (D10). https://doi.org/10.1029/2006JD007689.

(29) Veres, P.; Roberts, J. M.; Warneke, C.; Welsh-Bon, D.; Zahniser, M.; Herndon, S.; Fall, R.; de Gouw, J. Development of Negative-Ion Proton-Transfer Chemical-Ionization Mass Spectrometry (NI-PT-CIMS) for the Measurement of Gas-Phase Organic Acids in the Atmosphere. *Int. J. Mass Spectrom.* **2008**, *274* (1–3), 48–55. https://doi.org/10.1016/j.ijms.2008.04.032.

(30) Karellas, N. S.; Chen, Q. F.; De Brou, G. B.; Milburn, R. K. Real Time Air Monitoring of

Hydrogen Chloride and Chlorine Gas during a Chemical Fire. *J. Hazard. Mater.* **2003**, *102* (1), 105–120. https://doi.org/https://doi.org/10.1016/S0304-3894(03)00205-X.

(31) Hagen, C. L.; Lee, B. C.; Franka, I. S.; Rath, J. L.; Vandenboer, T. C.; Roberts, J. M.; Brown, S. S.; Yalin, A. P. Cavity Ring-down Spectroscopy Sensor for Detection of Hydrogen Chloride. *Atmos. Meas. Tech.* **2014**, *7* (2), 345–357. https://doi.org/10.5194/amt-7-345-2014.

(32) Wilkerson, J.; Sayres, D. S.; Smith, J. B.; Allen, N.; Rivero, M.; Greenberg, M.; Martin, T.; Anderson, J. G. In Situ Observations of Stratospheric HCl Using Three-Mirror Integrated Cavity Output Spectroscopy. *Atmos. Meas. Tech. Discuss.* **2021**, *2021*, 1–38. https://doi.org/10.5194/amt-2021-6.

(33) Crosson, E. R. A Cavity Ring-down Analyzer for Measuring Atmospheric Levels of Methane, Carbon Dioxide, and Water Vapor. *Appl. Phys. B* **2008**, *92* (3), 403–408. https://doi.org/10.1007/s00340-008-3135-y.

(34) Thaler, R. D.; Mielke, L. H.; Osthoff, H. D. Quantification of Nitryl Chloride at Part Per Trillion Mixing Ratios by Thermal Dissociation Cavity Ring-Down Spectroscopy. *Anal. Chem.* **2011**, *83* (7), 2761–2766. https://doi.org/10.1021/ac200055z.

(35) Lao, M.; Crilley, L. R.; Salehpoor, L.; Furlani, T. C.; Bourgeois, I.; Neuman, J. A.; Rollins, A. W.; Veres, P. R.; Washenfelder, R. A.; Womack, C. C.; et al. A Portable, Robust, Stable and Tunable Calibration Source for Gas-Phase Nitrous Acid (HONO). *Atmos. Meas. Tech.* **2020**, *13*, 5873–5890. https://doi.org/10.5194/amt-13-5873-2020.

(36) Place, B. K.; Young, C. J.; Ziegler, S. E.; Edwards, K. A.; Salehpoor, L.; VandenBoer, T. C. Passive Sampling Capabilities for Ultra-Trace Quantitation of Atmospheric Nitric Acid

(HNO3) in Remote Environments. *Atmos. Environ.* **2018**, *191* (November 2017), 360–369. https://doi.org/10.1016/j.atmosenv.2018.08.030.

(37) Gordon, I. E.; Rothman, L. S.; Hill, C.; Kochanov, R. V; Tan, Y.; Bernath, P. F.; Birk, M.; Boudon, V.; Campargue, A.; Chance, K. V; et al. The HITRAN2016 Molecular Spectroscopic Database. *J. Quant. Spectrosc. Radiat. Transf.* **2017**, *203*, 3–69. https://doi.org/https://doi.org/10.1016/j.jqsrt.2017.06.038.

(38) Kochanov, R. V; Gordon, I. E.; Rothman, L. S.; Shine, K. P.; Sharpe, S. W.; Johnson, T. J.; Wallington, T. J.; Harrison, J. J.; Bernath, P. F.; Birk, M.; et al. Infrared Absorption Cross-Sections in HITRAN2016 and beyond: Expansion for Climate, Environment, and Atmospheric Applications. *J. Quant. Spectrosc. Radiat. Transf.* **2019**, *230*, 172–221. https://doi.org/https://doi.org/10.1016/j.jqsrt.2019.04.001.

(39) MacInnis, J. J.; VandenBoer, T. C.; Young, C. J. Development of a Gas Phase Source for Perfluoroalkyl Acids to Examine Atmospheric Sampling Methods. *Analyst* **2016**, *141* (12), 3765–3775. https://doi.org/10.1039/C6AN00313C.

(40) Webster, C. R.; May, R. D.; Trimble, C. A.; Chave, R. G.; Kendall, J. Aircraft (ER-2) Laser Infrared Absorption Spectrometer (ALIAS) for in-Situ Stratospheric Measurements of HCl, N2O, CH4, NO2, and HNO3. *Appl. Opt.* **1994**, *33* (3), 454–472. https://doi.org/10.1364/AO.33.000454.

(41) Voss, P. B.; Stimpfle, R. M.; Cohen, R. C.; Hanisco, T. F.; Bonne, G. P.; Perkins, K. K.; Lanzendorf, E. J.; Anderson, J. G.; Salawitch, R. J.; Webster, C. R.; et al. Inorganic Chlorine Partitioning in the Summer Lower Stratosphere: Modeled and Measured [ClONO2]/[HCl] during POLARIS. *J. Geophys. Res. Atmos.* **2001**, *106* (D2), 1713–1732.

https://doi.org/https://doi.org/10.1029/2000JD900494.

(42) Ma, Y.; He, Y.; Yu, X.; Chen, C.; Sun, R.; Tittel, F. K. HCl Ppb-Level Detection Based on QEPAS Sensor Using a Low Resonance Frequency Quartz Tuning Fork. *Sensors Actuators, B Chem.* **2016**, *233*, 388–393. https://doi.org/10.1016/j.snb.2016.04.114.

(43) Lee, B. H.; Lopez-Hilfiker, F. D.; Schroder, J. C.; Campuzano-Jost, P.; Jimenez, J. L.; McDuffie, E. E.; Fibiger, D. L.; Veres, P. R.; Brown, S. S.; Campos, T. L.; et al. Airborne Observations of Reactive Inorganic Chlorine and Bromine Species in the Exhaust of Coal-Fired Power Plants. *J. Geophys. Res. Atmos.* **2018**, *123* (19), 11,225-11,237. https://doi.org/10.1029/2018JD029284.

(44) Jurkat, T.; Voigt, C.; Arnold, F.; Schlager, H.; Aufmhoff, H.; Schmale, J.; Schneider, J.; Lichtenstern, M.; Dörnbrack, A. Airborne Stratospheric ITCIMS Measurements of SO2, HCl, and HNO3 in the Aged Plume of Volcano Kasatochi. *J. Geophys. Res. Atmos.* **2010**, *115* (D2). https://doi.org/https://doi.org/10.1029/2010JD013890.

(45) Neuman, J. A.; Huey, L. G.; Ryerson, T. B.; Fahey, D. W. Study of Inlet Materials for Sampling Atmospheric Nitric Acid. *Environ. Sci. Technol.* **1999**, *33* (7), 1133–1136. https://doi.org/10.1021/es980767f.

(46) Eisele, F. L.; Tanner, D. J. Measurement of the Gas Phase Concentration of H2SO4 and Methane Sulfonic Acid and Estimates of H2SO4 Production and Loss in the Atmosphere. *J. Geophys. Res. Atmos.* **1993**, *98* (D5), 9001–9010. https://doi.org/10.1029/93JD00031.

(47) Pszenny, A. A. P.; Keene, W. C.; Jacob, D. J.; Fan, S.; Maben, J. R.; Zetwo, M. P.; Springer-Young, M.; Galloway, J. N. Evidence of Inorganic Chlorine Gases Other than Hydrogen Chloride in Marine Surface Air. *Geophys. Res. Lett.* **1993**, *20* (8), 699–702.

https://doi.org/10.1029/93GL00047.

(48) Kim, S.; Huey, L. G.; Stickel, R. E.; Pierce, R. B.; Chen, G.; Avery, M. A.; Dibb, J. E.; Diskin, G. S.; Sachse, G. W.; McNaughton, C. S.; et al. Airborne Measurements of HCl from the Marine Boundary Layer to the Lower Stratosphere over the North Pacific Ocean during INTEX-B. *Atmos. Chem. Phys. Discuss.* **2008**, *2008*, 3563–3595. https://doi.org/10.5194/acpd-8-3563-2008.

(49) Roscioli, J. R.; Zahniser, M. S.; Nelson, D. D.; Herndon, S. C.; Kolb, C. E. New Approaches to Measuring Sticky Molecules: Improvement of Instrumental Response Times Using Active Passivation. *J. Phys. Chem. A* **2016**, *120* (9), 1347–1357. https://doi.org/10.1021/acs.jpca.5b04395.

(50) Ellis, R. a; Murphy, J. G.; Pattey, E.; Haarlem, R. Van; Brien, J. M. O. Characterizing a Quantum Cascade Tunable Infrared Laser Differential Absorption Spectrometer (QC-TILDAS) for Measurements of Atmospheric Ammonia. *Atmos. Meas. Tech.* **2010**, 3309–3338.

(51) Pollack, I. B.; Lindaas, J.; Roscioli, J. R.; Agnese, M.; Permar, W.; Hu, L.; Fischer, E. V. Evaluation of Ambient Ammonia Measurements from a Research Aircraft Using a Closed-Path QC-TILDAS Operated with Active Continuous Passivation. *Atmos. Meas. Tech.* **2019**, *12* (7), 3717–3742. https://doi.org/10.5194/amt-12-3717-2019.

(52) Deming, B. L.; Pagonis, D.; Liu, X.; Day, D. A.; Talukdar, R.; Krechmer, J. E.; Gouw, J. A. De; Jimenez, J. L.; Ziemann, P. J. Measurements of Delays of Gas-Phase Compounds in a Wide Variety of Tubing Materials Due to Gas – Wall Interactions. **2019**, No. 1, 3453–3461.

(53) Pagonis, D.; Krechmer, J. E.; de Gouw, J.; Jimenez, J. L.; Ziemann, P. J. Effects of Gas–Wall Partitioning in Teflon Tubing and Instrumentation on Time-Resolved Measurements of Gas-Phase Organic Compounds. *Atmos. Meas. Tech.* **2017**, *10* (12), 4687–4696. https://doi.org/10.5194/amt-10-4687-2017.

(54) Zahniser, M. S.; Nelson, D. D.; McManus, B.; Kebabian, P. L.; Lloyd, D.; Fowler, D.; Jenkinson, D. S.; Monteith, J. L.; Unsworth, M. H. Measurement of Trace Gas Fluxes Using Tunable Diode Laser Spectroscopy. *Philos. Trans. R. Soc. London. Ser. A Phys. Eng. Sci.* **1995**, *351* (1696), 371–382. https://doi.org/10.1098/rsta.1995.0040.

(55) Moravek, A.; Singh, S.; Pattey, E.; Pelletier, L.; Murphy, J. Measurements and Quality Control of Ammonia Eddy Covariance Fluxes: A New Strategy for High-Frequency Attenuation Correction. *Atmos. Meas. Tech.* **2019**, *12*, 6059–6078. https://doi.org/10.5194/amt-12-6059-2019.

(56) Whitehead, J. D.; Twigg, M.; Famulari, D.; Nemitz, E.; Sutton, M. A.; Gallagher, M. W.; Fowler, D. Evaluation of Laser Absorption Spectroscopic Techniques for Eddy Covariance Flux Measurements of Ammonia. *Environ. Sci. Technol.* **2008**, *42* (6), 2041–2046. https://doi.org/10.1021/es071596u.

(57) Sintermann, J.; Spirig, C.; Jordan, A.; Kuhn, U.; Ammann, C.; Neftel, A. Eddy Covariance Flux Measurements of Ammonia by High Temperature Chemical Ionisation Mass Spectrometry. *Atmos. Meas. Tech.* **2011**, *4* (3), 599–616. https://doi.org/10.5194/amt-4-599-2011.

(58) Cousins, I. T.; DeWitt, J. C.; Gluege, J.; Goldenman, G.; Herzke, D.; Lohmann, R.; Ng, C.; Scheringer, M.; Wang, Z. The High Persistence of PFAS Is Sufficient for Their

Management as a Chemical Class. *Environ. Sci. Process. Impacts* **2020**. https://doi.org/10.1039/D0EM00355G.

(59) Sunderland, E. M.; Hu, X. C.; Dassuncao, C.; Tokranov, A. K.; Wagner, C. C.; Allen, J. G. A Review of the Pathways of Human Exposure to Poly- and Perfluoroalkyl Substances (PFASs) and Present Understanding of Health Effects. *J. Expo. Sci. Environ. Epidemiol.* **2019**, *29* (2), 131–147. https://doi.org/10.1038/s41370-018-0094-1.

(60) Benskin, J. P.; Muir, D. C. G.; Scott, B. F.; Spencer, C.; De Silva, A. O.; Kylin, H.; Martin, J. W.; Morris, A.; Lohmann, R.; Tomy, G.; et al. Perfluoroalkyl Acids in the Atlantic and Canadian Arctic Oceans. *Environ. Sci. Technol.* **2012**, *46* (11), 5815–5823. https://doi.org/10.1021/es300578x.

(61) ECHA. Four new substances added to Candidate List https://www.echa.europa.eu/-/four-new-substances-added-to-candidate-list (accessed Jun 30, 2020).

Chapter 4.

Hydrogen Chloride (HCl) as a Tracer for Morning Reactive Chlorine Cycling in the Polluted Marine Boundary Layer during the Halifax Fog and Air Quality Study (HaliFAQS)

Abstract

Chlorine atom (Cl) initiated oxidation yields hydrogen chloride (HCl) that can be detected using a high time-resolution cavity ringdown spectrometer (CRDS). We present in this study continuous HCl measurements in the polluted marine boundary layer during the Halifax Fog and Air Quality Study (HaliFAQS) and demonstrate the efficacy of HCl as a morning tracer of photochemical Cl formation. HCl throughout the campaign was elevated when high irradiance was observed. Bimodal HCl features in the high irradiance days are consistent with two known photochemical processes; (1) morning photolysis of Cl precursors, and (2) midday formation of nitric acid (HNO_3) followed by acid displacement onto chloride (Cl^-) containing aerosols. Morning rates of HCl increase and solar irradiance were used in conjunction with a rate constant fitting function to estimate sunrise $ClNO_2$ mixing ratios. The estimated $ClNO_2$ was then used to model HCl for 8 days. Within this period there were 6 days with high irradiance and high levels of HCl and 2 days with low levels. The modelled HCl agrees well for high irradiance days and captures the features of the first (morning) mode within combined uncertainty in the regression analysis and deposition uncertainty. We compared the production of Cl from photolysis of the estimated $ClNO_2$ ($P(Cl)_{ClNO_2}$) to the production of hydroxyl radical (OH) from the photolysis of measured ozone ($P(HO_x)_{O_3}$). For high irradiance days, it was observed that $P(Cl)_{ClNO_2}$ was 13% of $P(HO_x)_{O_3}$ when considering the full day, and 37% when considering only the morning. This observational data shows that HCl can be used to estimate nighttime mixing ratios of $ClNO_2$ and the overall influence of Cl on morning tropospheric oxidation chemistry.

4.1 Introduction

Tropospheric halogen chemistry influences the fate of atmospheric chemicals, including ozone (O_3), methane, and volatile organic compounds (VOCs) in the troposphere.[1,2] Halogen radicals, in particular atomic chlorine (Cl), can deplete O_3 and will react rapidly with VOCs

(R4.1.1). Methane and VOC loss through reaction with Cl is 16 and 10–200 times faster, respectively, than the hydroxyl radical (OH), and is an important methane sink in regions with high activity of chlorine chemistry.[3–5] Discerning the global tropospheric budget for Cl atoms is difficult due to a lack of direct measurements, and it remains uncertain on a global scale. As there are no methods currently able to measure tropospheric Cl, the levels of Cl are typically inferred through models that monitor major sinks (e.g. methane loss via R4.1.1).[6]

$$Cl\,(g) + RH\,(g) \rightarrow HCl\,(g) + R\,(g) \qquad \text{R4.1.1}$$

The dominant radical in the global atmosphere is OH, which impacts the lifetime of methane and VOCs, as well as initiates the reactions that lead to formation of tropospheric O_3. Primary radicals are generally formed through photolysis of precursor molecules and secondary radicals are formed through radical propagation. Secondary radicals produced in the atmosphere from reactions of primary radicals are almost exclusively OH. Cl has been demonstrated to act as an important primary radical source in some cases (e.g., Young et al., (2012), Young et al., (2014), Kim et al., (2014), and Riedel et al., (2014)).[5,7–9] Understanding the production of Cl is important due to its high reactivity. Higher levels of tropospheric Cl will lead to shorter methane and VOC lifetimes but would vary depending on the VOC mixture. For example, Cl initiated reactions are much faster than OH for saturated hydrocarbons.[7] The amount of Cl present in the atmosphere is small relative to OH, and are typically on the order of 10^3 atoms cm^{-3}, but can be as high as 10^5 atoms cm^{-3} in the early morning.[5,6,9,10] Elevated levels in the morning can influence the chemistry throughout the rest of the day through the production of secondary radicals.[7] For example, during the CalNex campaign in Los Angeles, Cl from the photolysis of $ClNO_2$ (R4.1.2) accounted for more than 50% of primary radicals in the morning on sunny days.[8,11]

$$ClNO_2\,(g) + h\nu \rightarrow Cl\,(g) + NO_2\,(g) \qquad \text{R4.1.2}$$

Such sources of Cl are termed reactive chlorine (Cl_y) and have been of emerging importance to understanding atmospheric oxidation. In this work Cl_y represents all chlorine-containing species that can undergo common atmospheric reactions to yield a Cl atom. Mobilization of chloride (Cl^-) from sea spray aerosol (SSA) that mixes with emissions of nitrogen oxides ($NO_x \equiv NO+NO_2$) in the marine boundary layer (MBL) can transform relatively unreactive aqueous Cl^- into Cl_y; these transformations are known as chlorine activation. Two major pathways for chlorine activation include; hydrogen chloride (HCl) production via acid displacement (R4.1.3, where M is a cation (e.g., Na^+) and HX is a strong acid),[12–17] and nighttime formation of $ClNO_2$ from reactive dinitrogen pentoxide (N_2O_5) uptake into aqueous aerosols (R4.1.4).[18–24]

$$HX + MCl\,(s \text{ or } aq) \rightarrow MX\,(s \text{ or } aq) + HCl\,(g) \qquad \text{R4.1.3}$$

$$N_2O_5\,(g) + Cl^-\,(aq) + H^+\,(aq) \rightarrow ClNO_2\,(g) + HNO_3\,(aq) \qquad \text{R4.1.4}$$

The most common acid and salt combination for HCl acid displacement are nitric acid (HNO_3, R4.1.5) and sodium chloride (NaCl, found in SSA).[25,26] The rate of acid displacement in the MBL is typically limited by HNO_3 (formed photochemically from R4.1.6). The formation of HNO_3 is typically photochemical (i.e. driven by irradiance), meaning that production is highest when OH is highest and NO_x levels are not limiting, which is typically midday in moderately polluted environments.[27,28]

$$HNO_3\,(g) + NaCl\,(s \text{ or } aq) \rightarrow NaNO_3\,(s \text{ or } aq) + HCl\,(g) \qquad \text{R4.1.5}$$

$$NO_2\,(g) + OH\,(g) \rightarrow HNO_3\,(g) \qquad \text{R4.1.6}$$

In the MBL the dominant Cl_y species that dictate Cl atom production in the morning and afternoon are $ClNO_2$ and HCl, respectively. Riedel et al., (2012), found that $ClNO_2$ photolysis

(R4.1.2) and the reaction of HCl with OH (R4.1.7) each accounted for 45% of the integrated Cl atom production over the entire day along the Santa Monica Bay of Los Angeles.[21]

$$HCl\ (g) + OH\ (g) \rightarrow Cl\ (g) + H_2O\ (g) \qquad \text{R4.1.7}$$

Distinguishing between the two Cl activation mechanisms is challenging as it typically requires complete measurements of precursors (e.g., $ClNO_2$, HNO_3, etc.) and the factors that influence each pathway (e.g., irradiance and relative humidity (RH)). Photolabile Cl_y builds up during the night and is readily photolyzed in the early morning. The resulting Cl production and subsequent HCl formation (R4.1.1) during the morning has mostly be attributed to $ClNO_2$.[5,8] Since HNO_3 concentration peaks midday (R4.1.6), the HCl formed from R4.4 will follow the same temporal trend. Thus, it may be possible to distinguish the two mechanisms using high time resolution and sensitive HCl measurements.

Tropospheric HCl levels commonly range from 10 to 1000 parts per trillion by volume (pptv).[29–31] In-situ high-time response measurements are challenging due to the fact HCl is a surface active gas that readily sorbs to inlet materials.[29,32,33] Online measurements have been generally accomplished by acetate or iodide chemical ionization time of flight mass spectrometry (CI-ToF-MS) or CI quadrupole MS (CI-QMS),[29,34,35] but emerging spectroscopy based techniques have been shown to have desirable qualities for field deployment, including high accuracy, simple operation, and portability.[30,31,33,36] In-situ high time-response measurements provide more information on HCl sources of sinks when compared to traditionally-used methods which rely on time integrated (2 hours – days) scrubbing of ambient air followed by offline analysis.[25,37,38] It is imperative that we can make measurements on the same timescale as the reactions/processes which influence Cl_y sources and sinks, so that we can identify the contributing processes and their relative importance to Cl and HCl production. The objectives of

this work are to: (i) make continuous, high time-resolution measurements of HCl in an urban MBL; (ii) estimate the importance of photolabile Cl precursor compounds to observed HCl levels; and (iii) assess the contribution of photolabile Cl_y to radical formation.

4.2 Methods

4.2.1 HaliFAQS campaign

Sampling was conducted as part of the Halifax Fog and Air Quality Study (HaliFAQS) in Halifax, Nova Scotia, Canada (population ~400,000) from May 25 to June 25, 2019. All measurements were made from the rooftop of the five story St Mary's University student union building (44°37'55.8"N, 63°34'48.4"W, ~50 m above sea level, including building height). The outdoor temperatures ranged from 5–25 °C (mean of 13.3 °C) and the RH ranged from 26–98% (mean of 76%). Air masses arrived at the observation site predominantly from the Atlantic Ocean (southeast), and a wind rose plot showed correlation between HCl and southeastern winds (see Figure B-1). The port of Halifax is the fourth largest port in Canada (measured by container volume) and connected to more than 150 countries via 18 direct shipping lines.[39] The port is integrated into the downtown area of the city and roughly 1.5 km from the measurement site. Therefore, the emissions from this shipping traffic may influence the chemistry reported in this study.

4.2.2 HCl measurement

HCl was measured at 0.5 Hz using a cavity ring-down spectrometer (CRDS, Picarro G2108). The instrument is described in detail in Chapter 3. All indoor inlet lines and fittings were kept in a thermostated room that fluctuated from 25–30 °C. All inlet lines and fittings were made of perfluoroalkoxy (PFA) unless stated otherwise. A full schematic of the sampling apparatus indicating the separation between the outdoor and indoor inlet line lengths is provided

in Figure B-2. A mass flow controller (GM50A, MKS instruments, Andover, Massachusetts, USA) regulated a sampling flow of 14.7 L min^{-1} using a diaphragm pump through a 2.4 m sampling inlet (i.d. of 0.375") from the ambient outdoor environment. The outdoor air was pulled through a URG teflon coated aluminum cyclone (URG Corporation, Chapel Hill, North Carolina, USA) with a 2.5 µm aerodynamic diameter cut-off for particulate matter to prevent deposition of local sea spray. The CRDS sampled 2.0 L min^{-1} from the main inlet line, yielding a total inlet flow of 16.7 L min^{-1}, which gave a residence time of 0.75 seconds. The CRDS sample flow passed through a polytetrafluoroethylene (PTFE) filter (2 µm pore size, 47 mm diameter, TISCH scientific, North Bend, Ohio, USA) and then two high efficiency particulate air (HEPA) filters contained within the CRDS outer cavity metal compartment heat-regulated to 45 °C. Instances of flagged instrument errors in the CRDS data during ambient observations were removed as standard practice in quality control procedures.

4.2.3 Supporting measurements

Supporting measurements for the HaliFAQS campaign were collocated with the HCl measurements described in Section 4.2.1 and included NO, NO_x, O_3, formaldehyde (HCHO), solar irradiance, and meteorological data. NO and NO_x were measured using chemiluminescence (American EcoTech EC9841) and NO_2 levels were calculated as the difference between NO_x and NO. O_3 was measured using absorption spectroscopy (American EcoTech Serinus 10). The NO, NO_x, and O_3 measurements were made through the same inlet as HCl (Figure B-3). Gas-phase HCHO (spectral window 2745–2800 cm^{-1}) was measured using open-path Fourier transform infrared spectroscopy (OP-FTIR).[39] The active broadband IR source is modulated by a low-resolution Fourier transform spectrometer arranged in a monostatic configuration. Collimated radiation is focused on a mercury-cadmium-telluride broadband IR detector (spectral window of

700 and 6000 cm^{-1}). Solar irradiance measurements (kW m^{-2}) were captured using a HOBO S-LIB-M003 Solar Radiation Smart Sensor paired with a HOBO H21-USB Micro Station data logger. The Davis Vantage Pro 2 weather station was used to monitor outdoor pressure, temperature, wind speed, and wind direction. Planetary boundary layer height was extracted for the campaign period from the Environment and Climate Change Canada (ECCC) High Resolution Deterministic Prediction System (HRDPS) Global Environmental Multiscale (GEM) model (2.5-km resolution) forecast archives (Figure B-4).[40] Photolysis rate coefficients were calculated using the National Center for Atmospheric Research (NCAR) tropospheric ultraviolet and visible (TUV) radiation model-version 5.3.[41]

4.2.4 Estimating mixing ratios of morning chlorine precursors

The dominant photolabile morning Cl precursor is $ClNO_2$, with Cl_2 generally playing a minor role (< 1%) (e.g., Riedel et al., 2012; Riedel et al., 2014; Sarwar et al., 2012; Sarwar et al., 2014; Thornton et al., 2010; Young et al., 2012; Haskins et al., 2018).[5,8,21,22,35,42,43] To explore this further, we selected days in which photolabile Cl precursors were likely to be major contributors to observed HCl. These were determined through the combination of early morning high irradiance conditions and a fast-morning rise of HCl. We also selected days that do not meet the aforementioned criterion for quality control. Quality control days were chosen due to their slow morning rise in HCl and low morning irradiance relative to the average. Eight days were selected: June 3, 5, 7, 13, 15, 17, 18, and 19, 2019. Days with an early morning high irradiance include June 13, 17, 18, and 19, while days chosen for their low irradiance include June 3, 5, 7 and 15. Using the TUV model, photolysis rate coefficients ($jClNO_2$) were calculated under clear-sky conditions at 15-minute intervals for the full days. The clear-sky j-values were scaled to observed irradiance using the ratio of 15-minute measured irradiance to the theoretical maximum

clear sky irradiance at each time point (described in the Appendix B1).[41,44–46] Assuming that the increase in HCl in the early morning is solely from R4.1.1 due to Cl atoms generated by photolysis of $ClNO_2$ (R4.1.2), the following equation can be written:

$$\Delta HCl = 900\, jClNO_2([ClNO2]_i - \Sigma HCl) \quad \text{(E1)}$$

Where ΔHCl is the change in HCl mixing ratio (calculated as the difference between deposition-corrected $[HCl]_t$ - $[HCl]_{t-1}$ for each 15-min interval from sunrise (04:30) to 10:30 (Atlantic Daylight Time (ADT)), with all negative values represented as zero), $[ClNO_2]_i$ is the mixing ratio of $ClNO_2$ present at sunrise, and ΣHCl is the sum of HCl formed since sunrise (determined using the deposition-corrected measured HCl mixing ratios from 04:30 to 10:30 ADT). Deposition was considered for both ΔHCl and ΣHCl. To account for the continual loss of HCl by deposition, we generated two sets of the independent variables ΔHCl and ΣHCl for low (1 cm s^{-1}) and high (6 cm s^{-1}) deposition velocities. The estimated loss of HCl was determined from modelled boundary layer height and measured HCl. The estimated loss by deposition of HCl in the 15-min timeframe was added to the existing measurement of HCl to generate deposition-corrected values of ΔHCl and ΣHCl that were used in the regression analysis. The three independent measured variables ΔHCl, $jClNO_2$, and ΣHCl were used to determine $[ClNO_2]_i$. The coefficient $[ClNO_2]_i$ was calculated using least-squares regression analysis on E1 in Igor Pro 8 (Wavemetrics, OR, USA). Two initial $ClNO_2$ mixing ratios corresponding to high and low deposition conditions were calculated. Using the calculated mixing ratios, the production of HCl can be modelled from the resulting photolysis, where the two mixing ratios represent the upper and lower bounds of predicted HCl. This assumes that all Cl reacts to form HCl. The uncertainty introduced through this assumption is heavily dependent on the VOC profile and does not necessary reflect a systematic loss. The reactivity of Cl in the ambient atmosphere is not well

constrained. One study has examined Cl reactivity in a polluted MBL (Los Angeles during early summer) and from that data approximately 75% of the reactions result in H abstraction via R4.1.1.[7] This reactivity is highly location- and condition-dependent and cannot be directly applied to our measurements. Our assumption that all Cl reactions that yield HCl via R4.1.1 results in a conservative estimate of $[ClNO_2]_i$ that is a lower limit to the true value. This assumption does not affect the modelled HCl. Another assumption made is that $ClNO_2$ is the only photolabile precursor that yields HCl, attempts to use Cl_2 was deemed to be ineffectual and not included in this work (see Figure B-5). Simulating and comparing the measured HCl allows us to validate this method as an indirect estimate of the lower limit of $ClNO_2$ as the Cl, which is discussed further is Section 4.3.2.

4.2.5 Calculating radical production

We calculated hydrogen oxides ($HO_x \equiv OH + HO_2$) primary radical production using surface level measurements of O_3 and HCHO (R4.2.1–2.5). Clear days that exhibited good correlation between modelled HCl and measured HCl were chosen to compare Cl production with HO_x. Two days were selected for calculating radical production: June 13 and 18. Using both the upper and lower ranges of HCl deposition velocity, the $[ClNO_2]_i$ was determined and their mean to calculate Cl production. Photolysis of nighttime $[ClNO_2]_i$ was calculated in 15-minute intervals to match the irradiance-normalized photolysis rate constants. We assumed no sources of $ClNO_2$ after sunrise and the continual loss due to photolysis was tracked. Photolysis rate coefficients for O_3 (jO_3) and HCHO (jHCHO) were calculated as described above for $jClNO_2$. Ozone measurements for June 13 and 18 were averaged over 15-minutes over the same time frame as jO_3. This was combined with pressure and RH data to generate the production of OH ($P(HO_x)_{O3}$), accounting for the quenching of O (^1D) with M (O_2 or N_2) via R4.2.2. HCHO was

diurnally averaged for the full campaign due to data gaps and averaged again into 15-minute bins to match jHCHO. The reaction of H atoms with molecular oxygen (R4.2.5) is assumed to be instantaneous, such that R4.2.4 determines $P(HO_x)_{HCHO}$.

$O_3\,(g) + h\nu \rightarrow O_2\,(g) + O\,(^1D, g)$ R4.2.1

$O\,(^1D, g) + M \rightarrow O\,(^3P, g) + M$ R4.2.2

$O\,(^1D, g) + H_2O\,(g) \rightarrow 2OH\,(g)$ R4.2.3

$HCHO\,(g) + h\nu \rightarrow H\,(g) + CHO\,(g)$ R4.2.4

$H\,(g) + O_2\,(g) \rightarrow HO_2\,(g)$ R4.2.5

4.3 Results and discussion

4.3.1 HCl measurements and sources

Measurements of HCl during HaliFAQS ranged between a daytime maximum of 572 pptv and a nighttime minimum of 55 pptv, with a mean value of 97 pptv (Figure 4-1). In most cases, HCl levels were higher during the day than at night. We typically observed higher HCl on days with high solar irradiance compared to those with low solar irradiance (Figures 4-1 and B-5). These trends are generally consistent with the literature (Tables 4-1 and B-1), where HCl formation has been attributed to photochemical processes, either acid displacement by photochemically-generated HNO_3 (R4.1.5, 4.1.6) or reaction of photochemically-generated Cl with organics (R4.1.1). Elevated levels of HCl observed at night are likely caused by direct emissions,[31] for example, suspected direct emissions of HCl were observed during the night of May 27 (Figure 4-1). Low levels of HCl and irradiance from May 26 — June 6 are due to observed fog events and overall cloudy conditions. Incidences of light raining events during this timeframe could also explain lower levels of HCl due to greater loss by wet deposition. Temperatures tended to be lower and could be indicative of a poorly mixed boundary layer

which might explain rapid and unpredictable changes (e.g., May 29 at ~ 14:00) in HCl from advection. Meteorological conditions can be used to better understand and complement observed trends of our local HCl levels.

Our results are similar to those reported using the same technique in another Atlantic Canadian city (St. John's, Newfoundland and Labrador, ~900 km east of Halifax) in early spring.[31] The HCl level for our dataset is higher than that observed in St John's (63 pptv), likely due to the greater overall available irradiance during HaliFAQS; however, the maximum value observed in St John's (1220 pptv) exceeds our highest observed value and also coincided with high irradiance. To explore the importance of photochemical processes further, we examined diurnal trends separated by irradiance levels. We defined high irradiance days as those within 25% of maximum integrated irradiance and defined the remaining days as low irradiance (Figure 4-2).

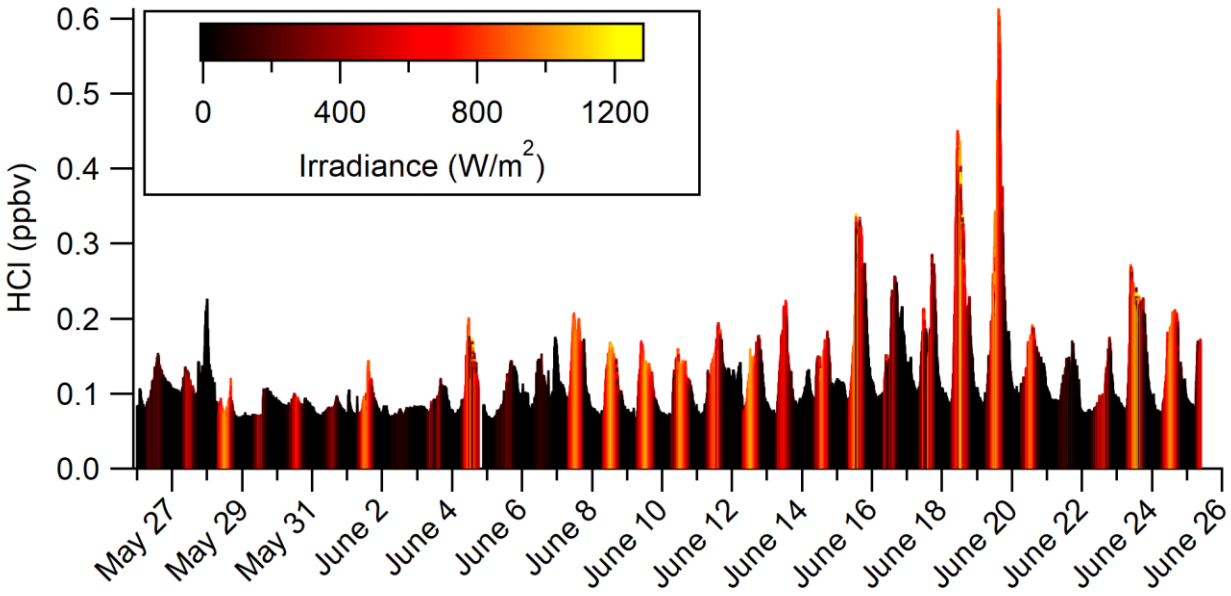

Figure 4-1. HCl timeseries from May 25 to June 25, 2019, for the HaliFAQS campaign colored by irradiance**.**

We observed bimodal features in many high irradiance days, with HCl peaking at about 10:00 and 14:00 ADT. On some high-irradiance days, we also observed days that had only a single mode, corresponding to high HCl in the morning or afternoon. The bimodal feature supports the inference that two major photochemical mechanisms previously established as HCl sources are responsible for its production in the MBL: photolysis of photolabile Cl_y (likely more important earlier in the day) and acid displacement (likely more important after mid-day). Both previously described photochemical mechanisms are important for HCl production and are heavily influenced by NO_x pollution. Figure B-6 illustrates the two mechanisms for elevated HCl levels, both required high irradiance. The first mechanism is limited by NO_2 and therefore low HNO_3, and elevated HCl is likely to be from R4.1.1. The second mechanism shows the slight increase in HCl with elevated HNO_3 as expected via R4.1.5. The two mechanisms rely on many of the same external factors such as irradiance, NO_x and Cl^- containing SSA. By examining the relationship between HCl, time of day, and irradiance, we can better understand the relative importance of these two mechanisms. Days with an observed afternoon mode of HCl formation (June 3, 5, 7, 17, 18, and 19) tended to have HCl peak between 14:00–18:00 ADT, which is consistent with the expected photochemical production of HNO_3. Predicting the days that will have single or bimodal features is complex and heavily dependent on the temporal and spatial trends for daily local emissions of the precursor compounds for HCl formation. We observed that quick-rising HCl in the morning leading to a mid-day maximum was often correlated with irradiance. The relationship between irradiance and HCl in the early morning in 22 of our 31 measurement days suggests photolysis of photolabile precursors as a likely mechanism. Only one day was observed (May 28) on which there was high morning irradiance and low HCl, which we hypothesize was

due to limited Cl precursor production the previous night. The formation of HCl from photolysis of photolabile precursors was explored further using a box model.

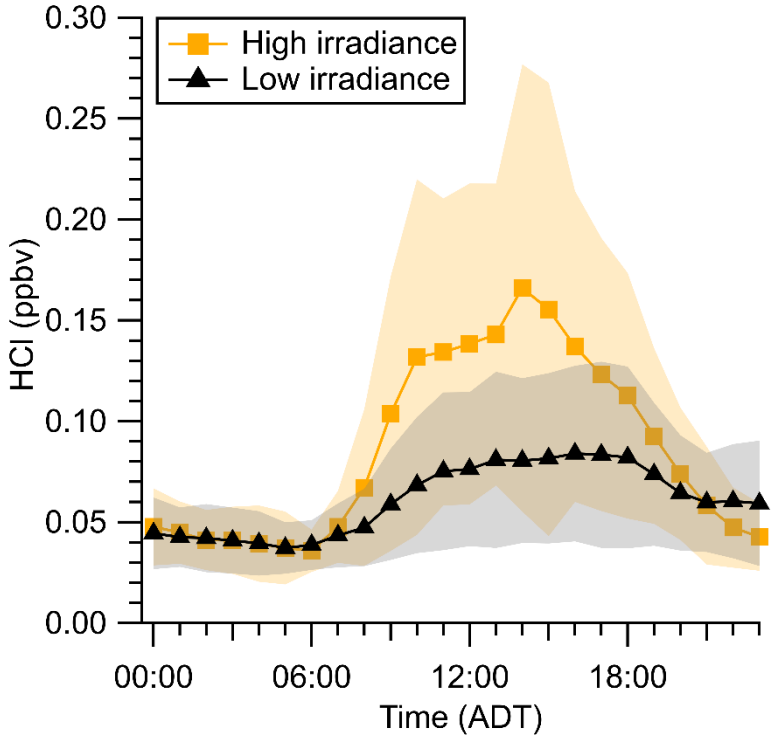

Figure 4-2. Diurnally averaged hourly observations of HCl for the full HaliFAQS campaign. Measurements are separated by days with high and low irradiance. See the text for a description of the definition of high and low irradiance days. Shaded areas represent the standard deviation in the hourly HCl measurement.

Table 4-1. Summary of selected modern measurements of HCl in the MBL reported starting from December 2000. Numbers in brackets represent the mean value.

Location	Date	Method	HCl mixing ratio range (pptv)	Reference
Halifax, Nova Scotia, Canada	May–June 2019	CRDS	55–572(97)	This study
St John's, Newfoundland, Canada	April 2017	CRDS	<20–1210(63)	Angelucci et al.,(2021)[31]
Northern California Coast, US	February–March 2015	Iodide CI-TOF-MS	100–380(199)	Haskins et al.,(2018)[35]
Southern	February–	Iodide CI-TOF-MS	530–2700(1300)	Haskins et

California Coast, US	March 2015			al.,(2018)[35]
Cyprus	July–August 2014	Iodide CI-QMS	<135–3000(790)	Eger et al., (2019)[34]
Central California Coast, US	May–June 2010	Acetate CI-TOF-MS	0–2800(440)	Crisp et al.,(2014)[29]
Southern California Coast, US	May–June 2010	Acetate CI-TOF-MS	0 to >16000(2200)	Crisp et al., (2014)[29]
Sao Vicente Island, Cape Verde	May–June 2007	Tandem Mist Chamber/IC	50–600	Lawler et al.,(2009)[47]
Appledore Island, Maine, US	July–August 2004	Tandem Mist Chamber/IC	5–5800(600)	Keene et al., (2007)[25]
Germany to South Africa	October–November 2003	Tandem Mist Chamber/IC	20–1400	Keene et al., (2009)[38]
Dumont d'Urville, Antarctica	December 2000—December 2001	Tandem Mist Chamber/IC	30–300	Jourdain and Legrand., (2002)[48]
S. Carolina, US to Canadian Coast	July–August 2002	Tandem Mist Chamber/IC	<25–4500	Keene et al., (2004)[49]

4.3.2 A box model to explore HCl formation and assess the contribution of photolabile Cl_y to radical formation

A box model was used to predict HCl from the photochemical production of Cl atoms from $ClNO_2$ (Figures 4-4 and B-7). This approach to modelling HCl does not include other parameters that could affect the HCl mixing ratio, including direct emissions or advection. As discussed in Section 4.3.1, meteorological conditions can affect observed levels of HCl and are currently not used in this model to decouple impacts of higher temperatures and/or the varying degrees on mixing within the boundary layer. Predicting the HCl from the photolysis of our estimated $[ClNO_2]_i$ and comparing it back to the measured HCl is used here to illustrate that using the rate

of change in measured HCl from 4:30 to 10:30 AM is valid. A good indication of the validity of the box model used to estimate $[ClNO_2]_i$ is the agreement between the time that predicted and measured HCl begin to rise in the morning and the ability to explain observed HCl past the modelled timeframe (i.e., later than 10:30 AM). The day-to-day variability of HCl observed in Section 4.3.1 indicates that HCl can potentially form by either or both photolysis of Cl_y precursors and/or acid displacement reactions. Most days show good agreement between predicted and measured HCl for the first morning mode. The days we modelled can be described by one of the following: (i) Days with primarily early morning HCl formation; (ii) Days with both morning and afternoon formation HCl; and (iii) days with broad and indistinguishable mechanisms of daytime HCl formation.

The days that solely have HCl production in the morning mode (category (i)) were June 13 and 18 (Figure 4-4c, e); these days had a single early and fast-rising HCl peak that coincided with high irradiance in the early morning. On these days we argue that photolysis of $ClNO_2$ is the dominant source of Cl into the MBL. The absence of a strong afternoon peak of HCl on these days is presumably due to a lack of photochemical HNO_3 and is consistent with low NO_2 (~5.5 ppbv) when compared to ~15 ppbv of NO_2 for days with observed second mode (Figure B-7). We do not expect to capture the totality of the HCl with our model, but a close match between measurement and model data on these days strongly indicates that photolysis can be the dominant source of HCl, and ultimately Cl, in the polluted MBL. The use of high time resolution measurements that are similar to the timescale of $ClNO_2$ photochemistry support this assertion further.

The days on which two clear peaks of HCl were observed (category (ii)) were June 5, 15, 17 and 19 (Figure 4-4d, f and B-8a, b). The predicted HCl maximum agreed well with the

measured HCl maximum only early in the day and did not agree with measurements later in the day. This suggests the peak mixing ratio and rate of increase corresponding to the morning mode for HCl is influenced by photolytic formation of Cl, while formation later in the day is likely caused by acid displacement. These bimodal days illustrate the two competing chemical pathways in daily HCl production. As expected, the box model can accurately capture the first mode attributed to photolytic production of Cl but not the second mode corresponding to the suspected acid displacement as the chemistry and measurements required to model it are not included.

The days that had an indistinguishable dominant mechanism (category (iii)) were June 3, and 7 (Figure 4-4a, b). June 7 had similar integrated irradiance levels to category (i) days and showed fair agreement between the initial modelled and measured HCl rate but failed to capture the totality of the initial peak and loss processes in the afternoon. It is possible that direct emissions or other HCl sources could be influencing HCl levels on these days. There is need for more routine measurements under different ambient conditions and for different regions, to better interpret and differentiate direct and photochemical sources for HCl and better understand the contributions of morning Cl_y photolysis in initiating radical production.

We also tested our model on June 3 and 5 (Figure 4-4a and B-8a) where irradiance was lowest (<10% of maximum irradiance). These days had some of the lowest mean levels of HCl (40 and 48 pptv, respectively) and served as negative controls for our model. As expected, these days had some of the poorest agreement between model and measurement.

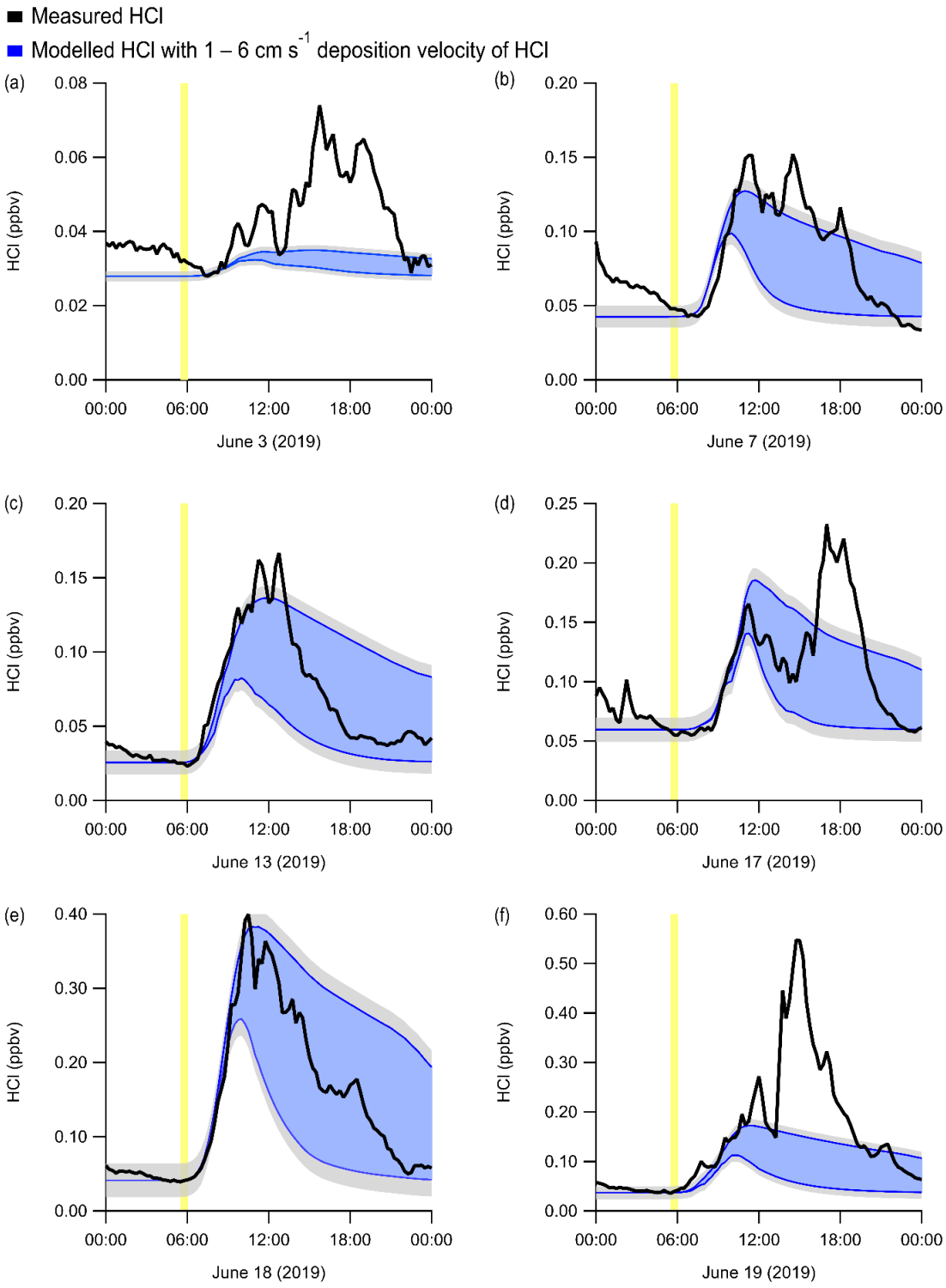

Figure 4-3. Modelled HCl (blue) formed via the photolysis of predicted $ClNO_2$ and measured HCl (black). Blue shading indicates the uncertainty in the modelled HCl from the range of deposition velocities. Yellow vertical line denotes time at sunrise. Grey shaded region is the error (σ) associated with the fitting function. (a) June 3, (b) June 7, (c) June 13, (d) June 17, (e) June 18, and (f) June 19. Note different y-axis scales.

4.3.3 Estimated influence of Cl as a primary radical source

We used the predicted Cl formed from photolysis of $ClNO_2$ ($(P(Cl)_{ClNO_2}$) for the two days with high irradiance and a single morning mode (and good agreement in the modelled to measured HCl) to assess the strength of this radical source compared to other major radical sources (Figures 4-5 and 4-6). It should be noted that this is not a radical budget, since we were unable to determine radical production from all primary radical sources that have been shown to be important in urban areas. For example, we cannot estimate the production of OH from the photolysis of nitrous acid.[8,9,50] $P(Cl)_{ClNO_2}$ was determined from the conservative estimates of $[ClNO_2]_i$ determined in Section 4.3.2 and is therefore a lower limit based on the assumptions discussed in Section 4.2.4. Photolysis of O_3 (R4.2.1) and the subsequent reaction of $O(^1D)$ with water (R4.2.3) to yield OH ($P(HO_x)_{O_3}$) is the dominant HaliFAQS radical producer, followed by photolysis of HCHO (R4.2.4, $P(HO_x)_{HCHO}$), and finally $P(Cl)_{ClNO_2}$. The contribution of Cl to morning time radicals in Halifax is important relative to these other radical sources. The timing and impact are different because $P(HO_x)_{O_3}$ and $P(HO_x)_{HCHO}$ both peak near midday, while production of Cl from $ClNO_2$ peaks in mid-morning, around 10:00 am (Figure 4-5). On June 13, $P(Cl)_{ClNO_2}$ was 8% of $P(HO_x)_{O_3}$ when considering the full day, and 19% when considering only the morning (Figure 4-6). On June 18, $P(Cl)_{ClNO_2}$ was 13% of $P(HO_x)_{O_3}$ when considering the full day, and 37% when considering only the morning. Only a few studies have calculated $P(Cl)_{ClNO_2}$ and $P(HO_x)_{O_3}$ to which we can compare. A radical budget during the early summer 2010 CalNex campaign in Los Angeles showed $P(Cl)_{ClNO_2}$ was 11% of $P(HO_x)_{O_3}$ when considering the full days averaged over 8 sunny days, while it accounted for 37% in the mornings.[8] Comparing the averaged data in Los Angeles to the radical production in Halifax on June 18, $P(HO_x)_{O_3}$ in Halifax was lower by approximately 45%, $P(HO_x)_{HCHO}$ was lower by approximately 90%, and $P(Cl)_{ClNO_2}$ was lower by approximately 50%.[8] Despite the maximum radical production

determined during HaliFAQS being approximately half of what was observed during CalNex, the relative contributions of $P(Cl)_{ClNO_2}$ to $P(HO_x)_{O_3}$ between the two cities are similar. High levels of $ClNO_2$ in the morning will photolyze yielding Cl to initiate oxidation and radical propagation earlier with respect to classic OH-initiated oxidation, which subsequently influences the degradation of VOCs that have slow loss through reaction with OH. These new VOC radical precursors then continue to produce secondary OH and O_3 that go on to further impact air quality compared to an atmosphere devoid of Cl atoms. Photolabile Cl_y is therefore an important radical source and these findings are consistent with previous studies that measured $ClNO_2$ in the MBL.[5,8] Another primary source of Cl that has been shown to be important in the MBL is reaction between OH and HCl (R4.1.7).[21] We cannot estimate its importance during HaliFAQS, but it likely also contributes to the available Cl.

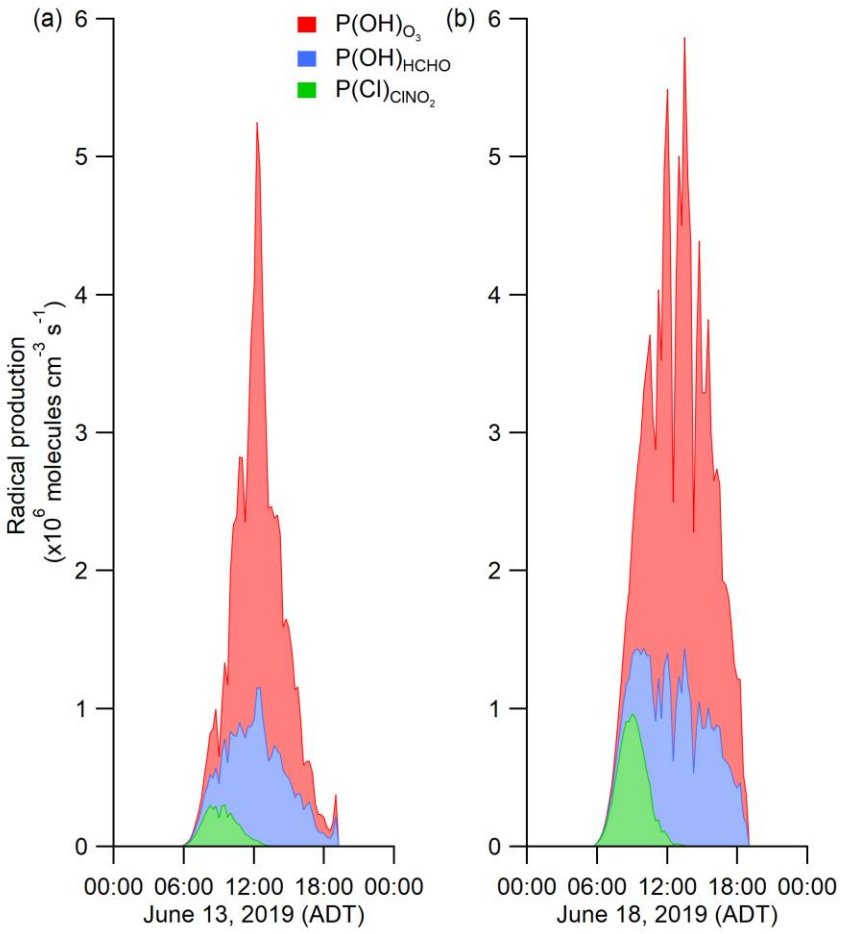

Figure 4-4. Comparison of major ground-level radical sources: $P(HO_x)$ from reaction of $O(^1D)$ with water (red), $P(HO_x)$ from diurnally averaged HCHO photolysis (blue), and P(Cl) from predicted $ClNO_2$ photolysis (green), for (a) June 13, and (b) June 18. Traces are stacked.

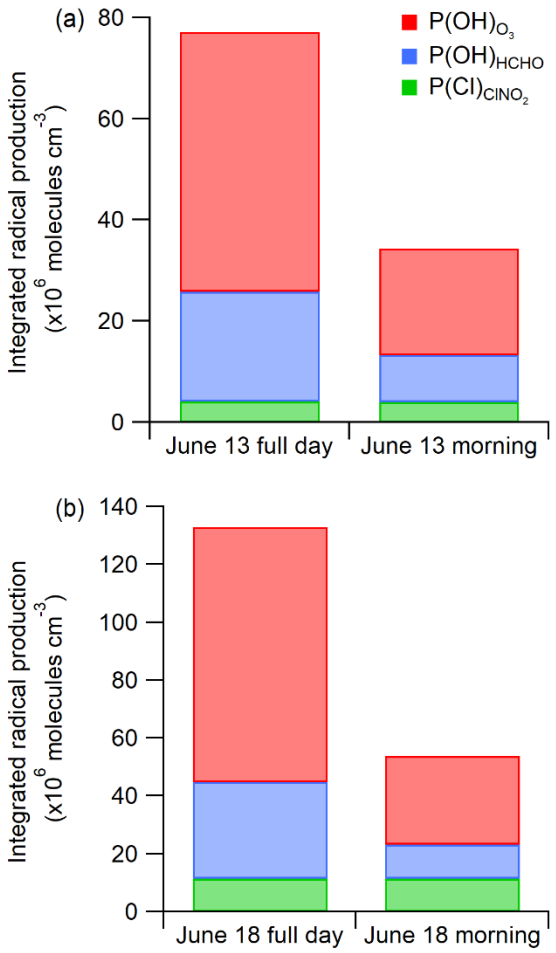

Figure 4-5. Integrated ground-level radical production during the HaliFAQS campaign for three radical sources: $P(HO_x)$ from reaction of $O(^1D)$ with water (red), $P(HO_x)$ from diurnally averaged HCHO photolysis (blue), and P(Cl) from predicted $ClNO_2$ photolysis (green) for (a) June 13 and (b) June 18 showing radical contributions for both the full day and morning (06:00 – 12:00).

4.4 Conclusions

In this work we made continuous, high time-resolution measurements of HCl in an urban MBL during the HaliFAQS field campaign and compared with previous measurements in the MBL. Bimodal peaks of HCl during days with high irradiance showed the presence of two photochemical mechanisms. The first mode was from the photolysis of Cl precursor compounds followed R4.1.1, and the second mode is suspected to be from the midday formation of HNO_3 followed by acid displacement onto Cl^- containing SSA. We used the rate of measured HCl to

determine the contribution of photolabile precursor $ClNO_2$ to observed morning HCl rates for 8 days. Predicted HCl from the photolysis of the determined initial $ClNO_2$ showed good agreement for high irradiance days during and past the modelling timeframe (i.e., 4:30 to 10:30 AM). In the absence of determining instantaneous deposition velocities, we accounted for the continual loss of HCl by deposition by generating two sets of data for low (1 cm s^{-1}) and high (6 cm s^{-1}) deposition velocities and display the data as a conservative range. On the most active day for Cl chemistry (June 18), it was observed that $P(Cl)_{ClNO_2}$ was 13% as large as $P(HO_x)_{O_3}$ when considering the full day, and 37% in the morning. Thus, it is important that Cl contributions to total radical production continue to be explored in the MBL to further understand the differences between full day and morning tropospheric oxidative capacity.

4.5 References

(1) Simpson, W. R.; Brown, S. S.; Saiz-Lopez, A.; Thornton, J. A.; Von Glasow, R. Tropospheric Halogen Chemistry: Sources, Cycling, and Impacts. *Chem. Rev.* **2015**, *115* (10), 4035–4062. https://doi.org/10.1021/cr5006638.

(2) Saiz-Lopez, A.; von Glasow, R. Reactive Halogen Chemistry in the Troposphere. *Chem. Soc. Rev.* **2012**, *41* (19), 6448–6472. https://doi.org/10.1039/C2CS35208G.

(3) Burkholder, J. B.; Sander, S. P.; Abbatt, J. P. D.; Barker, J. R.; Cappa, C.; Crounse, J. D.; Dibble, T. S.; Huie, R. E.; Kolb, C. E.; Kurylo, M. J.; et al. Chemical Kinetics and Photochemical Data for Use in Atmospheric Studies Evaluation Number 19. *Pasadena, CA Jet Propuls. Lab. Natl. Aeronaut. Sp. Adm. 2020* **2020**, No. 19–5.

(4) Hossaini, R.; Chipperfield, M. P.; Saiz-Lopez, A.; Fernandez, R.; Monks, S.; Feng, W.; Brauer, P.; von Glasow, R. A Global Model of Tropospheric Chlorine Chemistry: Organic versus Inorganic Sources and Impact on Methane Oxidation. *J. Geophys. Res. Atmos.* **2016**, *121* (23), 14,214-271,297. https://doi.org/10.1002/2016JD025756.

(5) Riedel, T. P.; Wolfe, G. M.; Danas, K. T.; Gilman, J. B.; Kuster, W. C.; Bon, D. M.; Vlasenko, A.; Li, S.-M.; Williams, E. J.; Lerner, B. M.; et al. An MCM Modeling Study of Nitryl Chloride ($ClNO_2$) Impacts on Oxidation, Ozone Production and Nitrogen Oxide Partitioning in Polluted Continental Outflow. *Atmos. Chem. Phys.* **2014**, *14* (8), 3789–3800. https://doi.org/10.5194/acp-14-3789-2014.

(6) Allan, W.; Struthers, H.; Lowe, D. C. Methane Carbon Isotope Effects Caused by Atomic Chlorine in the Marine Boundary Layer : Global Model Results Compared with Southern Hemisphere Measurements. **2007**, *112*, 1–10. https://doi.org/10.1029/2006JD007369.

(7) Young, C. J.; Washenfelder, R. A.; Edwards, P. M.; Parrish, D. D.; Gilman, J. B.; Kuster, W. C.; Mielke, L. H.; Osthoff, H. D.; Tsai, C.; Pikelnaya, O.; et al. Chlorine as a Primary Radical: Evaluation of Methods to Understand Its Role in Initiation of Oxidative Cycles. *Atmos. Chem. Phys.* **2014**, *14* (7), 3427–3440. https://doi.org/10.5194/acp-14-3427-2014.

(8) Young, C. J.; Washenfelder, R. A.; Roberts, J. M.; Mielke, L. H.; Osthoff, H. D.; Tsai, C.; Pikelnaya, O.; Stutz, J.; Veres, P. R.; Cochran, A. K.; et al. Vertically Resolved Measurements of Nighttime Radical Reservoirs in Los Angeles and Their Contribution to the Urban Radical Budget. *Environ. Sci. Technol.* **2012**, *46* (20), 10965–10973. https://doi.org/10.1021/es302206a.

(9) Kim, S.; VandenBoer, T. C.; Young, C. J.; Riedel, T. P.; Thornton, J. A.; Swarthout, B.; Sive, B.; Lerner, B.; Gilman, J. B.; Warneke, C.; et al. The Primary and Recycling Sources of OH during the NACHTT-2011 Campaign: HONO as an Important OH Primary Source in the Wintertime. *J. Geophys. Res. Atmos.* **2014**, *119* (11), 6886–6896. https://doi.org/https://doi.org/10.1002/2013JD019784.

(10) Singh, H. B.; Gregory, G. L.; Anderson, B.; Browell, E.; Sachse, G. W.; Davis, D. D.; Crawford, J.; Bradshaw, J. D.; Talbot, R.; Blake, D. R.; et al. Low Ozone in the Marine Boundary Layer of the Tropical Pacific Ocean: Photochemical Loss, Chlorine Atoms, and Entrainment. *J. Geophys. Res. Atmos.* **1996**, *101* (D1), 1907–1917. https://doi.org/https://doi.org/10.1029/95JD01028.

(11) Mielke, L. H.; Stutz, J.; Tsai, C.; Hurlock, S. C.; Roberts, J. M.; Veres, P. R.; Froyd, K. D.; Hayes, P. L.; Cubison, M. J.; Jimenez, J. L.; et al. Heterogeneous Formation of Nitryl Chloride and Its Role as a Nocturnal NOx Reservoir Species during CalNex-LA 2010. *J.*

Geophys. Res. Atmos. **2013**, *118* (18), 10,610-638,652. https://doi.org/https://doi.org/10.1002/jgrd.50783.

(12) Saul, T. D.; Tolocka, M. P.; Johnston, M. V. Reactive Uptake of Nitric Acid onto Sodium Chloride Aerosols Across a Wide Range of Relative Humidities. *J. Phys. Chem. A* **2006**, *110* (24), 7614–7620. https://doi.org/10.1021/jp060639a.

(13) Gard, E. E.; Kleeman, M. J.; Gross, D. S.; Hughes, L. S.; Allen, J. O.; Morrical, B. D.; Fergenson, D. P.; Dienes, T.; E. Gälli, M.; Johnson, R. J.; et al. Direct Observation of Heterogeneous Chemistry in the Atmosphere. *Science (80-.).* **1998**, *279* (5354), 1184 LP – 1187. https://doi.org/10.1126/science.279.5354.1184.

(14) Laskin, A.; Moffet, R. C.; Gilles, M. K.; Fast, J. D.; Zaveri, R. A.; Wang, B.; Nigge, P.; Shutthanandan, J. Tropospheric Chemistry of Internally Mixed Sea Salt and Organic Particles: Surprising Reactivity of NaCl with Weak Organic Acids. *J. Geophys. Res. Atmos.* **2012**, *117* (D15). https://doi.org/10.1029/2012JD017743.

(15) Pechtl, S.; von Glasow, R. Reactive Chlorine in the Marine Boundary Layer in the Outflow of Polluted Continental Air: A Model Study. *Geophys. Res. Lett.* **2007**, *34* (11). https://doi.org/10.1029/2007GL029761.

(16) Rossi, M. J. Heterogeneous Reactions on Salts. *Chem. Rev.* **2003**, *103* (12), 4823–4882. https://doi.org/10.1021/cr020507n.

(17) Raff, J. D.; Njegic, B.; Chang, W. L.; Gordon, M. S.; Dabdub, D.; Gerber, R. B.; Finlayson-Pitts, B. J. Chlorine Activation Indoors and Outdoors via Surface-Mediated Reactions of Nitrogen Oxides with Hydrogen Chloride. *Proc. Natl. Acad. Sci.* **2009**, *106* (33), 13647 LP – 13654. https://doi.org/10.1073/pnas.0904195106.

(18) Finlayson-Pitts, B. J.; Ezell, M. J.; Pitts, J. N. Formation of Chemically Active Chlorine Compounds by Reactions of Atmospheric NaCl Particles with Gaseous N2O5 and ClONO2. *Nature* **1989**, *337* (6204), 241–244. https://doi.org/10.1038/337241a0.

(19) Roberts, J. M.; Osthoff, H. D.; Brown, S. S.; Ravishankara, A. R.; Coffman, D.; Quinn, P.; Bates, T. Laboratory Studies of Products of N2O5 Uptake on Cl− Containing Substrates. *Geophys. Res. Lett.* **2009**, *36* (20). https://doi.org/10.1029/2009GL040448.

(20) Li, Q.; Zhang, L.; Wang, T.; Tham, Y. J.; Ahmadov, R.; Xue, L.; Zhang, Q.; Zheng, J. Impacts of Heterogeneous Uptake of Dinitrogen Pentoxide and Chlorine Activation on Ozone and Reactive Nitrogen Partitioning: Improvement and Application of the WRF-Chem Model in Southern China. *Atmos. Chem. Phys.* **2016**, *16* (23), 14875–14890. https://doi.org/10.5194/acp-16-14875-2016.

(21) Riedel, T. P.; Bertram, T. H.; Crisp, T. A.; Williams, E. J.; Lerner, B. M.; Vlasenko, A.; Li, S.-M.; Gilman, J.; de Gouw, J.; Bon, D. M.; et al. Nitryl Chloride and Molecular Chlorine in the Coastal Marine Boundary Layer. *Environ. Sci. Technol.* **2012**, *46* (19), 10463–10470. https://doi.org/10.1021/es204632r.

(22) Sarwar, G.; Simon, H.; Xing, J.; Mathur, R. Importance of Tropospheric ClNO2 Chemistry across the Northern Hemisphere. *Geophys. Res. Lett.* **2014**, *41* (11), 4050–4058. https://doi.org/10.1002/2014GL059962.

(23) Roberts, J. M.; Osthoff, H. D.; Brown, S. S.; Ravishankara, A. R. N2O5 Oxidizes Chloride to Cl2 in Acidic Atmospheric Aerosol. *Science (80-.).* **2008**, *321* (5892), 1059–1059. https://doi.org/10.1126/science.1158777.

(24) Thornton, J. A.; Abbatt, J. P. D. N2O5 Reaction on Submicron Sea Salt Aerosol:

Kinetics, Products, and the Effect of Surface Active Organics. *J. Phys. Chem. A* **2005**, *109* (44), 10004–10012. https://doi.org/10.1021/jp054183t.

(25) Keene, W. C.; Stutz, J.; Pszenny, A. A. P.; Maben, J. R.; Fischer, E. V; Smith, A. M.; von Glasow, R.; Pechtl, S.; Sive, B. C.; Varner, R. K. Inorganic Chlorine and Bromine in Coastal New England Air during Summer. *J. Geophys. Res. Atmos.* **2007**, *112* (D10). https://doi.org/10.1029/2006JD007689.

(26) Keene, W. C.; Khalil, M. A. K.; Erickson, D. J.; McCulloch, A.; Graedel, T. E.; Lobert, J. M.; Aucott, M. L.; Gong, S. L.; Harper, D. B.; Kleiman, G.; et al. Composite Global Emissions of Reactive Chlorine from Anthropogenic and Natural Sources: Reactive Chlorine Emissions Inventory. *J. Geophys. Res. Atmos.* **1999**, *104* (D7), 8429–8440. https://doi.org/10.1029/1998JD100084.

(27) Le Breton, M.; Bacak, A.; Muller, J. B. A.; Xiao, P.; Shallcross, B. M. A.; Batt, R.; Cooke, M. C.; Shallcross, D. E.; Bauguitte, S. J. B.; Percival, C. J. Simultaneous Airborne Nitric Acid and Formic Acid Measurements Using a Chemical Ionization Mass Spectrometer around the UK: Analysis of Primary and Secondary Production Pathways. *Atmos. Environ.* **2014**, *83* (3), 166–175. https://doi.org/10.1016/j.atmosenv.2013.10.008.

(28) Rodhe, H.; Crutzen, P.; Vanderpol, A. Formation of Sulfuric and Nitric Acid in the Atmosphere during Long-Range Transport. *Tellus* **1981**, *33* (2), 132–141. https://doi.org/https://doi.org/10.1111/j.2153-3490.1981.tb01739.x.

(29) Crisp, T. a; Lerner, B. M.; Williams, E. J.; Quinn, P. K.; Bates, T. S.; Bertram, T. H. Observations of Gas Phase Hydrochloric Acid in the Polluted Marine Boundary Layer. *J. Geophys. Res. Atmos.* **2014**, 6897–6915. https://doi.org/10.1002/2013JD020992.Received.

(30) Furlani, T. C.; Veres, P. R.; Dawe, K. E. R.; Neuman, J. A.; Brown, S. S.; VandenBoer, T. C.; Young, C. J. Validation of a New Cavity Ring-down Spectrometer for Measuring Tropospheric Gaseous Hydrogen Chloride. *Atmos. Meas. Tech. Discuss.* **2021**, *2021*, 1–30. https://doi.org/10.5194/amt-2021-105.

(31) Angelucci, A. A.; Furlani, T. C.; Wang, X.; Jacob, D. J.; VandenBoer, T. C.; Young, C. J. Understanding Sources of Atmospheric Hydrogen Chloride in Coastal Spring and Continental Winter. *ACS Earth Sp. Chem.* **2021**. https://doi.org/10.1021/acsearthspacechem.1c00193.

(32) Hagen, C. L.; Lee, B. C.; Franka, I. S.; Rath, J. L.; Vandenboer, T. C.; Roberts, J. M.; Brown, S. S.; Yalin, A. P. Cavity Ring-down Spectroscopy Sensor for Detection of Hydrogen Chloride. *Atmos. Meas. Tech.* **2014**, *7* (2), 345–357. https://doi.org/10.5194/amt-7-345-2014.

(33) Wilkerson, J.; Sayres, D. S.; Smith, J. B.; Allen, N.; Rivero, M.; Greenberg, M.; Martin, T.; Anderson, J. G. In Situ Observations of Stratospheric HCl Using Three-Mirror Integrated Cavity Output Spectroscopy. *Atmos. Meas. Tech. Discuss.* **2021**, *2021*, 1–38. https://doi.org/10.5194/amt-2021-6.

(34) Eger, P. G.; Helleis, F.; Schuster, G.; Phillips, G. J.; Lelieveld, J.; Crowley, J. N. Chemical Ionization Quadrupole Mass Spectrometer with an Electrical Discharge Ion Source for Atmospheric Trace Gas Measurement. *Atmos. Meas. Tech.* **2019**, *12* (3), 1935–1954. https://doi.org/10.5194/amt-12-1935-2019.

(35) Haskins, J. D.; Jaeglé, L.; Shah, V.; Lee, B. H.; Lopez-Hilfiker, F. D.; Campuzano-Jost, P.; Schroder, J. C.; Day, D. A.; Guo, H.; Sullivan, A. P.; et al. Wintertime Gas-Particle

Partitioning and Speciation of Inorganic Chlorine in the Lower Troposphere Over the Northeast United States and Coastal Ocean. *J. Geophys. Res. Atmos.* **2018**, *123* (22), 12,812-897,916. https://doi.org/10.1029/2018JD028786.

(36) Dawe, K. E. R.; Furlani, T. C.; Kowal, S. F.; Kahan, T. F.; Vandenboer, T. C.; Young, C. J. Formation and Emission of Hydrogen Chloride in Indoor Air. *Indoor Air* **2019**, No. April 2018, 70–78. https://doi.org/10.1111/ina.12509.

(37) United States Environmental Protection Agency. Compendium of Methods for the Determination of Inorganic Compounds in Ambient Air: Determination of Reactive Acidic and Basic Gases and Strong Acidity of Atmospheric Fine Particles (<2.5 Mm) (Compendium Method IO-4.2). **1999**.

(38) Keene, W. C.; Long, M. S.; Pszenny, A. A. P.; Sander, R.; Maben, J. R.; Wall, A. J.; O'Halloran, T. L.; Kerkweg, A.; Fischer, E. V; Schrems, O. Latitudinal Variation in the Multiphase Chemical Processing of Inorganic Halogens and Related Species over the Eastern North and South Atlantic Oceans. *Atmos. Chem. Phys.* **2009**, *9* (19), 7361–7385. https://doi.org/10.5194/acp-9-7361-2009.

(39) Wiacek, A.; Li, L.; Tobin, K.; Mitchell, M. Characterization of Trace Gas Emissions at an Intermediate Port. *Atmos. Chem. Phys.* **2018**, *18* (19), 13787–13812. https://doi.org/10.5194/acp-18-13787-2018.

(40) Milbrandt, J. A.; Bélair, S.; Faucher, M.; Vallée, M.; Carrera, M. L.; Glazer, A. The Pan-Canadian High Resolution (2.5 Km) Deterministic Prediction System. *Weather Forecast.* **2016**, *31* (6), 1791–1816. https://doi.org/10.1175/WAF-D-16-0035.1.

(41) Madronich, S.; Flocke, S. The Role of Solar Radiation in Atmospheric Chemistry, in

Handbook of Environmental Chemistry. *Springer-Verlag, Heidelb.* **1998**, *P. Boule*, 1–26.

(42) Sarwar, G.; Simon, H.; Bhave, P.; Yarwood, G. Examining the Impact of Heterogeneous Nitryl Chloride Production on Air Quality across the United States. *Atmos. Chem. Phys.* **2012**, *12* (14), 6455–6473. https://doi.org/10.5194/acp-12-6455-2012.

(43) Thornton, J. A.; Kercher, J. P.; Riedel, T. P.; Wagner, N. L.; Cozic, J.; Holloway, J. S.; Dubé, W. P.; Wolfe, G. M.; Quinn, P. K.; Middlebrook, A. M.; et al. A Large Atomic Chlorine Source Inferred from Mid-Continental Reactive Nitrogen Chemistry. *Nature* **2010**, *464*, 271.

(44) Meinel, A. B.; Meinel, M. P. Applied Solar Energy Addison. Wesley Publishing Co 1976.

(45) Woolf, H. On the Computation of Solar Elevation Angles and the Determination of Sunrise and Sunset Times; 1968.

(46) Kasten, F.; Young, A. T. Revised Optical Air Mass Tables and Approximation Formula. *Appl. Opt.* **1989**, *28* (22), 4735–4738. https://doi.org/10.1364/AO.28.004735.

(47) Lawler, M. J.; Finley, B. D.; Keene, W. C.; Pszenny, A. A. P.; Read, K. A.; von Glasow, R.; Saltzman, E. S. Pollution-Enhanced Reactive Chlorine Chemistry in the Eastern Tropical Atlantic Boundary Layer. *Geophys. Res. Lett.* **2009**, *36* (8). https://doi.org/10.1029/2008GL036666.

(48) Jourdain, B.; Legrand, M. Year-Round Records of Bulk and Size-Segregated Aerosol Composition and HCl and HNO3 Levels in the Dumont d'Urville (Coastal Antarctica) Atmosphere: Implications for Sea-Salt Aerosol Fractionation in the Winter and Summer. *J. Geophys. Res. Atmos.* **2002**, *107* (D22), ACH 20-1-ACH 20-13.

https://doi.org/https://doi.org/10.1029/2002JD002471.

(49) Keene, W. C.; Pszenny, A. A. P.; Maben, J. R.; Stevenson, E.; Wall, A. Closure Evaluation of Size-Resolved Aerosol PH in the New England Coastal Atmosphere during Summer. *J. Geophys. Res. Atmos.* **2004**, *109* (D23). https://doi.org/https://doi.org/10.1029/2004JD004801.

(50) Alicke, B.; Platt, U.; Stutz, J. Impact of Nitrous Acid Photolysis on the Total Hydroxyl Radical Budget during the Limitation of Oxidant Production/Pianura Padana Produzione Di Ozono Study in Milan. *J. Geophys. Res. Atmos.* **2002**, *107* (D22), LOP 9-1-LOP 9-17. https://doi.org/https://doi.org/10.1029/2000JD000075.

Chapter 5.

Characterization of a Conversion Technique to Measure Total Chlorine in Ambient Air

Abstract

Total gaseous chlorine (TCl_g) measurements can illuminate unknown sources of Cl to the atmosphere. Techniques for measuring TCl_g have been limited to offline analysis of extracted filters and do not provide suitable temporal information on fast atmospheric process. High time-resolution in-situ measurements of TCl_g can be captured by combusting ambient air on a catalytic platinum (Pt) substrate contained in high temperature furnace that is coupled to a cavity ring-down spectrometer (CRDS). The method relies on the complete combustion of TCl_g to release Cl atoms that react to form HCl, detection of HCl by CRDS has been shown to be fast and reliable. We constructed custom organochlorine permeation devices (PDs) to generate low emitting gas-phase standards for dichloromethane (DCM), 1-chlorobutane (CB), and 1, 3-dichloropropene (DCP). The optimal conversion temperature and residence time through the high-temperature furnace was 825 °C and 1.5 seconds, respectively. Complete conversion is indicated by the near unity orthogonal distance regression analysis slope (±σ) of 0.996 ± 0.012, 1.048 ± 0.006, and 1.027 ± 0.061 for DCM, CB, and DCP, respectively. Breaking these strong C-Cl bonds represents a proof of concept for complete conversion of all similar or weaker bonds that characterize all other TCl_g. We applied this technique to both outdoor and indoor environments and found reasonable comparisons in ambient background mixing ratios with the sum of expected HCl from known Cl species. We measured the converted TCl_g in an indoor environment during bleaching events and observed varying increases of 5–18 ppbv of TCl_g. The method validated here is capable of measuring in-situ TCl_g and has a broad range of applications to make routine TCl_g measurements in a variety of regions.

5.1 Introduction

Chlorine (Cl) containing compounds in the atmosphere can impact air quality, climate, and health.[1–4] Gaseous chlorinated compounds are either organic (e.g., chloroform, dichloromethane, and methyl chloride) or inorganic (e.g., Cl_2, hydrogen chloride (HCl), and nitryl chloride ($ClNO_2$)), with the latter being more reactive under most atmospheric conditions. Impacts on air quality and climate are due to the high reactivity of atomic Cl produced by common atmospheric reactions (e.g., photolysis and oxidation) of Cl containing compounds.[5–7] The Cl cycle can affect air pollutants and climate forcing agents, such as methane, ozone, and particles (formation and composition), which will influence climate through direct and indirect radiative effects[7] and are important in both the stratosphere and the troposphere.[6,8,9] High levels of some total gaseous chlorine (TCl_g) species (e.g., Cl_2) are known to be toxic.[4] The implications of all TCl_g species on human health are not well understood for low level exposure for extended periods of time. Some potential impacts include the chlorination of squalene, a major part of human skin oils, by hypochlorous acid (HOCl);[10] respiratory irritation and airway obstruction by Cl_2;[4] and increased incidence of asthma and other chronic respiratory issues following exposure to chloramines.[3] Sources of Cl to the atmosphere are highly variable and depend on both direct emissions and indirect regional Cl activation chemistry.[11–13] Cl activation occurs when atmospheric processes transform relatively unreactive chloride (Cl^-) into reactive gaseous chlorine (Cl_y) and will contribute to TCl_g. In this work, TCl_g represents all gas-phase chlorine-containing species, including both inorganic and organic species.

Understanding global levels of TCl_g is difficult due to changes in emissions and chemistry, and our best estimate comes from modelling studies combined with collaborative efforts to compose routine reports on halogenated substances, such as the World Meteorological

Organization scientific assessment of stratospheric ozone depletion.[14] Mixing ratio estimates of halogenated species from this report are from individual measurements from different groups (e.g., National Oceanic and Atmospheric Administration (NOAA) and Advanced Global Atmospheric Gases Experiment (AGAGE)). These measurements combine flask (captured gas from clean air sectors) and in-situ measurements typically by gas chromatography from most recent field campaigns and routine sampling sites (e.g., CONvective Transport of Active Species in the Tropics (CONTRAST)).[15–19] From the 2018 report there was an observed rate of -12.7 ± 0.9 pptv Cl yr^{-1} in total tropospheric chlorine yields from Montreal Protocol-controlled substances (e.g., chlorofluorocarbons (CFCs) and hydrochlorofluorocarbons (HCFCs)).[14] The decrease in controlled Cl emissions has been slightly offset by an increase in observed natural halogenated very short-lived substances (VSLS) that are not controlled by the Montreal Protocol. Increases in dichloromethane accounts for the majority of the 20 pptv rise in total chlorine from VSLSs.[14] Total chlorine from all HCFCs has continued to increase in the atmosphere since 2016 ozone assessment and reached 309 ppt.[14] A recent study by Zhai et. al., (2021), estimated an increase of up to 170% of Cl_y since preindustrial 1970s can be attributed to anthropogenic sources.[20] Unexpected and new sources of TCl_g that affect the Cl budget have been discovered in the recent past indicating our understanding of the Cl budget is incomplete. For example, unexpected increases in CFC-11 emissions suggests new production not reported to United Nations Environment.[14] A new source of chloroform was also recently identified and attributed to halide containing organic matter derived from penguin excrement in the Antarctic tundra.[21]

Understanding TCl_g source and sink chemistry is not only important for the ambient atmosphere but indoor environments as well. Uncertainty in sources and levels of chemicals, including TCl_g, indoors is related to a large number of potential sources, heterogeneity in

individual indoor environments, and the relatively few studies that have focused on indoor chemistry relative to outdoor. The role of TCl_g on indoor air quality has been investigated in a few studies.[22–28] The most common active form of TCl_g indoors is HOCl, which has a broad range of applications, such as an antimicrobial agent in water systems or as the active ingredient in household and commercial cleaning agents. Some studies have reported the presence of VSLSs such as chloroform and carbon tetrachloride above bleach cleaning solutions indoors,[29,30] and chloroform has been observed during water-based cleaning activities, such as showering and clothing washing.[25,26,28]

Constraining the Cl budget is critical to better understanding its contributions to climate, air quality, and human health. Robust total Cl measurements are desirable because individual measurements are not feasible due to the large number of species (Table 5-1). Currently, TCl_g has been assessed using complex models and combined estimates from known species,[2,14,16,20,38,39] and it is a combination of both these modelled and measured measurements that help to elucidate unknowns that can not be captured solely by models. It is therefore essential to have a method capable of measuring true TCl_g to explain discrepancies between model and measured estimates due to unknown species. Measurements of total elemental composition, including total Cl, have been used for monitoring and managing both known and unknown compounds in the condensed phase.[31–37] TCl_g methods have been limited to offline analysis of scrubbed sample gas (e.g., flue); these methods rely on multiple extraction steps and the combustion (800–900 °C) of halogenated compounds that are extracted into aqueous solutions and detected by either ion chromatography or microcoulometric titration.[32,40] Other methods to measure extractable organic halogens involve neutron activation analysis.[35,36,41] The aforementioned methods all suffer from inherent uncertainties from extraction methods. Because offline techniques do not have the temporal

resolution to effectively probe fast source and sink chemistry in the atmosphere, in-situ measurements of total elemental gaseous composition have been developed.[42–45] Total nitrogen has been measured using Pt-catalyzed combustion coupled to online chemiluminescence technique (see Figures C-1 and C-2).[46] Using a similar approach, we describe here a method that converts TCl_g into HCl that is amenable to measurement by a high time-resolution cavity ring-down spectrometer (CRDS). This technique relies on the complete combustion of TCl_g, which yields chlorine atoms. These Cl atoms readily form HCl via hydrogen abstraction (R5.1.1), in this case from propane which is supplied in excess.

$$Cl\ (g) + C_3H_8\ (g) \rightarrow HCl\ (g) + C_3H_7\ (g) \qquad \text{R5.1.1}$$

The objectives of this paper are to: (i) Develop and validate an instrument capable of in situ measurement of TCl_g through conversion to HCl and detection by CRDS; and (ii) Demonstrate its applications to outdoor and indoor air TCl_g measurements.

Table 5-1. Summary of observed mixing ratios, bond dissociation energies, and atmospheric lifetimes for most chlorinated species expected to be present in appreciable amounts in the troposphere.

Chemical formula	Observed mixing ratio (pptv)		Atmospheric lifetime (years)	Cl-containing bond dissociation energy (kJ mol^{-1})	Expected TCl_g (pptv)*	
	Outdoor	Indoor			Outdoor	Indoor**
	Chlorofluorocarbons (CFCs)					
CCl_3F (CFC-11)	228.9[a]	-	52[a]	305[b]	686.8	686.8
CCl_2F_2 (CFC-12)	514.6[a]	-	102[a]	344[c]	1029.3	1029.3
$CClF_3$ (CFC-13)	3.04[a]	-	640[a]	364[c]	3.04	3.04
CCl_2FCCl_2F (CFC-112)	0.42[a]	-	63.6[a]	-	1.68	1.68
CCl_3CClF_2 (CFC-112a)	0.067[a]	-	52[a]	351[c]	0.27	0.27
CCl_2FCClF_2 (CFC-113)	71.3[a]	-	93[a]	-	214	214
CCl_3CF_3 (CFC-113a)	0.66[a]	-	55[a]	309[c]	1.98	1.98
$CClF_2CClF_2$ (CFC-114)	15.45[a]	-	189[a]	365[c]	30.9	30.9
CCl_2FCF_3 (CFC-114a)	1.04[a]	-	105[a]	-	2.08	2.08
$CClF_2CF_3$ (CFC-115)	8.58[a]	-	540[a]	365[c]	8.58	8.58
	Hydrochlorofluorocarbons (HCFCs)					
$CHClF_2$ (HCFC-22)	239.1[a]	-	11.9[a]	360[c]	239.1	239.1
CH_2ClCF_3 (HCFC-133a)	0.39[a]	-	4.6[a]	360[c]	0.39	0.39
CH_3CCl_2F (HCFC-141b)	24.53[a]	-	9.4[a]	388[c]	49.1	49.1
CH_3CClF_2 (HCFC-142b)	22.6[a]	-	18[a]	410[c]	22.6	22.6
	Halons					
$CBrClF_2$ (Halon-1211)	3.6[a]	-	16[a]	-	3.6	3.6
	Chlorocarbons					
CH_3Cl	555.9[a]	-	0.9[a]	339[b]	555.9	555.9

(Methyl chloride)						
CCl_4 (Carbon tetrachloride)	81[a]	-	26[a]	293[b]	324	324
CH_3CCl_3 (Methyl chloroform)	2.7[a]	-	5[a]	368[c]	8.26	8.26
CH_2Cl_2 (Dichloro-methane)	35.95[a]	-	180 days[a]	310[b]	71.9	71.9
$CHCl_3$ (Chloroform)	8.9[a]	-	183 days[a]	311[c]	26.7	26.7
CH_2ClCH_2Cl (1,2-Dichloroethane)	12.8[a]	-	82 days[a]	-	25.6	25.6
C_2Cl_4 (Tetrachloro-ethylene)	1.1[a]	-	110 days[a]	350[c]	4.54	4.54
	Inorganic chlorine					
HCl	0–8000[d]	0–700[n]	1–2 days [15 days][j]	432[b]	0–8000[d]	0–700
Cl_2	0–20[e]	0–100 ppbv[i]	<1 min[g]	242[b]	0–20[e]	0–200 ppbv
HOCl	0–60[e]	0–300 ppbv[i]	<1 min[g]	251[b]	0–60[e]	0–300 ppbv
ClO	0–10[f]	-	-	272[b]	0–10[f]	-
ClNO	0–3[d]	-	5–45 min[k]	159[b]	0–3[d]	-
$ClNO_2$	0–8000[d]	0–20 ppbv[i]	0.73–31 hrs[l]	142[b]	0–8000[d]	0–20 ppbv
$ClONO_2$	0–10[g]	-	-	109[h]	0–10[g]	-
	Chloramines					
NH_2Cl	-	0–60[i]	-	251[b]	-	0–60 ppbv
$NHCl_2$	-	0–20 ppbv[i]	9.1 min[m]	280[b]	-	0–40 ppbv
NCl_3	-	0–4 pbbv[i]	5.3 min[m]	381[b]	-	0–12 ppbv
	Expected TCl_g				3.3–19 ppbv**	3.3–640 ppbv***

(a) Tropospheric mixing ratios from 2018 world meteorological organization scientific ozone depletion assessment.[14] (b) Bond dissociation energies, data from Huheey and Cottrell, 1958.[47] (c) Bond dissociation energies, data from Shi et al., 2011.[48] Tropospheric mixing ratios for inorganic chlorines are highly variable given local conditions, a conservative range is given. (d) Data from Raff et al., 2009.[12] (e) Data from Lawler et al., 2011.[49] (f) Data from Platt and Janssen, 1995.[50] (g) Data estimated from Wang et al., 2019.[38] (h) Data taken from Casper et al., 1993.[51] (i) Data taken from Mattila et al., 2020, during an indoor air study; emissions after bleaching events represent a worst case scenario.[22] (j) Lifetime with respect to deposition and lifetime with respect to OH in brackets, Data taken from Crisp et al., 2014.[52] (k) Data taken from Keene et al., 1990.[53] (l) lifetime ranges with solar zenith angle, data taken from

Ganske et al., 1992.[54] (m) Lifetimes calculated from first order photolysis decay rates in a well lit room, data taken from Wong et al., 2017.[55] (n) This study during bleaching event (see Section 5.3.4.).(*) Expected TCl_g mixing ratio represents the total number of Cl atom yielded from complete conversion. (**) Indoor levels of CFCs, HCFCs, and chlorocarbons are assumed to be the same as outdoor (***) Upper estimates are highly depended on local conditions and direct emissions.

5.2 Materials and experimental methods

5.2.1 Chemicals

Commercially available reagents were purchased from Sigma-Aldrich: Dichloromethane (DCM, HPLC grade, Oakville, Ontario, Canada), cis-1,3-dichloropropene (DCP, 97%, Milwaukee, Wisconsin, USA), 1-chlorobutane (CB, 99.5%, Milwaukee, Wisconsin, USA), and 52 mesh sized platinum catalyst (99.9 %, Milwaukee, Wisconsin, USA). Nitrogen (grade 4.8) and propane (C_3H_8, 12.7% in nitrogen, v/v) gas was from Praxair (Toronto, Ontario, Canada). Experiments used deionized water generated by a Barnstead Infinity Ultrapure Water System (Thermo Fisher Scientific, Waltham, Massachusetts, USA; 18.2 MΩ cm^{-1}). All clean air was generated by a custom lab made zero-air generator (see Figure C-3).

5.2.2 HCl and total chlorine (HCl-TCl) instrument

The main components of the HCl-TCl (Figure 5-1) are platinum catalyst mesh, quartz glass flow tube, and a split-tube furnace (Protégé Compact, 1100°C max temperature, Thermcraft incorporated, North Carolina, USA). A crucial component for conversion is the platinum catalyst, which was ~2 grams platinum mesh and a total combined surface area of 134 cm^2. Sample gas was mixed with critical orifice-regulated propane gas (62 ± 6.2 sccm), provided in excess prior to introduction to HCl-TCl to promote (R5.1.1). Added uncombusted propane can cause spectral interferences at temperatures < 650 °C (see Figure C4), and is recommended here to only add when temperatures exceed 650 °C. The mixing line carrying clean air dilution flows was controlled by a 10 L min^{-1} mass flow controller (MFC, GM50A, MKS instruments, Andover, Massachusetts, USA). Length of the sample gas tubing to the HCl-TCl was 0.6 m, and the transfer line out of the

HCl-TCl to CRDS was 0.2 m. The coupled CRDS (Picarro G2108 Hydrogen Chloride Gas Analyzer) can capture transient fast HCl formation processes (as discussed in Chapters 3 and 4). The CRDS collects data at 0.5 Hz, which was averaged to 30 sec for the purposes of this work. The limit of detection (LOD) for this instrument 30 sec is 18 pptv and well below expected HCl from TCl_g conversion.

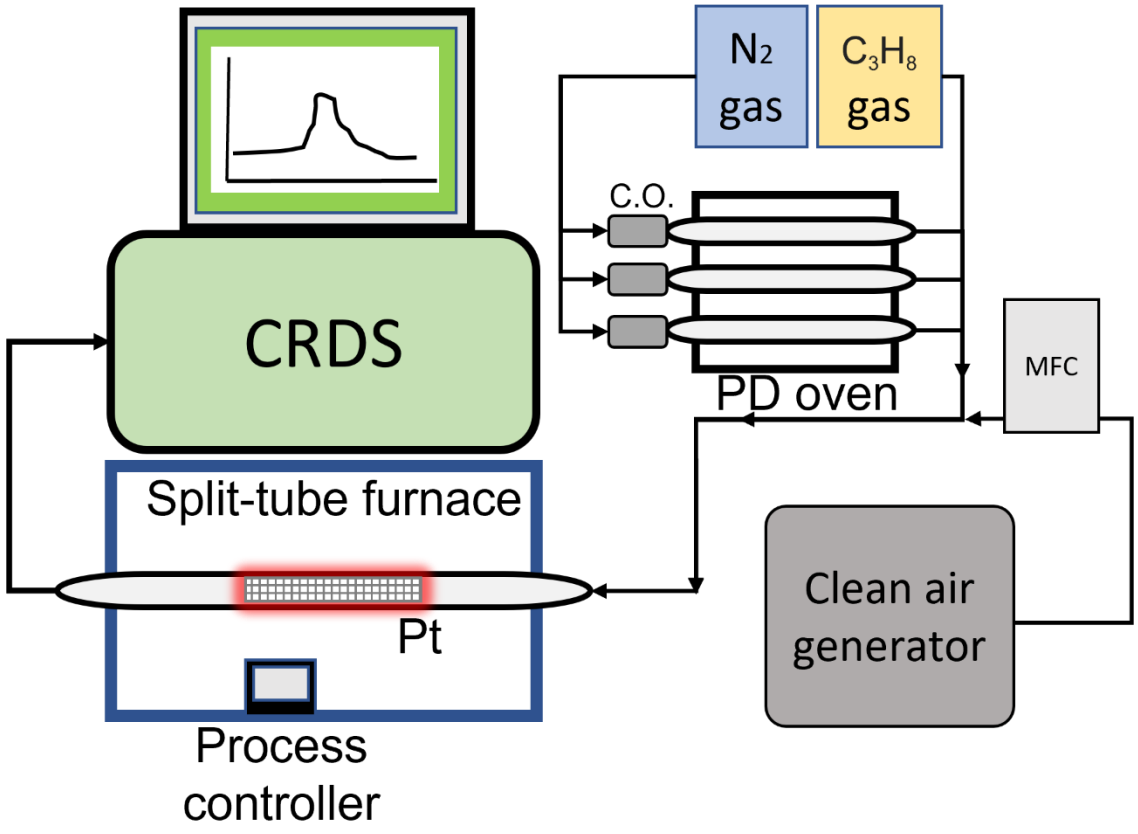

Figure 5-1. Sampling schematic showing the key components of the HCl-TCl coupled to CRDS analyzer. Not to scale.

5.2.3 Preparation of permeation devices (PDs)

The in-house assembly of permeation devices (PDs) is as follows; approximately 200 µL of each organo chlorine liquid was pipetted into a 50 mm perfluoroalkoxy (PFA) tube (3 mm i.d. with 1 mm thickness), thermally sealed at one and plugged at the other end with porous polytetrafluoroethylene (PTFE) (13 mm length by 3.17 mm o.d.). The polymers allow a consistent

mass of standard gas to permeate at a given temperature and pressure. An aluminum block that was temperature-controlled (Omega^{TM}; CN 7823, Saint-Eustache, QC, Canada) using a cartridge heater (Omega^{TM}; CIR-2081/120V, Saint-Eustache, QC, Canada) housed the PD and was regulated to 30.0 ± 0.1 °C. Dry N_2 gas flowed through a PFA housing tube (1.27 cm o.d.) in the block, containing the PD. Stable flows of 120 ± 12, 99 ± 9.9, and 120 ± 12 standard cubic centimeters per minute (sccm) for DCM, CB, and DCP, respectively, carrier gases passed through the housing tube in the oven were maintained using a 50 µm diameter critical orifice (Lenox laser, Glen Arm, Maryland, USA, 30 psi; SS-4-VCR-2-50). Flows were measured using a DryCal Definer 220 (Mesa Labs, Lakewood, Colorado, USA). The mass emission rate of each organochlorine from the PDs was quantified gravimetrically over a period approximately 4 weeks. Mass emission rates for each PD were determined as 640 ± 13, 240 ± 36, and $1.20\times10^4 \pm 0.02\times10^4$ ng min^{-1} (n=3, ± 1σ) at 30 °C for DCM, CB, and DCP, respectively.

5.2.4 HCl-TCl optimization

Gas phase standards were used to test the conversion efficiency of chlorinated compounds to form HCl. The standards were generated using PDs containing DCM, CB, and DCP. Bond dissociation energies for carbon-chlorine bonds typically range between 310 and 410 kJ mol^{-1} (Tables 5-1 and C-1). Determining the temperature at which we could provide enough energy to break these bonds was an important step. The split-tube furnace has a process controller capable of increasing or decreasing at a set °C min^{-1}. By introducing a consistent amount of each of the organochlorines, separately, to the HCl-TCl set over a simple temperature ramping program we can monitor in real-time when the bonds start to break by measuring the formation of the resulting HCl. The breakthrough temperature is determined when the measured HCl begins to plateau at 100% conversion. All inlet lines and fittings were made of PFA unless stated otherwise.

To optimize residence time in the hot-tube with the Pt catalyst, flows containing DCM sample gas in clean air ranged from 0.6–5.5 L min^{-1}, yielding a range of residence times of 0.5–4.5 sec in the HCl-TCl. Temperature remained a constant 825 °C throughout the experiment and dilution flow after exiting the HCl-TCl remained a constant 4.0 L min^{-1}.

We tested the HCl-TCl conversion for 5 different mixing ratios of all three PDs standards, DCM, CB, and DCP, under three conditions: (1) both Pt catalyst and added propane, (2) only Pt catalyst, and (3) only added propane. Each gas was tested individually under the same conditions; sample gas from PDs was mixed with propane and immediately diluted into clean air using a 10 L min^{-1} MFC (GM50A, MKS instruments, Andover, Massachusetts, USA). The dilution flows ranged from 2.2–9.0 L min^{-1}. The sampling lines were the same lengths as stated previously. In this experiment the CRDS flowrate of 2 L min^{-1} was sufficient to give an optimal residence time of 1.5 sec through the HCl-TCl (see Section 5.3.1). In all experiments the CRDS subsampled through the HCl-TCl off the main transfer line and the excess sampling gas was directed outdoors through a carbon trap waste line.

5.2.5 Outdoor air HCl-TCl measurement

Outdoor air sampling was performed from November 17–19, 2021 (Eastern daylight time, EDT). The sampling site was the air quality research station, located on the roof of the Petrie Science and Engineering building at York University in Toronto, Ontario, Canada (43.7738° N, 79.5071° W, 220 m above sea level). The HCl-TCl was co-located with a Campbell scientific weather station paired with a cr300 datalogger, for meteorological data. All indoor inlet lines and fittings were kept at room temperature while the outdoor temperature ranged from 16 to 24 °C. All inlet lines and fittings were made of PFA unless stated otherwise. All indoor inlet lines and fittings were kept in a thermostated room that fluctuated from 20–25 °C. A mass flow controller (GM50A,

MKS instruments, Andover, Massachusetts, USA) regulated a sampling flow of 14.7 L min^{-1} using a diaphragm pump through a 2.4 m sampling inlet (I.D. of 0.375") from the ambient outdoor environment. The outdoor air was pulled through a URG Teflon Coated Aluminum Cyclone (URG Corporation, Chapel Hill, North Carolina, USA) with a 2.5 µm cut-off for particulate matter. The CRDS sampled 2 L min^{-1} through the HCl-TCl and the from the main inlet line, yielding a total inlet flow of 16.7 L min^{-1}. The CRDS sample flow passed through a polytetrafluoroethylene (PTFE) filter (2 µm pore size, 47 mm diameter, TISCH scientific, North Bend, Ohio, USA) and then two high efficiency particulate air (HEPA) filters contained within the CRDS outer cavity metal compartment heat-regulated to 45 °C. Instances of flagged instrument errors in the CRDS data during ambient observations were removed as standard practice in quality control procedures.

5.2.6 Indoor air HCl-TCl bleach measurement

Commercial cleaning products containing sodium hypochlorite are known to emit reactive chlorine species indoors, HOCl and Cl_2.[55] To test indoor applications of the HCl-TCl, four separate 2 m x 2 m areas of the laboratory floor were cleaned with a common household bleach. The bleach solution was mixed as per manufacturers instruction (100 times dilution of a 6 % w/v sodium hypochlorite solution) and ~400 mL was applied using a mop to the designated area for 1 minute. The distance from the suspended 2 m transfer line to the floor was ~1 m. The flowrate through the HCl-TCl and inlet was the 2 L min^{-1} CRDS flowrate. Each sectioned area was bleached, for a total of 4 separate bleaching events separated in time by ~1 hour. Three of these events were measured using the HCl-TCl, while one event was measured without (measuring HCl only).

5.3 Results and Discussion

5.3.1 HCl-TCl temperature and residence time optimization

We present a critical approach to validate this method by testing conversion efficiency of organochlorines under different operating parameters and conditions. Testing all TCl_g species is

not feasible, but by testing compounds that contain strong Cl-containing bonds, we can assume at least equal efficacy of the system in the breakage of weaker Cl-containing bonds. We selected very strong Cl–C bonds (primary alkyl chlorides) and use them as a proxy for compounds containing weaker Cl bonds; therefore, by demonstrating their complete conversion we set good precedent for conversion of all TCl_g. The temperature of the furnace is a key factor in accomplishing complete combustion, and the minimum temperature to break these C-Cl bonds was determined. A simple temperature ramping program was used to determine the breakthrough temperature as follows; The temperature was increased at a rate of 2.7 °C min^{-1} starting at 300 °C and ending at 800 °C and required 3 hours to complete. The temperature breakthrough was found to be ~800 °C for the tested organochlorines (Figure C-5).

Determining the optimal residence time of sample gas in the HCl-TCl was the first test in achieving an optimized method for TCl_g conversion. Using a temperature slightly above the observed breakthrough of 800 °C determined above (825 °C, see Figure C-6), six residence times were tested, ranging from 0.5 to 4.5 seconds in the HCl-TCl (Figure 5-2). At each residence time the conversion efficiency was determined, where conversion efficiency is calculated as follows;

$$\text{Conversion efficiency} = \frac{\text{Measured } TCl_g}{\text{Expected } TCl_g} \times 100\ \% \qquad \text{E1}$$

The optimal residence time was at ~1.5 seconds, corresponding to a conversion efficiency of 100.1 ± 0.1 %. When residence times were lower (i.e., sample gas travels quicker through the system) than 1.5 seconds the conversion efficiencies were lower by 2 – 10%, the measured HCl signal was more erratic, and it took longer to stabilize. When residence times were higher (i.e., sample gas travels slower through the system) than 1.5 seconds the conversion efficiencies were comparable

(±2 %), but the measured HCl suffered from longer equilibration times due to increased surface effects. A residence time of 1.5 seconds was selected for all HCl-TCl experiments.

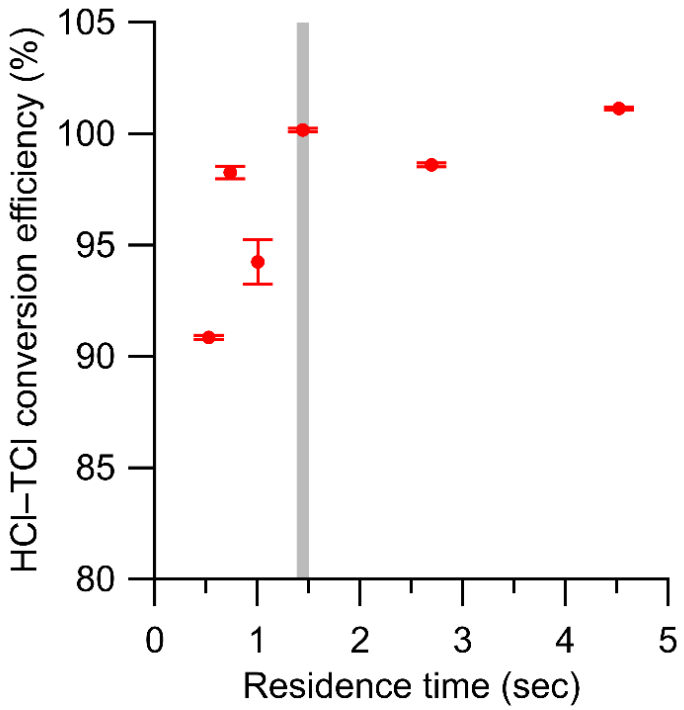

Figure 5-2. Conversion efficiency of DCM plotted against the residence time in the HCl-TCl. Error bars represent the percent relative standard deviation of the measured HCl by the CRDS over ~30 minutes, after signal has plateaued. Grey vertical line denotes selected residence time.

5.3.2 HCl-TCl Conversion efficiency

The conversion of each of the three chosen organochlorines using the HCl-TCl was tested at 5 different mixing ratios. The mixing ratios tested for DCM were 41, 54, 80, 111, and 165 ppbv. The mixing ratios tested for CB were 3.5, 4.6, 6.8, 9.5, and 14 ppbv. The mixing ratios tested for DCP were 121, 259, 468, 651, and 967 ppbv. All three showed good linearity and near 1:1 correlation with the HCl expected to be formed from the PD under standard operating conditions (solid circles in Figure 5-3). Due to differences in PD emission rates, the values are normalized to the highest mixing ratio to more easily visualize comparisons. Under condition (1) with both Pt and propane the orthogonal distance regression slope (±σ) was 0.996 ± 0.012, 1.048 ± 0.006, and

1.027 ± 0.061 for DCM, CB, and DCP, respectively. This corresponds to near-100% conversion efficiency for all three compounds (Table 5-2). With only the Pt catalyst (condition (2)), the HCl-TCl conversion was 80.7 ± 0.4, 54.1 ± 1.6, 54.3 ± 3.5% for DCM, CB, and DCP, respectively. The added hydrogen source (propane) is needed to promote R5.1.1. The hydrogen dependence for near unity conversion could be crucial in applications to ambient air measurements where total Cl levels are expected to be equal to (or exceed if measuring direct emission sources) the mixing ratios tested here. When the Pt catalyst was removed (condition (3)) the HCl-TCl conversion was 94.4 ± 4.6, 44.2 ± 0.9, 41.7 ± 3.4% for DCM, CB, and DCP, respectively. The observed dependence of the Pt catalyst indicates that a reactive surface in important to aid complete combustion. The better conversion for DCM in the absence of the Pt catalyst or hydrogen source may be attributed to its lower BDE (310 kJ mol^{-1}) compared to estimated BDEs for CB and DCP (CB inferred from Table C-1 (~410 kJ mol^{-1}), and DCP from Tetrachloroethylene (350 kJ mol^{-1} in Table 5-1)). The good linearity for all three compounds shows that the HCl-TCl is capable of complete conversion of mono and polychlorinated species on sp^3 and sp^2 carbons. The complete combustion of the strong C-Cl bond on the primary alkyl chloride (CB) demonstrates the efficacy of the HCl-TCl. Breaking these relatively strong C-Cl bonds is a good proof of concept for complete conversion of all similar or weaker bonds that characterize all other TCl_g.

The comparison presented here is a worst-case scenario because the sampled mixing ratios (as high as almost 1 ppmv for DCP) were greater than expected for ambient monitoring and therefore required more time to equilibrate to reach a stable signal. Although, the good linearity for these high mixing ratios shows precedent that it is capable of capture events as high as 1 ppmv of HCl for a litany of experimental applications that is further explored in Section 5.3.4. To practically validate the HCl-TCl under real-world conditions and atmospherically relevant mixing

ratios we deployed and configured the system to measure ambient air, discussed further in Section 5.3.3.

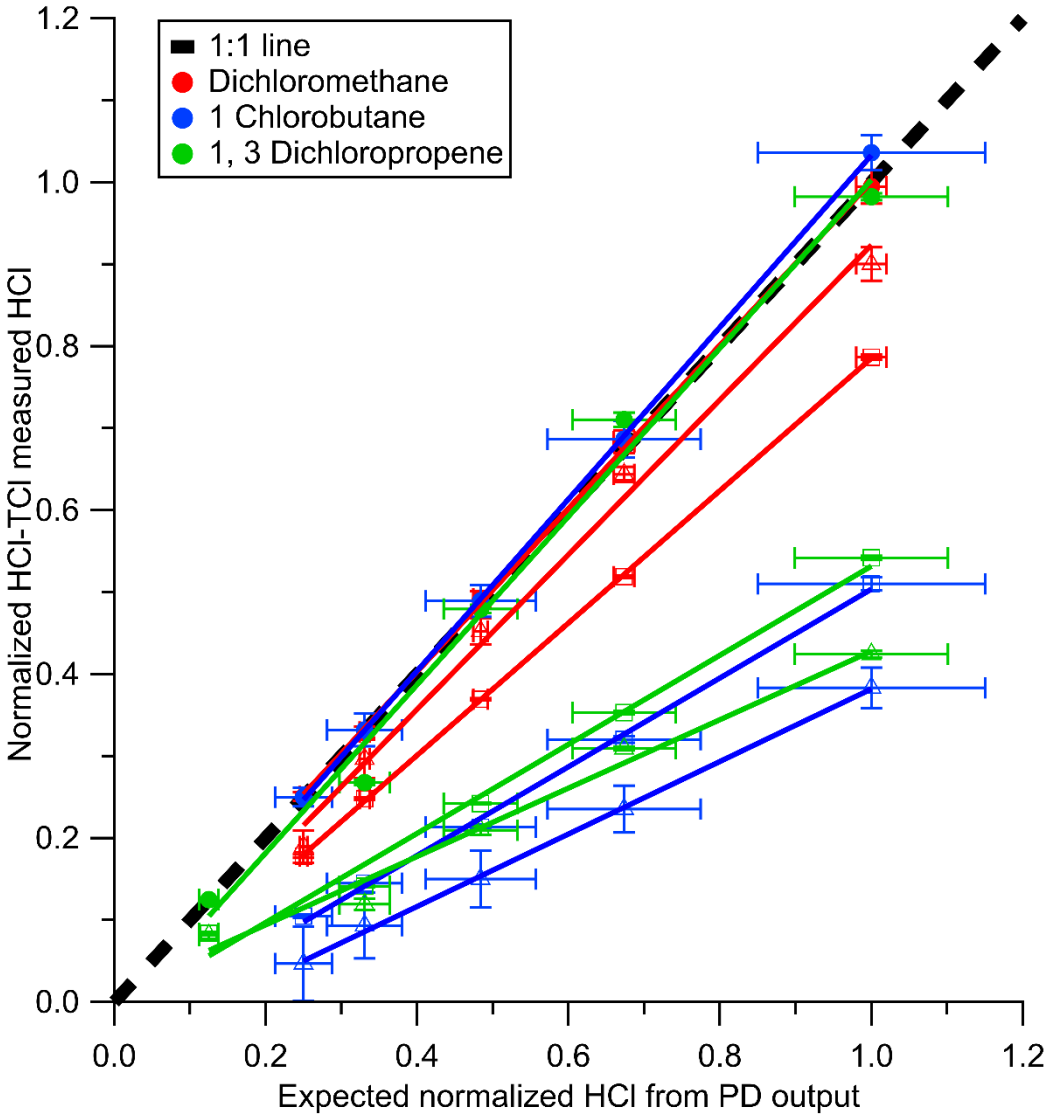

Figure 5-3. HCl measured by CRDS plotted against the expected HCl from HCl-TCl converted DCM (red), 1 Chlorobutane (blue), and 1, 3 Dichloropropene (green) under three conditions. All values are normalized to the highest expected HCl concentration to better illustrate deviations from unity (dashed black line). HCl-TCl conversion is shown for both Pt and propane added (condition (1), solid circles), with only Pt (condition (2), hollow squares), and only propane (condition (3), hollow triangles). Error bars on the y-axis represents 1σ in the HCl signal for 10 minutes. Error bars on the x-axis represent the error in the PD used to generate DCM.

Table 5-2. Conversion efficiency for tested organochlorine compounds under the three conditions. Conversion efficiency was determined from the orthogonal distance regression slope and ± σ and propagated error from individual PDs.

Compound	BDE ($kJ\ mol^{-1}$)	Conversion efficiency (%)		
		Condition 1	Condition 2	Condition 3
DCM	310	99.6 ± 3.2	80.7 ± 2.4	94.4 ± 6.6
CB	410	104.8 ± 5.6	54.1 ± 6.6	44.2 ± 5.9
DCP	350	102.7 ± 7.8	54.3 ± 5.2	41.7 ± 5.1

5.3.3 HCl-TCl applications to outdoor air

We deployed and configured the system to measure ambient air, which we compare to the expected TCl_g range from complete combustion of total Cl (Table 5-1). The apparatus subsampled off a main inlet pulling ambient air and combusting trace gases on a reactive catalyst from November 17–19, 2021 (Figure 5-4). The apparatus had zero air overflow the inlet 1 hour prior to and after outdoor sampling. Reported HCl mean mixing ratios from Chapter 3 and Angelucci et al., (2021), for this sampling location are 106 and 67 pptv, respectively, and ranged from 10 – 600 and <4 – 541 pptv, respectively.[56] The maximum, minimum, and mean of observed TCl_g was 3.5 ppbv, 2.0, and 2.5 ppbv, respectively. The mean TCl_g is higher than the observed HCl levels at this location and but below the range (3.3–19 ppbv, Table 5-1) of expected mixing ratios of TCl_g. The high observed relative humidity (RH) likely led to greater wet deposition of TCl_g species and lower observed levels. There was no observed impact on observed TCl_g dues to changes in wind direction or wind speed and likely indicates a well mixed boundary layer. Data compiled in Table 5-1 is not a complete representation of the total chlorine in the troposphere and represents measurements from many different regions, making it difficult to compare absolute magnitudes. The high variability (2.0–3.5) of measured TCl_g in this urban environment shows that direct sources or indirect formation is changing the observed abundance by an appreciable amount over the few-

hour sampling period. Demonstrating reasonable conversion of ambient TCl_g sets good precedent for applications of this method to future field campaigns and to different ambient environments, such as indoors. The detection of elevated Cl_{tot} during indoors activities that used chlorine containing cleaning product is an application explored here.

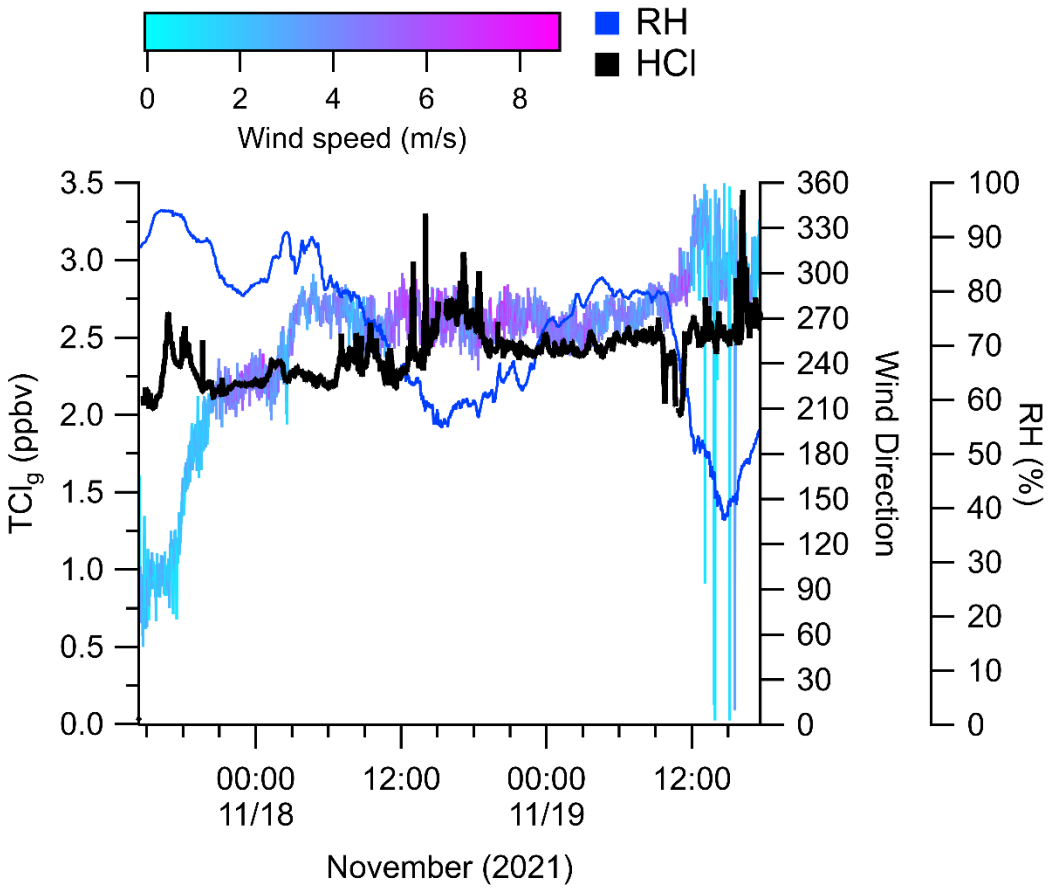

Figure 5-4. Monitoring TCl_g in outdoor air through HCl-TCl.

5.3.4 HCl-TCl applications to indoor cleaning events

We performed four bleaching events in a well-lit indoor room and measured TCl_g using the HCl-TCl (Figure 5-5). The first cleaning event was done without the HCl-TCl and has a local maximum of 656 pptv HCl (black). These levels are comparable to peak HCl levels of ~500 pptv observed from surface application of bleach in an occupied home.[24] Observed mixing ratios during bleaching events monitored by the HCl-TCl are much higher than that seen with just the CRDS,

indicating the presence of reactive Cl compounds. The maximum values of TCl_g from HCl-TCl operated cleaning event 1 (purple), 2 (blue), and 3 (red), were 18.3, 12.1, and 6.62 ppbv, respectively (Figure 5-5). These levels are much higher than observed in outdoor air (Section 5.3.3) and are within the range of expected TCl_g from Table 5-1. Reactive chlorine species that have previously been observed to be emitted from surface bleaching are Cl_2, HOCl, $ClNO_2$, NH_2Cl, $NHCl_2$, and NCl_3,[22,55] all of which have been observed by chemical ionization mass spectrometry. The levels of reactive chlorine observed during bleaching events is highly variable but can be >100s of ppbv,[22,23,29,57] by comparison our highest levels are around 20 ppbv. Because the multiphase chemical processes involved in bleach application are complex and poorly understood (e.g., surface or aerosol acidity[22]), it is difficult to compare levels between experiments and studies. For example, studies have observed that gaseous NH_3 partitioning into aqueous bleach can produce large and variable amounts of chloramines, NH_2Cl, $NHCl_2$, and NCl_3.[22,23] One possible explanation for the decreasing trend of TCl_g after each bleaching experiment is a NH_3 limitation in producing these chloramines. Not enough is known about the complex multiphase chemical pathways that influence indoor air quality, and more measurements should be made to properly assess the impacts of human activity-based emissions.

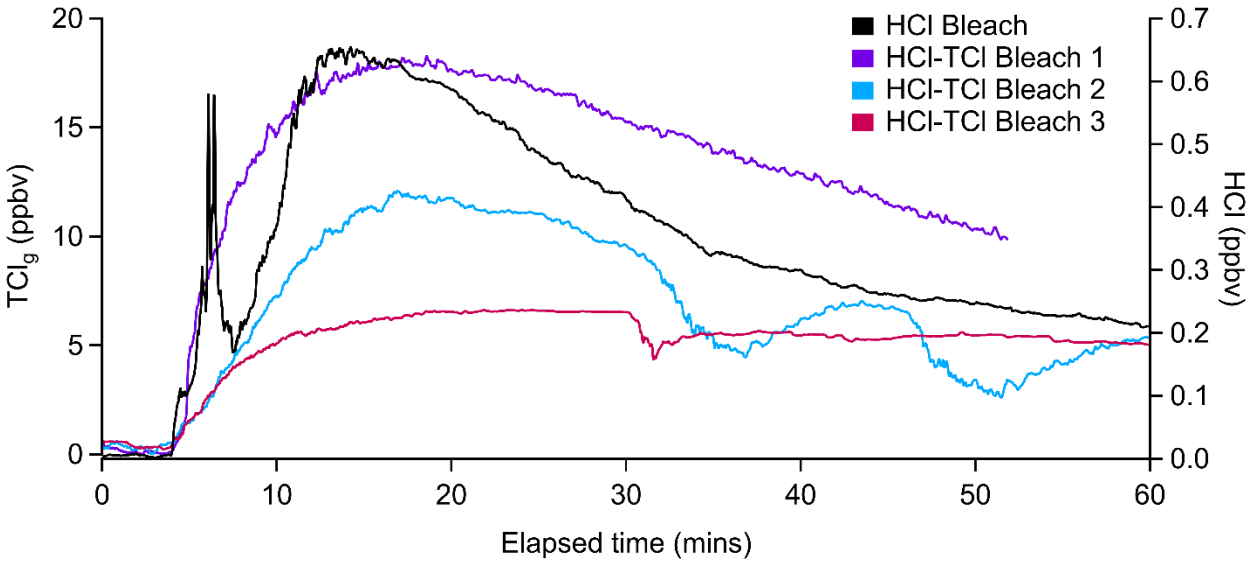

Figure 5-5. HCl-TCl bleaching experiment background corrected to levels prior to bleaching event. Bleaching events monitored by CRDS (black) and HCl-TCl (purple, blue, red).

5.4 Conclusions

In this work we developed, optimized, validated, and applied a method capable of converting TCl_g into gaseous HCl amenable to CRDS detection. Our TCl_g converting instrument, the HCl-TCl, was primarily composed of a platinum catalyst mesh inside a quartz glass flow tube all contained in a split-tube furnace. To test the conversion of TCl_g, we generated low-level gas-phase standards of three organochlorines, which had among the strongest Cl-containing bonds. We determined the breakthrough temperature for DCM to be 800 °C and used 825 °C to provide additional energy for conversion. The optimal residence time in the quartz flow-tube was also explored using DCM and it was determined that the optimal residence time was 1.5 seconds in the flow-tube, which corresponded to a flowrate of ~ 2 L min^{-1}. Once the optimal temperature and optimal flow rate through the quartz flow-tube was determined we could completely convert the three organochlorines, each chosen for their relatively strong C-Cl bond strength. The complete conversion of these TCl_g was demonstrated, as well as the necessity of both the Pt catalyst and hydrogen source. We applied the HCl-TCl conversion under different conditions for two different

environments. First, we monitored the conversion of outdoor air for ~2 days and observed a range of 2.0–3.5 ppbv. The observed outdoor mixing ratio is comparable to the expected HCl from known TCl_g species (3.3–19 ppbv, Table 5-1). Secondly, we measured TCl_g in an indoor environment during bleaching events and observed varying increases (5–18 ppbv) during each event. We have shown that the HCl-TCl can be applied to a variety of different experiments and environments. The utility of this novel TCl_g measurement technique will be crucial to future estimates and assessments of chlorinated compounds and their impact on air quality, climate, and health.

5.5 References

(1) Saiz-Lopez, A.; Von Glasow, R. Reactive Halogen Chemistry in the Troposphere. *Chem. Soc. Rev.* **2012**, *41* (19), 6448–6472. https://doi.org/10.1039/c2cs35208g.

(2) Simpson, W. R.; Brown, S. S.; Saiz-Lopez, A.; Thornton, J. A.; Von Glasow, R. Tropospheric Halogen Chemistry: Sources, Cycling, and Impacts. *Chem. Rev.* **2015**, *115* (10), 4035–4062. https://doi.org/10.1021/cr5006638.

(3) Massin, N.; Bohadana, A. B.; Wild, P.; Héry, M.; Toamain, J. P.; Hubert, G. Respiratory Symptoms and Bronchial Responsiveness in Lifeguards Exposed to Nitrogen Trichloride in Indoor Swimming Pools. *Occup. Environ. Med.* **1998**, *55* (4), 258 LP – 263. https://doi.org/10.1136/oem.55.4.258.

(4) White, C. W.; Martin, J. G. Chlorine Gas Inhalation. *Proc. Am. Thorac. Soc.* **2010**, *7* (4), 257–263. https://doi.org/10.1513/pats.201001-008SM.

(5) Haskins, J. D.; Jaeglé, L.; Shah, V.; Lee, B. H.; Lopez-Hilfiker, F. D.; Campuzano-Jost, P.; Schroder, J. C.; Day, D. A.; Guo, H.; Sullivan, A. P.; et al. Wintertime Gas-Particle Partitioning and Speciation of Inorganic Chlorine in the Lower Troposphere Over the Northeast United States and Coastal Ocean. *J. Geophys. Res. Atmos.* **2018**, *123* (22), 12,812-897,916. https://doi.org/10.1029/2018JD028786.

(6) Riedel, T. P.; Wolfe, G. M.; Danas, K. T.; Gilman, J. B.; Kuster, W. C.; Bon, D. M.; Vlasenko, A.; Li, S.-M.; Williams, E. J.; Lerner, B. M.; et al. An MCM Modeling Study of Nitryl Chloride ($ClNO_2$) Impacts on Oxidation, Ozone Production and Nitrogen Oxide Partitioning in Polluted Continental Outflow. *Atmos. Chem. Phys.* **2014**, *14* (8), 3789–3800. https://doi.org/10.5194/acp-14-3789-2014.

(7) Sherwen, T.; Schmidt, J. A.; Evans, M. J.; Carpenter, L. J.; Großmann, K.; Eastham, S. D.; Jacob, D. J.; Dix, B.; Koenig, T. K.; Sinreich, R.; et al. Global Impacts of Tropospheric Halogens (Cl, Br, I) on Oxidants and Composition in GEOS-Chem. *Atmos. Chem. Phys.* **2016**, *16* (18), 12239–12271. https://doi.org/10.5194/acp-16-12239-2016.

(8) Solomon, S. Stratospheric Ozone Depletion: A Review of Concepts and History. *Rev. Geophys.* **1999**, *37* (3), 275–316. https://doi.org/10.1029/1999RG900008.

(9) Young, C. J.; Washenfelder, R. A.; Edwards, P. M.; Parrish, D. D.; Gilman, J. B.; Kuster, W. C.; Mielke, L. H.; Osthoff, H. D.; Tsai, C.; Pikelnaya, O.; et al. Chlorine as a Primary Radical: Evaluation of Methods to Understand Its Role in Initiation of Oxidative Cycles. *Atmos. Chem. Phys.* **2014**, *14* (7), 3427–3440. https://doi.org/10.5194/acp-14-3427-2014.

(10) Schwartz-Narbonne, H.; Wang, C.; Zhou, S.; Abbatt, J. P. D.; Faust, J. Heterogeneous Chlorination of Squalene and Oleic Acid. *Environ. Sci. Technol.* **2019**, *53* (3), 1217–1224. https://doi.org/10.1021/acs.est.8b04248.

(11) Finlayson-Pitts, B. J. Chlorine Atoms as a Potential Tropospheric Oxidant in the Marine Boundary Layer. *Res. Chem. Intermed.* **1993**, *19* (3), 235–249. https://doi.org/10.1163/156856793X00091.

(12) Raff, J. D.; Njegic, B.; Chang, W. L.; Gordon, M. S.; Dabdub, D.; Gerber, R. B.; Finlayson-Pitts, B. J. Chlorine Activation Indoors and Outdoors via Surface-Mediated Reactions of Nitrogen Oxides with Hydrogen Chloride. *Proc. Natl. Acad. Sci.* **2009**, *106* (33), 13647 LP – 13654. https://doi.org/10.1073/pnas.0904195106.

(13) Khalil, M. A. K.; Moore, R. M.; Harper, D. B.; Lobert, J. M.; Erickson, D. J.; Koropalov, V.; Sturges, W. T.; Keene, W. C. Natural Emissions of Chlorine-Containing Gases:

Reactive Chlorine Emissions Inventory. *J. Geophys. Res. Atmos.* **1999**, *104* (D7), 8333–8346. https://doi.org/10.1029/1998JD100079.

(14) World Meteorological Organization; States., U.; National Oceanic and Atmospheric Administration; States., U.; National Aeronautics and Space Administration; United Nations Environment Programme; European Commission. *Scientific Assessment of Ozone Depletion: 2018.*; 2019.

(15) Prinn, R. G.; Weiss, R. F.; Arduini, J.; Arnold, T.; DeWitt, H. L.; Fraser, P. J.; Ganesan, A. L.; Gasore, J.; Harth, C. M.; Hermansen, O.; et al. History of Chemically and Radiatively Important Atmospheric Gases from the Advanced Global Atmospheric Gases Experiment (AGAGE). *Earth Syst. Sci. Data* **2018**, *10* (2), 985–1018. https://doi.org/10.5194/essd-10-985-2018.

(16) Pan, L. L.; Atlas, E. L.; Salawitch, R. J.; Honomichl, S. B.; Bresch, J. F.; Randel, W. J.; Apel, E. C.; Hornbrook, R. S.; Weinheimer, A. J.; Anderson, D. C.; et al. The Convective Transport of Active Species in the Tropics (CONTRAST) Experiment. *Bull. Am. Meteorol. Soc.* **2017**, *98* (1), 106–128. https://doi.org/10.1175/BAMS-D-14-00272.1.

(17) Andrews, S. J.; Carpenter, L. J.; Apel, E. C.; Atlas, E.; Donets, V.; Hopkins, J. R.; Hornbrook, R. S.; Lewis, A. C.; Lidster, R. T.; Lueb, R.; et al. A Comparison of Very Short Lived Halocarbon (VSLS) and DMS Aircraft Measurements in the Tropical West Pacific from CAST, ATTREX and CONTRAST. *Atmos. Meas. Tech.* **2016**, *9* (10), 5213–5225. https://doi.org/10.5194/amt-9-5213-2016.

(18) Montzka, S. A.; Dutton, G. S.; Portmann, R. W.; Chipperfield, M. P.; Davis, S.; Feng, W.; Manning, A. J.; Ray, E.; Rigby, M.; Hall, B. D.; et al. A Decline in Global CFC-11

Emissions during 2018−2019. *Nature* **2021**, *590* (7846), 428–432. https://doi.org/10.1038/s41586-021-03260-5.

(19) Adcock, K. E.; Reeves, C. E.; Gooch, L. J.; Leedham Elvidge, E. C.; Ashfold, M. J.; Brenninkmeijer, C. A. M.; Chou, C.; Fraser, P. J.; Langenfelds, R. L.; Mohd Hanif, N.; et al. Continued Increase of CFC-113a (CCl3CF3) Mixing Ratios in the Global Atmosphere: Emissions, Occurrence and Potential Sources. *Atmos. Chem. Phys.* **2018**, *18* (7), 4737–4751. https://doi.org/10.5194/acp-18-4737-2018.

(20) Zhai, S.; Wang, X.; McConnell, J. R.; Geng, L.; Cole-Dai, J.; Sigl, M.; Chellman, N.; Sherwen, T.; Pound, R.; Fujita, K.; et al. Anthropogenic Impacts on Tropospheric Reactive Chlorine Since the Preindustrial. *Geophys. Res. Lett.* **2021**, *48* (14), e2021GL093808. https://doi.org/https://doi.org/10.1029/2021GL093808.

(21) Zhang, W.; Jiao, Y.; Zhu, R.; Rhew, R. C.; Sun, B.; Dai, H. Chloroform (CHCl3) Emissions From Coastal Antarctic Tundra. *Geophys. Res. Lett.* **2021**, *48* (18), e2021GL093811. https://doi.org/https://doi.org/10.1029/2021GL093811.

(22) Mattila, J. M.; Lakey, P. S. J.; Shiraiwa, M.; Wang, C.; Abbatt, J. P. D.; Arata, C.; Goldstein, A. H.; Ampollini, L.; Katz, E. F.; DeCarlo, P. F.; et al. Multiphase Chemistry Controls Inorganic Chlorinated and Nitrogenated Compounds in Indoor Air during Bleach Cleaning. *Environ. Sci. Technol.* **2020**, *54* (3), 1730–1739. https://doi.org/10.1021/acs.est.9b05767.

(23) Wong, J. P. S.; Carslaw, N.; Zhao, R.; Zhou, S.; Abbatt, J. P. D. Observations and Impacts of Bleach Washing on Indoor Chlorine Chemistry. *Indoor Air* **2017**, *27* (6), 1082–1090. https://doi.org/10.1111/ina.12402.

(24) Dawe, K. E. R.; Furlani, T. C.; Kowal, S. F.; Kahan, T. F.; Vandenboer, T. C.; Young, C. J. Formation and Emission of Hydrogen Chloride in Indoor Air. *Indoor Air* **2019**, No. April 2018, 70–78. https://doi.org/10.1111/ina.12509.

(25) Giardino, N. J.; Andelman, J. B. Characterization of the Emissions of Trichloroethylene, Chloroform, and 1,2-Dibromo-3-Chloropropane in a Full-Size, Experimental Shower. *J. Expo. Anal. Environ. Epidemiol.* **1996**, *6* (4), 413–423.

(26) Shepherd, J. L.; Corsi, R. L.; Kemp, J. Chloroform in Indoor Air and Wastewater: The Role of Residential Washing Machines. *J. Air Waste Manag. Assoc.* **1996**, *46* (7), 631–642. https://doi.org/10.1080/10473289.1996.10467497.

(27) Doucette, W. J.; Wetzel, T. A.; Dettenmaier, E.; Gorder, K. Emission Rates of Chlorinated Volatile Organics from New and Used Consumer Products Found during Vapor Intrusion Investigations: Impact on Indoor Air Concentrations. *Environ. Forensics* **2018**, *19* (3), 185–190. https://doi.org/10.1080/15275922.2018.1475433.

(28) Nuckols, J. R.; Ashley, D. L.; Lyu, C.; Gordon, S. M.; Hinckley, A. F.; Singer, P. Influence of Tap Water Quality and Household Water Use Activities on Indoor Air and Internal Dose Levels of Trihalomethanes. *Environ. Health Perspect.* **2005**, *113* (7), 863–870. https://doi.org/10.1289/ehp.7141.

(29) Odabasi, M. Halogenated Volatile Organic Compounds from the Use of Chlorine-Bleach-Containing Household Products. *Environ. Sci. Technol.* **2008**, *42* (5), 1445–1451. https://doi.org/10.1021/es702355u.

(30) Odabasi, M.; Elbir, T.; Dumanoglu, Y.; Sofuoglu, S. Halogenated Volatile Organic Compounds in Chlorine-Bleach-Containing Household Products and Implications for

Their Use. *Atmos. Environ.* **2014**, *92*, 376–383. https://doi.org/10.1016/j.atmosenv.2014.04.049.

(31) Miyake, Y.; Yamashita, N.; So, M. K.; Rostkowski, P.; Taniyasu, S.; Lam, P. K. S.; Kannan, K. Trace Analysis of Total Fluorine in Human Blood Using Combustion Ion Chromatography for Fluorine: A Mass Balance Approach for the Determination of Known and Unknown Organofluorine Compounds. *J. Chromatogr. A* **2007**, *1154* (1), 214–221. https://doi.org/https://doi.org/10.1016/j.chroma.2007.03.084.

(32) Miyake, Y.; Kato, M.; Urano, K. A Method for Measuring Semi- and Non-Volatile Organic Halogens by Combustion Ion Chromatography. *J. Chromatogr. A* **2007**, *1139* (1), 63–69. https://doi.org/https://doi.org/10.1016/j.chroma.2006.10.078.

(33) Yeung, L. W. Y.; Miyake, Y.; Taniyasu, S.; Wang, Y.; Yu, H.; So, M. K.; Jiang, G.; Wu, Y.; Li, J.; Giesy, J. P.; et al. Perfluorinated Compounds and Total and Extractable Organic Fluorine in Human Blood Samples from China. *Environ. Sci. Technol.* **2008**, *42* (21), 8140–8145. https://doi.org/10.1021/es800631n.

(34) Miyake, Y.; Yamashita, N.; Rostkowski, P.; So, M. K.; Taniyasu, S.; Lam, P. K. S.; Kannan, K. Determination of Trace Levels of Total Fluorine in Water Using Combustion Ion Chromatography for Fluorine: A Mass Balance Approach to Determine Individual Perfluorinated Chemicals in Water. *J. Chromatogr. A* **2007**, *1143* (1), 98–104. https://doi.org/https://doi.org/10.1016/j.chroma.2006.12.071.

(35) Kannan, K.; Kawano, M.; Kashima, Y.; Matsui, M.; Giesy, J. P. Extractable Organohalogens (EOX) in Sediment and Biota Collected at an Estuarine Marsh near a Former Chloralkali Facility. *Environ. Sci. Technol.* **1999**, *33* (7), 1004–1008.

https://doi.org/10.1021/es9811142.

(36) Xu, D.; Zhong, W.; Deng, L.; Chai, Z.; Mao, X. Levels of Extractable Organohalogens in Pine Needles in China. *Environ. Sci. Technol.* **2003**, *37* (1), 1–6. https://doi.org/10.1021/es025799o.

(37) Kawano, M.; Falandysz, J.; Wakimoto, T. Instrumental Neutron Activation Analysis of Extractable Organohalogens in the Antarctic Weddell Seal (Leptonychotes Weddelli). *J. Radioanal. Nucl. Chem.* **2007**, *272* (3), 501–504. https://doi.org/10.1007/s10967-007-0611-5.

(38) Wang, X.; Jacob, D. J.; Eastham, S. D.; Sulprizio, M. P.; Zhu, L.; Chen, Q.; Alexander, B.; Sherwen, T.; Evans, M. J.; Lee, B. H.; et al. The Role of Chlorine in Global Tropospheric Chemistry. **2019**, 3981–4003.

(39) Hossaini, R.; Chipperfield, M. P.; Saiz-Lopez, A.; Fernandez, R.; Monks, S.; Feng, W.; Brauer, P.; von Glasow, R. A Global Model of Tropospheric Chlorine Chemistry: Organic versus Inorganic Sources and Impact on Methane Oxidation. *J. Geophys. Res. Atmos.* **2016**, *121* (23), 14,214-271,297. https://doi.org/10.1002/2016JD025756.

(40) Kato, M.; Urano, K.; Tasaki, T. Development of Semi- and Nonvolatile Organic Halogen as a New Hazardous Index of Flue Gas. *Environ. Sci. Technol.* **2000**, *34* (19), 4071–4075. https://doi.org/10.1021/es000881+.

(41) Berg, W. W.; Crutzen, P. J.; Grahek, F. E.; Gitlin, S. N.; Sedlacek, W. A. First Measurements of Total Chlorine and Bromine in the Lower Stratosphere. *Geophys. Res. Lett.* **1980**, *7* (11), 937–940. https://doi.org/https://doi.org/10.1029/GL007i011p00937.

(42) Hardy, J. E.; Knarr, J. J. Technique for Measuring the Total Concentration of Gaseous Fixed Nitrogen Species. *J. Air Pollut. Control Assoc.* **1982**, *32* (4), 376–379. https://doi.org/10.1080/00022470.1982.10465412.

(43) Veres, P.; Gilman, J. B.; Roberts, J. M.; Kuster, W. C.; Warneke, C.; Burling, I. R.; de Gouw, J. Development and Validation of a Portable Gas Phase Standard Generation and Calibration System for Volatile Organic Compounds. *Atmos. Meas. Tech.* **2010**, *3* (3), 683–691. https://doi.org/10.5194/amt-3-683-2010.

(44) Roberts, J. M.; Bertman, S. B.; Jobson, T.; Niki, H.; Tanner, R. Measurement of Total Nonmethane Organic Carbon (Cy): Development and Application at Chebogue Point, Nova Scotia, during the 1993 North Atlantic Regional Experiment Campaign. *J. Geophys. Res. Atmos.* **1998**, *103* (D11), 13581–13592. https://doi.org/https://doi.org/10.1029/97JD02240.

(45) Maris, C.; Chung, M. Y.; Lueb, R.; Krischke, U.; Meller, R.; Fox, M. J.; Paulson, S. E. Development of Instrumentation for Simultaneous Analysis of Total Non-Methane Organic Carbon and Volatile Organic Compounds in Ambient Air. *Atmos. Environ.* **2003**, *37*, 149–158. https://doi.org/https://doi.org/10.1016/S1352-2310(03)00387-X.

(46) Stockwell, C. E.; Kupc, A.; Witkowski, B.; Talukdar, R. K.; Liu, Y. Characterization of a Catalyst-Based Conversion Technique to Measure Total Particulate Nitrogen and Organic Carbon and Comparison to a Particle Mass Measurement Instrument. *Atmos. Meas. Tech* **2018**, 2749–2768.

(47) Huheey, J.; Cottrell, T. The Strengths of Chemical Bonds. Butterworths, London MA, USA 1958.

(48) Shi, J.; He, J.; Wang, H.-J. A Computational Study of C-X (X = H, C, F, Cl) Bond Dissociation Enthalpies (BDEs) in Polyhalogenated Methanes and Ethanes. *J. Phys. Org. Chem.* **2011**, *24* (1), 65–73. https://doi.org/https://doi.org/10.1002/poc.1704.

(49) Lawler, M. J.; Sander, R.; Carpenter, L. J.; Lee, J. D.; von Glasow, R.; Sommariva, R.; Saltzman, E. S. HOCl and Cl_2 Observations in Marine Air. *Atmos. Chem. Phys.* **2011**, *11* (15), 7617–7628. https://doi.org/10.5194/acp-11-7617-2011.

(50) Platt, U.; Janssen, C. Observation and Role of the Free Radicals NO3, ClO, BrO and IO in the Troposphere. *Faraday Discuss.* **1995**, *100* (0), 175–198. https://doi.org/10.1039/FD9950000175.

(51) Casper, B.; Lambotte, P.; Minkwitz, R.; Oberhammer, H. Gas-Phase Structures of Chlorine and Bromine Nitrate (ClONO2 and BrONO2). *J. Phys. Chem.* **1993**, *97* (39), 9992–9995. https://doi.org/10.1021/j100141a017.

(52) Crisp, T. a; Lerner, B. M.; Williams, E. J.; Quinn, P. K.; Bates, T. S.; Bertram, T. H. Observations of Gas Phase Hydrochloric Acid in the Polluted Marine Boundary Layer. *J. Geophys. Res. Atmos.* **2014**, 6897–6915. https://doi.org/10.1002/2013JD020992.Received.

(53) Keene, W. C.; Pszenny, A. A. P.; Jacob, D. J.; Duce, R. A.; Galloway, J. N.; Schultz-Tokos, J. J.; Sievering, H.; Boatman, J. F. The Geochemical Cycling of Reactive Chlorine through the Marine Troposphere. *Global Biogeochem. Cycles* **1990**, *4* (4), 407–430. https://doi.org/https://doi.org/10.1029/GB004i004p00407.

(54) Ganske, J. A.; Berko, H. N.; Finlayson-Pitts, B. J. Absorption Cross Sections for Gaseous ClNO2 and Cl2 at 298 K: Potential Organic Oxidant Source in the Marine Troposphere. *J. Geophys. Res. Atmos.* **1992**, *97* (D7), 7651–7656.

https://doi.org/https://doi.org/10.1029/92JD00414.

(55) Wong, J. P. S.; Carslaw, N.; Zhao, R.; Zhou, S.; Abbatt, J. P. D. Observations and Impacts of Bleach Washing on Indoor Chlorine Chemistry. *Indoor Air* **2017**, No. June, 1082–1090. https://doi.org/10.1111/ina.12402.

(56) Angelucci, A. A.; Furlani, T. C.; Wang, X.; Jacob, D. J.; VandenBoer, T. C.; Young, C. J. Understanding Sources of Atmospheric Hydrogen Chloride in Coastal Spring and Continental Winter. *ACS Earth Sp. Chem.* **2021**. https://doi.org/10.1021/acsearthspacechem.1c00193.

(57) Wang, C.; Collins, D. B.; Abbatt, J. P. D. Indoor Illumination of Terpenes and Bleach Emissions Leads to Particle Formation and Growth. *Environ. Sci. Technol.* **2019**, *53* (20), 11792–11800. https://doi.org/10.1021/acs.est.9b04261.

Chapter 6.

Conclusions and Future Directions

6.1 Conclusions

The work that comprises this thesis was a comprehensive analytical approach to measuring reactive chlorine (Cl_y) species and elucidating tropospheric Cl_y mechanisms. To accomplish this the three main objectives were met by: (1) Validating a new spectroscopic instrument for HCl; (2) Applying validated HCl measurements to elucidate chlorine chemistry trends in an urban marine boundary layer; and (3) Developing and applying novel instrumentation to measure total Cl_y. To meet these objectives, we first described in detail in Chapter 2 how to generate low-emitting gas-phase standards by constructing custom permeation devices (PDs). We show two calibration techniques to determine PD emission rates; gravimetric and offline collection followed by ion chromatography with conductive detection (IC-CD) analysis. Both methods have their advantages, and the choice of method will depend on analyte properties and method availability. We illustrated the temperature dependence and the importance of maintaining a constant temperature due to the Arrhenius behavior of the PD emission rates. The stability of a PDs was monitored using a cavity ring-down spectrometer (CRDS) and the fluctuation/precision and were ±0.2% at best. We recognize that the stability is a combination of the true error of the emission rate and the uncertainty of the method we used to determine it.

Chapter 3 combined multiple approaches to validate a new commercial CRDS HCl analyzer for ambient measurements of HCl. We compared the method performance characteristics (e.g., limit of detection (LOD)) to other reported instrumentation and observed the CRDS performed similar to or better than the most sensitive HCl techniques. The most significant limitation to in-situ techniques is adsorption/desorption loss and release on inlet surfaces. Our results showed that these deposition effects increase with increasing relative humidity and decreasing HCl mixing ratios. Several chemical and physical options to circumvent or lessen surface effects were

discussed and are important factors to incorporate for faster response times in any methods that measures surface active gases (e.g., HCl, ammonia, and nitric acid (HNO_3)). The recommended simplest approach was to increase the flowrate of the sampling inlet while maintaining laminar flow. Spectra capturing errors in the measurement of HCl for the CRDS can occur at high levels of volatile organic compounds (VOCs, e.g., near emission point sources or biomass burning plumes) or instrument instabilities (e.g., pressure fluctuations), however potential instrument errors are minimal under most operating and atmospheric conditions. To validate our CRDS method, we presented comparisons with two established methods for measuring strong acids and our observations agreed within the combined uncertainties.

To further demonstrate the environmental applicability of the now validated CRDS, we measured HCl during the Halifax Fog and Air Quality Study (HaliFAQS) and reported the results in Chapter 4. Using the measured HCl and supporting measurements, we explained some of the major sources of HCl. We used continuous, high time-resolution measurements of HCl in an urban marine boundary layer (MBL) during the HaliFAQS field campaign and compared with previous measurements in the MBL. Two peaks of HCl were common in days with higher the average irradiance, indicating the presence of two photochemical mechanisms. The first peak was likely from the photolysis of Cl precursor compounds (e.g., nitryl chloride ($ClNO_2$)) followed hydrogen abstraction of methane or volatile organic compounds (VOCs). The second peak of HCl was likely from the midday photochemical formation of HNO_3 followed by acid displacement onto Cl^- containing sea spray aerosols. Trends observed in the diurnal HCl were used to develop an irradiance-dependent box model to estimate initial Cl precursor compound, $ClNO_2$, mixing ratios. Using the rate of measured HCl we determined the contribution of $ClNO_2$ to observed morning HCl rates for 8 days. Modelled HCl from the photolysis of the determined initial $ClNO_2$ showed

good agreement for high irradiance days. We accounted for the continual loss of HCl by deposition by generating two sets of data for low (1 cm s^{-1}) and high (6 cm s^{-1}) deposition velocities and display the estimated $ClNO_2$ data as a conservative range. On the most active day for Cl chemistry (June 18), it was observed that $P(Cl)_{ClNO_2}$ was 13% as large as $P(HO_x)_{O_3}$ when considering the full day, and 37% in the morning. It is important to include Cl contributions in total radical production studies in the marine boundary layer to further understand the differences between full day and morning time tropospheric chemistry.

In the third and final main objective we developed a novel total gaseous Cl (TCl_g) method, which was described in Chapter 5. This was achieved using a high-temperature platinum (Pt) catalyzed flow tube capable of combusting chlorine species and transforming them into HCl that is amenable to measurement by the CRDS. This work was presented in two steps; (i) Develop and validate an instrument capable of in-situ measurement of TCl_g through conversion to HCl and detection by CRDS; and (ii) Demonstrate its applications to outdoor and indoor air TCl_g measurements. Briefly, the HCl-TCl was composed of a platinum catalyst inside a quartz glass flow tube in a split-tube furnace that was provided with excess propane. After developing the instrument, we had to first determine the temperature breakthrough of strong C-Cl containing bond from a dichloromethane (DCM) PD standard. We determined this breakthrough by ramping the temperature and monitoring the formation of the resulting HCl. The determined temperature was 800 °C and we used 825 °C in the following experiments to provide a surplus of energy. The optimal residence time in the quartz flow-tube was explored by monitoring DCM conversion and found that the optimal residence time was 1.5 seconds in the flow-tube, which corresponded to a flowrate through the tube of ~ 2 L min^{-1}. Once the optimal temperature and flow-rate was determined we could validate the method by showing the complete conversion of three

organochlorines (DCM, 1-chlorobutane, and 1,3-dichloropropene), each chosen for their relatively strong C-Cl bond strength. The complete conversion of these TCl_g species were demonstrated, and a dependence of the Pt catalyst and propane hydrogen source was observed. We applied the HCl-TCl method under different conditions for two contrasting environments. We first monitored the conversion of outdoor ambient air for ~2.5 hours and observed a range of 3.5–6 ppbv. The observed outdoor mixing ratio is comparable to the expected HCl from known TCl_g species (Table 5.1). Secondly, we measured the headspace in an indoor environment during bleaching events, we observed varying increases during these events which corresponded to range of 5–18 ppbv of TCl_g. The CRDS and HCl-TCl can be applied to a variety of different experiments and environments. The utility of this novel TCl_g measurement technique will be crucial to future estimates and assessments of chlorinated compounds and their impact on air quality, climate, and health.

6.2 Future Directions

One of the greatest advantages of the CRDS HCl analyzer that could not be achieved with the methods to which we compared was the ability to capture transient events that are important to constraining atmospheric chlorine chemistry (e.g., photolysis of precursors, thermodynamic partitioning, and direct emissions). We have demonstrated in Chapters 3 and 4 the utility of the CRDS for environmental applications in future field campaigns and experiments that require high time-resolved HCl measurements (e.g., mobile and aircraft measurements). This ability to make high time-resolved measurements will be important for constraining fast formation processes and direct sources of HCl.

In Chapter 4 we explained how high time-resolved HCl measurements can be used in a simple box model to ascertain Cl production in the morning. Characterizing the unknown degrees of mixing from the residual layer into the boundary layer during the morning be very important to

properly constrain the sources of morning Cl chemistry. Future applications of this modelling approach could include different locations in the MBL with varying degrees of Cl precursors, as well as locations in-land that have been shown to have Cl activation chemistry (e.g., saline lakes). As two photochemical processes were observed, future experiments should focus on also modelling HCl formation from HNO_3 combined with measurements of both $ClNO_2$ and HNO_3. A full field campaign with all the measurements required to properly characterize a total radical budget would complement this modelling approach and allow us to better understand Cl contributions. Cl production from photolabile precursors is the greatest source of daily Cl, while not accounted for here the production of Cl from HCl reaction with OH can be very important and would serve as an important addition in future applications.

The newly validated HCl-TCl technique will complement future outdoor and indoor field campaigns where chlorine in concerned. Future projects that combine separate measurements of Cl_y and known TCl_g will helps elucidate contributions unknown chlorinated species to a given environment under ambient conditions or during active emitting events. Understanding the effects that meteorological conditions (e.g., Temperature and RH) can have on local TCl_g levels will be a key next step to explain trends in TCl_g. We have shown the efficacy of this method for measuring TCl_g and we propose that it can be applied to other halogenated species (i.e., fluorine) of concern provided there is an appropriate online measuring instrument.

~fin~

Appendix A: Supporting information for Chapter 3.

A.1 Ion chromatography analysis

Aqueous chloride samples collected into an impinger from the HCl PD were analyzed by IC-CD using an ICS-2100 (Thermo Fisher Scientific, Sunnyvale, California, USA) according to the method described by Place et al., (2018).[1] An AS-DV autosampler loaded 1.0 mL of sample onto a concentration column (5 x 23mm, TAC-ULP1, P/N: 061400) and injected into the IC-CD. Anions were analyzed at a flowrate of 1.5 mL min^{-1} using an eluent gradient from 1–60 mM KOH controlled by a Dionex EGC III KOH Potassium Hydroxide Eluent Generator Cartridge (Thermo Fisher Scientific, Sunnyvale, California, USA), and separated on an AS11-HC analytical column thermostated to 30°C, and protected by an IonPac AG11 guard column (4 × 250 mm, P/N: 052960, and 4 x 50 mm, P/N: 052962, respectively). The gradient program started with 1.0 mM KOH held for 7 min followed by a linear increase to 16 mM KOH over the next 9 min. The KOH was held at 16 mM for 4 min then linearly increased to 25 mM from 20 min to 25 min. At 25 min the concentration was linearly increased to 60 mM over a period of 8 min, followed by a stepped decrease to 10 mM KOH and held for 1 min to re-equilibrate the column, yielding a total run time of 33 min. The eluent was suppressed in legacy mode with 124 mA (AERS 500, 4 mm, P/N: 082540) before Cl^- was detected by the CD (DS6 heated conductivity cell, 30 °C).

Annular denuder extracts were analyzed by IC-CD using an ICS-6000 (Thermo Fisher Scientific, Sunnyvale, California, USA). An AS-AP autosampler loaded 250 µL of sample onto a loop and injected into the IC-CD. The sample loop was cut from 0.75mm i.d. polyetheretherketone (PEEK; Thermo Fisher Scientific, Sunnyvale, California, USA, P/N: 052305) tubing, with a length of 56.59 cm. Anions were separated at a flow rate of 1.0 mL min^{-1} using an eluent gradient from 10–60 mM NaOH on an IonPac AS23 analytical column protected by an AG23 guard column

(4 × 250 mm, P/N:064149 and 4 × 50 mm, P/N:064147, respectively). Eluent of 100 mM NaOH was prepared from a 9.5 mL aliquot of 50% w/w NaOH diluted to 1800 mL in deionized water, the eluent was purged with N_2 for 15 minutes to remove trace CO_2. The gradient program held 1.0 mM NaOH for the first 15 min followed by a linear increase to 60 mM NaOH over the next 5 min. The NaOH was held at 60 mM for 5 min, followed by a stepped decrease to 10 mM NaOH and held for 5 min to re-equilibrate the column, yielding a total run time of 30 min. The eluent was dynamically suppressed (ADRS 600, 4 mm, P/N:088666) before Cl^- was detected by conductivity (ICS-6000 CD heated conductivity cell).

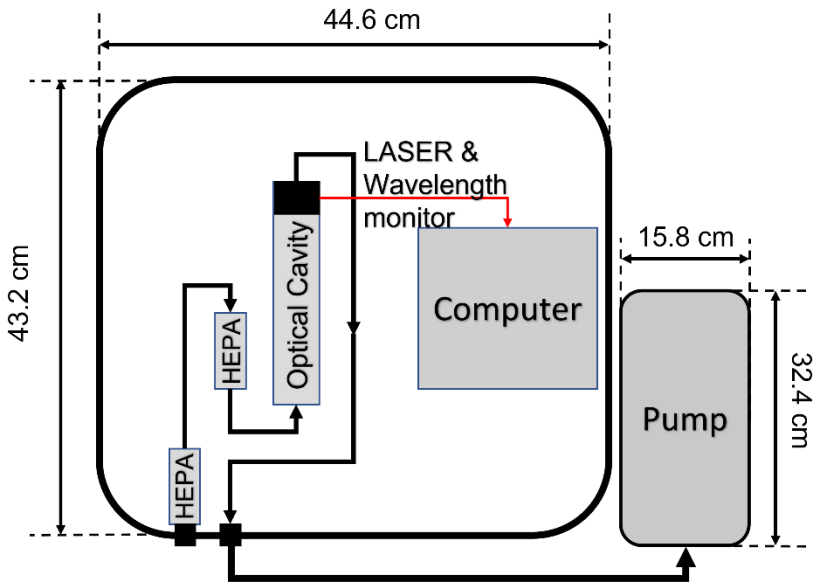

Figure A-1. Simple schematic for the Picarro CRDS.

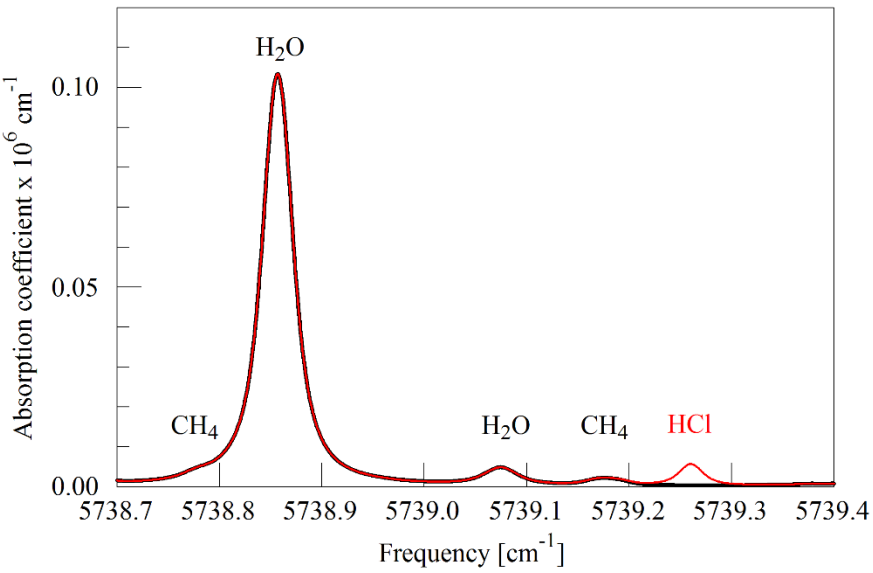

Figure A-2. Absorption coefficients modeled from Hitran database for common atmospheric interfering compounds within the relevant wavenumber range of the CRDS laser.[2,3]

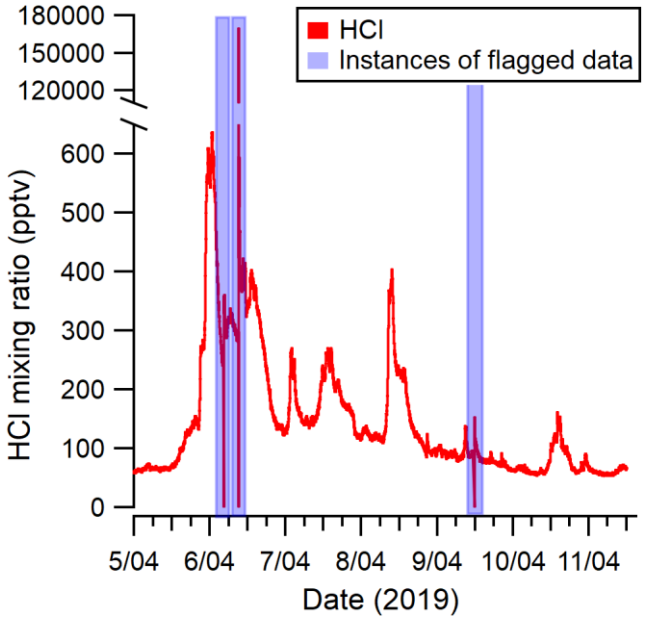

Figure A-3. Spectral error for HCl dataset measured in April 2019. Filtered data constituted a 3.5% loss of total data points for the 24-hour averaged CRDS April 6 denuder comparison.

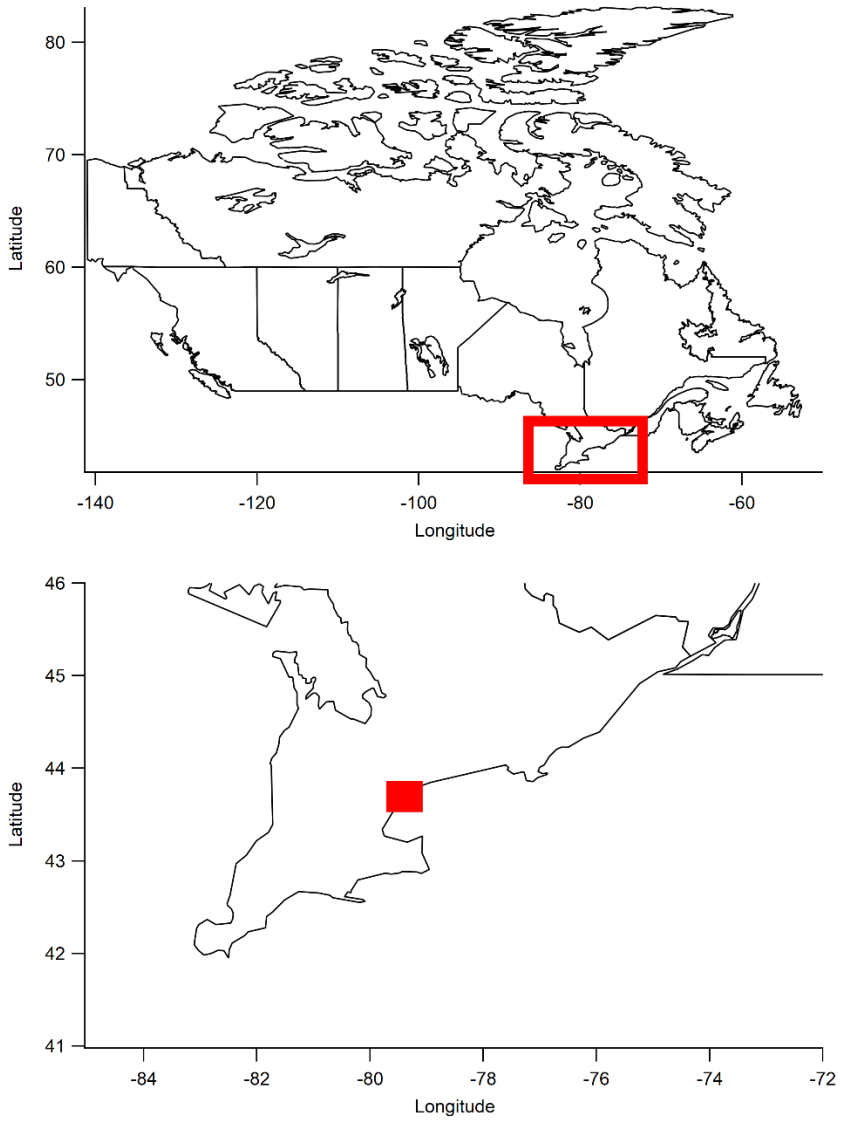

Figure A-4. Map of sampling location for ambient measurements.

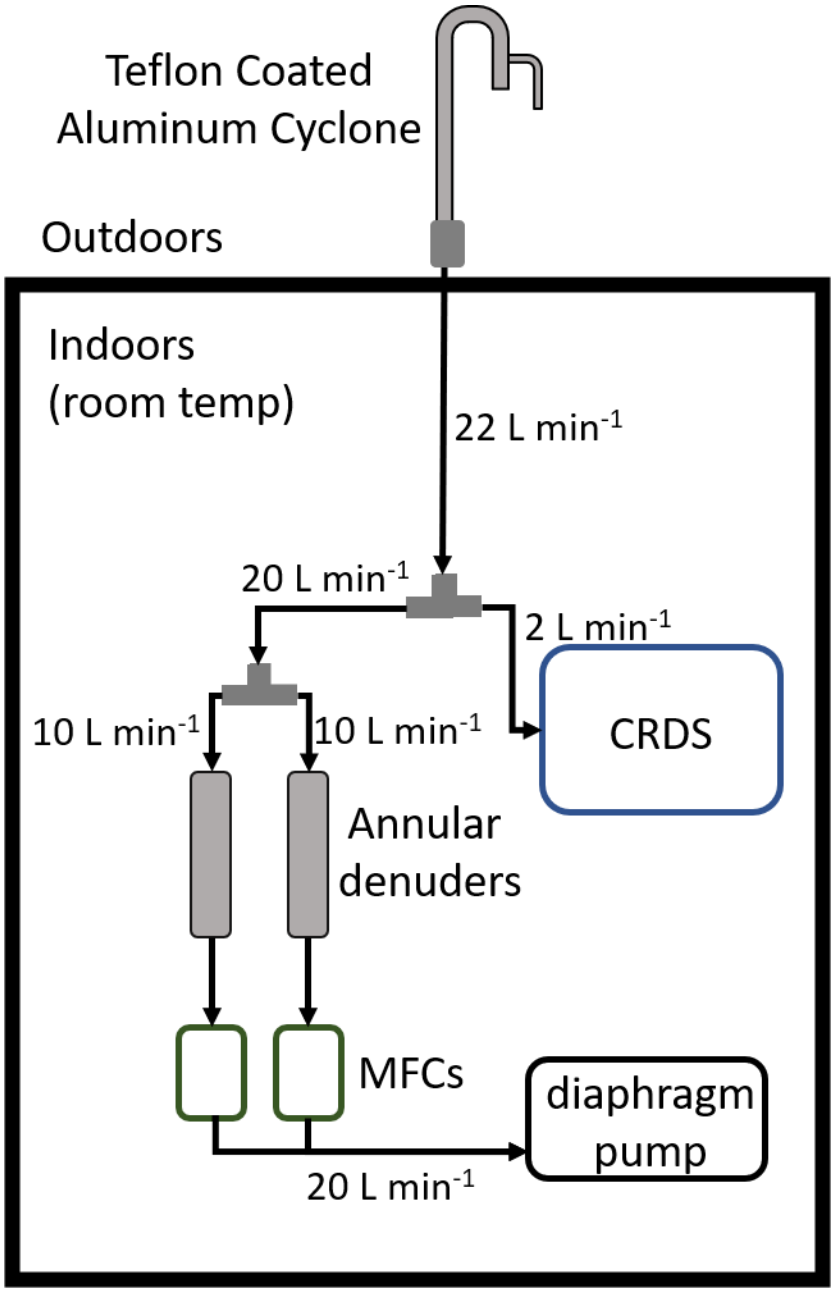

Figure A-5. Ambient intercomparison sampling schematic.

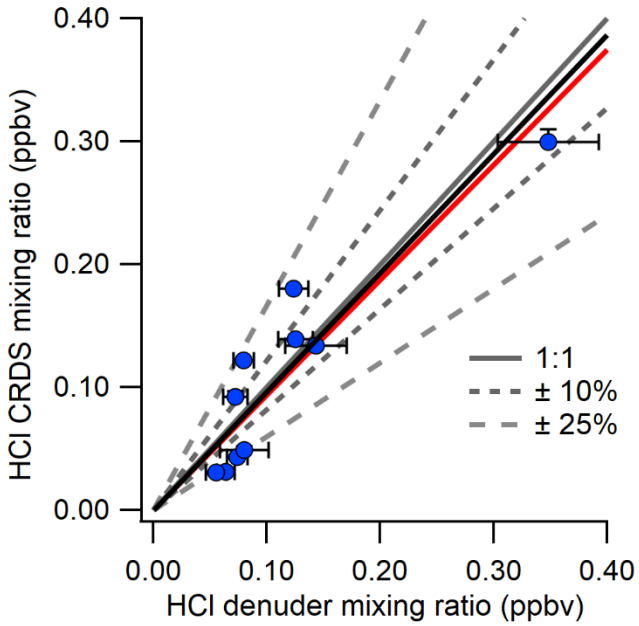

Figure A-6. Comparison of HCl measured 4-11 April 2019 using annular denuders and CRDS (averaged to the collection time of denuders. Also shown are a 1:1 correlation line (solid grey), 10 % (short grey dash) and 25 % (long grey dash) deviation from 1:1, orthogonal distance regression (solid black), and the least squares regression (solid red).

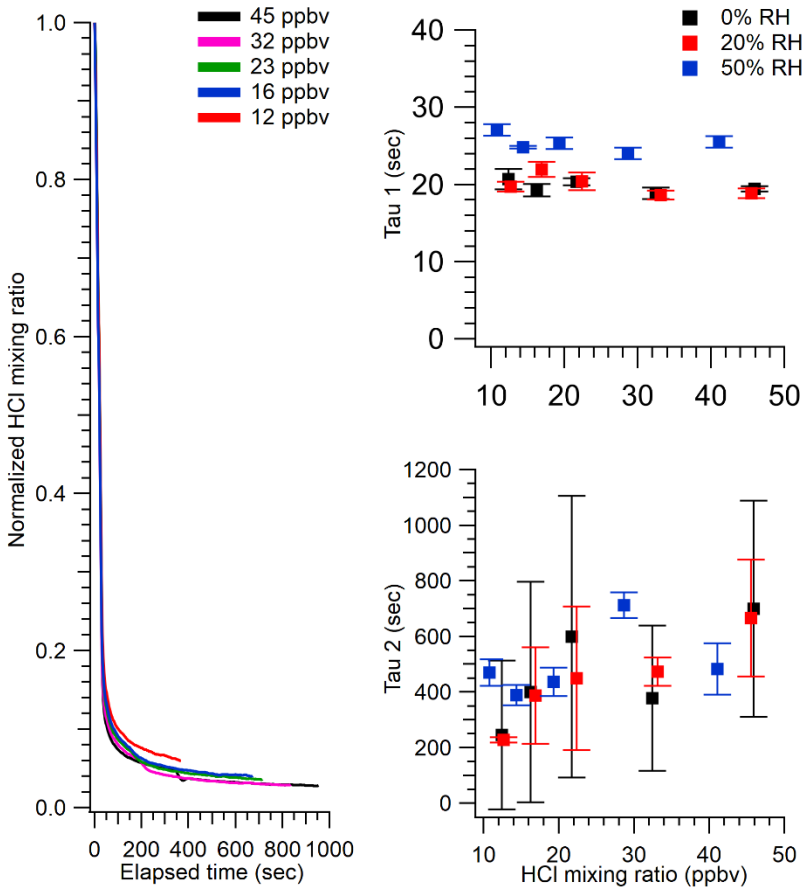

Figure A-7. a) Normalized decay curves for 0% RH. b) Tau 1's for increasing humidity. c) Tau 2's for increasing humidity. b) and c) calculated by fitting decays curves to E2.

Table A-1. Signal loss decay times for select input HCl mixing ratios, mapping signal loss from zero input.

~Mixing ratio (ppbv)	0% RH		20% RH		50% RH		
	$1/e$ (sec)	90% (sec)	$1/e$ (sec)	90% (sec)	$1/e$ (sec)	90% (sec)	Residence time (ms)
12	26.5	101	30.8	229	38.0	458	21.0
16	24.7	82	31.3	214	34.3	415	28.0
21	26.4	74	30.1	178	33.4	310	37.2
32	24.5	62	28.9	167	29.9	199	55.6
45	25.6	54	28.3	152	31.9	186	78.8

Table A-2. Signal loss decay ratios for HCl decay times to residence time.

~Mixing ratio (ppbv)	0% RH		20% RH		50% RH	
	$1/e$	90%	$1/e$	90%	$1/e$	90%
12	0.126	0.481	0.147	1.090	0.181	2.181
16	0.088	0.293	0.112	0.764	0.123	1.482
21	0.071	0.199	0.081	0.478	0.090	0.833
32	0.044	0.112	0.052	0.300	0.054	0.358
45	0.032	0.069	0.036	0.193	0.040	0.236

Table A-3. Signal increase upswing times for select input HCl mixing ratios, mapping signal rise from zero input to signal plateau.

~Mixing ratio (ppbv)	0% RH		20% RH		50% RH		
	$1 - \frac{1}{e}$ (sec)	90% (sec)	$1 - \frac{1}{e}$ (sec)	90% (sec)	$1 - \frac{1}{e}$ (sec)	90% (sec)	Residence time (ms)
12	27.2	64	27.2	64	50.8	197	21.0
16	26.4	62	27.9	58	49.3	204	28.0
21	26.3	61	26.8	60	48.5	198	37.2
32	25.7	61	29.3	60	31.8	174	55.6
45	28.2	117	33.3	128	62.9	452	78.8

Table A-4. Signal loss upswing ratios for HCl upswing times to residence time.

~Mixing ratio (ppbv)	0% RH		20% RH		50% RH	
	$1 - \frac{1}{e}$ (sec)	90% (sec)	$1 - \frac{1}{e}$ (sec)	90% (sec)	$1 - \frac{1}{e}$ (sec)	90% (sec)
12	0.130	0.305	0.130	0.305	0.242	0.938
16	0.094	0.221	0.100	0.207	0.176	0.729
21	0.071	0.164	0.072	0.161	0.130	0.532
32	0.046	0.110	0.053	0.108	0.057	0.313
45	0.036	0.148	0.042	0.162	0.080	0.574

Table A-5. Denuder extraction list.

Extract #	Time and Date	Duration (min)	Mixing ratio (ppbv)
1	21:07 April 4 → 21:00 April 5	1433	0.074
2	9:30 April 5 → 10:06 April 6	1476	N/A*
3	21:00 April 5 → 21:00 April 6	1440	0.347
4	10:06 April 6 → 10:12 April 7	1446	0.123
5	21:00 April 6 → 20:34 April 7	1414	0.125
6	10:12 April 7 → 9:30 April 8	1398	0.143
7	20:34 April 7 → 21:03 April 8	1469	0.079
8	9:30 April 8 → 10:45 April 9	1515	0.072
9	21:03 April 8 → 21:00 April 9	1437	0.080
10	10:45 April 9 → 10:53 April 10	1448	0.064
11	21:00 April 9 → 10:06 April 11	2226	0.055

* Sample lost

Annular denuder codes were recorded for determining and applying systematic error corrections.

A. 2 References

(1) Place, B. K.; Young, C. J.; Ziegler, S. E.; Edwards, K. A.; Salehpoor, L.; VandenBoer, T. C. Passive Sampling Capabilities for Ultra-Trace Quantitation of Atmospheric Nitric Acid (HNO3) in Remote Environments. *Atmos. Environ.* **2018**, *191* (November 2017), 360–369. https://doi.org/10.1016/j.atmosenv.2018.08.030.

(2) Gordon, I. E.; Rothman, L. S.; Hill, C.; Kochanov, R. V; Tan, Y.; Bernath, P. F.; Birk, M.; Boudon, V.; Campargue, A.; Chance, K. V; et al. The HITRAN2016 Molecular Spectroscopic Database. *J. Quant. Spectrosc. Radiat. Transf.* **2017**, *203*, 3–69. https://doi.org/https://doi.org/10.1016/j.jqsrt.2017.06.038.

(3) Kochanov, R. V; Gordon, I. E.; Rothman, L. S.; Shine, K. P.; Sharpe, S. W.; Johnson, T. J.; Wallington, T. J.; Harrison, J. J.; Bernath, P. F.; Birk, M.; et al. Infrared Absorption Cross-Sections in HITRAN2016 and beyond: Expansion for Climate, Environment, and Atmospheric Applications. *J. Quant. Spectrosc. Radiat. Transf.* **2019**, *230*, 172–221. https://doi.org/https://doi.org/10.1016/j.jqsrt.2019.04.001.

Appendix B: Supporting information for Chapter 4.

B.1 Clear sky irradiance calculation

Clear sky solar irradiance was calculated in kW m^{-2} by;[1]

$$I_D = 1.353 \times 1.1 \times \left[(1 - ah)0.7^{AM^{0.678}} + ah\right] \quad \text{(BE1)}$$

I_D is the solar intensity on a plane perpendicular to the sun's rays in units of kW m^{-2}. AM is the air mass zenith. 1.353 kW m^{-2} is the solar constant. 0.7 is due the fact that only 70% of the incident radiation on the atmosphere is transmitted to the Earth. The coefficient of 1.1 is calculated from the 10% diffusion component through the atmosphere. The coefficient 0.678 is an empirical fit to the observed data and considers the non-uniformities in the atmospheric layers. α = 0.14 and h is the location height above sea level in kilometers. AM is a function of latitude and calculated by;[2]

$$AM = \frac{1}{\cos\theta} \quad \text{(BE2)}$$

Where θ is the vertical solar zenith angle and calculated by;

$$\cos\theta = \sin\delta \sin\varphi + \cos\delta \cos\varphi \cos\omega \quad \text{(BE3)}$$

Where δ is declination of the sun, φ is the latitude (defined as positive in the northern hemisphere), and ω is the hour angle. The solar declination is a function of the day of the year and calculated by;[3]

$$\delta = -23.45° \times \cos\left(\frac{360}{365} \times (d + 10)\right) \quad \text{(BE4)}$$

Where d is the day of the year on the Gregorian calendar. ω is a measure of the local time determined by;[3]

$$\omega = 15^{\circ}((LT + \frac{4(\text{Longitude} - 15^{0}\Delta T_{UTC}) + 9.87\sin\left(2(\frac{360}{365}(d-81))\right) - 7.53\cos\left(\frac{360}{365}(d-81)\right) - 1.5\sin\left(\frac{360}{365}(d-81)\right)}{60}) - 12) \qquad \text{(BE5)}$$

Where LT is local time and ΔT_{UTC} is the time difference in UTC.

B.2 Deposition of HCl calculation

The deposition of HCl in 15 min data is calculated for two deposition velocities: 1 and 6 cm s^{-1}.

$$\Delta HCl = -900 \times [HCl]_{t-900} \times \frac{D_V}{PBLH} \qquad \text{(BE6)}$$

Where ΔHCl is the loss in HCl over 15 min (900 sec), $[HCl]_{t-900}$ is mixing ratio of HCl initially, D_v is the deposition velocity, and PBLH is the planetary boundary layer height in cm. HCl data is corrected for estimated deposition for the two D_v, generating two data sets prior to modelling [$ClNO_2$] at sunrise.

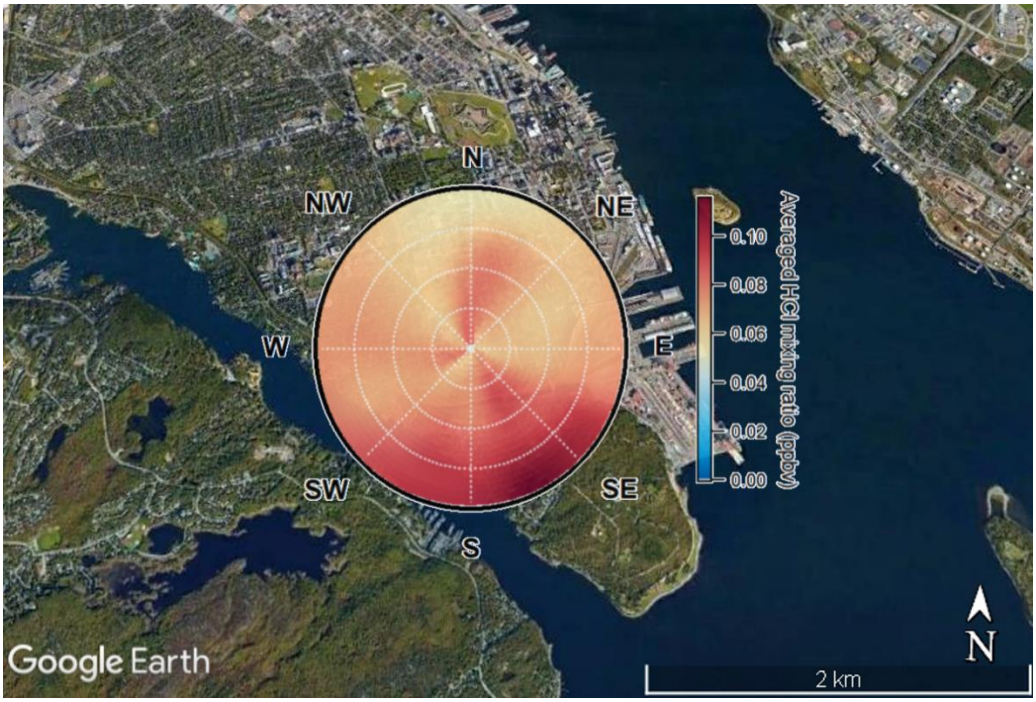

Figure B-1. Wind rose plot of HCl overlayed on a Google Earth image of the campaign location.

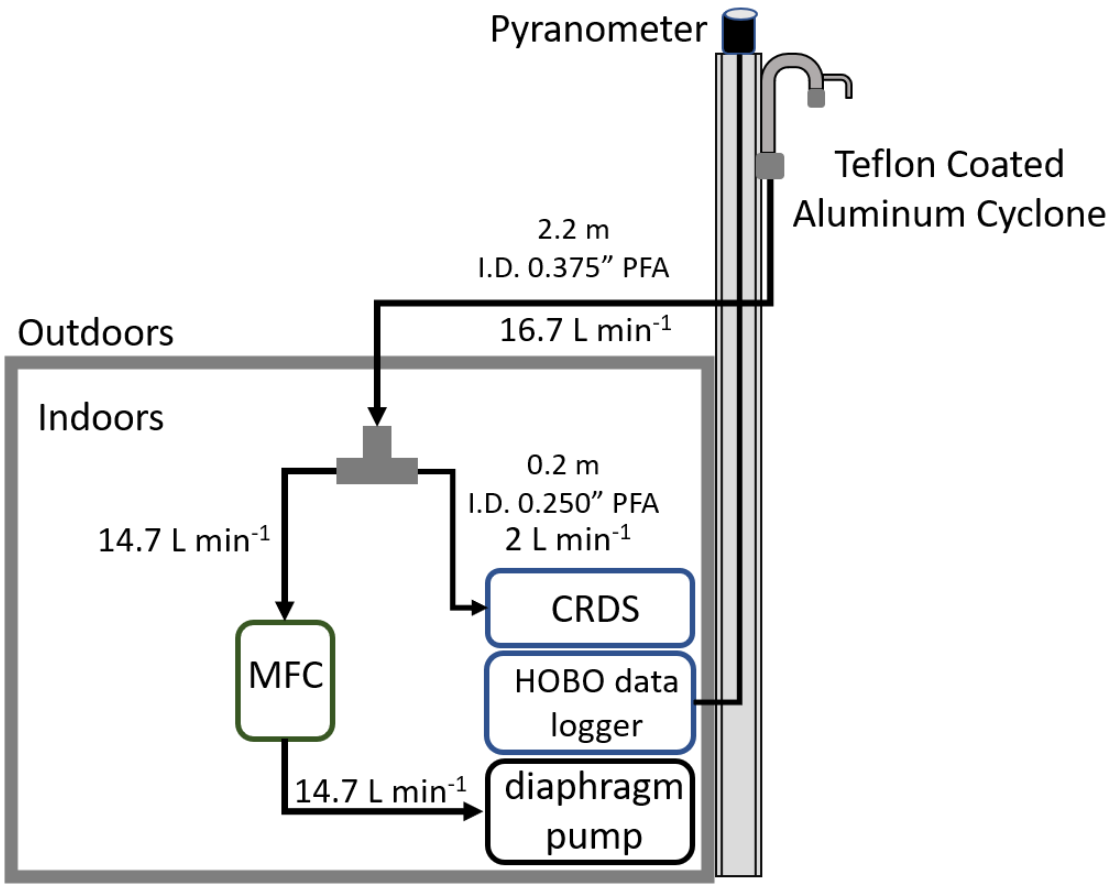

Figure B-2. Sampling schematic for the CRDS and pyranometer.

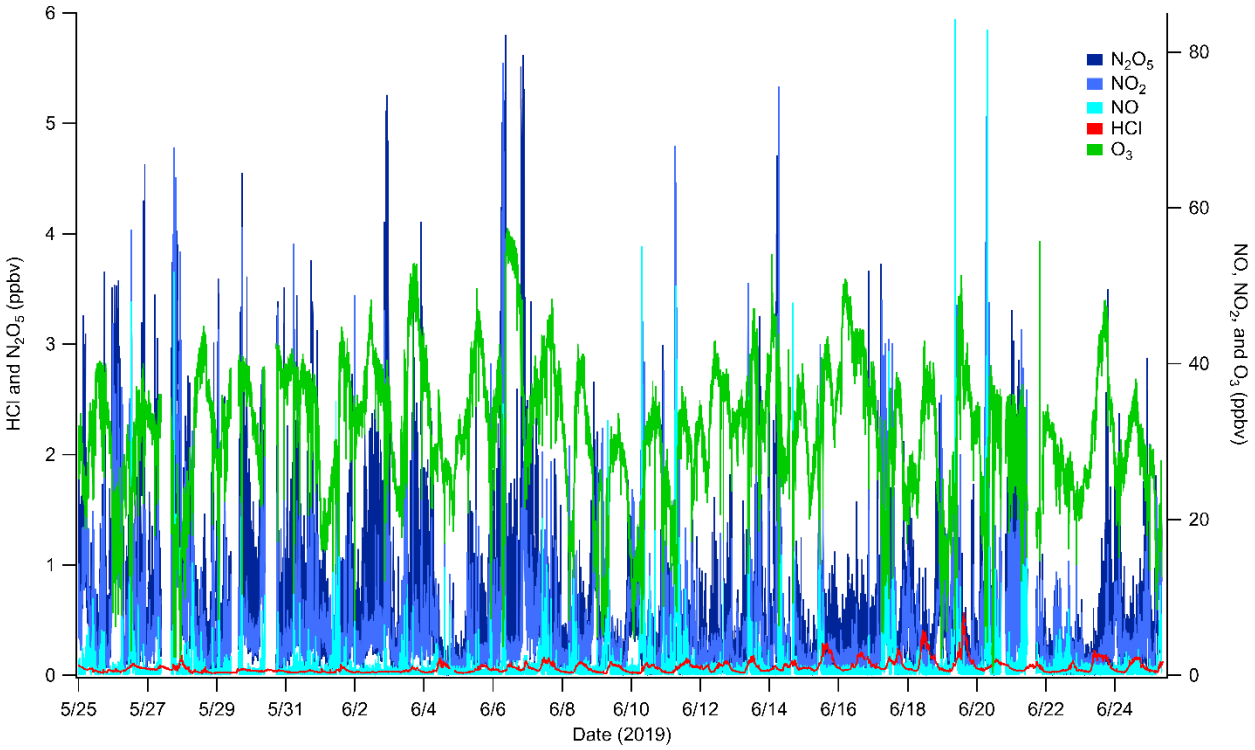

Figure B-3. Time-series of predicted N_2O_5 formation and measured HCl, NO, NO_2, and O_3. N_2O_5 formation was estimated from measured NO, NO_2, and O_3.

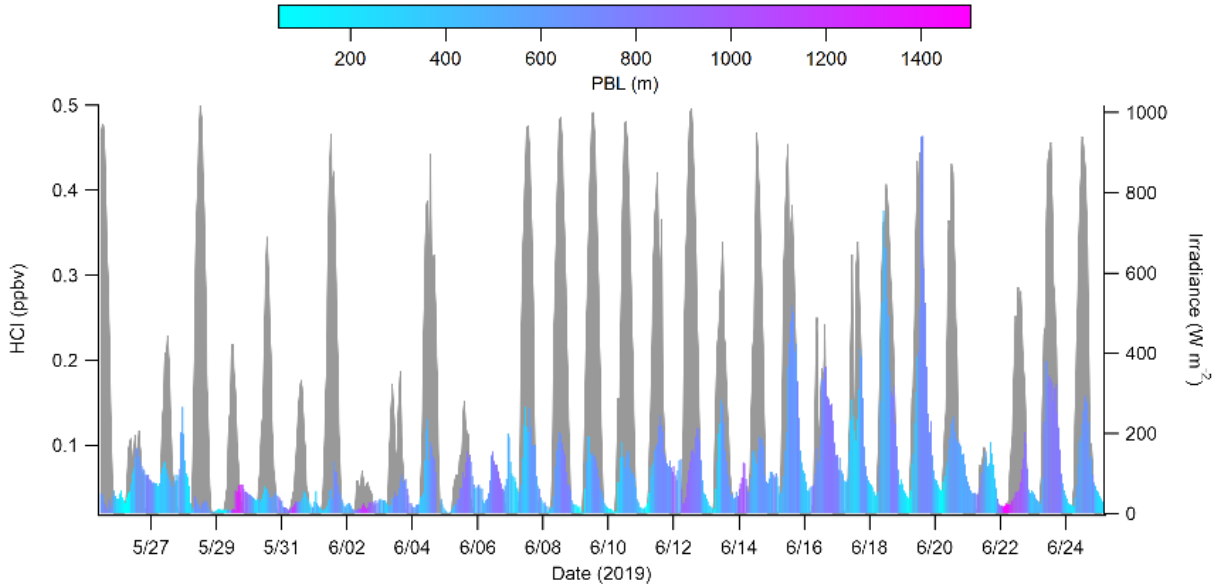

Figure B-4. HCl colored by planetary boundary layer height plotted with irradiance (Gray).

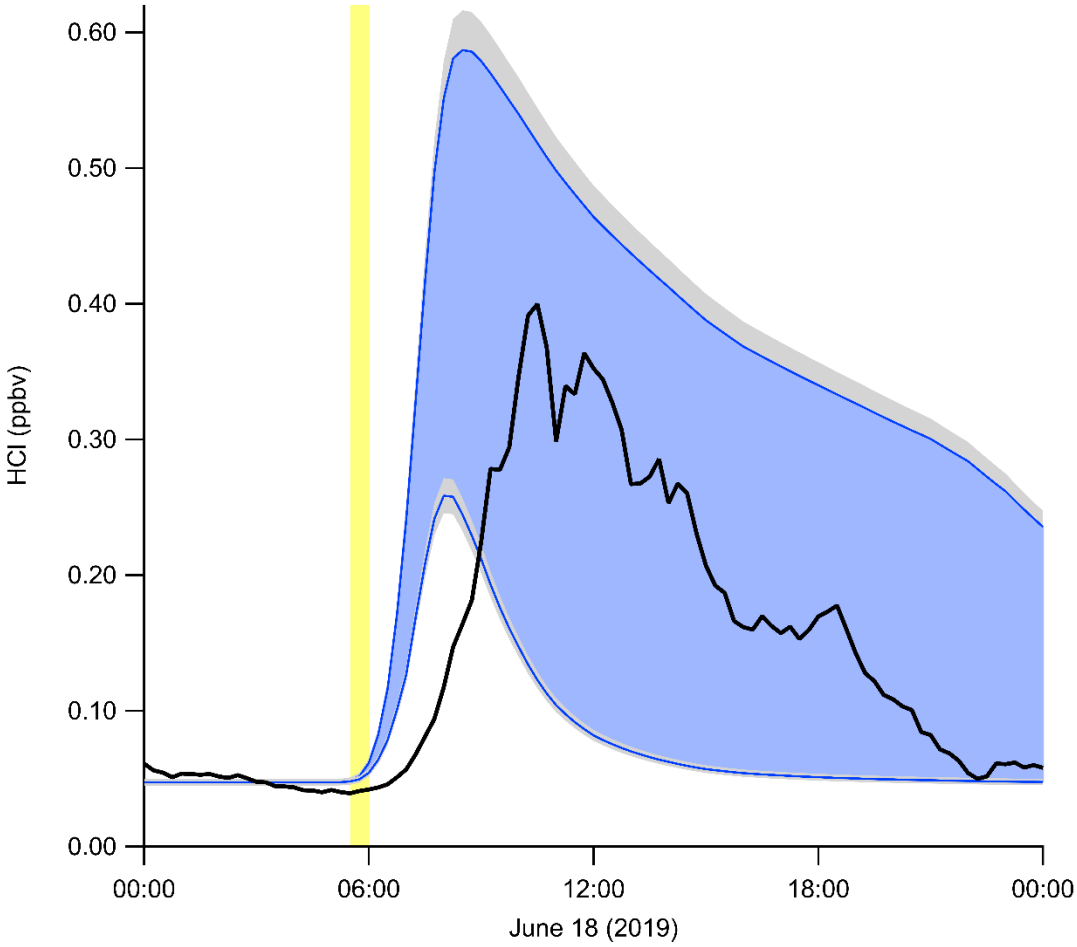

Figure B-5. Modelled HCl (blue) formed via the photolysis of predicted Cl_2 and measured HCl (black) on June 18. Blue shading on the figure indicates the uncertainty in the modelled HCl from the range of deposition velocities. Yellow vertical line denotes time at sunrise.

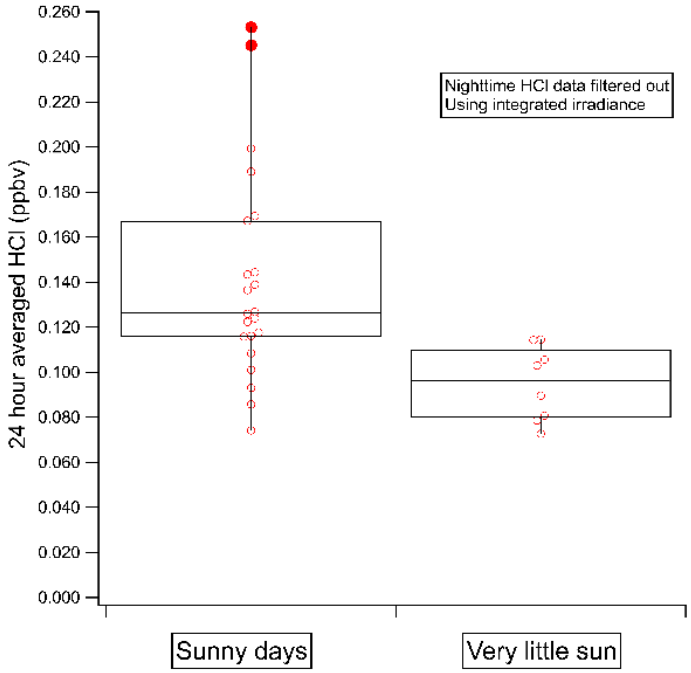

Figure B-6. Box and whisker plot for sunny days and limited sun days, irradiance data was integrated for the day and the plotted with daytime HCl.

Table B-1. Full summary of select measurements for HCl in the marine boundary layer.

Location	Date	Method	HCl mixing ratio range (pptv)[a]	Reference
Halifax, Nova Scotia, Canada	May–June 2019	CRDS	55–572(97)	This study
Central California Coast, US	May–June 2010	Acetate CI-TOFMS	0–2800(440)	Crisp et al.[4]
Southern California Coast, US	May–June 2010	Acetate CI-TOFMS	0 to >16000(2200)	Crisp et al.[4]
Claremont, California, US	September 1985	Denuder/IC	0–2000	Appel et al.[5]
Claremont, California, US	September 1985	Dichotomous sampler	0–1600	John et al.[6]
Glendora, California, US	August 1986	Filter/LC	0–850(500)	Grosjean.[7]
Southern California, US	1986	Denuder/IC	400–1300	Eldering et al.[8]
Colchester, UK	March–April 1987	Filter/IC	100–1200	Sturges and Harrison.[9]

Colchester, UK	Feb 1987 — Jan 1988	Filter/IC	200–1200(500)	Harrison and Allen.[10]
Petten, Netherlands	March–August 1987	Denuder/IC	70–3000	Keuken et al.[11]
Umeå, Sweden	January 1990	Diffusion Scrubber/IC	200–1000	Lindgren.[12]
Umeå, Sweden	July 1990	Diffusion Scrubber/IC	100–600	Lindgren.[12]
Umeå, Sweden	September 1990	Diffusion Scrubber/IC	20–300	Lindgren.[12]
Manhattan, New York, US	July 1999—June 2000	Denuder/IC	10–2000 (300)	Bari et al.[13]
Bronx, New York, US	July 1999—June 2000	Denuder/IC	10–1800 (300)	Bari et al.[13]
Sydney, Florida, US	May 2002	Denuder/IC	<10–5600 (700)	Dasgupta et al.[14]
Bermuda	July–September 1988	Filter/IC	200–400	Keene et al.[15]
East Coast, US	July–September 1988	Filter/IC	500–1200	Keene et al.[15]
Miami, Florida, US	January 1992	Tandem Mist Chamber/IC	40–270	Pszenny et al.[16]
Tudor Hill, Bermuda	April–May 1996	Tandem Mist Chamber/IC	100–900	Keene and Savoie.[17]
Oahu, Hawaii, US	September 1999	Tandem Mist Chamber/IC	30–300	Pszenny et al.[18]
Dumont d'Urville, Antarctica	Dec 2000—Dec 2001	Tandem Mist Chamber/IC	30–300	Jourdain and Legrand. [19]
S. Carolina, US to Canadian Coast	July–August 2002	Tandem Mist Chamber/IC	<25–4500	Keene et al.[20]
Germany to South Africa	October–November 2003	Tandem Mist Chamber/IC	20–1400	Keene et al.[21]
Appledore Island, Maine, US	July–August 2004	Tandem Mist Chamber/IC	5–5800(600)	Keene et al.[22]
N. Pacific Ocean near Alaska, US	May 2006	SF_6 CIMS	6–100(30)	Kim et al.[23]

Sao Vicente Island, Cape Verde	May–June 2007	Tandem Mist Chamber/IC	50–600	Lawler et al.[24]
Cyprus	July–August 2014	Iodide CI-QMS	<135–3000(790)	Eger et al.[25]
East Coast, US	February–March 2015	Iodide CI-TOFMS	199–380	Haskins et al.[26]
St John's, Newfoundland, Canada	April 2017	CRDS	<20–1210(63)	Andrea paper citation

(a) Numbers in brackets represent the measurement average.

Table B-2. List of modelled dates and the ranges of predicted $ClNO_2$.

Date	Mixing ratio range (pptv)
June 3	9.7–10.5
June 5	71–78
June 7	105–118
June 13	151–168
June 15	71–75
June 17	166–188
June 18	426–465
June 19	175–193

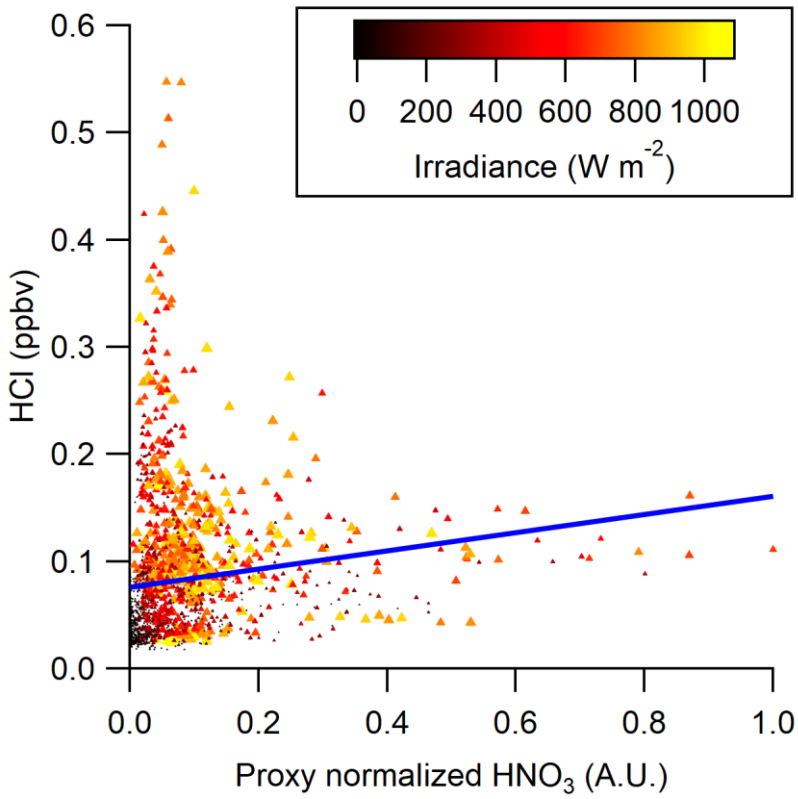

Figure B-7. Measured HCl plotted against normalized HNO_3 colored by irradiance. Blue line is the linear regression best fit line (slope=0.085, R^2=0.018). Proxy HNO_3 is calculated by multiplying the mixing ratio of NO_2 by the irradiance, to mimic OH reaction with NO_2.

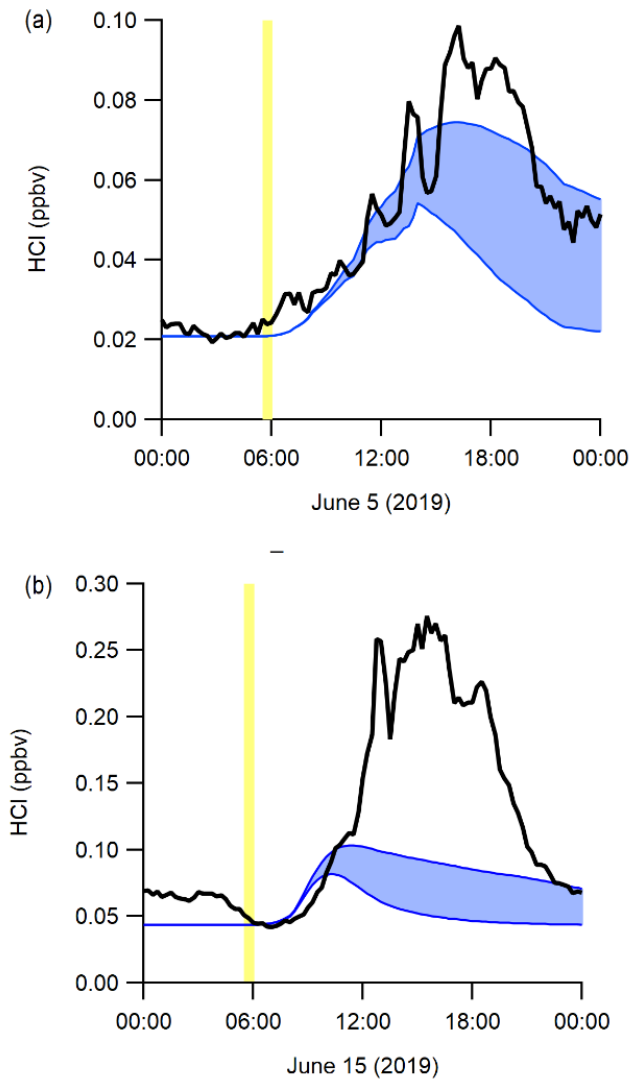

Figure B-8. Modelled HCl (blue) formed via the photolysis of predicted $ClNO_2$ and measured HCl (black). Blue shading on the figure indicates the uncertainty in the modelled HCl from the range of deposition velocities. Yellow vertical line denotes time at sunrise. (a) June 5 and (b) June 15.

B.2 References

(1) Meinel, A. B.; Meinel, M. P. Applied Solar Energy Addison. Wesley Publishing Co **1976**.

(2) Kasten, F.; Young, A. T. Revised Optical Air Mass Tables and Approximation Formula. *Appl. Opt.* **1989**, *28* (22), 4735–4738. https://doi.org/10.1364/AO.28.004735.

(3) Woolf, H. On the Computation of Solar Elevation Angles and the Determination of Sunrise and Sunset Times; **1968**.

(4) Crisp, T. a; Lerner, B. M.; Williams, E. J.; Quinn, P. K.; Bates, T. S.; Bertram, T. H. Observations of Gas Phase Hydrochloric Acid in the Polluted Marine Boundary Layer. *J. Geophys. Res. Atmos.* **2014**, 6897–6915. https://doi.org/10.1002/2013JD020992.Received.

(5) Appel, B. R.; Tokiwa, Y.; Povard, V.; Kothny, E. L. The Measurement of Atmospheric Hydrochloric Acid in Southern California. *Atmos. Environ. Part A. Gen. Top.* **1991**, *25* (2), 525–527. https://doi.org/https://doi.org/10.1016/0960-1686(91)90325-2.

(6) John, W.; Wall, S. M.; Ondo, J. L. A New Method for Nitric Acid and Nitrate Aerosol Measurement Using the Dichotomous Sampler. *Atmos. Environ.* **1988**, *22* (8), 1627–1635. https://doi.org/https://doi.org/10.1016/0004-6981(88)90390-3.

(7) Grosjean, D. Liquid-Chromatography Analysis of Chloride and Nitrate with "Negative" Ultraviolet Detection: Ambient Levels and Relative Abundance of Gas-Phase Inorganic and Organic Acids in Southern California. *Environ. Sci. Technol.* **1990**, *24* (1), 77–81. https://doi.org/10.1021/es00071a007.

(8) Eldering, A. M.; Solomon, P. A.; Salmon, L. G.; Fall, T.; Cass, G. R. Hydrochloric Acid: A Regional Perspective on Concentrations and Formation in the Atmosphere of Southern California. *Atmos. Environ. Part A, Gen. Top.* **1991**, *25* (10), 2091–2102.

https://doi.org/10.1016/0960-1686(91)90086-M.

(9) Sturges, W. T.; Harrison, R. M. The Use of Nylon Filters to Collect Hcl: Efficiencies, Interferences and Ambient Concentrations. *Atmos. Environ.* **1989**, *23* (9), 1987–1996. https://doi.org/https://doi.org/10.1016/0004-6981(89)90525-8.

(10) Harrison, R. M.; Allen, A. G. Measurements of Atmospheric HNO3, HCl and Associated Species on a Small Network in Eastern England. *Atmos. Environ. Part A. Gen. Top.* **1990**, *24* (2), 369–376. https://doi.org/https://doi.org/10.1016/0960-1686(90)90116-5.

(11) Keuken, M. P.; Schoonebeek, C. A. M.; van Wensveen-Louter, A.; Slanina, J. Simultaneous Sampling of NH3, HNO3, HC1, SO2 and H2O2 in Ambient Air by a Wet Annular Denuder System. *Atmos. Environ.* **1988**, *22* (11), 2541–2548. https://doi.org/https://doi.org/10.1016/0004-6981(88)90486-6.

(12) Lindgren, P. F. Diffusion Scrubber-Ion Chromatography for the Measurement of Trace Levels of Atmospheric HCl. *Atmos. Environ. Part A. Gen. Top.* **1992**, *26* (1), 43–49. https://doi.org/https://doi.org/10.1016/0960-1686(92)90259-N.

(13) Bari, A.; Ferraro, V.; Wilson, L. R.; Luttinger, D.; Husain, L. Measurements of Gaseous HONO, HNO3, SO2, HCl, NH3, Particulate Sulfate and PM2.5 in New York, NY. *Atmos. Environ.* **2003**, *37* (20), 2825–2835. https://doi.org/10.1016/S1352-2310(03)00199-7.

(14) Dasgupta, P. K.; Campbell, S. W.; Al-Horr, R. S.; Ullah, S. M. R.; Li, J.; Amalfitano, C.; Poor, N. D. Conversion of Sea Salt Aerosol to NaNO3 and the Production of HCl: Analysis of Temporal Behavior of Aerosol Chloride/Nitrate and Gaseous HCl/HNO3 Concentrations with AIM. *Atmos. Environ.* **2007**, *41* (20), 4242–4257. https://doi.org/https://doi.org/10.1016/j.atmosenv.2006.09.054.

(15) Keene, W. C.; Pszenny, A. A. P.; Jacob, D. J.; Duce, R. A.; Galloway, J. N.; Schultz-Tokos, J. J.; Sievering, H.; Boatman, J. F. The Geochemical Cycling of Reactive Chlorine through the Marine Troposphere. *Global Biogeochem. Cycles* **1990**, *4* (4), 407–430. https://doi.org/https://doi.org/10.1029/GB004i004p00407.

(16) Pszenny, A. A. P.; Keene, W. C.; Jacob, D. J.; Fan, S.; Maben, J. R.; Zetwo, M. P.; Springer-Young, M.; Galloway, J. N. Evidence of Inorganic Chlorine Gases Other than Hydrogen Chloride in Marine Surface Air. *Geophys. Res. Lett.* **1993**, *20* (8), 699–702. https://doi.org/10.1029/93GL00047.

(17) Keene, W. C.; Savoie, D. L. The PH of Deliquesced Sea-Salt Aerosol in Polluted Marine Air. *Geophys. Res. Lett.* **1998**, *25* (12), 2181–2184. https://doi.org/https://doi.org/10.1029/98GL01591.

(18) Pszenny, A. A. P.; Moldanová, J.; Keene, W. C.; Sander, R.; Maben, J. R.; Martinez, M.; Crutzen, P. J.; Perner, D.; Prinn, R. G. Halogen Cycling and Aerosol PH in the Hawaiian Marine Boundary Layer. *Atmos. Chem. Phys.* **2004**, *4* (1), 147–168. https://doi.org/10.5194/acp-4-147-2004.

(19) Jourdain, B.; Legrand, M. Year-Round Records of Bulk and Size-Segregated Aerosol Composition and HCl and HNO3 Levels in the Dumont d'Urville (Coastal Antarctica) Atmosphere: Implications for Sea-Salt Aerosol Fractionation in the Winter and Summer. *J. Geophys. Res. Atmos.* **2002**, *107* (D22), ACH 20-1-ACH 20-13. https://doi.org/https://doi.org/10.1029/2002JD002471.

(20) Keene, W. C.; Pszenny, A. A. P.; Maben, J. R.; Stevenson, E.; Wall, A. Closure Evaluation of Size-Resolved Aerosol PH in the New England Coastal Atmosphere during

Summer. *J. Geophys. Res. Atmos.* **2004**, *109* (D23). https://doi.org/https://doi.org/10.1029/2004JD004801.

(21) Keene, W. C.; Long, M. S.; Pszenny, A. A. P.; Sander, R.; Maben, J. R.; Wall, A. J.; O'Halloran, T. L.; Kerkweg, A.; Fischer, E. V; Schrems, O. Latitudinal Variation in the Multiphase Chemical Processing of Inorganic Halogens and Related Species over the Eastern North and South Atlantic Oceans. *Atmos. Chem. Phys.* **2009**, *9* (19), 7361–7385. https://doi.org/10.5194/acp-9-7361-2009.

(22) Keene, W. C.; Stutz, J.; Pszenny, A. A. P.; Maben, J. R.; Fischer, E. V; Smith, A. M.; von Glasow, R.; Pechtl, S.; Sive, B. C.; Varner, R. K. Inorganic Chlorine and Bromine in Coastal New England Air during Summer. *J. Geophys. Res. Atmos.* **2007**, *112* (D10). https://doi.org/10.1029/2006JD007689.

(23) Kim, S.; Huey, L. G.; Stickel, R. E.; Pierce, R. B.; Chen, G.; Avery, M. A.; Dibb, J. E.; Diskin, G. S.; Sachse, G. W.; McNaughton, C. S.; et al. Airborne Measurements of HCl from the Marine Boundary Layer to the Lower Stratosphere over the North Pacific Ocean during INTEX-B. *Atmos. Chem. Phys. Discuss.* **2008**, *2008*, 3563–3595. https://doi.org/10.5194/acpd-8-3563-2008.

(24) Lawler, M. J.; Finley, B. D.; Keene, W. C.; Pszenny, A. A. P.; Read, K. A.; von Glasow, R.; Saltzman, E. S. Pollution-Enhanced Reactive Chlorine Chemistry in the Eastern Tropical Atlantic Boundary Layer. *Geophys. Res. Lett.* **2009**, *36* (8). https://doi.org/10.1029/2008GL036666.

(25) Eger, P. G.; Helleis, F.; Schuster, G.; Phillips, G. J.; Lelieveld, J.; Crowley, J. N. Chemical Ionization Quadrupole Mass Spectrometer with an Electrical Discharge Ion Source for

Atmospheric Trace Gas Measurement. *Atmos. Meas. Tech.* **2019**, *12* (3), 1935–1954. https://doi.org/10.5194/amt-12-1935-2019.

(26) Haskins, J. D.; Jaeglé, L.; Shah, V.; Lee, B. H.; Lopez-Hilfiker, F. D.; Campuzano-Jost, P.; Schroder, J. C.; Day, D. A.; Guo, H.; Sullivan, A. P.; et al. Wintertime Gas-Particle Partitioning and Speciation of Inorganic Chlorine in the Lower Troposphere Over the Northeast United States and Coastal Ocean. *J. Geophys. Res. Atmos.* **2018**, *123* (22), 12,812-897,916. https://doi.org/10.1029/2018JD028786.

Appendix C: Supporting information for Chapter 5.

Table C-1. Typical bond dissociation energies for sp^3 alkyl chlorides.[1]

Carbon Type	Dissociation Energy (kJ/mol)
Primary	~410
Secondary	~400
Tertiary	~380

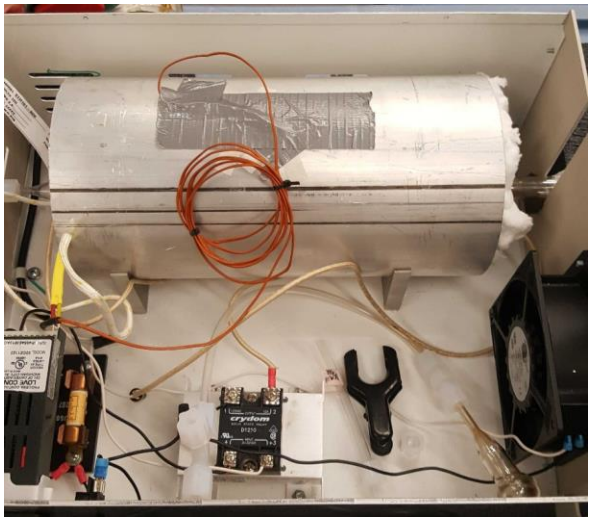

Figure C-1. Initial prototype HCl-TCl based off of Stockwell et al., (2018).[2]

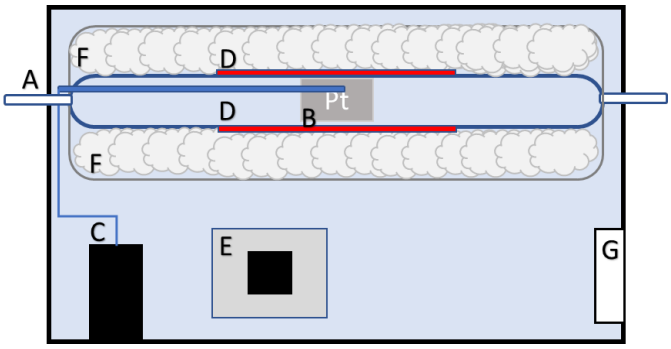

Figure C-2. Schematic for initial HCl-TCl prototype; (A) Quartz flow-tube, (B) platinum catalyst bed, (C) thermocouple & process controller, (D) heaters, (E) solid state relay, (F) insulation, and (G) fan.

A higher stable operating temperature was required for total chlorine combustion, which led to the implementing the split-tube furnace.

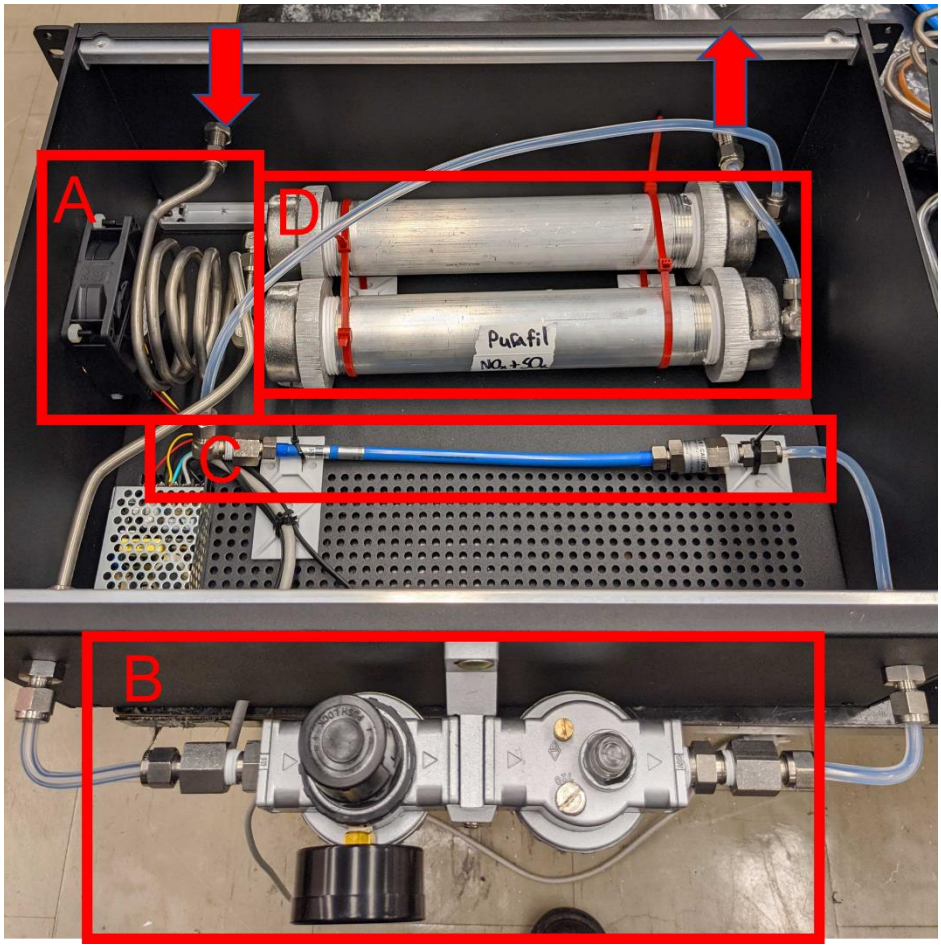

Figure C-3. Custom lab built clean air generator. (A) cooling fan, (B) water condenser and pressure regulator, (C) SMC membrane dryer (SMCIDG1N02, Proax Technologies Ltd, Oakville, Ont, Canada), and (D) two scrubbers containing Purakol and Purafil SP (Purafil, incorporated, Doraville, GA, USA).

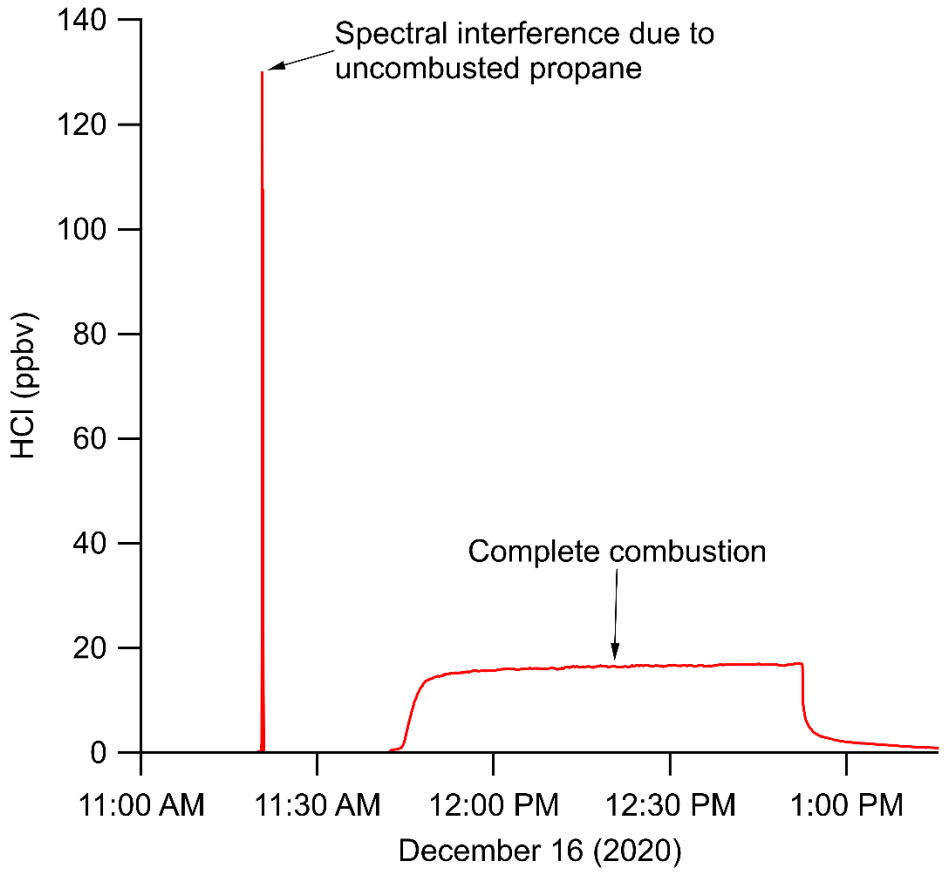

Figure C-4. High spectral interference of added propane at low temperatures (<650 °C).

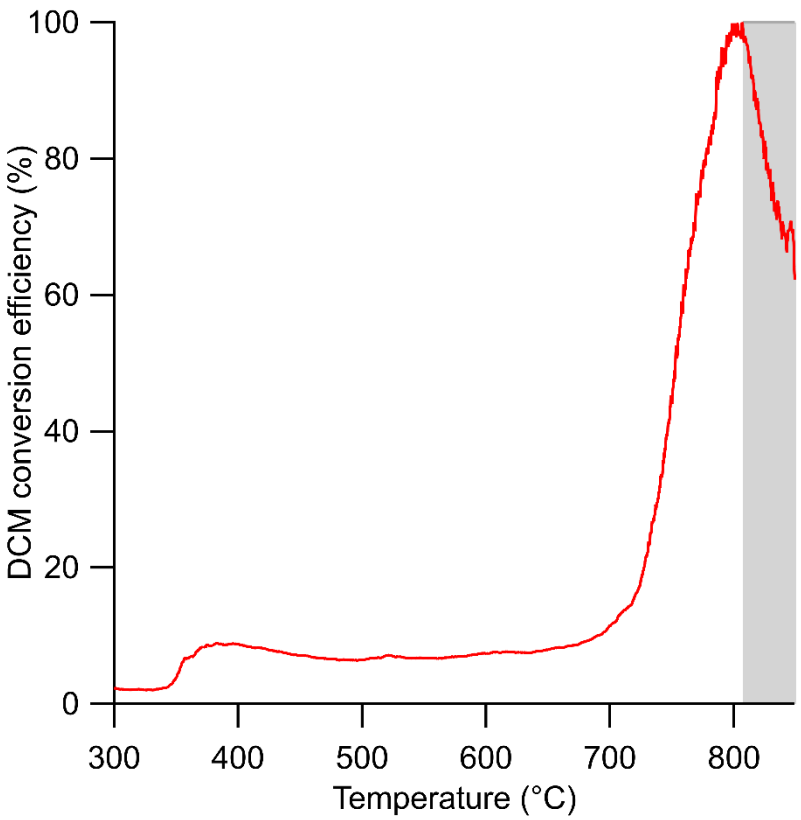

Figure C-5. Monitoring DCM conversion from 300–800 °C. Gray shaded region indicates when temperature was turned off.

Figure C-6. Output of the flow-tube in the Split-tube furnace held at 825 °C.

C.1 References

(1) Wade, L. G. *Organic Chemistry*; Prentice Hall: Upper Saddle River, N.J., 1999.

(2) Stockwell, C. E.; Kupc, A.; Witkowski, B.; Talukdar, R. K.; Liu, Y. Characterization of a Catalyst-Based Conversion Technique to Measure Total Particulate Nitrogen and Organic Carbon and Comparison to a Particle Mass Measurement Instrument. *Atmos. Meas. Tech* **2018**, 2749–2768.